DOCTORAL THESIS

Optical Detection Methods for Droplet Microfluidic Applications

Kaiser Pärnamets

TALLINNA TEHNIKAÜLIKOOL
TALLINN UNIVERSITY OF TECHNOLOGY
TALLINN 2023

TALLINN UNIVERSITY OF TECHNOLOGY
DOCTORAL THESIS
31/2023

Optical Detection Methods for Droplet Microfluidic Applications

KAISER PÄRNAMETS

TAL TECH PRESS

TALLINN UNIVERSITY OF TECHNOLOGY
School of Information Technologies
Thomas Johann Seebeck Department of Electronics
This dissertation was accepted for the defence of the degree 25/07/2023

Supervisor: Dr. Tamás Pardy, Senior Researcher
Department of Chemistry and Biotechnology
Tallinn University of Technology
Tallinn, Estonia

Co-supervisor: Dr. Ants Koel, Senior Researcher
Department of Chemistry and Biotechnology
Tallinn University of Technology
Tallinn, Estonia

Opponents: Dr. Ferenc Ender, Associate Professor
Department of Electron Devices
Budapest University of Technology and Economics
Budapest, Hungary

Prof. Serge Dos Santos, Associate Professor
Department of Industrial Systems
INSA Centre Val de Loire, Blois Campus, France
Inserm-University of Tours, France

Defence of the thesis: 29/08/2023, Tallinn

Declaration:
Hereby I declare that this doctoral thesis, my original investigation and achievement, submitted for the doctoral degree at Tallinn University of Technology has not been submitted for doctoral or equivalent academic degree.

Kaiser Pärnamets

---
signature

European Union
European Regional
Development Fund

Investing
in your future

ISSN 2585-6898 (publication)
ISBN 978-9916-80-022-5 (publication)
ISSN 2585-6901 (PDF)
ISBN 978-9916-80-023-2 (PDF)
Printed by Koopia Niini & Rauam

TALLINNA TEHNIKAÜLIKOOL
DOKTORITÖÖ
31/2023

Optilised tuvastusmeetodid tilkade mikrofluidiliste rakenduste jaoks

KAISER PÄRNAMETS

TAL TECH
KIRJASTUS

Contents

List of Publications

The list of author's publications, on the basis of which the thesis has been prepared.

Publications

I **K. Pärnamets** *et al.*, "Optical Detection Methods for High-Throughput Fluorescent Droplet Microflow Cytometry," *Micromachines 2021, Vol. 12, Page 345*, vol. 12, no. 3, p. 345, Mar. 2021, doi: 10.3390/MI12030345.

II **K. Parnamets**, A. Koel, T. Pardy, and T. Rang, "Open Source Hardware Cost-Effective Imaging Sensors for High-Throughput Droplet Microfluidic Systems," *Proc. 2022 26th Int. Conf. Electron. Electron. 2022*, 2022, doi: 10.1109/IEEECONF55059.2022.9810383.

III **K. Parnamets**, A. Udal, A. Koel, T. Pardy, N. Gyimah, and T. Rang, "Compact Empirical Model for Droplet Generation in a Lab-on-Chip Cytometry System," *IEEE Access*, vol. 10, pp. 127708–127717, 2022, doi: 10.1109/ACCESS.2022.3226623.

Other publications

IV N. Gyimah, R. Jõemaa, **K. Pärnamets**, O. Scheler, T. Rang, and T. Pardy, "PID Controller Tuning Optimization Using Genetic Algorithm for Droplet Size Control in Microfluidics". BEC2022.

Papers under review

V R. Jõemaa, N. Gyimah, K. Ashraf, **K. Pärnamets**, A. W. Zaft, O. Scheler, T. Rang, and T. Pardy, "CogniFlow-Drop: Integrated modular system for automated generation of droplets in microfluidic applications". *Submitted to IEEE Access by May 2023*.

Author's Contribution to the Publications

Contribution to the papers in this thesis are:

I As the first author of the publication, I carried out the literature search regarding light sources and sensors used in droplet microfluidic applications. The tables and figures were prepared by me, and I wrote the bulk of the manuscript except for the sections on commercial platforms and perspectives (paper's Sections 4.1 and 4.2).

II As the first author of the publication, I developed an experimental platform for droplet microfluidic studies. I used an open-source and cost-effective set of imaging sensors specifically designed for the Raspberry Pi platform, along with freeware code designed to increase the framerate capabilities of the sensors. I conducted a variety of experiments and analyses to determine the maximum droplet detection rate for each sensor. I analysed the results, prepared the figures and tables, and I wrote the manuscript.

III I was the first author and proposed the idea of mathematically expressing droplet generation estimation based on flow rates in dispersed and continuous phases. I was responsible for collecting data, evaluating the results, and writing the introduction, the description of the measurement setup, the summary of the experimental results, and the conclusion.

V I was a co-author and proposed a novel methodology for cost-effective and portable solution for non-imaging droplet detection. It was my responsibility to develop a microfluidic measurement setup, conduct the experiments, and prepare the chapters covering the detection setup. The paper is submitted to IEEE Access for review at end of May 2023.

Abbreviations

μTAS	Miniaturized Total Analysis Systems
ADC	Analogue to Digital Converter
AI	Artificial Intelligence
APD	Avalanche Photodiode
CCD	Charge Coupled Device
CMOS	Complementary Metal Oxide Semiconductor
DC	Direct current
DL	Deep Learning
DMF	Droplet microfluidics
dps	Droplets per second
EMCCD	Electron Multiplied Charge Coupled Device
FITC	Fluorescein Isothiocyanate
fps	Frames per second
I.D.	Inner Diameter
ICCD	Intensified Charge Coupled Device
IR	Infrared
LED	Light Emitting Diode
LOC	Lab-On-a-Chip
MCP-PMT	Microchannel plate photomultiplier tube
ML	Machine Learning
O.D.	Outer Diameter
PC	Personal Computer
PCB	Printed Circuit Board
PD	Photodiode
PDMS	Polydimethylsiloxane
PIN	Photodiode with intrinsic layer
PMT	Photomultiplier Tube
POCT	Point-Of-Care Test
PTFE	Polytetrafluoroethylene (Teflon™)
sCMOS	Scientific complementary metal oxide semiconductor
SNR	Signal to Noise Ratio
TIA	Transimpedance amplifier
UV	Ultraviolet

1 Introduction

As the field of biomedical research continues to evolve, Lab on a Chip (LOC) has emerged as a ground-breaking technology combining various laboratory functions on a single microchip. As a result of this remarkable integration, new opportunities have been opened up for diagnostics, healthcare, and research. It is common for traditional laboratory techniques to require time-consuming processes, bulky equipment, and large quantities of samples. By miniaturizing and automating laboratory processes, LOC addresses these challenges by increasing efficiency, reducing costs, and improving portability. With LOC, researchers and healthcare professionals are able to perform complex analyses using minute samples, resulting in more accurate and faster results. It is possible to detect and monitor diseases such as infectious diseases, cancers, and genetic disorders using LOC devices in clinical diagnostics. In resource-limited settings, these portable devices facilitate point-of-care testing (POCT) and facilitate diagnostic capabilities for underserved populations.

There are many areas of interest and trends within LOC, but recent research has identified three major objectives: developing POCT, increasing the number of tests per microfluidic chip, and developing portable applications. A growing emphasis is being placed on the development of POCT devices that could be utilized in doctor's offices, clinics, and even at home. This trend aims to provide rapid and accurate diagnostics, eliminating the need for sending samples to centralized laboratories and enabling immediate decision-making and treatment initiation. Furthermore, ongoing research efforts seek to incorporate additional functions into a single microchip, enabling diverse analytical processes to be performed seamlessly on the same device, including sample preparation, amplification, separation, and detection. Lastly, the shrinking size of LOC devices allows for greater portability, which makes them suitable for use in remote or resource-limited areas. Moreover, with the addition of wireless connectivity, portable LOC devices can transmit data in real time, enabling remote monitoring and data analysis.

LOC's most important objective is to provide access to advanced diagnostic capabilities to make healthcare more accessible and equitable. LOC also allows laboratory processes to be optimized, resulting in improved patient outcomes, reduced healthcare costs, and early detection and intervention of a wide range of diseases.

1.1 Background and motivation

The concept of Micro Total Analysis Systems (μTAS), also known as LOC devices, has been of interest to scientists for almost four decades [1]–[7] The field of LOC started to emerge with the advancement of microelectromechanical systems in the beginning of the 90s based on the developments in microfabrication techniques developed for the silicon microprocessor industry in the 80s [1], [8]. Those technologies enabled to develop and manufacture microfluidic chips with channels sizes in the range of 10 to 100 μm [1]. As a result of miniaturization of LOC devices, it became evident that vast quantities of expensive reagents could be saved by reducing the size of the devices. The lower volume of reagents allows the sample to be heated and cooled more rapidly, and the reaction times are greatly improved. Moreover, LOC devices can now be miniaturized to a smaller form factor, leading to the possibility of producing more compact μTAS devices and opening the market for home medical devices (and more generally for in-the-field devices), which are known as POCT, a term first used by Dr Kost in the early 1980s [9]–[12]. Such approaches, or combinations thereof, are particularly interesting because they enable

the results of an analysis to be obtained substantially more rapidly than conventional laboratory experiments. Some of the most commonly known microfluidic POCT devices on the market are pregnancy tests and blood glucose tests that usually provide answer to the experiment under 30 minutes and are approved for home use [13]–[15].

Despite the fact that there are already POCT solutions available that can provide analysis to some extent [15], [16], there is a need for more. A prime example surged in 2020, when there was a rapidly increasing interest and need for POCT solutions that can detect COVID19 quickly and easily, especially in the case of home use [10], [11], [17], [18]. There is no doubt that this type of solution is of great interest, as it gives results within minutes, is portable, is cost-effective, and is easy to use by non-qualified personnel, which is exactly what is required for rapid testing in order to contain an outbreak.

Out of many sub-fields in microfluidics (paper-based microfluidics, digital microfluidics, droplet-based microfluidics, open microfluidics and continuous-flow microfluidics), droplet-based microfluidic solutions are increasingly gaining attention for a variety of reasons, including their ability to handle droplets as single-cell incubators and create a high numbers of droplets per second (dps) [19]–[21]. There are multiple benefits associated with using droplet microfluidics in biological experiments. First, the sample is packed into small droplets with a volume in the range of microliters to picolitres, allowing a significant reduction in the required sample volume, which is often limited and costly. In addition to its ability to separate droplets from each other, droplet microfluidics is also capable of generating large numbers of dps (high-throughput), allowing virtually a multitude of experiments to be conducted simultaneously. Droplet microfluidics has numerous applications, but it is particularly popular in biomedical research, particularly drug discovery [22], [23]. Droplet-based detection devices incorporate some form of electronic readout circuitry in their final configuration.The droplets are detected either using optical, mechanical or chemical methods, whereas the optical method is most widely used due to excellent sensitivity [24]–[29] A wide variety of tasks can be addressed with the optical technique, including counting droplets, detecting droplet size and speed, and analysing the morphology of droplets to detect multiple parameters simultaneously [30]–[32]. The wide range of applications, the high sensitivity, and the capability to analyse multiple parameters simultaneously make the optical technique an attractive detection option in comparison to other available options.

The droplets serve as individual microreactors and there is a clear motivation to generate a large number of droplets in order to increase the statistical significance of the experiment. However, it is not just about generating a large number of droplets, but also to produce as many droplets containing only a single cell as possible. During the encapsulation of the droplets, the percentage of encapsulated cells is completely random, but real-life experiments indicate a typical rate percentage of 10% [33], [34]. It has been demonstrated that droplet detection systems can detect up to a million dps, but these applications heavily depend on the parallelization of the microfluidic chip [35], [36]. Using a single channel approach (or when parallelization is used, then performance per channel), it has been reported that the number of droplets generated can reach upwards of 2000 dps [35], [37]–[44]. Due to the high quantity of droplets generated, methods of detection with ever-better performance are required to handle the increased demand. In the case of high-throughput droplet applications, the collected dataset can include tens to hundreds of thousands of individual images of droplets per experiment. It is inevitable that such a large volume of data needs to be analysed with potent approaches. A number of approaches have been described in the literature that rely on

artificial intelligence (AI) to analyse a large number of droplets captured in images, videos, or electrical signals. [45]–[49].

In microfluidics, there are two possible optical detection approaches: imaging and non-imaging. When employing an imaging approach, a camera is used as a detector and the result is an image or video which is then analysed. For such imaging approaches, there are two types of sensors, either charge couple devices (CCDs) or complementary metal oxide semiconductors (CMOSs) [25], [50]–[52]. Regarding the light sources for imaging approaches, early microfluidic devices used water-cooled light sources such as mercury arcs, xenon arcs, and lasers as light sources [53]–[55]. These bulky light sources have since been replaced by solid state lasers and LEDs, enabling the devices to be compact, energy efficient, and portable [56]–[59]. Non-imaging approaches capture light intensity as an electrical signal via photodiodes or photomultiplier tubes (PMTs) [30], [50], [60]. For analysis, artificial intelligence and machine learning can be applied to both imaging and non-imaging detection approaches.

1.2 Challenges in Lab-on-a-Chip

The LOC's objective is to provide a device that works according to the principle of "sample in – answer out" or also known as "sample-to-answer" [15], [16], [61], [62] and would cover all required steps, from sample preparation to detection and analysing the earlier section, droplet microfluidics was discussed as an area of great interest to researchers. Due to the requirement for portable high-throughput systems, there are challenges that must be addressed. These challenges are highlighted in bold.

In order to perform high-throughput analysis in droplets, a microfluidic setup is needed, which enables both high-speed generation of droplets as well as detection of the massive number of droplets that are generated. The microfluidic setup usually includes a droplet generator with adaptive pumping, and a high-speed fluorometer, which together form a droplet microfluidic flow cytometer (Figure 1). It is important to note that one of the critical components of a flow cytometer is either a non-imaging detector, or an imaging detector combined with a light source, usually a laser or an LED; however, xenon and mercury arc lamps with filters or monochromators may also be used.

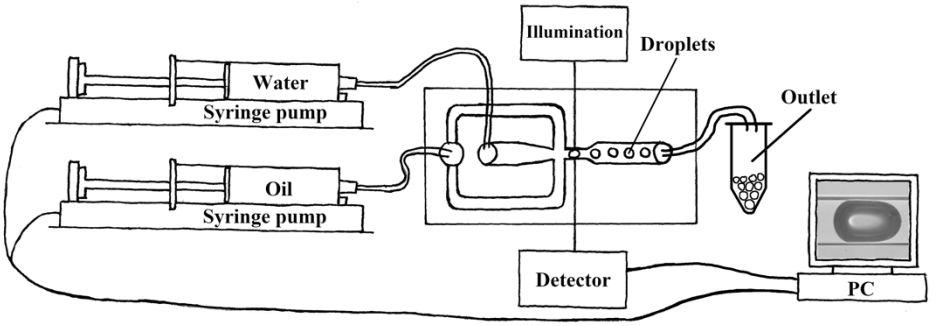

Figure 1. Overview of droplet microfluidic flow cytometer. The system contains a droplet generator, to which an illumination source and an imaging detector are added. Droplets are generated by pumping water and oil into the microfluidic chip using syringe pumps. The detector and pumps are controlled by the personal computer (PC) and the images of the droplets can be seen on the screen. In case a non-imaging sensor is used, additionally an oscilloscope may be used to capture the electrical signal from the detector.

While LOC has been used for many decades, there is a limited number of ready-made devices available on the market that follow the aforementioned approach, especially in a portable form-factor [63]. In the past, equipment capable of performing this task was of the size of a desk (e.g., Coulter Epics V from 1979–1985) [64]. A state-of-the-art flow cytometer can be used on a desktop and is expected to cost between 100 000 euros and 500 000 euros [63], [65]. Although a desktop flow cytometer is well suited for biological experiments and analyses in laboratories, there is a need for a portable, user-friendly, and affordable device, particularly for use in non-laboratory environments [13], [16], [19], [66]–[68]. However, this has not been possible until recently due to the absence of commercially available mobile embedded platforms with sufficient computing power [53], [69], [70]. The present day offers a wide range of portable cost-effective devices with affordable computing power in a small form factor, such as mobile devices, embedded platforms, and other portable devices. Based on the aforementioned devices or platforms, some portable microfluidic applications have been proposed, which use some combination of detector and illumination [67], [69]–[71]. There were several high-power, air- or water-cooled light sources available in the early days, including lasers, mercury arc lamps, and xenon arc lamps. However, today, a wide array of powerful LEDs and solid state lasers are also available as an alternative to these light sources that are affordable and portable [53]. **Embedded hardware platforms can often be used to solve portable microfluidic applications with minimal computational requirements; however, light sources and detectors may not always be suitable for portable applications; this is still an open research issue**.

During the last decade, much research has been conducted on the advancement of LOC microfluidic systems, especially on sample preparation and detection. The focus is now shifting to digital and automated sample analysis. Some recent papers in the field of LOC have shown the use of some form of automated analysis of the detected results, whether using AI-based approaches, such as machine learning (ML), deep learning (DL) [13], [46]–[49], [61], [72]. From the perspective of analysis, this clearly sets the direction for the research, however the need for lower costing, portable and perhaps even disposable devices has not diminished [20], [47]. **However, this poses a challenge to existing preparation and detection methods in terms of their suitability for use in automated systems, i.e. whether they are capable of being automated themselves. In addition, since AI based tools enable the analysis of very large numbers of droplets, the portable platform must be capable of integrating with DL, AI, or ML methods.**

Microscopes are often used to detect droplets, since they are available in laboratories, provide good built-in illumination, magnification, and detection capabilities, but they can't be automated as they require manual settings to adjust the focus, brightness and are not portable. In addition, since microscopes are widely used in microfluidic experiments, the illumination and detection they provide are a benchmark for portable applications' illumination and detection [73]–[79]. The current illumination and detection methods using microscope, however, are not capable of being adopted by ML. **Two challenges arise from this. First, the performance of illumination and detection in portable platforms should be on par with that for microscopes. In addition, the proposed combination of detection and illumination should facilitate easy integration with machine learning, if necessary.**

1.3 Problem statement and Research questions

The above paragraphs about background and motivation, and challenges in Lab-on-a-Chip, present a brief overview of the current focus of research in the field of microfluidics. Although these paragraphs identify the challenges in the field, they do not identify any potential research gaps, questions, or hypotheses that could lead to solutions to those challenges.

From the scientific literature, it is clearly seen that there is a pressing need for cost-effective and portable solutions, especially such solutions that could be used at home or in the non-laboratory environments [3]. Some of the already existing solutions work well for certain use cases, but there is certainly a need to make more sensitive tests or microfluidic solutions [16], [80]. Some papers show that the issue of sensitivity could be solved by using high throughput droplet microfluidics with a properly selected set of illumination, detection and sample handling mechanisms as optical detection methods are the most sensitive compared to other existing solutions [39], [81]–[84].

Based on the background, motivation and challenges of this doctoral dissertation, it is possible to formulate the following **hypothesis**:

"**A portable, cost-effective droplet-based cell analysis platform can be built using an optimal combination of readout frequency, excitation, and sensing to detect cell fluorescence. Furthermore, the same platform will, by design, be compatible with machine learning for automated droplet analysis.**"

The goal for this thesis is to focus on the illumination and sensorics aspects; thus, the other parts of MF setups are not thoroughly analysed.

Before advancing to the specific microfluidic solution stage, one must clearly understand the currently existing illumination and imaging options and propose a suitable combination of technologies suitable for cost-effective, portable MF setup. This leads to the first research question (RQ1). Upon identifying the types of sensors that have been used, it is wise to determine how the selected sensors will perform. This leads to the second research question (RQ2). In all likelihood, the sensors have some limitations in terms of detection rate. In cases where droplet generation rate is half or more the sensor framerate, it is not possible to visually differentiate if droplets are generated or there is a continuous flow of liquids instead. Additionally, as the droplet generation rates can be experimentally determined, it is often time consuming, requires multiple experiments and is not cost-effective due to the excessive volume of expensive reagents wasted. It would be valuable to mathematically represent the droplet generation rate in the microfluidic chip by observing the behaviour of the droplet generation at lower droplet generation speeds, enabling to estimate droplet generation rate at other speeds. This leads to the third research question (RQ3).

RQ1 – Three types of sensors are mostly used in microfluidics – optical, mechanical and chemical, whereas optical sensor is the most frequently used due to high sensitivity. Although optical sensors are widely used it might require different approach for high-throughput droplet applications. This brings up the question, what are the capabilities of optical sensors for droplet detection and how does high-throughput limit sensor selection i.e. **what are the sensitivity and sensor speed requirements for reliable droplet detection? Also, are the sensor requirements different for droplet detection if the droplets are fluorescently labelled or not?**

RQ2 – In microfluidics, non-imaging and imaging sensors are used as optical sensors, the latter of which provides more details about the droplets (size, morphology, velocity etc.) and is thus an attractive choice for droplet detection in the early stages of development of microfluidic devices. The question arises as to what **possible cost-effective and open-source solutions** exist that could be **suitable for high-throughput droplet detection with and without fluorescence.** Also, what could be the **suitable lighting solution**, i.e. are LEDs sufficient or should lasers be used instead? **How to evaluate the quality of captured images,** i.e. which tool to use and which parameters to monitor (sharpness, resolution)?

RQ3 – Droplet generation experiments can be performed by experimentally finding suitable oil and water flow rates that produce stable droplet generation at a measurable rate. However, in high-throughput applications, the droplet generation rate exceeds the capabilities of the detection camera, and thus the camera may no longer distinguish the droplets, and therefore it is unknown whether droplet generation continues to be stable. The question arises, **is it possible to model droplet generation to predict stable steady state of generation at high flowrates by knowing the system behaviour at lower flow rates**?

RQ4 – Is it possible to find a new approach to achieve non-imaging high-speed droplet detection without requiring the use of conventional microscope lenses, while still achieving a sensitivity comparable to state-of-the-art solutions? Most of the current state-of-the-art microfluidic solutions rely on precise focusing of illumination, detector, or both, to the microfluidic channel.

1.4 Contributions of the thesis

This PhD thesis makes the following contributions:

1. Contributing to RQ1, a comprehensive study of illumination and detectors was carried out. A thorough review of illumination sources for biomedical applications is presented, as well as identification of which of the sources is particularly suitable for cost-effective and portable droplet microfluidic applications. In addition, a similar review is provided for imaging and non-imaging sensors used in biomedical applications with a focus on which of these are suitable for cost-effective and portable droplet microfluidic applications.
2. Contributing to RQ2, an analysis and evaluation of cost-effective imaging sensors is presented. A comprehensive study evaluates the maximum performance of each imaging sensor in order to determine the maximum detectable droplet rate. An assessment of the suitability of LEDs and lasers is made, as well as the detection of droplets containing and without fluorescein.
3. Contributing to RQ3, a mathematical model is developed based on empirical research data; the model is capable of determining the droplet generation rate in microfluidic chips based on continuous and dispersed flow rates.
4. Contributing to RQ4, a novel method for the non-imaging detection of droplets is presented by incorporating a pinhole into the measurement setup. Compared to state-of-the-art measurement setups, the proposed setup is more compact and provides comparable performance. In addition, it outperforms the current state-of-the-art measurement setups by providing a solution that does not require the precise alignment of the microfluidic chip with the measurement electronics.

Table 1 summarizes the above-mentioned contributions in relation to research papers (listed in Appendices A-D).

Table 1. Publications containing the thesis' contributions.

Contributions	Publication I	Publication II	Publication III	Paper V (under review)
1 – Review	✓	✓		
2 – Comparison of imaging sensors		✓		
3 – Compact empirical model			✓	
4 – Non-imaging approach				✓

1.5 Thesis organization

The following is an outline of the remainder of this PhD thesis. Figure 2 shows the workflow of the chapters from mapping out the state-of-the-art all the way to proposing a novel non-imaging detection technique.

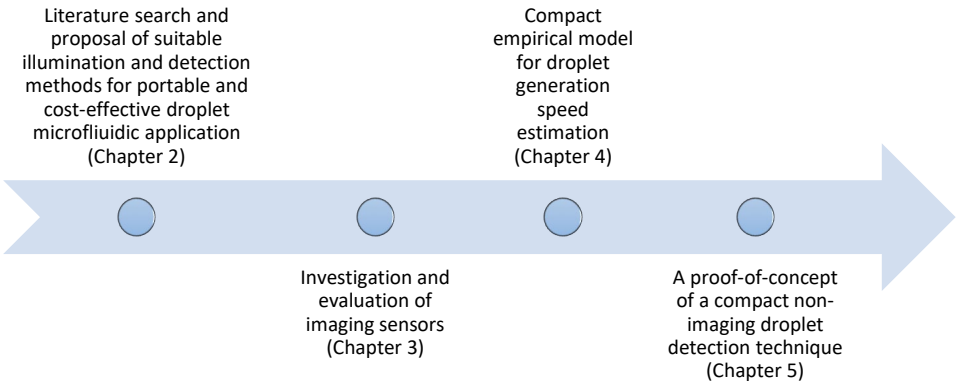

Figure 2. Workflow of the thesis.

- Chapter 2: Based on Publication I, this chapter provides an overview of optical detection methods used in high-throughput fluorescent droplet microflow cytometry. A discussion of imaging and non-imaging sensors used in biomedical applications and droplet microfluidics is presented in this chapter as well as a discussion of different illumination options. In conclusion, this chapter highlights the contributions of my research to the positioning of this PhD dissertation.

- Chapter 3: Based on Publication II, this chapter examines three cost-effective imaging sensors that are suitable for open-source applications, and their performance is evaluated for high-throughput droplet microfluidic systems. In addition to measuring the dps performance for brightfield illumination, the sensor performance is also evaluated for fluorescent stained cells. Furthermore, different use scenarios are discussed.

- Chapter 4: Based on Publication III, this chapter proposes a mathematical model that can be used to estimate droplet generation rate in microfluidic channel. Based on a series of real-life experiments, an empirical model is developed for flow focusing microfluidic chips.

- Chapter 5: Based on Publication V, and as an extension of Chapter 3, this chapter presents a proof-of-concept setup and method to microfluidic droplet detection that eliminates the need for microscope lenses by a pinhole addon. The non-imaging setup is evaluated in comparison to the imaging setup in Chapter 3 for measuring droplet generation rates. The proposed setup is more cost-effective, and due to its placement with rough tolerances, it may be suitable for use in portable applications, for example, point-of-care diagnostic equipment.

- Chapter 6: This chapter gives a summary of the thesis, presents the conclusions, and outlines possible directions for future research.

2 Evaluation of imaging and illumination options in biology and microfluidics

This chapter discusses imaging and non-imaging sensors for high throughput fluorescent droplet microflow systems. In addition, light sources for high-throughput fluorescent droplet microfluidic applications are discussed.

This chapter is based on the following publication:

- K. Pärnamets et al., "**Optical Detection Methods for High-Throughput Fluorescent Droplet Microflow Cytometry**," Micromachines 2021, Vol. 12, Page 345, vol. 12, no. 3, p. 345, Mar. 2021, doi: 10.3390/MI12030345.

2.1 Overview of Lab-On-a-Chip

The fields of LOC, µTAS, microfluidics and droplet microfluidics all share something in common – most of the experiments conducted involve some type of biological sample. An important component of any biological experiment is the sample itself, but in order to analyse it properly it is necessary to use the proper combination of illumination and detection methods. In many state-of-the-art papers, the sample is typically analysed using only an optical microscope [73]–[79]. Optical microscopes are suitable, as the sample under test is often very small, especially in cases of droplet microfluidics where droplets have diameters around 100 µm, and a microscope provides the necessary magnification. Moreover, optical microscopes have built-in light source that provides a good source of illumination, making it a readymade tool with the necessary combination of illumination and detection. In conventional optical microscopes, the detection is performed through the eyepiece, where a human is required to observe and analyse the sample. Although this method may be convenient for most tests and analyses, it cannot be automated and relies heavily on human perception. Furthermore, if the sample is moving rapidly (for example, hundreds or thousands of droplets are generated within a second), it is impossible to detect them using the human eye. Newer optical microscopes, however, come with an additional eyepiece for connecting a camera, making it possible to use them in automated systems.

Using an optical microscope to analyse biological samples, three key modules emerge, illumination, sample handling, and detection [20], [25], [50], [85], [86]. Microfluidic setups (droplet or otherwise) that give some analytical answer to the sample under test can also be divided into three modules, i.e. a. droplet generation, b. droplet detection, and c. data processing, as shown in Figure 3.

The description of the droplet generation module contains information about the design of the microfluidic chip, pumping parameters, and liquid parameters [73], [87]–[89]. The droplet detection module is concerned with all aspects of detecting the droplets or other substances in the microfluidic chip, including some form of detector and a light source for illumination [71], [90]–[92]. The final module focuses on data processing. In this module, the electronic signals captured in the droplet detection module are converted into readable data and sometimes the data can also be analysed [77], [93]–[96].

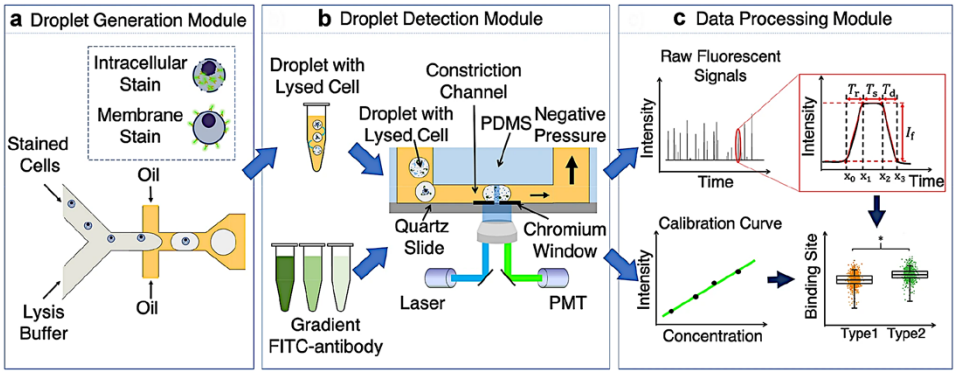

Figure 3. Microfluidic system modules. The modules are (a) a droplet generation module where droplets are produced, (b) a detection module which is employed in the same system, typically imaging or non-imaging detectors are employed, in combination with some form of illumination, (c) data collected by the detector will be analysed by using either a personal computer or an embedded system. Figure reproduced from: [97].

The focus of this PhD thesis is on the detection module in order to find the most appropriate combination of lighting and detection for portable applications, as well as to provide input for machine learning based data processing to operate on the selected technology. A thorough understanding of the illumination and detection technologies that are already being used in the field of biology is essential before proposing an appropriate combination for portable platforms. Additionally, as the final application of the illumination-detection combination will be used in droplet microfluidics, it is crucial to understand the working principles of droplet generation and mapping possible limitations of using the illumination-detection combination in droplet microfluidic systems. The above issues are discussed in what follows.

2.2 Principles of flow cytometer used in LOC applications

The optical excitation and detection system that is at the core of every droplet microfluidic setup works similarly to that of a flow cytometer [58], [90], [91], [98]–[100]. A cytometer is a device used in biology to measure the properties of cells. The operation of a flow cytometer is no different, with the exception that the cells suspended in a liquid are moving through the measurement device with the help of sheath fluid (Figure 4). It is important to distinguish between cells and droplets. A cell is the smallest form of life, whereas a droplet is the result of pushing two immiscible fluids together (for instance, when oil is poured on water, large oil droplets form). In flow cytometry, sample cells are focused using hydrodynamic focusing into a stream of single cells within a microfluidic channel.

An illumination and detector combination is used to detect the cells. A flow cytometer typically uses a laser as an illumination source and a non-imaging sensor as a detector (e.g., a photodiode, an avalanche photodiode, a photomultiplier tube). Instead of non-imaging sensor, an imaging sensor (e.g., a CCD or CMOS camera) can be used, resulting imaging flow cytometry [72], [99], [101], [102]. Laser illumination is frequently used because of its narrow beam, which is further narrowed by using lenses to focus on a single cell [58], [91], [103]–[105]. Moreover, lasers are optically powerful and have a

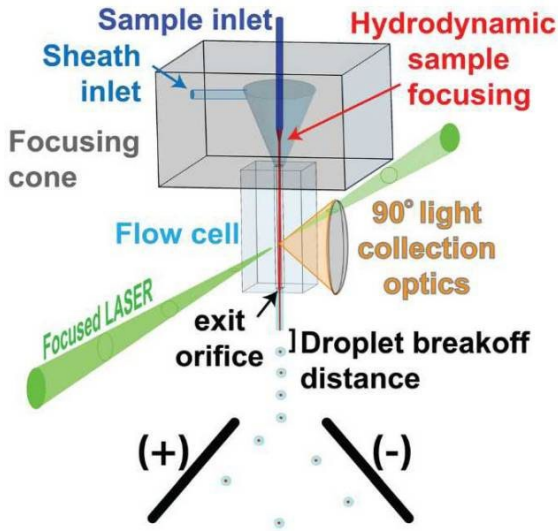

Figure 4. Overview of flow cytometer. The cells are suspended in a liquid sample, which is added to the flow cytometer's inlet. With the aid of a hydrodynamic focuser and sheath fluid, the sample is hydrodynamically focused, resulting in the flow of cells in a flow cell. In order to illuminate one cell at a time, a laser beam must be focused. Excitation light emission is collected at a 90-degree angle with respect to illumination. As the cells exit the flow cell, they form droplets and are then sorted. Figure reproduced from: [44].

narrow spectrum, making it possible to incorporate multiple lasers into one flow cytometer and to use multiple fluorophores simultaneously [103], [104]. However, the number of lasers that can be used is limited, as each laser must be focused on the flow cell separately and be spatially positioned in order to avoid overlapping fluorescence emission. The current state of the art flow cytometer is able to detect up to 17 fluorophores using a combination of three lasers [104]. A number of high efficiency and optically powerful LEDs have also been developed over the past two decades that are suitable for flow cytometry applications, despite lasers' narrow spectrum and potent optical power [106]. Due to their ease of use, these illumination sources are often used in smartphone-based flow cytometry [66], [70]. In addition to the light source, lenses and filters are often used to focus the light on a flow cell. It is common to use filtering with light sources that have a wide spectrum of wavelengths (e.g., xenon lamps or LEDs) to narrow down the excitation wavelength to a desired range. LEDs are single colour devices, but their single colour spectrum can range from 20 to 40 nanometres, which may require the use of optical filters [107]. The optical parameters of each light source are discussed in more detail in the next section.

2.3 Light source specifications for this PhD work

In order to determine the most appropriate combination of lighting and detection for portable applications, a set of specifications is formulated that seem suitable for portable applications. It would be possible to conduct experiments with droplets labelled with fluorescein (e.g. FITC) if the suitable light source had a spectrum of 488 nm. Additionally, a white light source is required in order for droplets to be clearly visible to the human

eye. Due to its portability, the system is intended to work off grid and on batteries, so the power consumption of the light source should be lower than 10 W. It is also expected that the price of the light solution will not exceed 100 €. To eliminate the need to replace the light source, it should have a lifespan of at least 10000 hours. Since the lifespan criterion is fairly high and the light source is unlikely to require replacement, it would still be beneficial if no alignment is required when a bulb or light module is replaced. In portable applications, it is also important that the light solution is robust, which means that it can withstand smaller shocks and vibrations. In addition, it would be preferred if the light source's power supply was relatively simple and could be operated from a battery (e.g. low voltage, low current, DC regulator). Portability is also improved if the module's overall dimensions are less than 10 cm x 10 cm x 10 cm and is lightweight, e.g. 100 grams or less. The requirements for the light source are outlined in Table 2.

Table 2. Requirements for light source for portable droplet microfluidic detector.

Property	Value
Spectrum	Peak at 488 nm for detection of droplets containing fluorescein (e.g. FITC) and white for detecting empty droplets
Power consumption	<10 W
Price	<100 €
Battery operated	Yes
Lifespan	>10k hours
Light output	Immediate (no warmup needed) and adjustable
Alignment	Flexible
Power supply architecture (in terms of circuitry)	Simplest possible
Handling	Robust for portable operation
Size	Maximum of 10x10x10 cm
Weight	<100 g for light source

2.4 Light sources for biological experiments

Every scientific measurement in the field of biomedical application requires appropriate illumination, and it is essential to fully understand the advantages, drawbacks, and technical specifications of each type of lighting. Given the focus of this thesis on optical sensors for droplet microfluidics, a sensible approach would be to investigate the light sources used in microfluidics, particularly in droplet microfluidics. However, since experiments in the field of microfluidics share many characteristics with experiments in biology, it therefore seems appropriate to examine how illumination is used in biology, with possible references to microfluidics as a field of application. In addition, since the thesis focuses on portable applications, light sources suitable for these applications are thoroughly investigated, whereas other light sources are only briefly examined. As was discussed in earlier paragraphs, a microscope is often used to observe microfluidic and biological experiments in order to avoid the development of a complicated optical setup [73]–[79]. Therefore, the analysis of light sources are primarily focused on those that are

used in microscopes, but also on those that are used in microfluidic experiments without the use of a microscope.

A microscope can image a sample in a variety of ways (brightfield, darkfield, confocal microscope, etc.); however, knowing this does not clearly indicate the type of light source type that is used. For brightfield and darkfield illumination, light sources with white colour are favoured [50], [108]–[110]. In such experiments, either tungsten, mercury arc, xenon arc, metal halide or LED light sources are typically used. Other experiments may require a specific wavelength of light, such as those involving fluorescent dyes, which require a narrow spectrum of light for excitation. As a result, lasers are usually preferred due to their narrow spectrum, although it is also possible to use white light with a broad spectrum by adding either filters or monochromators to the setup in order to narrow down the broad spectrum [54], [111].

2.4.1 LED

For many years, light emitting diodes were not considered to be suitable light sources for microscope illumination due to their limited optical power and spectrum [106], [112], [113]. As LED technology has improved over the past few decades, there is a wide variety of power LEDs available that can compete with traditional microscope illumination sources.

LEDs are attractive option for fluorescence microscopy for many reasons. In the first place, LEDs are available with a spectrum ranging from ultraviolet to infrared, with various single colour options to choose from. Below are visible two graphs, showing the spectrum of white LEDs and single colour LEDs from blue to red (Figure 5 (a) and Figure 5 (b)). It may be possible to eliminate the need to use optical filters by using single-colour LEDs instead of broad-spectrum lights that require optical filters or monochromators for selecting single colour for excitation [54]. A single colour light source's performance can be evaluated in terms of the full width half maximum (FWHM), which indicates the width of the spectrum at half the optical power maximum. Due to the broad spectrum of light, FWHM does not apply to broad spectrum light sources. Although LEDs are single colour light sources, their FWHM is typically around 20–40 nm, making them suitable for use without optical filters. However, if the excitation and emission wavelengths are relatively close, filtering may still be necessary. Furthermore, LEDs are compact, although power LEDs require some form of cooling, which usually involves adding a radiator and a fan, making them less compact. Two examples of LEDs are shown below, one LED has mechanical dimensions of 3.5 mm times 3.5mm (Figure 5 (c)), while is other LED is intended to be used in a compact design, having mechanical dimensions of 1.6 mm by 1.6 mm (Figure 5 (d)).

While it is true that metal halide lamps are compact, and some of the low-power (less than 50 W) lamps could also be used for mobile applications, there remains the requirement for a complex supply capable of producing high voltage arc. This is where LEDs have a distinct advantage over metal halide lamps, as LEDs only require a low supply voltage and a suitable current, thus making them more suitable for mobile applications. In addition, LEDs can be easily controlled in terms of light output by adjusting the output current of a supply. Light is produced immediately after LEDs are turned on, eliminating the tedious cycle of turning on and turning off associated with mercury arc (HBO), xenon arc (XBO) or metal halide bulbs. LEDs have a lifespan of up to 50000 hours, and their optical power does not decrease with time. Moreover, compared to HBO, XBO or metal halide lamps, the LED are more cost-effective. The initial cost of single LED is 10–100 times

lower. When multiple LEDs are used in a light source, it makes the overall light source slightly more expensive. However, since LEDs have a lifetime of up to 250 times longer than conventional light sources, the overall operating cost is significantly lower.

Due to the benefits discussed above, manufactures have developed light sources that are direct replacements for xenon arc lamps, e.g. Zeiss Hal 100 light source or Zeiss Colibri [114], [115]. Typically, these light sources have multiple single colour LEDs covering the full spectrum. Below is a comparison graph of Zeiss Calibri 7 LED illumination compared to common mixed gas lamp (the type is not mentioned in Zeiss documentation, but the spectrum is similar to that of a metal halide lamp (Figure 8)). LEDs cover a wide range of wavelengths and are even capable of reaching near infrared wavelengths. Additionally, LED light sources exhibit greater intensities in some cases than a typical mixed gas lamp. As an attractive light source, LEDs have also been incorporated into a number of biomedical applications. [111] have written an extensive review about analytical devices based on LEDS. Another thorough review was conducted by [116] where LEDs are used in analytical chemistry. When LEDs were first introduced in the early 21st century, custom setups began to emerge using LEDs as alternative light sources [118]–[120]. While commercial solutions weren't available at a time [121] successfully used a combination of blue and infrared LED to provide illumination for widefield Olympus microscope. As LEDs are fairly easy to drive and use, they are also used in custom microfluidic setups. [57] developed a multi-LED light source to be synchronised with custom acousto-optical spectral imaging module added to microscope for biomedical imaging. [106] presented a LED based imaging cytometer prototype to detect bead-based immunoassay samples. In their previous experiments lasers were used, LEDs nowadays provide required optical power to be on par with lasers.

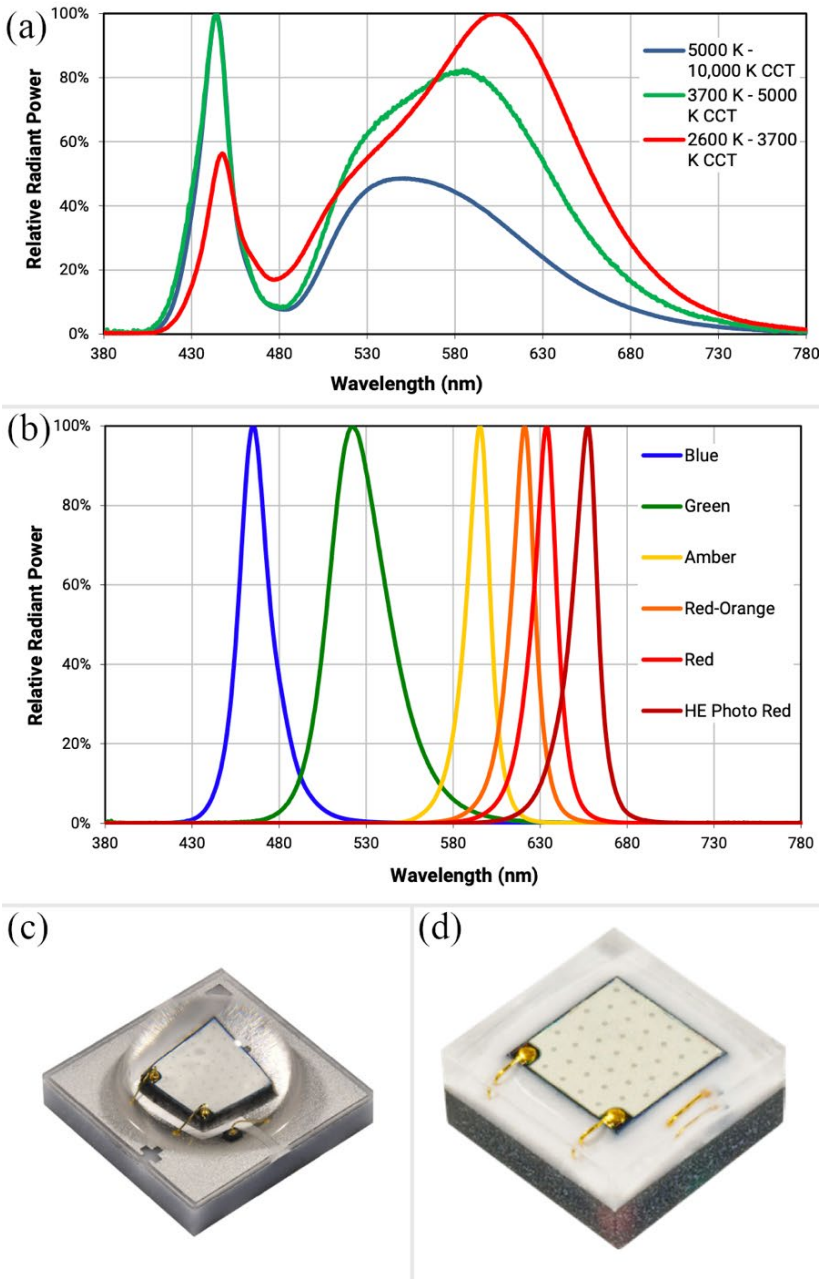

Figure 5. Spectrum and an element of light emitting diode. In figure is seen: (a) white LED spectrum and (b) spectrums of blue, green, amber, red-orange, red and high efficiency (HE) red LEDs. (c) is a single LED with size of 3.45 mm by 3.45 mm from Cree Xlamp XP-E series and (d) is a single LED for compact designs with size of 1.6 mm by 1.6mm from Cree Xlamp XQ-E series. Figures reproduced from: [107] *and* [117].

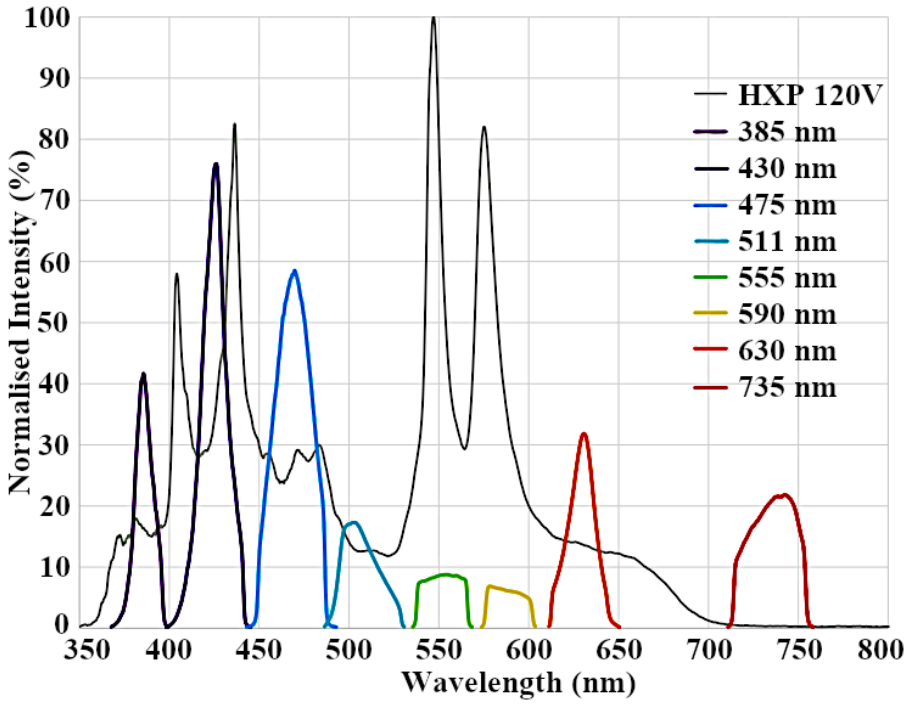

Figure 6. Spectrum of Zeiss Colibri 7. The illumination consists of 7 LEDs, which spectrum is compared to typical mixed gas lamp. Image reproduced from: [115].

2.4.2 Laser

Another important light source for biomedical applications is laser which is popular for the monochrome and powerful optical output. In the early days of flow cytometry only either air cooled argon laser with 488 nm wavelength or water-cooled krypton-ion laser with wavelength configurable from 400 to 700 nm were available [103], [122]. In spite of their superior optical performance, such light sources were ineffective since only a small portion of input electrical power was converted into optical power (about 0.01% to 0.0001%) [103]. There are four types of lasers: gas lasers, liquid lasers, solid lasers, and semiconductor lasers [123]. Two types of lasers that offer a compact and power efficient alternative to existing wide spectrum light sources have recently emerged – solid state lasers and semiconductor lasers [103], [124]. This work is not intended to discuss how lasers operate, however, [123] has published a book on principles of lasers, which may be of interest to those who wish to gain a deeper understanding of lasers' principles of operation, types, etc. Here only a brief overview of solid-state lasers and semiconductor lasers is provided.

As the name implies, solid state lasers emit light from solid materials. The majority of solid state lasers use crystals as the medium, which are composed of yttrium, aluminium, and garnet, commonly referred to as a YAG laser [123]. An external light source is used to excite the crystal, such as another laser, a xenon arc lamp, or some other source suitable for excitation of laser crystals (Figure 7 (a)). There are two reflectors at the ends of the crystal, one of which is a full reflector, and the other is a partial reflector, through which the laser beam can be emitted. After the beam exits the crystal, some beam forming optics are used. In semiconductor lasers, the operation is similar to that of LEDs,

except that the light emitting intrinsic layer is sandwiched between n-type and p-type materials (Figure 7 (b)). The intrinsic layer starts to emit photons, if current is applied to the n-type and p-type material. Typically, the layer has a thickness of only a few microns. The sides of the layer are polished, which allows photons to bounce multiple times within it. The intrinsic layer's small size prevents photons from easily escaping, so they bounce multiple times within it and interact with incoming electrons to produce even more photons, resulting in an amplification of the light output. [123], [125]. Due to the length and narrowness of the intrinsic layer, the majority of the photons are emitted as parallel beams of light from the end. Additionally, such beam shapes are useful for flow cytometry, where a small area needs to be illuminated by the excitation light. By using beam forming optics, it is possible to narrow the beam to less than 1 mm in diameter.

Lasers are attractive light sources due to the fact that their spectrum is narrow and they produce a monochrome light (Figure 7 (c)). This is especially relevant to fluorescence microscopy, where the excitation of biological samples requires a single-colour light with a narrow spectrum. While a wide spectrum XBO light source and a monochromator can achieve a similar spectrum of light, using a laser here has several advantages, including the fact that it does not require additional filters and is low power and compact in comparison to HBO and monochromator setups. Compared with HBO, XBO and metal halide lamps, which had lifetimes in range of 200 to 2000 hours, solid state lasers lifetime is in the range of 5000 to 10000 hours [103], [123], [124] It is relatively easy to drive semiconductor lasers, although a specific driving circuit that accurately drives the laser's current may be required.

Since the time lasers have been available, they have been considered as suitable sources of light for fluorescence microscopy; the first commercial flow cytometers utilized lasers as a source of illumination. [124] and [103] conducted reviews of the use of lasers for flow cytometry, including information on laser characteristics, the types of lasers, wavelengths, and other factors. [126] proposed a design and construction of a microfluidic workstation that is high-throughput and uses multiple lasers to excite fluorescence. Three lasers with wavelengths of 405 nm, 473 nm and 561 nm are used, which are focused to droplets using an array of dichroic mirrors.
An optical microscope with a photomultiplier tube was used for detection. [127] described the use of integrated pneumatic valve droplet microfluidic chips in the sorting of single cells. Droplets containing fluorescent dye were illuminated with a laser of wavelength 473 nm in their setup. Fluorescence emission was filtered by a 525 bandpass filter and collected by a photomultiplier tube. Additionally, a digital high-speed camera was added to the setup to capture images of the generation and screening of droplets. [128] proposed an analysis of the real-time interaction between triglyceride digestion and lipophilic micronutrient bio accessibility using droplet microfluidics. To detect the fluorescence in the droplets, a laser with wavelength of 488 nm was used. The emission from fluorescence was filtered between 500–530 nm. [43] proposed a method to virtually freeze the movement of droplets by syncing the laser movement with the scanning speed of the imaging sensor. In the setup, two lasers were used having wavelengths of 488 nm and 560 nm. For imaging, a charge coupled device sensor (CCD) camera sensor was used, that employs a time delay and integration (TDI). TDI can be used to move the collected photo charge along with the channel and thus be able to have multiple exposures of one droplet. The virtual freezing enabled to move the focused illumination from laser in the same phase as droplet and sensor exposure, resulting in better detection performance.

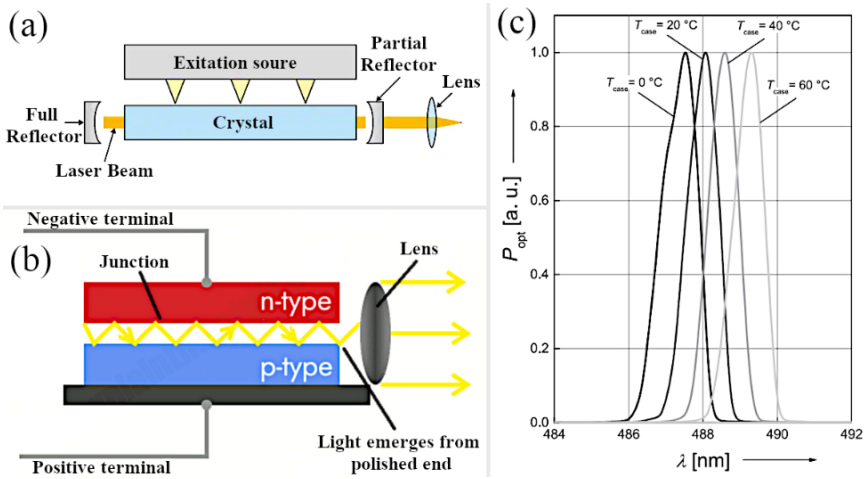

Figure 7. Construction and spectrum of solid-state laser. In figure is seen: (a) solid-state laser and (b) a semiconductor laser. Additionally (c) a relative output over the spectrum of Osram PLT5 488nm cyan laser is shown. Figures reproduced from: [125], [129] *and* [130].

2.4.3 Other type of light sources commonly used in biological experiments

In spite of the fact that LED and semiconductor laser light sources seem to be suitable illumination options for portable droplet microfluidic applications, there are other light sources that have historically been widely used in microscope illumination. Such light sources are: mercury arc lamp, xenon arc lamp, tungsten lamp and metal halide lamp.

Mercury arc lamps were historically one of the first electronic lights used in microscopy; so, many fluorescent markers were developed to respond to the light spectrum of such lamp [54], [112]. Using these light sources for fluorescent experiments have demonstrated excellent response. The lamp's spectrum ranges from 200 to 800 nanometres, covering both the visible spectrum and portions of the ultraviolet spectrum. Since half of the lamp's optical power lies in the UV region, special precautions must be taken when operating the lamp in order to protect the eyes as well as the living cells from UV radiation [131]. Although the bulb has a good spectrum and is suitable for a wide variation of experiments in biology, there are several hazards and precautions to be considered. It should be noted that the bulb contains mercury - in the event that the bulb is to break, the room must be ventilated for at least 30 minutes to air out the mercury and collect the remains of it [132]. Additionally, the lifetime of the bulb is around 200 hours and to get the bulb operational, there is a 30-minute warmup time. Before the next turn-on time, the bulb has to cool down, which also takes roughly 30 minutes and the total number of turn on cycles the bulb can withstand is half the maximum operating hours (100 times for a bulb with a maximum operating time of 200 hours) [133] [132]. Although mercury arc lamps use a direct current (DC) power source, they require complicated power supplies that can produce a pulse at start-up reaching tens of kilovolts to ionize the gas in the arc gap. In spite of the fact that the bulb itself measures 82mm in length and 10mm in diameter, it requires a special housing, which is usually larger than 10cm x 10cm x 10cm as required [132]. Moreover the lamp module itself consumes 155 W of power [132].

Despite the shortcomings, there are numerous examples of usage of the lamp in the literature for biological experiments. [73] used Zeiss HBO100 Mercury vapor short-arc lamp with a set of excitation and emission filters to illuminate the microfluidic setup, which was used to evaluate event based cameras as cost-effective alternative to particle detection and tracking using microbeads ranging in size from 1 µm to 10 µm. [134] used fluorescence imaging with an inverted microscope (Olympus IX71) equipped with a 130 W mercury arc lamp and a set of filters to detect Escherichia coli cells trapped in droplets at 105 dps using a high frame rate camera (Phantom V210).

Another light source that is often used in microscopes and for biological experiments is the xenon arc lamp that produces white light output. Since xenon gas is not poisonous, if the bulb were to break, there would be no imminent danger to the personnel in the room, however, since the bulb is made of quartz, sharp quartz shards might be present. Since xenon arc lamps have a relatively linear visible spectrum, they are ideal for fluorescence microscopy, where the excitation of multiple fluorophores is needed. In the IR spectrum, the bulb has multiple peaks, so it may be necessary to use some IR filters to eliminate that portion of the spectrum. The lifetime is also improved compared to HBO lamps, where in some cases it is up to 400 hours or more [54], [113]. Although the bulb has similar size as HBO lamps, XBO lamps include high pressure bulbs and must only be used in lamp housing to protect the surroundings in case of bulb explosion. Additionally such light sources are greater in size than 10 cm x 10 cm x 10 cm as required [135]. It is expected that XBO lamps will last approximately 400 to 600 hours [136], [137]. A XBO lamp can be reignited while still hot, whereas HBO bulbs require about 30 minutes to cool before they can be used again however when the lamp is frequently turned on and off, the electrodes are subjected to accelerated wear, which shortens its lifetime. The spectral output of a xenon lamp remains the same as it ages (even at the end of its lifespan), and unlike mercury arc lamps, the entire emission profile is visible when the lamp is switched on [137]. Despite this, it takes some time for the xenon gas to reach its maximum brightness. As with HBO lamps, XBO lamps are powered by DC power supplies and require a pulse reaching several kilovolts to ignite [137].

Xenon arc lamps have been used as light sources in a variety of applications, some of which are highlighted here. A study by [138], used fluorescence anisotropy imaging to monitor insulin production from a small number of islets simultaneously. A Nikon Eclipse Ti-S inverted microscope equipped with a xenon arc lamp and a set of filters was used to illuminate the microfluidic system. [139] proposed an approach for the synthesis of spectrally encoded polymer beads containing multiple lanthanide nanophosphors through programmable microfluidic synthesis. A custom microfluidic setup was constructed, which included a xenon arc lamp of 300 W and a set of filters that could be selected by a filter wheel. [140] proposed a high-throughput droplet microfluidic system for absorbance measurements in microfluidic droplets. To conduct experiments, a custom measurement platform was proposed, that included microfluidic platform, camera with monochromator and a xenon arc lamp with adjustable power of 150 W to 600 W. Droplets with volume in the picolitre range are always difficult to detect by detection systems. To improve the performance of the droplet analysis using picolitre droplet volumes, [141] used a broad-band spectrum and high-sensitivity absorbance spectroscopy. In order to perform measurements, a custom-built setup was proposed which included a medium power xenon arc lamp which was focused on a microfluidic channel via a combination of lenses and collimators. By using additional lenses and mirrors, light was collected and focused on the spectrometer.

One of the most common sources for illumination currently used in microscopy is tungsten lamp (sometimes also called tungsten halogen, quartz-halogen quartz iodine lamps). Such lamps are also commonly found in households, where the filament is sealed into glass bulb, that is usually filled with inert gas. Microscopes use either a regular type of bulb or a bulb with a reflector. There are several advantages to using tungsten lamps, including ease of use, flexibility regarding the power supply, and a relatively long lifetime (up to 2000 hours) [142]. The bulb emits white light, however most of the spectrum is in the range of infrared[142]. Similarly to XBO lamps that also had intense IR spectrum, using a tungsten lamp might require the use of IR filter. Moreover it has quite poor performance below 400 nm, so it is not suitable for experiments requiring UV.

Tungsten is one of the most common light source used in microscopy, it is often not noted in the literature itself, as it is part of the microscope. It was reported by [143] that an ultra-high efficiency droplet microfluidic platform was developed, where experiments containing droplets were imaged with an optical microscope. There is no mention of the light source in the paper, but according to the specification on the manufacturer's webpage it is a 50 W halogen light source [144]. Furthermore, [145]proposed the use of neural networks to detect microfluidic droplets and compared it to conventional image analysis methods using the optical microscope model Ti/Ti2-U by Nikon. There is no mention of the light source in the paper, but according to the specifications on the manufacturer's website, it is a 100 watt halogen bulb [146]. [41] proposed a method for sorting droplets using fluorescence activated sorting (FACS). However, the sorting of droplets was done using laser as illumination source, they also used a white halogen light source incorporated into microscope to monitor droplets moving in the microfluidic channel. The make, model and power was not provided. From the physical perspectives, a metal halide arc lamp is similar to tungsten halogen reflector lamp; however, instead of a tungsten filament, a high-discharge bulb is used and built together with reflector. Although it has similar peaks in the visible spectrum to mercury arc lamps, the advantage lies in the off-peak areas, where the optical output is greater than that of HBOs. Higher off-peak intensity makes this light source suitable for fluorescence experiments. After the bulb was installed in HBO and XBO lamps, it was necessary to perform a tedious alignment process. Contrary to this, metal halide lamps are designed to have the beam focus always in the same place with respect to the bulb housing, which is precisely aligned at the time of bulb manufacturing [147]. While HBO and XBO lamps had lifetimes from 200 to 400 hours, the metal halide lamp has typical lifetime up to 2000 hours [147]. Even though there are some notable advantages over HBO and XBO lamps, an arc lamp requires a power supply that is capable of creating a high voltage impulse in the range of several tens of kilovolts in order to ionize the starter gas. Such a lamp contains mercury, takes up to 5 minutes to heat up, vaporizes mercury and other metal halides and produces stable spectrum output. Before turning off a lamp, it is important to allow it to reach the operating temperature, since prematurely turning off a lamp may cause mercury or metal halides to leave black marks on the envelope or worse, may deposit on the quartz envelope walls, resulting in a non-operational lamp.

The metal-halide lamp has been used in numerous experiments as an important source of light, particularly for imaging fluorophores. [148] developed a method for photolithographically patterning cell-laden hydrogels into freely standing, free-standing structures on a microfluidic chip. A Zeiss AxioZoom upright microscope equipped with a

metal halide lamp HXP 200C was used to image the experiments together with a set of filters for fluorescent imaging. [149] develop an integrated, high-sensitivity, low-cost, truly compact LOC quantitative fluorescence measurement system by filtering out excitation light from the emission signal. As part of the experiments, an Olympus IX 71 microscope equipped with a 100 watt metal halide lamp was used in conjunction with a filter cube in order to conduct fluorescence experiments. [150] proposes a method of determining single-cell intrinsic structural and electrical parameters using microfluidic flow cytometry. A metal halide lamp (X-Cite 120Q, Excelitas, Canada) was used to excite the cells and a photomultiplier tube limited by a bandpass filter was used to detect the fluorescence results.

2.4.4 Comparison of the spectrums of HBO, XBO, and metal halide lamps

Fluorescence experiments in biology are commonly performed using HBO, XBO, and metal halide lamps. In spite of the fact HBO and metal halide lamps have prominent peaks in their spectrums, it is often necessary to utilize multiple fluorophores when the excitation for some may lie in off-spectrum areas. Xenon arc lamps may be a suitable option for this purpose because they maintain a constant intensity and are more efficient in the off-peak spectrum than XBO and HBO lamps. What follows is a comparison of HBO, XBO, and metal halide lamps over the wavelength range of 300 to 800 nm (Figure 8).

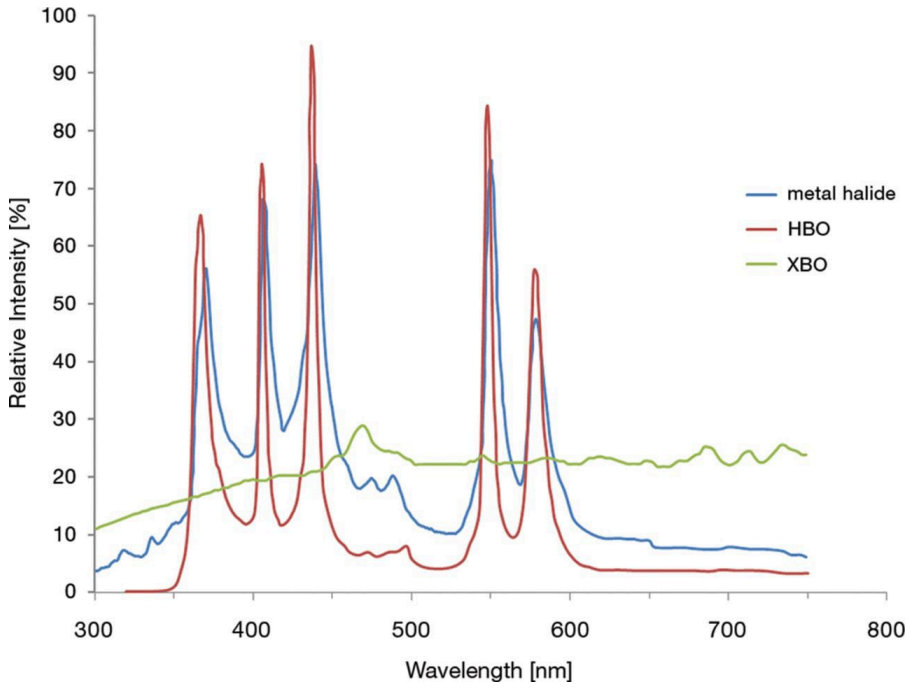

Figure 8. Comparison of the relative intensity of HBO, XBO, and metal halide lamps. The intensity is measured over the spectrum from 300 nm to 750 nm. Figure reproduced from: [54].

2.4.5 Evaluating the suitability of light sources for portable application

The specifications for the light source were previously outlined in Table 2. As a result of the previous overview of light sources, a comparative table of parameters is presented in Table 3 based on the specification table. There were six different light sources compared, with the parameters that met the criteria highlighted in bold. Because of their high power consumption and complex power supply requirements, HBO, XBO, and tungsten arc lamps cannot be used for battery-operated portable applications. The two most suitable options are LED and laser, both of which provide suitable spectrums in the required range. The laser emits monochromatic light that is generally suitable for fluorescence experiments (e.g. Sharp's 488 nm laser diode [151]), whereas LEDs offer both single colour options (e.g. LEDs with 480 nm wavelengths) and white LEDs for the illumination of droplets. It is important to note that both options consume less than 10 watts of power and require fairly simple power supply solutions. It is also possible to modify the light output of both light sources by modifying the output current of the supply. Both solutions are priced below 100 euros (included in the price are the LED or laser, and power supply). LEDs have an excellent lifespan of 50000 hours, whereas lasers have a lifespan of 10000 hours. They are both lightweight and offer maximum light output as soon as they are turned on. There is a possibility that some alignment will be required when a laser light source is used. It is important to note that both solutions are lightweight and offer excellent resistance to minor vibrations, making them suitable for portable applications.

Table 3. An overview of the light sources as compared to the specifications previously established.

Property	LED	Laser	HBO	XBO	Tungsten	Metal halide arc lamp
Spectrum (488nm + white)	**350-750nm**	**400-700 nm**	**200-800 nm**	**200-1100 nm**	**400-2500 nm**	**300-700 nm**
Power consumption (<10 W)	**Yes**	**Yes**	No	No	No	No
Price (< 100 €)	**Yes**	**Yes**	No	No	**Yes**	No
Can be battery operated	**Yes**	**Yes**	No	No	No	No
Lifespan (hours)	**50k**	**5k to 10k**	200	400-600	2000	2000
Light output (immediate and adjustable)	**Yes**	**Yes**	No (needs warmup)	No (needs warmup)	**Yes**	No (needs warmup)
Flexible alignment	**Yes**	**Somewhat**	No	No	**Yes**	**Yes**
Power supply architecture complexity (+ = simple; ++ = complex)	+	+	+ +	+ +	+ +	+ +
Handling (++ = suitable for portable operations; + = somewhat suitable; - = not suitable for portable operations)	++	++	-	-	+	+
Size (envelope within 10x10x10 cm?)	**Yes**	**Yes**	No	No	**Yes**	**Yes**
Weight (<100 g)	**Yes**	**Yes**	No	No	No	No

2.4.6 Conclusion about light sources for LOC

The previous chapters provided an overview of light sources used in biomedical applications or in microfluidic applications. The following six light sources emerged: mercury arc lamps, xenon arc lamps, tungsten halogen lamps, metal halide lamps, light emitting diode-based lamps, and lasers based light source, where lasers and LEDs seemed to suit the best for portable droplet microfluidic application. Analysing the aforementioned light sources was necessary in order to gain a better understanding of why and how these light sources are used in the field, as well as their advantages. A thorough overview was also required to determine which of these could be suitable for portable droplet microfluidic applications that have limited power supply capabilities and require compact light sources. Furthermore, the choice of the appropriate light source cannot solely be influenced by supply limitations, but also by its optical performance and suitability for droplet microfluidics.

Even though HBO, XBO, and metal halide lamps are historically some of the most commonly used light sources in the field of biomedical imaging, LEDs and semiconductor lasers are emerging as a competitive alternative, offering lower operating costs, longer lifetimes and lower power supply requirements. The selection of the light source, however, is only half of the solution because the light source must be compatible with the selected sensor technology. These technologies are discussed in the next section.

2.5 Sensor setup and technology

Sensor technology can be analysed using the same methodology as for light sources, i.e. only consider sensors used in microscopes or biological experiments. By considering just the microscope, only imaging sensors can be identified, because when a human uses the microscope, it is usually an image that is viewed thus imaging sensors are used with microscopes. For flow cytometry and droplet microfluidics either imaging or non-imaging sensor approaches are used.

A chart of optical sensors used in microscopy and droplet microscopy is provided in Figure 9. Sensors can be divided into two major classes – imaging and non-imaging. An imaging sensor produces an image as an output, while a non-imaging sensor produces an electrical signal (such as a sine wave). Sub-classes of these sensors are further analysed in what follows.

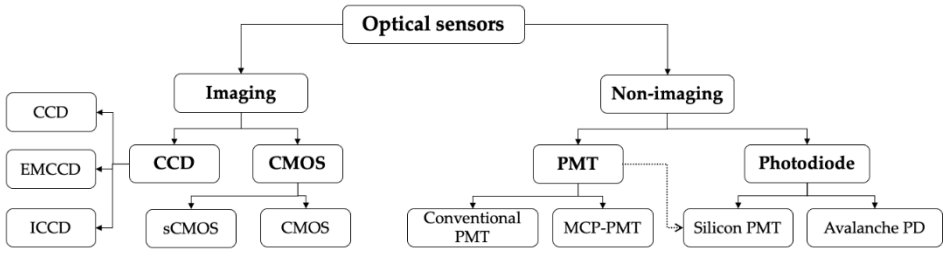

Figure 9. Map of imaging and non-imaging sensors used in biomedical applications. Figure reproduced from: [51].

2.5.1 Imaging sensors

For fluorescence microscopy, imaging sensors are most advantageous, since they allow not only the detection of fluorescence but also the determination of a cell's size and shape. Additionally, imaging sensors are widely used, as most microscopes include a third optical viewing port to which a camera can be attached, also known as a trinocular port. One of such microscopes is previously viewed Nikon LV100N which is equipped with a universal mounting system known as a C-mount [144]. One of such systems is seen in [52], where microscope with trinocular port is used to image droplet microfluidic setup (Figure 10 (a)). Many microscope cameras are equipped with the C-mount out of the box [152], [153]. Often, cameras that do not utilize C-mounts offer a special mounting adapter that can be used to convert the camera mount to C-mount, thus expanding the available selection of microscope cameras. Microscope lens mounts have a diameter of 20 millimetres, while C-mount camera mounts have a diameter of 1 inch or 25.4 millimetres. An adapter ring can be used to connect a microscope lens directly to a C-mount camera.

In the heart of every imaging sensor is a photosensitive area that converts photons into electrons. Electrons collected, sometimes amplified, and then transferred out from the sensor. For each imaging sensor, two indicators are important – frames per second (fps) and exposure time. The fps indicator determines how many frames a sensor can capture and send out in one second. Exposure time sets the maximum time per frame that photons are collected and converted to electrons. Typically, the exposure time is an inverse of framerate, but in cases of high light intensity it can be lowered to avoid the saturation of imaging sensor.

In the past, CCD sensors were used as imaging sensors since they were developed the earliest. With a CCD camera, photons are converted to electrons and collected as charge underneath each pixel. The charge is then transferred from the sensor to the readout electronics, which converts it into a digital image. Since the data from CCD sensors is read out in series, it hinders the frame rate performance, making it undesirable for droplet detection systems that require high throughput (1000+ dps) [43], [154]. With the increase of readout speed, increases the readout noise. The problem could be somewhat mitigated by the addition of a cooling system [155]. An intensified CCD sensor or ICCD was proposed in order to increase the sensitivity of the imaging sensor. In this system, an image intensifier is attached in front of the CCD sensor in order to enhance its sensitivity. Despite offering better sensitivity, the add-on increased noise, increased the complexity of sensors, and made them more expensive. Another CCD sensor is electron multiplying CCD sensor or EMCCD sensor, where after the readout circuitry a special electron multiplier is used to intensify the signal. The gain of the amplifier can be set so the sensor is able to detect single photons [155] [156]. There is a report in [157] which describes a setup using an EM-CCD camera to generate microdroplets filled with fluorescent dye at a rate of 30 Hz. The block diagram of such setup is shown in Figure 10 (b). However, as was discussed earlier, CCD sensors are not suitable for high-throughput applications requiring high frame rates. Although there are cases of some CCD sensor based cameras running at high framerates. [33] used Phantom V7.3 camera, that uses CCD sensor and was configured to run at 30000 fps to detect the microbeads in the microfluidic droplets.

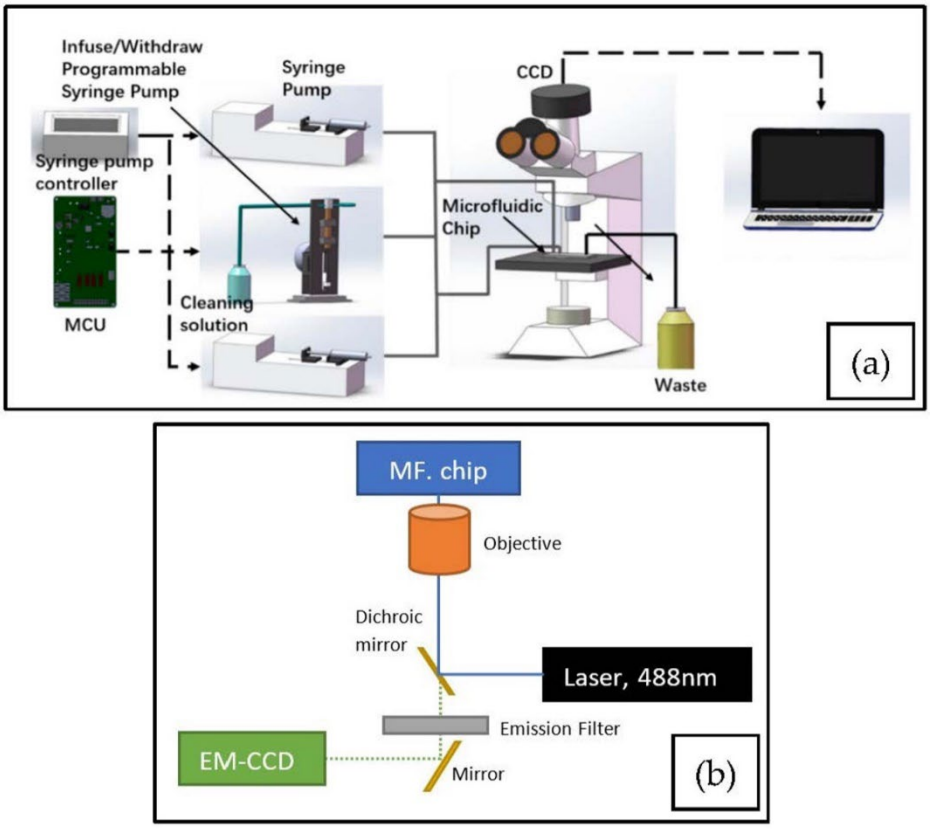

Figure 10. Charge Coupled Device (CCD) sensors are used as detectors in droplet microflow cytometry (DMFC). (a) an example of a microscope-based microfluidic measurement setup. Microfluidic chips are viewed and zoomed using a microscope with an integrated camera. Two syringe pumps are controlled by a controller to provide continuous flow of the fluid within the sheath (carrier) and sample. It is also possible to detect fluorescence-induced droplets at the rate of 30Hz with an electron multiplying charge coupled device (EMCCD) sensor system. Figure reproduced from: [51].

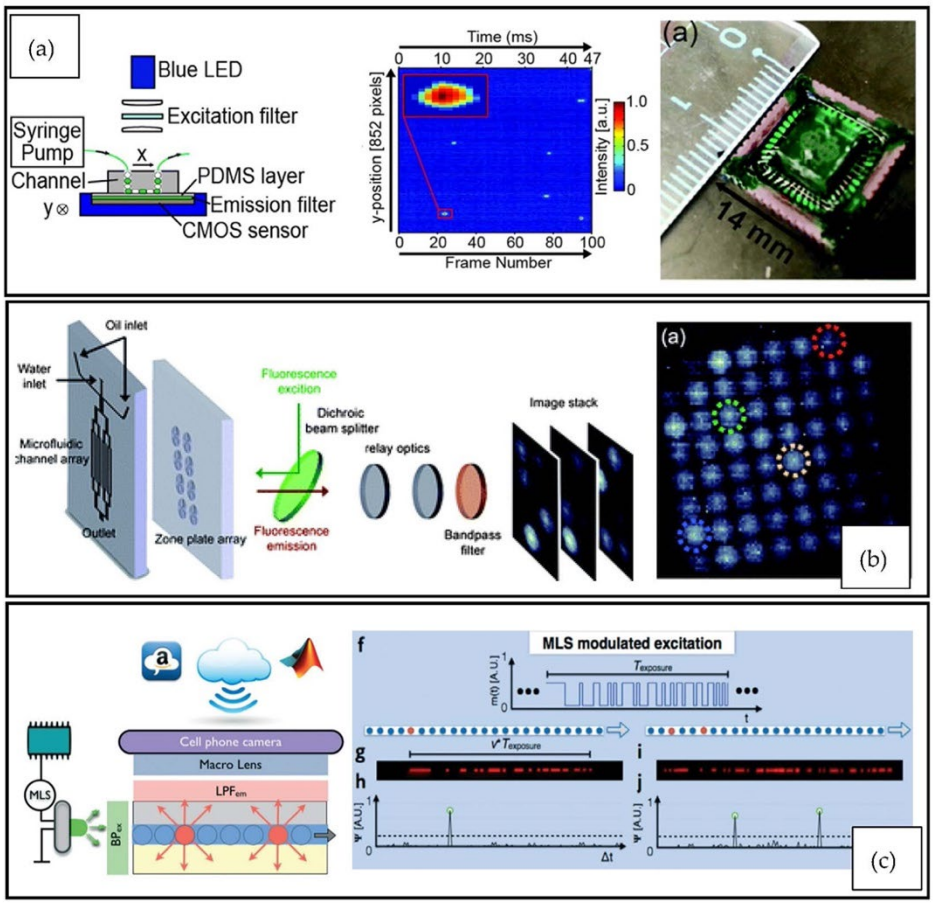

Figure 11. Demonstrated ultrahigh-throughput detection methods in the droplet microfluidic flow cytometers. (a) a compact LED-CMOS system capable of detecting fluorescent droplets at a rate of 254,000 dps. This system utilizes an optical path that is simple and compact as well as microfluidic channels that branch out into 16 parallel channels to maximize throughput [158]. *(b) the second type of system is a laser-CMOS system, which was capable of detecting droplets at a throughput of 184,000 dps. By dividing microfluidic channels into 64 parallel branches, an 8x8 zone plate array was used to image the microfluidic channels. On the right, you can see the resultant image* [40]. *(c) the system consists of an LED-CMOS detector that can detect droplets at a rate of 1,000,000 droplets per second. In order to accomplish this, the microfluidic channels were divided into 120 parallel branches. To prevent droplets from overlapping due to CMOS camera framerate limitations, pseudorandom maximum length sequences (MLS) were used for excitation* [39]. *Figure reproduced from:* [51].

Thanks to advancements in microelectronics, active-pixel sensors based on CMOS technology were developed. CMOS sensors are called active pixel sensors, due to the fact that the voltage generated by photodiode is amplified by the circuitry within the pixel. Although CCD cameras initially offered better sensitivity because of the larger active area of the pixels, CMOS sensors were providing faster readout times and higher frame rates (up to 10 times higher) due to the parallel readout scheme. In addition, CMOS sensors are cheaper, require less power, and are therefore more suitable for portable applications. It is therefore more appropriate to use CMOS sensors for portable high-throughput

droplet detection systems. In order to further improve low level detection, a special CMOS sensor has been developed, which improves the detection and amplification of signals in a pixel. This type of sensor is referred to as a scientific CMOS sensor, or simply sCMOS. However, while CMOS sensors are presently dominating the market, CCD sensors are still available, since they are sometimes more sensitive, especially when detecting low levels of fluorescence is needed.

As imaging sensors provide a great deal of information about the experiment, they are also very popular in the scientific literature. Compared to CCD sensors, it is more suitable to use CMOS sensors for high-throughput applications. There are many high-throughput applications found in the scientific literature. [43] proposed a novel virtual freezing method for droplet detection, that improved the typical high-throughput droplet detection rate of 1000 dps to 10000 dps. By using a polygon scanner, they were able to excite and track the droplets in the microfluidic chip, and droplets were imaged using scientific CMOS camera. In [158] it was possible to achieve a 100,000 events/s detection rate by spin coating a filter onto the CMOS sensor and bonding a 16-channel PDMS droplet generator chip to it (Figure 11 (a)). An LED with a peak wavelength of 490 nm was used as an excitation source. As a result of the filter blocking most of the excitation light, only a 4-pixel wide area of the sensor aligned with the chip was used for detection. The CMOS camera was operated at a speed of up to 2150 fps. In another demonstration, the chip and the camera were integrated (Figure 11 (b)). In [40] an sCMOS camera running at 16,000 frames per second was demonstrated to count cells at 184,000 droplets per second using a zone-plate array of 64 output channels. According to [39], a smartphone camera could detect up to one million fluorescent events per second (Figure 11 (c)). Using this setup, an ultra-bright LED was flashed in a pseudorandom sequence to excite droplets that would otherwise overlap. Additionally, a 120-channel massively parallelized droplet generator structure was used.

2.5.2 Non-imaging sensors

Another type of sensor that is used in biomedical applications is non-imaging sensor. Though imaging sensors provide a lot of information about droplets, non-imaging are not less useful and have other advantages. As a starting point, non-imaging sensors are capable of acting more rapidly than imaging sensors and provide information regarding the number and size of droplets. Non-imaging sensors can be divided into two categories – Photomultiplier tube (PMT) based solutions and photodiode-based solutions. It is important to note that there are three types of PMTs: conventional PMTs, microchannel plate photomultiplier tubes (MCP-PMT), and silicon photomultipliers; the latter combines photomultipliers and photodiodes.

Typically, a photomultiplier tube consists of a window containing a photocathode, an electron multiplier, focusing electrodes, and an anode that produces a current proportional to the amount of incident light. PMT-s have relatively quick response times, typically in range of tens of nanoseconds, making them suitable for fast droplet counting applications [159]. Another interesting photomultiplier tube microchannel plate photomultiplier tube, which is an advancement of conventional PMT, but where the dynode is replaced with microchannels in range of micrometres. In addition to improving the sensitivity of the PMT, such a microchannel add-on speeds up the detection speed of the photomultiplier to a range of picoseconds [160]. Although PMTs are sensitive devices, they require supply voltages that are in the range of several kilovolts, making them difficult to use in portable and mobile devices. Moreover conducting experiments that

requires multiple parameters to be detected at once have proven to be challenging with PMTs. By switching on multiple lasers separately, the excitation and detection wavelengths can be varied without the need for filters or multiple sensors [161]. An illustration of such a system can be found in Figure 12 (a). It is also possible to modulate the laser frequency by means of frequency-division multiplexing and to employ single-sensor setups [30]. Figure 12 (b) illustrates such a setup. For both sets-ups, PMTs, lasers, optical fibbers, and microfluidic chips were used as their optical components, which is the minimal number of components possible with PMTs.

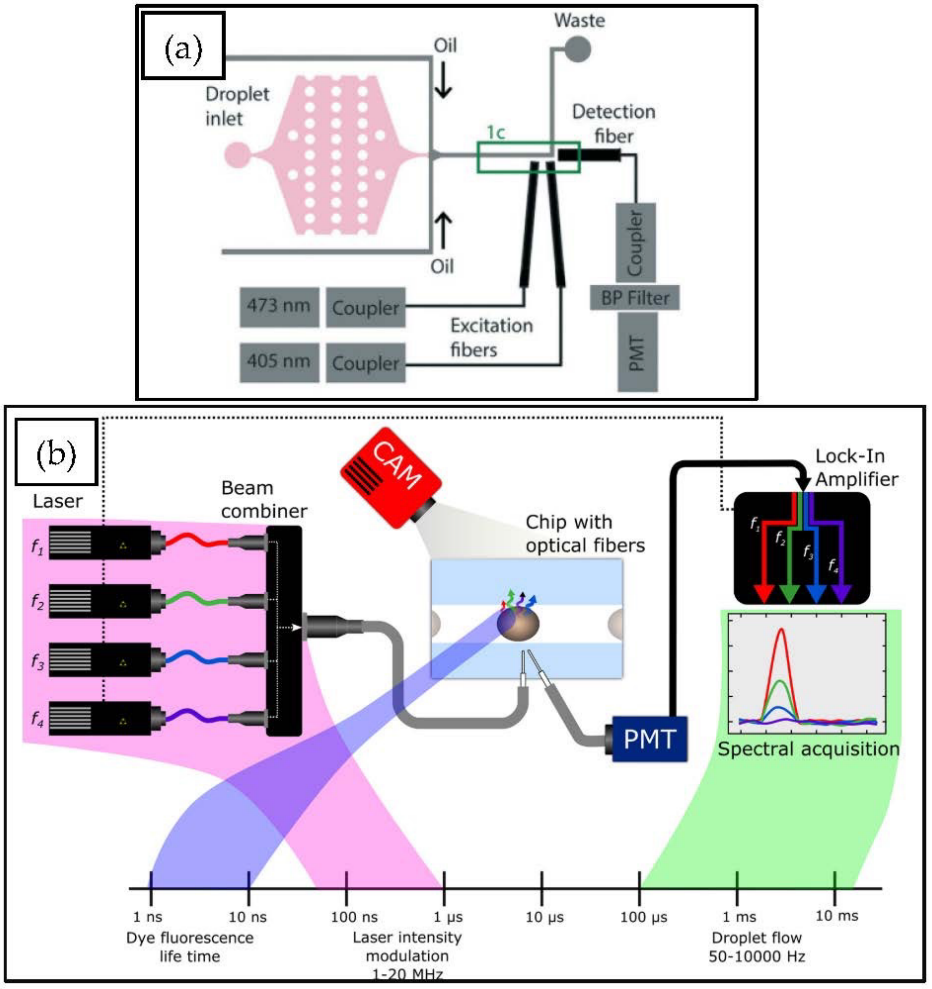

Figure 12. Photomultiplier tubes are used as detectors in droplet microflow cytometry. Using multiple lasers coupled to the microfluidic chip, a measurement system can be developed. A single PMT tube can be used to analyse multiple droplets when the flow speed is known [161]*; (b) the use of a measurement setup consisting of a PMT capable of measuring four parameters simultaneously, with a laser light source, beam combiner, and lock-in amplifier to compute the results* [30]*. Figure reproduced from:* [51].

A good semiconductor alternative to PMT is an avalanche photodiode (APD), which offers similar sensitivity and performance, but is more compact and requires lower supply voltages. Although it operates at a lower voltage, it is still within the range of few hundreds of volts, thus it is not an attractive option for battery operated portable applications [162], [163], though mechanically it is more compact compared to PMTs. The gain of APD is sensitive to temperature and in some cases internal temperature stabilization might be required [162]. The diode can be operated beyond the breakdown voltage, and it is capable of detecting single photons, although the output is not linear with the incident photons in such a mode. To overcome that issue, silicon photomultipliers were proposed, where an array of parallel avalanche photodiodes working after breakdown voltage is used and the output is summed [164]. In applications where high sensitivity is not needed a simple photodiode could be considered that has lower sensitivity, but also lower operating voltages.

In one experiment, APD was used to detect fluorescence emission from droplets, unfortunately the droplet detection rate was not reported. Additionally, a CCD camera was used to verify droplet generation [165]. The droplet detection setup can be seen in Figure 9 (a). A second experiment used an argon-ion laser, two sets of dichroic mirrors, two APDs, and a 50 Hz droplet generation rate to detect two fluorescent signals. A diagram of the droplet detection setup can be found in Figure 9 (b).

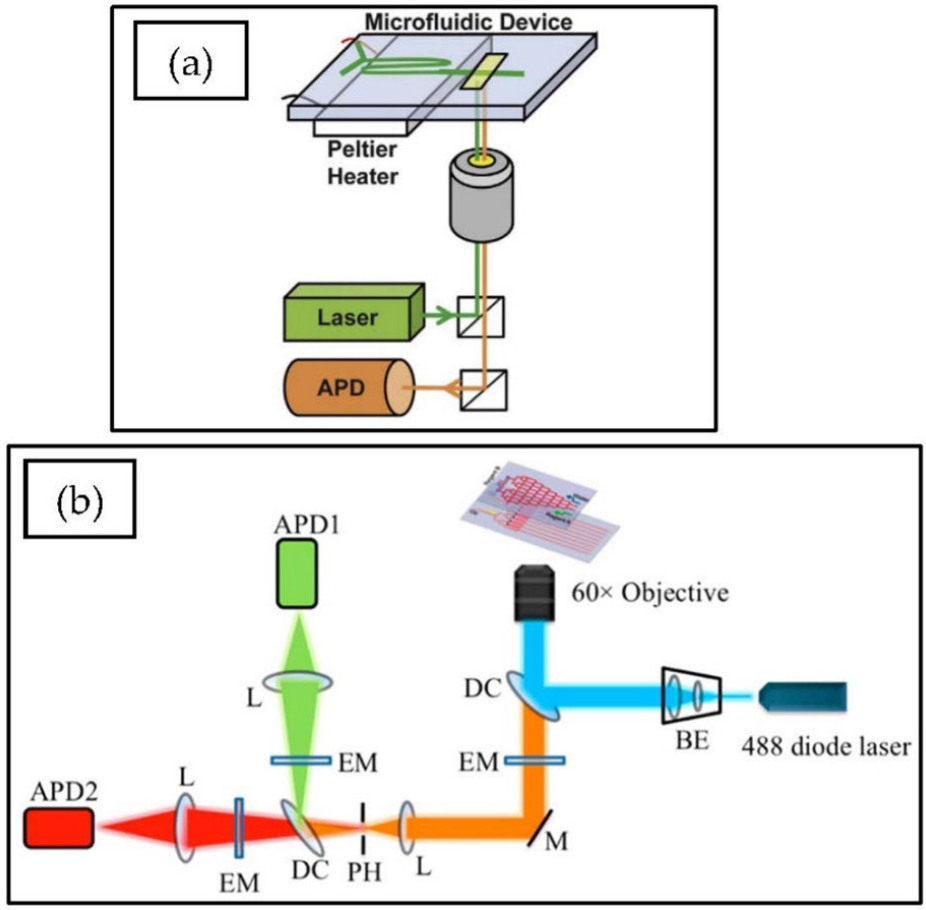

Figure 13. Droplet microflow cytometry detector setups utilizing photodiodes or avalanche photodiodes. (a) Microfluidic measurement system utilizing a laser for excitation and an APD for detection [165]. *In addition, light is focused on the sample using optics. (b) A microfluidic measurement system which utilizes differential detection photothermal interferometry and a lock-in amplifier to collect data, which is then analysed on a personal computer* [42]. *Figure reproduced from:* [51].

2.5.3 Performance and sensitivity requirements for droplet microfluidic flow cytometer setups

There is an analysis of the performance of currently available droplet microfluidic setups in [51] and a summary table is presented in Table 4. Detection setups utilizing fluorescence detection are examined as fluorescence experiments are commonly conducted in droplet microfluidics. The study further examines imaging as well as non-imaging methods.

Based on the literature, the following key metrics for sensors have been identified: a maximum throughput of droplets per second (dps), a sensor frame rate (fps), a sensor exposure time, and, if lenses are used, typically, lens numerical aperture is included as well. Numerical aperture defines the maximum angle of light that can be captured by the lens. Despite the fact that some papers specify high dps counts, this can be somewhat misleading since in such applications multiple parallel microfluidic channels are often employed, which does not define sensitivity requirements for a single channel (e.g. [39],

[102], [158] A single channel's dps can be calculated by dividing the maximum DPS by the number of parallel channels. Further, in some cases, only the detection of droplets is important, which implies that such an approach is not feasible for detecting droplet shape or morphology (e.g. [158]). It is common for papers to focus exclusively on the fps

Table 4. Detection setups used in droplet microflow cytometry are compared in terms of complexity and performance.

Optical sensor	Light source	Max throughput (dps)	Excitation wavelength (nm)	Complexity (No of optical components)	Portable/compact?	Imaging?	Ref
APD	Laser	50	488	>10	No	No	[165]
CCD	LED	1150	~449	4	No	Yes	[166]
CCD	lamp	100	470-495	>10	No	Yes	[167]
EM-CCD	Laser	40	488	6	No	Yes	[168]
CMOS	LED	1000000	530	3	Yes	No	[39]
CMOS	LED	254000	490	3	Yes	No	[158]
CMOS	Laser/LED	96000	488/640	>10	No	Yes	[102]
CMOS	Laser	70	532	2	Yes	Yes	[169]
sCMOS	Laser	184000	532	5	No	No	[40]
sCMOS	Laser	10000	488/560	>10	No	Yes	[43]
PMT	Laser	100000	488	5	No	No	[170]
PMT	Laser	10000	405/488/561/639	6	No	No	[30]
PMT	Laser	500	488	3	No	No	[171]
PMT	Laser	50	405/473	7	No	No	[161]
PMT	Laser	10	455	7	No	No	[172]

metrics of imaging sensors and the maximum dps is determined experimentally (e.g. [166] [167], [158], [169], [40]). It can be however concluded, that typically for single channel high speed detection a camera sensor with high framerate (1000+ fps) is needed. Also, it is mentioned that the droplet detection rate is limited by the frame rate, and dps cannot exceed fps since then droplets cannot be distinguished (e.g. [158]). Detection sensitivity and frequency are stated for non-imaging sensors, but no numerical values are provided (e.g. [30]).

For illumination, two types of light sources are commonly used, LEDs and lasers, with lasers being commonly used for fluorescence experiments. Following is a summary of the key metrics for light sources identified in the literature: wavelength, optical power, beam shape. One of the most important parameters that is always defined in the literature (e.g. [165]), is the wavelength of the illumination source, since it is essential to select the correct wavelength for proper fluorescence excitation. In addition, an optical power is provided. For lasers used for fluorescent experiments, the optical power has ranged from 1 milliwatt to hundreds of milliwatts (e.g. [165], [167]). For white colour LED an optical power of 440 mW is mentioned in [166] and for 490 nm (blue) LED an optical power of 250 mW is mentioned in [158]. What is additionally important for light sources is the beam pattern. LEDs have relatively wide beam pattern and usage of beam focusing lens is needed, however it can be omitted if the LED has relatively narrow beam shape (i.e. +- 10° as was in [158]).

2.5.4 Conclusion about sensors for LOC

The previous sections provided an overview of imaging and non-imaging sensors in biomedical applications or in microfluidic applications. In terms of imaging approaches, CCDs and CMOS sensors have emerged, while in terms of non-imaging approaches PMTs and photodiodes have emerged. By analysing the aforementioned sensors, it was possible to gain a deeper understanding of why and how these sensors are used in the field, as well as their advantages. A thorough overview was also required to determine which of these could be suitable for portable droplet microfluidic applications that have limited power supply.

2.6 Combination of light sources and imaging sensors

As one possible combination of excitation and detection, a laser light is focused on a microfluidic channel droplets are excited, and the scattered light is collected by the detector (Figure 14 (a)) [44], [173]. Laser light is typically focused on microfluidic channels using either a single lens approach or a multi-lens approach in these solutions. Another, more widely reported method is to focus illumination onto a microfluidic channel and collect emission light through the use of a microscope lens (Figure 14 (b)) [42], [165]. Fluorescence experiments are often conducted with this approach, which requires additional components to separate the excitation light from the emission light [174]–[176]. As a result, this is often preferred, since it allows illumination of droplets from the same side from which emission can be detected. An alternative approach is to use optical fibre cables, which are attached to a microfluidic chip, and which are used to guide the illumination from light source to microfluidic channel and guide the emission light to the detector (Figure 14 (c)) [30], [161], [177], [178]. Such an approach enables multiple optical fibres to be used, enabling multiple excitations and detections; however, it increases the complexity of the chip design. Additionally, there exist a methodology where microfluidic chips are directly bonded to sensor. Most often, such an approach is

employed when imaging sensors are used, but there are some examples in which non-imaging sensors are utilized (Figure 14 (d)) [60], [179], [180].

Currently, the state-of-the-art approach in the literature which performs the best in terms of droplet detection rate relies on photodiodes and is capable of detecting droplets in a single channel at a frequency of 10.3 kHz [82]. However, such an approach is somewhat cumbersome, since the optical detection method (illumination plus detection)

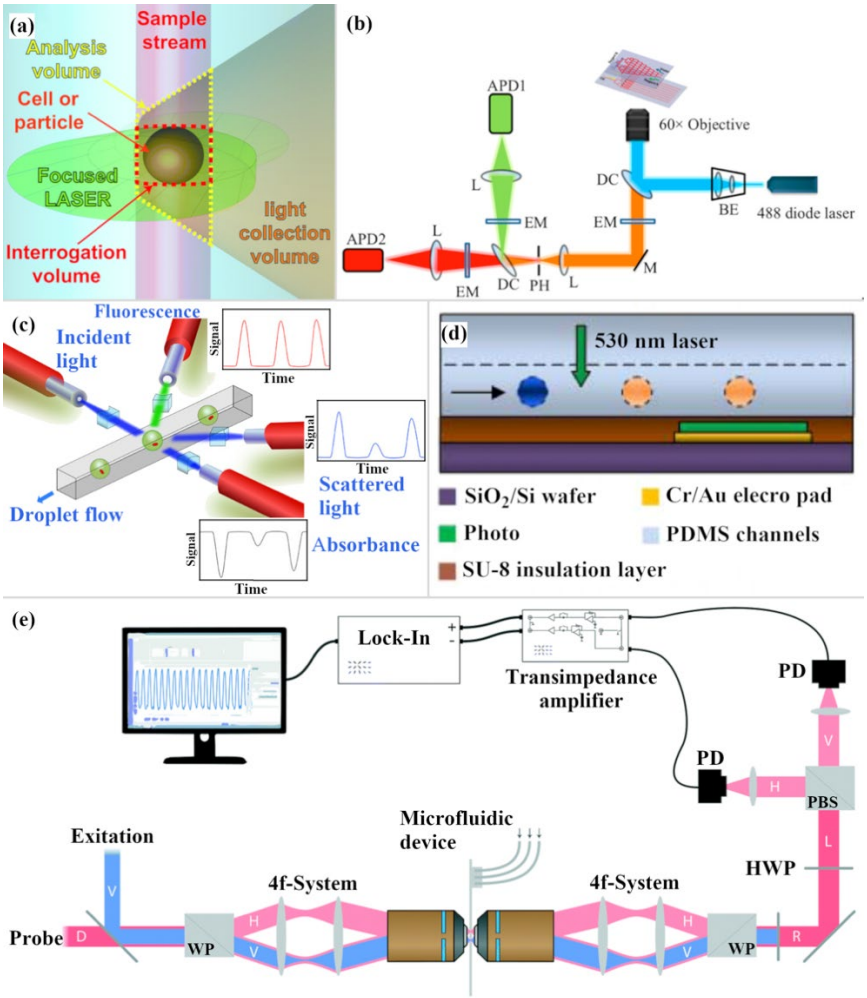

Figure 14. Overview of existing droplet detection systems. The systems are employing: (a) laser light focused to microfluidic channel and emitted light collected at an angle; (b) laser light source that is focused to microfluidic channel using microscope lens and where the same lens is used to collect the emission light; (c) using a set of optical fibres to provide a combination of different illumination and detection for microfluidic chip; (d) a PDMS chip directly bonded on top of non-imaging sensor, aligned with microfluidic channel; and (e) dual microscope lenses for excitation and emission collection reaching the droplet detection rate up to 10.3 kHz. Reproduced from – (a) [44]*, (b)* [42]*, (c)* [181] *, (d)* [179]*, and (e)* [82]*.*

employs a microscope lens in conjunction with photodiode detectors. Additionally, it requires a PC connected to a lock-in and transimpedance amplifier (Figure 14 (e)).

All of the approaches described previously have two significant technological shortcomings. A common feature of these setups is the incorporation of microscope lenses, which make them cumbersome and uneconomical for portable or cost-effective applications, as compared to approaches that use a single lens or a lens-less design. A second disadvantage is that the microfluidic channel must be precisely aligned with either the illumination source or the detector, or both, making it difficult to set up and use for experiments and potentially unsuitable for POCT applications. As part of the novel detection methodology presented here, a pinhole made out of a thin stainless steel sheet is combined with a photodiode and microfluidic chip. As a result, the pinhole was used instead of a lens, and it has been fitted between the microfluidic chip and the photodiode, whereas the photodiode is situated close to the pinhole.

2.7 Commercial cytometer platforms

There are multiple commercial flow cytometers available on the market; however, it is not reasonable to review all of them. To remain focused, a selection of the top 10 flow cytometer manufacturers were selected based on the market analysis published online [182], [183]. Then a Boolean search was conducted using the following keyword: *"Manufacturer" AND flow AND cytometry*. There were four manufacturers that were most frequently referenced, starting with the most popular: BD biosciences, Bio-Rad, Thermo Fisher, and Beckman Coulter.

A brief overview of the capacities and performance of the aforementioned manufacturers of top-of-the-line flow cytometers is provided below. In spite of the fact that some manufacturers offer more than one model, it is not feasible to review all of them in order to gain a comprehensive understanding of the state of the art. This is why only top-of-the-line instruments are examined. Table 5 summarizes the type of detection sensor, type of excitation light source, number of maximum detectable parameters, and weight of each flow cytometer.

Table 5. Comparison of commercial flow cytometer parameters.

Manufacturer	Model	Detection	Excitation light source	Number of parameters	Events in second	Weight [kg]
BD Biosciences	BD FACSymphony A5	PMT	Laser	50	40000	215
Bio-Rad	ZE5 Cell Analyzer	PMT	Laser	30	100000	110
Thermo Fiscer Scientific	Attune CytPix	PMT	Laser	34	65000	33
Beckman Coulter	CytoFlexLX	APD	Laser	23	30000	80

2.7.1 BD Biosciences

In the area of flow cytometers, BD Biosciences (New Jersey, United States) offers a variety of commercial devices, including clinical cell analysers, research cell analysers, and research cell sorters. One of the company's most advanced research cell analysers (BD FACSymphony A5) is capable of detecting up to 50 parameters. An optical filter set and a PMT are used for the detection, while lasers are used for the excitation. It is possible to choose between 25 solid state lasers, which range in wavelength from 355 nm to 980 nm [184], [185]. Using microbeads, 40000 events can be acquired per second [186]. In addition, it is important to note that the device weighs 215 kilograms. The price of the device is not publicly available as it is dependent on its configuration.

2.7.2 Bio-Rad

The company Bio-Rad (California, United States) offers only one flow cytometer, a ZE5 cell analyser, that is intended for research use only. [187]. The flow cytometer can be equipped with up to five water-cooled lasers and can detect up to 30 parameters using PMT tubes from Hamamatsu [188]. The flow cytometer is capable of detecting up to 100000 events per second [187]. Additionally, the device weighs 110 kilograms. The price of the device is not publicly available as it is dependent on its configuration.

2.7.3 Thermo Fisher Scientific

Thermo Fisher Scientific (Massachusetts, United States) offers a wide range of tools for scientists. The company offers two flow cytometers, with the Attune CytPix being the top-of-the-line model intended solely for research purposes [189]. These devices are equipped with 2 to 4 lasers and are able to detect up to 34 parameters. The system is capable of detecting as many as 65000 events per second or as many as 6000 images per second. Unfortunately, the type of imaging sensor is not specified, but the resolution can be set between 96 x 96 pixels and 248 x 248 pixels. When a non-imaging detection approach is utilized, a PMT with a set of filters is used. Among all flow cytometers viewed here, the Attune CytPix is the lightest, weighing only 33 kilograms [190]. There is no information publicly available about the price of this flow cytometer.

2.7.4 Beckman Coulter

As for the final commercial flow cytometer under investigation, the device is manufactured by Beckman Coulter and is intended for research purposes only. The CytoFlexLX is the top-of-the-line model, capable of detecting up to 23 parameters. In order to detect events, up to six lasers can be used for excitation, and a set of APDs can be used for detection [191]. It is capable of detecting up to 30000 events per second. In terms of weight, the cytometer can weigh up to 80 kilograms, depending on the selected options. As for the previous devices, there is no information regarding the price of the device since it is dependent on the final configuration.

2.8 Conclusion on the State-of-the-Art and positioning of this PhD thesis

The purpose of this chapter was to provide an overview of existing imaging and illumination devices used in biomedical applications, flow cytometry, and droplet microfluidics. In addition to analysing each component separately, an examination of existing illumination and detection combinations was also conducted where applicable.

The analysis of the state-of-the-art clearly showed that though historically arc lamps are used for illumination, a rapid development of high-power LEDs and semiconductor lasers is clearly driving the research as more and more arc light sources are being replaced by LEDs and lasers. Furthermore, these solutions can be used in portable applications due to high energy efficiency and compact mechanical form. This is also supported by the examination of commercial devices that used semiconductor lasers as an illumination source.

Clearly, imaging sensors provide more information than non-imaging sensors, but many solutions still use a non-imaging approach. While the reason for this is not clearly explained, even when looking at the most advanced commercial flow cytometers, only one of the devices used an imaging approach in conjunction with a non-imaging approach. The best assumption is that if an automated "sample-in-answer-out" device is needed, there are few existing tools to achieve automated image analysis. According to recent papers, novel machine learning methods have been applied to analysis in microfluidics, although this approach is still relatively new. Moreover, the existing illumination and detection hardware does not provide inputs that can be controlled by machine learning, making the integration of tools challenging.

2.8.1 Positioning of this PhD thesis

While the previous sections provided an overview of the state-of-the-art in biomedical applications and droplet microfluidics in general, they did not elaborate upon how such technologies could be used in a portable and cost-effective way. During the past few years, there has been a clear market demand and need for portable and cost-effective tools for virus detection and analysis, especially for applications in the field of POCT. Currently proposed analytical devices and methods are bulky or have low accuracy and could be improved by utilizing droplet microfluidics. This section highlights the positioning of this thesis as compared to the corresponding state-of-the-art.

After reviewing the existing detection methods, it became evident that commercial devices, but also other works in the state-of-the-art, lean towards non-imaging approaches. However, more informative imaging approaches are also employed, especially during the early stages of microfluidic setup development. To accommodate the need for a high frame rate for detecting a high number of dps, these setups tend to use expensive and high-performing camera solutions. In many cases, these cameras are limited to closed-source user interfaces and hardware, which makes it difficult to integrate them into a customized microfluidic system. High-speed cameras are clearly needed, but there has been little research into cost-effective solutions and their performance. It would also be beneficial if the solution were open source, allowing it to be customized to meet microfluidic setup needs. **Unlike existing research, this PhD thesis examines the use of open-source and cost-effective imaging sensors to detect microfluidic droplets on microfluidic chips. To evaluate the detection performance of sensors, two approaches are examined. The first one uses illumination from white**

LEDs, while the second one uses a laser to excite fluorescein in the droplets and detect their fluorescence. Furthermore, the use of open-source code is demonstrated, which allows for an increase in the maximum frame rate and a larger number of droplets to be detected at a time.

In the state-of-the-art, a number of tools and models have been proposed from the perspectives of science and technology to determine the size of droplets in microfluidic chips based on flows of continuous and dispersed phases. The current state-of-the-art for counting droplets relies either on imaging or non-imaging approaches. It is possible, however, that there might exist a case where the microfluidic chip starts jetting and the output looks as if the droplet generation rate exceeds the capabilities of the imaging solution. It would be possible to estimate the rate at which droplets are generated with the aid of a mathematical model, enabling one to determine if the rate at which droplets are generated exceeds the frame rate of the sensor. **Therefore, and in contrast to other studies, this thesis considers the possible situation where the microfluidic chip might start jetting and the output look as if the droplet generation rate exceeds the capabilities of the imaging solution; we hypothesize that it is possible to estimate the rate at which droplets are generated with the aid of a mathematical model, enabling one to determine if the rate at which droplets are generated exceeds the frame rate of the sensor. Thus, this thesis proposes a mathematical model to estimate the droplet generation rate in a flow-focused microfluidic chip using the flow rates of continuous and dispersed phases.**

As mentioned earlier, large portion of the state-of-the-art devices use non-imaging approach for detection. Additionally, often cumbersome optical solutions are used for droplet imaging or non-imaging detection. Most typical solutions are to use either microscope or microscope lenses and such approaches are not portable nor cost-effective. **This PhD thesis presents a novel non-imaging detection approach which is competitive with the state-of-the-art non-imaging methods in terms of droplet rate detection level, reaching detection rates up to 10 kdps (10000 dps), but with the advantage that it is a lens-less approach, making it less cumbersome compared to the existing methods; since it does not require the use of microscope lenses, it is both cost-effective and portable.**

This chapter presented the state-of-the-art of light sources and sensors used in droplet microfluidics. The next chapter is about analysing and evaluating three open-source and cost-effective imaging sensors for portable microfluidic application.

3 Imaging sensors for high-speed droplet microfluidics using embedded platform

In this chapter, camera solutions for portable and low-cost droplet microfluidic applications are reviewed and their performance is evaluated for droplet microfluidic applications.

This chapter is based on the following publications:

- K. Pärnamets et al., "**Optical Detection Methods for High-Throughput Fluorescent Droplet Microflow Cytometry**," Micromachines 2021, Vol. 12, Page 345, vol. 12, no. 3, p. 345, Mar. 2021, doi: 10.3390/MI12030345.
- K. Parnamets, A. Koel, T. Pardy, and T. Rang, "**Open Source Hardware Cost-Effective Imaging Sensors for High-Throughput Droplet Microfluidic Systems**," Proc. 2022 26th Int. Conf. Electron. Electron. 2022, 2022, doi: 10.1109/IEEECONF55059.2022.9810383.

3.1 Overview of droplet microfluidic setups using imaging sensor

As mentioned in the previous chapter, microscopes are often used for experiments in droplet microfluidics as they provide adequate optical magnification and illumination, and in some cases also include an input for a camera. Using a microscope in the early stages of microfluidic setup development can be beneficial; however, the user will be restricted to the magnification and illumination provided by the microscope as these parameters are rarely configurable. For the purpose of this thesis, it is evident that a microscope is not an appropriate tool, and a tailored setup must be used instead. As a result of the tailored setup, it should be possible to evaluate a combination of imaging and non-imaging sensors using a variety of light sources (laser or LED). Moreover, the setup must be able to accommodate microfluidic chips, and since the channels of a microfluidic chip are in the range of a few hundred micrometres, it must be able to provide a mechanism for positioning the chip or camera on a microscale level.

Aside from the overall setup, the detection setup or camera itself is also essential since it is the eyes of the entire system. In the early stages of the development of microfluidic devices, it is wise to rely heavily on imaging sensors since these provide the most information about the droplets and the microfluidic chip itself. The use of imaging sensors allows the user to examine the magnification provided by the lens, observe the droplet channel closely, and detect any defects in the microfluidic chip. Moreover, this allows the measurement of important parameters related to the operation of the microfluidic chip, such as the size, speed, and shape of the droplets.

A camera sensor can be purchased as a standalone component, as part of a camera module, or as part of a ready-made camera solution. It is not feasible to develop an imaging platform from a standalone sensor in the early stages. The use of ready-made camera solutions provides a suitable interface and enables the user to get started rapidly, but does not fall into the category of cost-effective and portable since a PC is still needed to operate the system. Another option would be to use an embedded system with a camera interface, which would provide a standalone operating system, be cost-effective, and be portable.

Out of many available solutions, one of such embedded platforms is Raspberry Pi – a microcomputer with camera interface. Despite the fact that there are similar alternatives available which operate similarly to Raspberry Pi, at the time of system development and

experiments, there was a shortage of chips on the global market, which significantly reduced the range of available platforms. Raspberry Pi is also an attractive option due to the fact that the platform offers three different camera modules with different resolutions and lenses. Raspberry Pi cameras, however, enable to capture images up to 120 fps only. An alternative, a Basler Ace [192] camera system was considered, as its framerate can reach up to 750 fps at full resolution (640 x 480 px) and can be extended when lowering the resolution. However, the Basler camera (in its entirety) does not meet the criterion as a camera running on an embedded platform because it requires a PC to operate. However, as the sensor of this camera is deemed suitable, a custom hardware system, incorporating the same sensor as in the Basler Ace camera is being prepared[1] to be used on a custom embedded platform. To date, a ready-made camera system has been considered equivalent to hardware of the same performance level.

3.2 Experimental setup for droplet detection and imaging sensor evaluation

To evaluate and analyse various combinations of imaging sensors and illuminations, a custom set-up has been developed for droplet microfluidics in accordance with the principles of flow cytometers discussed in earlier chapters. In terms of technology, the most important aspect of the setup is the fact that it can easily be configured with respect to sensors, lenses, illumination, and sensor alignment to the microfluidic chip.

The experimental setup can be seen in Figure 15 (a). In this setup, a part of a photo enlargement device is used to provide an arm to which a holder (I) of microfluidic chip is added (II). With the help of the arm, the chip holder can be moved on a relatively large scale, which is beneficial when testing different lenses (III) for the camera (IV), as each lens has a different focusing distance. It is also stable enough to allow the microfluidic chip to remain in place so that the channel with a width of 100 µm can be imaged without any major movement or shaking. An arm is attached to a photo enlarger suitcase that forms a table to which an adjustment table is attached (V). The adjustment table is directly under the chip holder, which allows very fine movements on the X, Y, and Z axes, enabling the camera to be positioned relative to the microfluidic chip and also adjust the focusing. The size of the experimental setup is not of importance at this stage, but the ability to customize it to a great extent is. The illumination is provided either by LEDs (VI) or by lasers (VII). In addition to the microfluidic measurement station, is shown one of the two syringe pumps (VIII), to which a syringe (IX) is attached, using a polytetrafluoroethylene (PTFE) tubing (X) to pump liquids to the microfluidic chip. A block diagram of the measurement setup is shown in Figure 15 (b), while a closeup of the microfluidic chip is shown in Figure 15 (c).

[1] This part of the work has been supported by several BSc and MSc theses conducted in the framework of the PRG620 project.

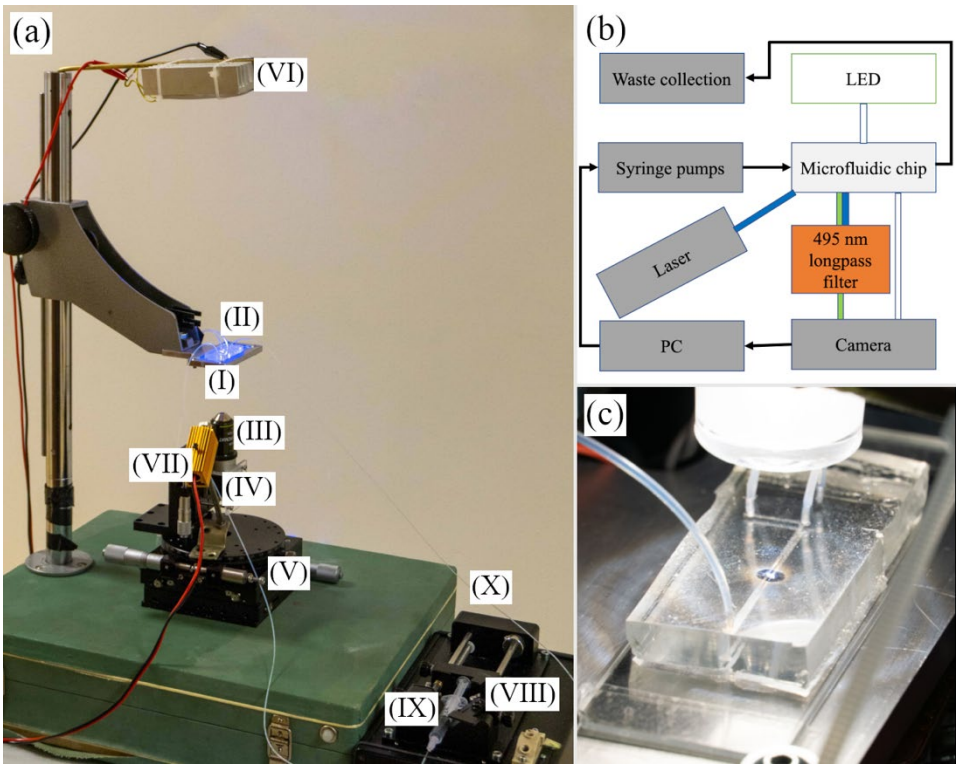

Figure 15. A custom microfluidic setup for camera comparison. In figure is seen: (a) a custom experimental setup comprising a mechanical arm for holding the microfluidic chip and a light source. Furthermore, there is a micromovement table to which a camera is connected, allowing for precise alignment of the camera with the microfluidic chip. (b) a block diagram of the same setup and (c) a close-up image of the microfluidic chip. Figures reproduced from: [193].

3.3 Microfluidic chip and droplet generation

An essential component of the setup is the microfluidic chip itself. This thesis does not focus on the design and manufacturing of the chip itself, but it is imperative that the basic parameters of the design are covered. The importance of this is heightened because every design of microfluidic chip behaves differently. By knowing the parameters, one can compare the results with other works and repeat the experiment if necessary. Note that for this part of the work, the microfluidic chip, liquids, and the initial flow rate parameters were provided by another workgroup in our department, whose research subject is manufacturing and working with microfluidic chips.

3.3.1 Design and manufacturing of microfluidic chip

The purpose of the microfluidic chip is to generate a stable flow of droplets with specific speed and size. Here is a brief description of the microfluidic chip, describing its design and manufacturing steps. To generate droplets two immiscible liquids must be pumped together. It is possible to configure microfluidic chips in a variety of ways, including

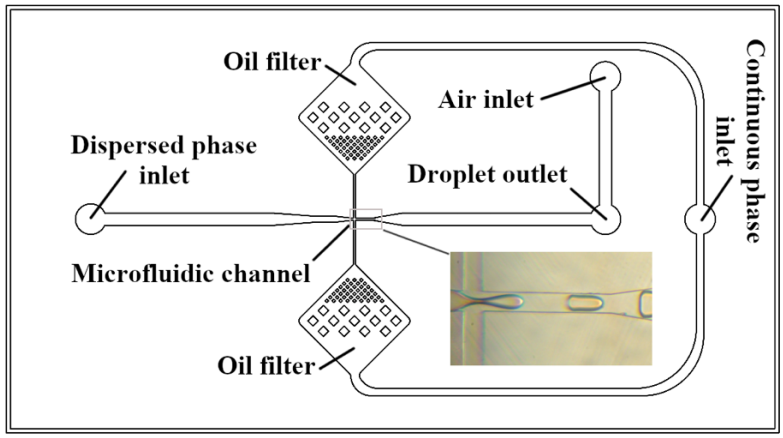

Figure 16. Design of a flow focusing microfluidic chip. Additionally, is shown an image from a camera from the junction of the chip where the formation of droplets can be observed.

changing junction configurations (i.e. co-flow, T-junction and flow focusing), varying the width and length of the droplet generation area, incorporating filters, etc. The design of a microfluidic chip can be seen in Figure 16, and it is configured to have a flow focusing junction, along with a droplet generation junction of 90 µm which widens to a 600 µm channel. In addition, filters are added to the continuous phase (oil) inlet, but not to dispersed phase (water) inlet. AutoDesk Inventor is used to design the chip, from which SU8 photoresist is used to create a positive master mould for polydimethylsiloxane (PDMS). The PDMS is bonded to a microscope glass slide (75 mm x 25 mm), holes are punched for inlet and outlet tubing, and thus the microfluidic chip is complete [194]. The SU8 photoresist has a height of approximately 100 µm, which also determines the channel height of the microfluidic chip to be also around 100 µm.

3.3.2 Pumps and tubing

The liquid handling apparatus consists of two syringe pumps, each mounted with a 3 ml syringe, one for oil, one for water. The pumps and the control software are both manufactured by the company SpinSplit [195]. The control software (SpinStudio) enables to set the flow rate in microliters per minute, which determines how rapidly the liquid is pumped out of the syringe. The syringes are made of polypropylene and have a Luer-lok™ connector, to which a needle with 0.63mm (23 gauge) outer diameter (O.D.) is attached. In order to connect the syringes to the microfluidic chip, a polytetrafluoroethylene (PTFE) tubing with an inner diameter (I.D.) of 0.5 mm and an outer diameter (O.D.) of 1 mm is used. Oil and water syringe tubing are connected to the oil and water inputs of the microfluidic chip, respectively. For oil, a mineral oil (Sigma Aldrich, 330779, viscosity cSt 14,2-17) is used, which is mixed with 2% surfactant (Span 80, Sigma Aldrich, S6760-250). For aqueous input, deionized water is used. In cases of fluorescent experiments, a fluorescein isothiocyanate (FITC) is mixed with water (Sigma Aldrich, FDS10S) [196]. Two different concentrations of FITC are used, 1 µg/ml and 10 µg/ml – a common background dye in biological experiments, which makes the results of this work comparable with what is already reported in the scientific literature [197]–[201].

3.3.3 Parameters for droplet generation

For the purpose of evaluating the performance of sensor and illumination combinations, a microfluidic chip that produces droplets is required since one of the most important performance indicators for a camera system is the number of detected droplets per second. The provided flow rates were 100 µl/min for water (Q_W) and 190 µl/min for oil (Q_O), with the expected droplet generation rate to be around 1000 droplets per second. The ratio of water to oil is 1:2, as the chip has flow-focusing design, which means that at the junction there is a single input for water and two inputs for oil. Conducting the first experiments with the provided flow rates and liquids, unfortunately the microfluidic chips started to leak after 10–15 seconds of operation. Multiple similar design chips were used to exclude issues with chip manufacturing or bonding. As a result of some investigation, it was found that the flow rates given were for fluorinated oil, HFE-7500, and not for the provided mineral oil, which is approximately 20 times more viscous than HFE-7500 [202]. The reason for using mineral oil instead of the HFE-7500 oil was purely economical, as the latter oil with suitable surfactant is considerably more expensive, whereas the droplets look similar or identical to the mineral oil droplets [203].

3.3.4 Finding flow speeds for droplet generation using mineral oil

The leakage of the chips indicated that the proposed flow rates were too high, and that new experiments were needed in order to find the appropriate parameters for mineral oil flow rates. According to the parameters previously provided by another workgroup (100 µl/min for water and 190 µl/min for oil), as a start, the oil-to-water ratio should be maintained at 1:2. The pump control software allows for setting the flow rate of liquids in µl/min, although it is possible to go below 1 µl/min, it was decided to begin pumping water at a rate of 1 µl/min, and oil at a rate of 2 µl/min. During the initial stages, only a stable flow of droplets was observed using the Basler Ace camera module, and neither the size nor the rate of droplet generation was of particular interest. The Basler Ace camera was set to a frame rate of 1000 fps, and it was assumed that the droplet generation rate from lower flow rates would be well below 1000 dps and easily detectable by camera. The first test was using flow rate of 1/2 µl/min (Q_W/Q_O) and resulted in stable flow of droplets, at frequency around 9 dps.

As individual still frames were exported from the captured video, it became evident that the highly compressed video and current lens magnification were not sufficient for performing morphology analysis of the droplets at this stage, which indicates that either video quality should be improved, or lens magnification should be increased to capture more detail. Nevertheless, the experiments demonstrated that for more viscous oils, lower flow rates were required, and the experimentally determined numbers showed great success with no leakage of the microfluidic chip. In the early stage the droplet generation frequency was not determined, as the goal was to solely test if the chip handles the flow speeds and if the droplets are generated. At later stages the droplet generation frequencies were also extrapolated from the recorded data and are shown in table below (Table 6). Additionally, still images are shown below (Figure 17 (a)–(f)).

Table 6. Frequencies of droplet generation for flow speeds ranging from 1/2 to 16/32 µl/min of water or oil.

Flow speeds [Q_W/Q_O]	1/2	2/4	4/8	8/16	16/32
Dps	9	30	67	190	670

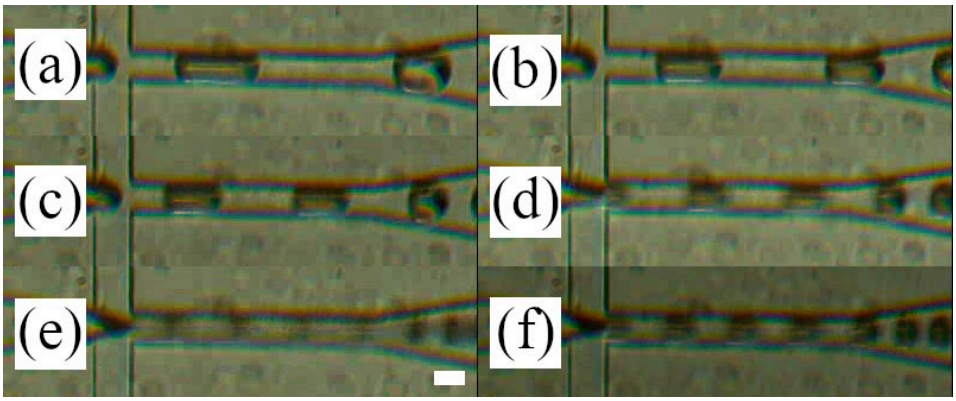

Figure 17. Still images of droplets saved from recorded videos using Basler Ace camera. Flow rates were varied for water and oil in microliters per second in the following steps (water/oil): 1/2 (a), 2/4 (b), 4/8 (c), 8/16 (d), 16/32 (e). For the last flow rate of 16/32, the droplets are generated at a frequency of 670 per second, and a camera running at 1000 fps is no longer capable of detecting the droplets. For the last experiment, the acquisition rate has been increased to 2000 fps (f). A scale of 100 µm is represented by the white horizontal bar at the bottom of the image.

It is evident from the results that the chip is capable of generating up to 670 dps without any signs of leakage, using flow rates of 16 µl/min for water and 32 µl/min for oil (Figure 17 (e)). Though as can be seen, the droplets are hardly distinguishable from the extracted image. As countermeasure, the camera framerate was increased to 2000 fps (Figure 17 (f)), but in order to achieve that, the resolution of the sensor has to be lowered – a common technique among high-speed cameras, in which only a portion of the full sensor is used as a sensor, improving the readout speed, and allowing for higher framerate performance [204]. With the resolution lowered to 400 x 200 pixels, the camera frame rate reached 2000 fps, resulting in more discernible droplets than before (Figure 17 (f)).

At a later stage during the research, the video format was changed to capturing images instead to increase the quality of droplet images (Figure 18 (a) and Figure 18 (b)). In addition to providing images with a much higher quality than previously captured videos, such an approach has also been incorporated into industry standard high framerate cameras [205]. Moreover, in view of a potential droplet morphology analysis, the lens was upgraded from 10x to 20x magnification (Figure 18 (c)). Eventually, the resolution of the captured images was further reduced in order to achieve a higher frame rate, up to 3000 fps (Figure 18 (d)). As a result of aforementioned modifications to the imaging system, the droplet generation was deemed to be successful at new flowrates reported in Table 6.

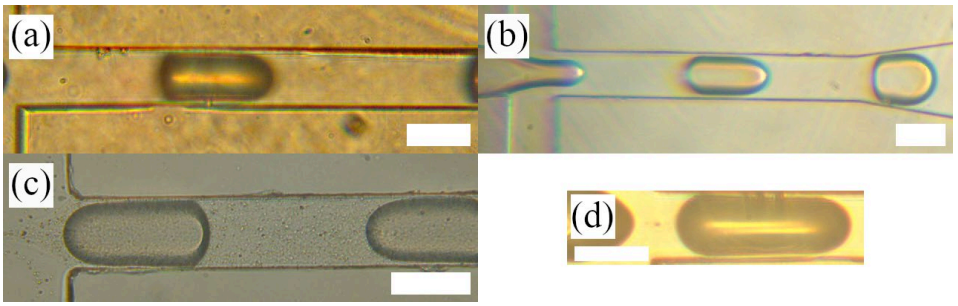

Figure 18. Still images captured instead of videos that provide higher image quality. In figure is seen: (a) and (b) the droplet is being detected similarly to how it was captured using videos and less distortion can be viewed from the images; (c) the lens is changed from 10x magnification to 20x magnification; (d) image resolution is decreased so only droplet is imaged and camera framerate can be pushed up to 3000 fps. A scale of 100 µm is represented by the white horizontal bar at the bottom of the image.

3.4 Open-source camera sensors

The introduction section of this chapter underscored the fact that imaging sensors are available as standalone components, as components of camera modules, and as component parts of ready-made camera solutions. Two possible solutions were considered, a Raspberry Pi and a Basler Ace camera system. The Raspberry Pi camera line-up consists of three different camera modules, the Raspberry Pi camera V1, the Raspberry Pi camera V2, and the Raspberry Pi HQ camera. The differences between camera versions 1 and 2 are not significant, so evaluating only the version 2 and the HQ cameras are considered. Additionally, the Basler Ace camera module is considered. Although the camera module itself is not open source, the sensor found in the camera module is used in separate BSc and MSc projects, resulting in custom hardware similar to Raspberry Pi.

3.4.1 Lens selection for C-mount

On the market, there is a myriad of lenses available for photography, microscopes, security cameras and so on, all having different optical parameters, but also different mounts. The most reasonable mount to be used appears to be C-mount; as there is a wide variety of small form factor lenses available, the microscope lenses can easily be adapted to C-mount using small adaptor ring; moreover, the Raspberry HQ and Basler Ace cameras have C-mount lens mount. There exist some camera modules that do not require external lenses (Raspberry V2), while others do require external lenses (Raspberry HQ and Basler Ace). In order to use the Raspberry V2 camera, the lens that was installed in the factory must be removed and a custom mount for the camera lens must be attached in place.

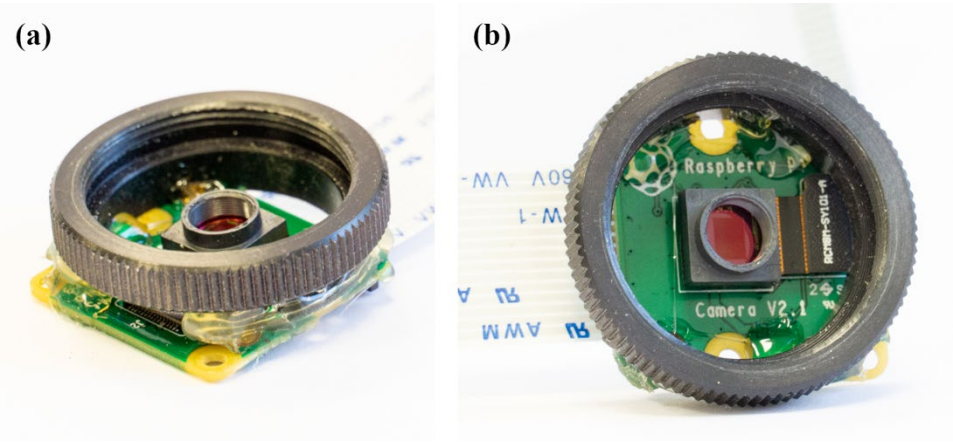

Figure 19. Raspberry Pi version 2 camera with a 5mm C-mount extension. As Raspberry Pi V2 camera does not have the mount for C-mount lenses, an extension tube was modified to fit to the camera board to create a mount for lenses. The extension tube was glued to the board using hot glue – a sturdy enough solution to keep the lens in place for experiments. The factory fitted lens was removed from the camera.

The factory lens is removed because it does not provide the necessary magnification for microfluidic chip imaging. Using a modified 5 mm C-mount extension tube and some notches machined to the extension tube, it is possible to attach it to the Raspberry V2 camera board, forming a suitable C-mount holder for lens (Figure 19 (a)). The holder is aligned so that the sensor would be centred within the holder as precisely as possible (Figure 19 (b)). The extension tube is attached to the board using hot glue – this approach is sufficient for the very first prototype.

A variety of lenses were tested in order to select a suitable lens, including some lenses used for security camera systems that also have a C-mount. These lenses, however, have a low magnification, which makes them only suitable for droplet counting applications. There are several different types of microscope lenses available, some of which offer a wide range of magnification (e.g. 5X, 10X, 20X, 40X 60X) and are therefore more suitable for imaging droplets.

3.4.2 Raspberry camera framerate limitation

The Raspbian operating system allows the Raspberry Pi to communicate and control the camera in order to take still photographs and to record videos, using the *raspistill* and *raspivid* commands, respectively. In previous chapters it was discussed that using videos is not suitable for droplet analysis due to the high compression rate of video resulting in low quality images. By switching to capturing images, the quality of droplet images was significantly improved. Using the *raspivid* command, one can capture videos up to 200 fps, and it would seem reasonable to expect that single images could also be recorded at a similar rate. Unfortunately, this is not true, as the *raspistill* command does not allow for such speed. Fortunately, there are some publicly available approaches on Github known as *raspiraw* wherein a similar approach to high-speed cameras has been applied, i.e. raw sensor data is captured to an onboard memory after which image processing is performed and single images are saved as a result [206], [207]. Using the *raspiraw* approach, the maximum framerates of raspberry sensors for capturing images

were pushed to 665 fps for V2 camera and to 200 fps for HQ camera. Both results could be obtained by reducing the image size, which is also a widely used approach for high-speed cameras. It was expected for HQ camera to reach similar performance range compared to Raspberry Pi camera version 2 and Basler Ace cameras at resolutions of 640 x 480 pixels, however the software was not able to set the resolution of the sensor below 1020 x 760 pixels and at such resolution, only a maximum of 200 fps was achieved. A comparison of sensors is provided in Table 7.

Table 7. Comparison of Raspberry Pi camera modules with Basler Ace camera.

Camera	Sensor manufacturer	Maximum resolution	Maximum fps @ resolution	Achieved dps
Raspberry V2	Sony IMX219	3280x2464px	200 @ 640x 480px	665 @ 640 x 480 px
Raspberry HQ	Sony IMX477R	4056x3040px	120 @ 1332x 990px	200 @ 1020 x 760 px
Basler Ace	Onsemi Python 300	640x480px	750 @ 640x 480px	Up to 3000 @ 400x 100px

3.4.3 Additional sensor parameters (global shutter vs rolling shutter and exposure vs fps)

The imaging microfluidic system captures moving objects, such as droplets. It is already inherent from photography that sometimes the moving objects will be blurry when imaged. A moving object's sharpness is determined primarily by its exposure time and its rate of movement over the exposure time – the faster the object, the shorter the exposure time should be. An exposure time is defined as the length of time during which the sensor pixels were collecting photons. The shorter the exposure time, the less movement there is in the object and the less motion blur is introduced to the captured image. The exposure time (t_{exp}) is always shorter or equal to the inverse of the framerate (fps), which can be expressed as:

$$t_{exp} \leq \frac{1}{fps} \tag{1}$$

In addition to exposure and framerate, there is another factor that affects how the image is captured. Many commercial cameras utilize a mechanical shutter to control the exposure time of the sensor. Mechanical shutters work by moving a shutter blind from one edge of the sensor to the opposite edge, and then moving another shutter blind in the same order. The time between the movement of two shutter blinds is defined as the exposure time. As a result, when photographing moving objects, the effect known as rolling shutter is introduced, causing the imaged object to be skewed.

The imaging solution of a microfluidic system consists only of a sensor, optics, and processing hardware, without any mechanical shutter. There are two types of readout methods available for imaging sensors without mechanical shutters: a rolling shutter and a global shutter. The rolling shutter operates similarly to a mechanical shutter, except

that the data from the sensor pixels is shifted out row by row. The global shutter sensor captures and transfers all pixel values simultaneously so that no rolling motion will occur. Although global shutter has its benefits, it does not render rolling shutter sensors useless. However, the system designer must be aware of the effects, so as to avoid getting a false impression regarding droplets size and shape.

3.5 Camera sensors experiments and evaluation

Previously in this chapter, the droplet generation setup has been demonstrated to be capable of generating droplets at a frequency as high as 670 dps, allowing the performance of various sensors to be assessed by capturing images of droplets. Three possible aqueous liquids can be used, i.e. i) deionised water, ii) FITC with concentration of 1 µg/ml, and iii) FITC with concentration of 10 µg/ml. When using deionizing water as an aqueous liquid, the principles of brightfield illumination are employed, whereas when using fluorescence, the principles of flow cytometry are employed, in which the illumination and detector are positioned at an angle, typically at a 90-degree angle. In the first case, the illumination is provided by four white high-power LEDs, while the laser light is produced by a solid state laser from Sharp with a peak wavelength of 488 nm [151].

Furthermore, there are three different camera configurations available, with the highest performing camera able to reach a frame rate of up to 3000 fps. The objective is to evaluate three camera sensors, first and foremost to determine the highest possible frame rate for each sensor and furthermore to determine the frequency at which droplets can be detected using the aforementioned sensors.

3.5.1 Imaging sensor performance with 200 fps limitation

First, experiments with deionized water are conducted so as to gain a better understanding of how sensors perform in terms of fps. Using deionized water and brightfield illumination, an image of the droplet can be obtained with a reasonably well discernible outline, allowing comparison of image quality as well as of droplet shape and size between different sensors. In order to maintain comparability between different sensors, the frame rates of all cameras are set the same value, choosing the frame rate of the sensor with the highest frame rate of its own. In the comparison table (Table 7), it can be seen that the Raspberry HQ sensor had a maximum frame rate limit of 200 fps.

A frame rate of 200 fps corresponds to a maximum exposure time of 5 ms based on Equation 1. On the basis of previous experiments with mineral oil flow rate experiments, it was determined that the camera framerate had to be 3 or more times higher than the droplet generation rate in order to provide discernible droplets. In this respect, it was expected that with a framerate of 200 fps, droplets with a frequency of up to 67 droplets could be detected without issues. As a first experiment, the droplets were generated at the frequency of 30 dps, using flow rates show in Table 6.

In Figure 20 (a), droplets are generated at 30 dps and detected with a camera running at 200 fps. Although the camera frame rate is six times faster than the droplet generation rate, some motion blur can still be observed (Figure 20 (a)). To further improve the quality of images and reduce the motion blur, the exposure time of the sensor was reduced by factor of 10, i.e. from 5000 µs to 500 µs. Using the same droplet generation speed, a much sharper and higher quality image of the droplet can be observed (Figure 20 (d)).

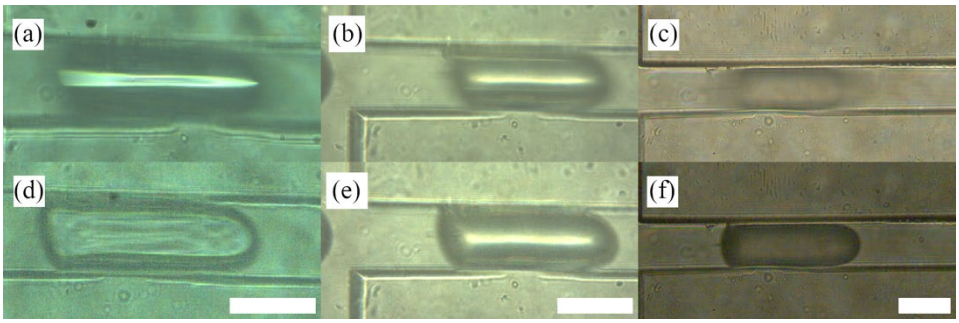

Figure 20. A comparison of droplet shapes and image quality captured with different cameras. The exposure times and framerates were kept constant between experiments and cameras. Droplets were generated at rate of 30 dps. The images (a) through (c) were captured with an exposure time of 5 ms. The exposure time for images (d)-(f) has been lowered to 500 µs. The images (a) and (d) were captured using the Raspberry HQ camera, the images (b) and (c) were captured using the Raspberry V2 camera, and the images (c) and (f) were captured using the Basler Ace camera. A scale of 100 µm is represented by the white horizontal bars at the bottom of the images. Reproduced from: [193].

It is evident that lowering the exposure time will result in sharper images. As a result of the shorter exposure time, the sensor has less time to collect photons, resulting in a darker image. Raspberry Pi cameras (Figure 20 (d)–(e)) were compensated for the shorter exposure time by increasing the illumination intensity, so that the exposure of the image would be with previous experiments (Figure 20 (a)–(b)). Just to illustrate, what happens, when the exposure time is not compensated and illumination intensity is kept same throughout the experiments, Basler Ace camera with shorter exposure time shows clearly a darker image (Figure 20 (f)) compared to experiment with longer exposure time (Figure 20 (c)). There is the possibility of lowering the exposure time even further (e.g., the Basler Ace exposure time can be set as low as 59 microseconds), however, it is important to find balance between illumination intensity, exposure time, and droplet sharpness. If a satisfactory level of detail for droplets has been achieved, it is not reasonable to increase the light output of illumination.

3.5.2 Rolling shutter distortion

As mentioned previously, Raspberry cameras have rolling shutters, but it is unclear how this might affect the capture of droplets. The effect of rolling shutter on droplet shape was investigated by comparing a rolling shutter sensor (Raspberry V2) with a global shutter sensor (Basler Ace). Although both the Raspberry V2 and Raspberry HQ cameras have rolling shutters, only the Raspberry V2 camera was used, since the effects of rolling shutter are similar between different rolling shutter sensors.

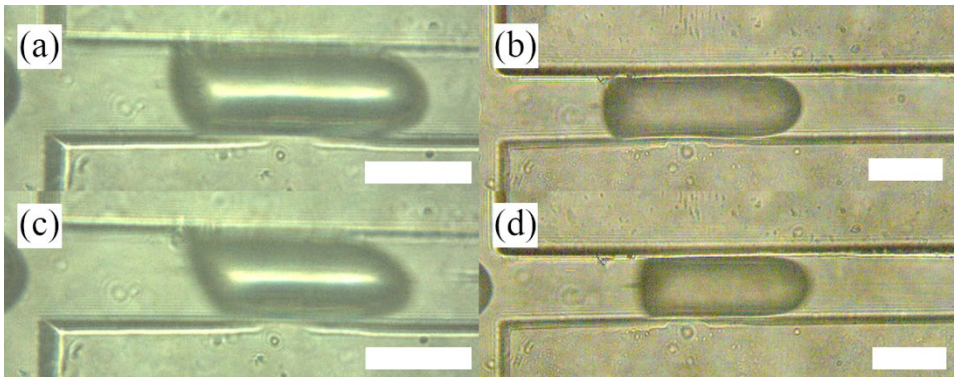

Figure 21. The effects of rolling shutter to the captured image of droplet. The shape of the droplet is affected by sensors with rolling shutters as opposed to sensors with global shutters. Using two droplet flow rates, the generation rate of droplets was 30 dps in (a) and (b), and 67 dps in (c) and (d). Using rolling shutter, droplet is skewed as the droplet generation frequency along with flow speeds increases. Global shutter sensors introduce only some motion blur with an increase in droplet generation frequency and flow speed, whereas the droplet has the expected bullet-like shape. A scale of 100 µm is represented by the white horizontal bars at the bottom of the images. Figure reproduced from: [193].

It is clearly visible, that the rolling shutter sensor will distort the final image, making droplets looking tilted (Figure 21 (a)). Images of droplets captured with global shutter sensor show no such issue (Figure 21 (b)). With an increase in flowrates and droplet generation frequency, the faster moving droplet (Figure 21 (d)) exhibits a bit more blur than the slower moving droplet (Figure 21 (b)). For the rolling shutter, the tilting effect is exacerbated as the droplet velocity increases with an increase in flowrates and droplet generation frequency (Figure 21 (c)). This is not a major issue, as long as the system designer is aware of the effect. Moreover, the image can be tilted in reverse using imaging software, making the droplet appear as if it were captured with a global shutter sensor (Figure 22).

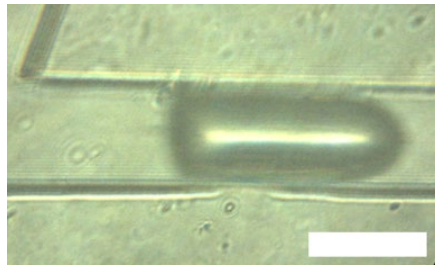

Figure 22. Modified image of the droplet after accounting for rolling shutter effect. The droplet presented in Figure 21 (c) was reoriented and tilted in the reverse direction to make it appear as if it was captured using global shutter, thus resembling its actual shape and size in the microfluidic channel, resembling size and shape of droplets captured with global shutter cameras. A scale of 100 µm is represented by the white horizontal bar at the bottom of the image.

3.5.3 Imaging sensor performance at higher framerates

As part of previous experiments, the framerates for all three sensors were set to 200 fps due to the limitation of the Raspberry HQ maximum framerate. However, the Raspberry V2 and Basler Ace can be configured to work at 665 fps and 750 fps, respectively. The framerate of the Raspberry V2 camera can theoretically be increased to 1000 fps, but this approach requires a significant reduction in the active area of the sensor, which renders the captured images to be very small and only a small portion of the droplet is visible. Using the Basler Ace, the framerate can be increased up to 3000 fps by reducing the sensor active area and preserving the ability to image droplets in full size. The Raspberry V2 camera was pushed to 665 fps while maintaining the ability to image full droplets, and the Basler Ace camera was operated at 750 fps at full resolution.

Each sensor has a 500 µs exposure time setting, which is similar to what was used in previous experiments to reduce motion blur. For the experiment, two flow rates were used: 4 µl/min for water and 8 µl/min for oil, resulting in 67 dps, and 8 µl/min for water and 16 µl/min for oil, resulting in 190 dps. First and foremost, the images clearly illustrate the heavy influence of rolling shutter for the Raspberry V2 camera (Figure 23 (a)), especially at higher flowrates (Figure 23 (c)). In addition, there is a noticeable motion blur, however the droplet is still well visible. By visually inspecting the droplets captured with the Basler Ace camera, the droplets have no visible skewing (Figure 23 (b)); however, for higher flow rates, the droplets have noticeable motion blur (Figure 23 (d)). In spite of the blurry droplets, both cameras captured droplets that were being generated at a rate of 190 dps. Comparing the droplet sizes of the Raspberry V2 sensor and the Basler Ace sensor for the same flow rate, they appear to be relatively similar. Additionally, it is interesting to note that as flow rates increase, the droplet generation frequency also increases and the droplet sizes decrease.

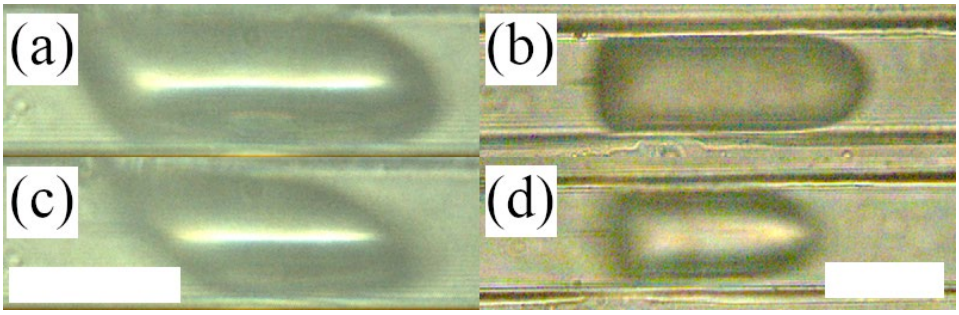

Figure 23. Size and shape of droplets when imaged with a rolling shutter and global shutter, as well as their effects at high droplet generation frequencies. Droplets are captured using two cameras, (a)(c) a Raspberry Pi V2 camera that utilizes a rolling shutter, and (b)(d) a Basler Ace camera that utilizes a global shutter. Two different flow rate configurations are used, that result in a droplet generation frequency of (a)(b) 67 dps and (c)(d) 190 dps. A scale of 100 µm is represented by the white horizontal bars at the bottom of the images. Reproduced from: [193].

3.5.4 Experiments with fluorescein isothiocyanate–dextran

Thus far, the capabilities of each sensor have been explored in terms of their capability to detect droplets when backlight illumination with LEDs have been used. The droplets in those experiments only contained deionized water; however, in droplet microfluidics, fluorescence experiments are often performed, and the droplets may contain fluorescent dyes (e.g. FITC, Alexa Fluor 488, green fluorescent protein (GFP)). Although the performance with back illumination is known, the light intensity for these experiments is expected to be considerably greater than that produced by droplets labelled by fluorescent dye. As the performance of the cameras was assessed by determining the maximum framerate, it is reasonable to believe, that lower intensity from fluorescence labelled droplets is more difficult to detect, thus it is reasonable to lower the camera framerate to 200 fps.

Since fluorescein requires a specific excitation wavelength that is specific to the fluorescein used, special consideration must be given when selecting illumination for fluorescent experiments. In the experiments, FITC is used, which has an excitation maximum of 490 nm [196]. A possible option would be to use LEDs; however, as discussed in Chapter 1, LEDs have an inherently wide spectrum in terms of FWHM. LEDs may still be a viable option, but a filter that blocks the spectrum above 490 nm would be needed. Since LEDs typically have a wide viewing angle, a focusing lens is required in order to focus most of their optical power on the microfluidic chip. Another approach is to use a laser that has a very narrow spectrum, resulting in monochrome light output, thus eliminating the need to use optical filters on the illumination side. Additionally, laser modules are equipped with some beam forming optics. Although the complexity of lasers is somewhat similar to that of LEDs, their advantages are their narrow spectrum and already included optics, which speak in favour of their use. As FITC has a maximum excitation wavelength of 490 nm, a solid-state laser with a peak wavelength of 488 nm has been chosen [151]. While the laser emits monochrome light, an optical longpass filter from Thorlabs with a cut-off wavelength of 495 nm is placed between the microfluidic chip and the detector optics in order to eliminate the excitation spectrum of 488 nm.

FITC at 1 µg/ml has a very low fluorescence intensity, and droplets are barely visible on the images. The camera sensor exposure time has been set to 5000 µs in order to collect as much light as possible. This is the maximum setting that is possible when using a framerate of 200 fps. In the case of the Raspberry V2 camera, the most visible droplet is observed (Figure 24 (a)). In the case of the Raspberry HQ camera, the droplet is very difficult to discern; however, when the droplets are moving, the contour lines stand out better compared to still images (Figure 24 (b)). The Basler Ace camera shows the lowest droplet intensity, but compared to other sensors, the droplet is best discernible (Figure 24 (c)). There appears to be some noise on the image, but when compared to the other images, it is relatively minor. It is important to note that the brightness of the images has been enhanced by equal amount for each image so that the droplets are more visible on print. The enhancement of brightness, however, always introduces some noise into the images.

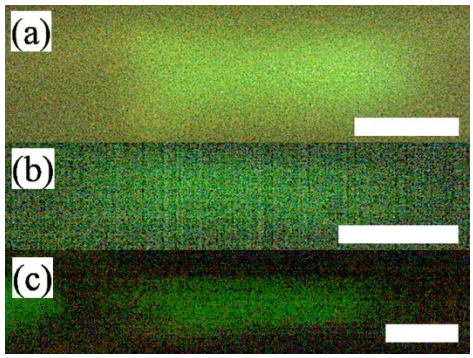

Figure 24. A microfluidic droplet containing FITC at a concentration of 1 µg/ml. The droplets are illuminated using laser light with a wavelength of 488 nm. The images were captured using (a) a Raspberry Pi V2 camera, (b) a Raspberry Pi HQ camera, and (c) a Basler Ace camera at a framerate of 200 fps. The droplets are generated at a frequency of 30 dps. A scale of 100 µm is represented by the white horizontal bars at the bottom of the images. Figure reproduced from: [193].

The images captured using 10 µg/ml FITC are more pronounced. The sensor settings are unchanged, which means the frame rate is kept at 200 fps and the exposure time is kept at 5000 µs. Furthermore, the droplets are generated at a rate of 30 dps, which matches the flow rate settings for 1 µg/ml FITC experiments, so that the droplet size and shape remain the same throughout. There is already a clear indication that the droplets

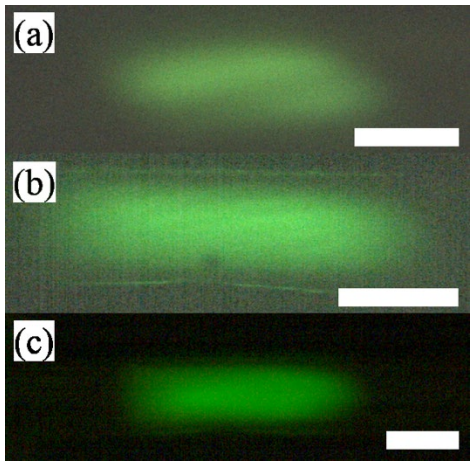

Figure 25. A microfluidic droplet containing FITC at a concentration of 10 µg/ml. The droplets are illuminated using laser light with a wavelength of 488 nm. The images were captured using (a) a Raspberry Pi V2 camera, (b) a Raspberry Pi HQ camera, and (c) a Basler Ace camera at a framerate of 200 fps. The droplets are generated at a frequency of 30 dps. A scale of 100 µm is represented by the white horizontal bars at the bottom of the images. Figure reproduced from: [193].

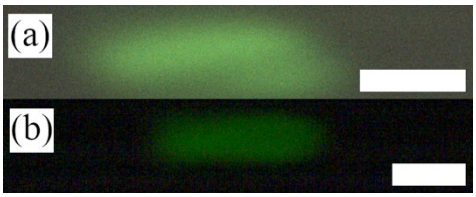

Figure 26. High framerate detection of a microfluidic droplet containing FITC at a concentration of 10 µg/ml. The droplets are illuminated using laser light with a wavelength of 488 nm. The images were captured using (a) a Raspberry Pi V2 camera, and (c) a Basler Ace camera at a framerate of 665 fps and a 750 fps, respectively. The droplets are generated at a frequency of 67 dps. A scale of 100 µm is represented by the white horizontal bars at the bottom of the images.

are more prominent at higher concentrations of FITC. As a result of not increasing the brightness of the images, there is also less visible noise in the images. In the case of the Raspberry V2 sensor, the edges of the droplet are more visible, and the effects of rolling shutter are even visible to some extent (Figure 25 (a)). According to the Raspberry HQ camera, the channel edges are also visible, indicating some contamination, likely caused by the fact, that before droplet formation the FITC was flowing through the channel (Figure 25 (b)). As for the Basler Ace camera, the droplet shape and size are similar to those previously captured using back illumination (Figure 20 (f)). In addition, the Basler Ace camera has one of the lowest levels of noise among all the sensors used (Figure 25 (c)).

The previous experiment was conducted at 200 fps, but the Raspberry V2 and Basler Ace cameras are capable of higher fps, and it is important to know whether the fluorescence can still be detected at higher fps, where the exposure time is reduced. For this purpose, a similar experiment was conducted, in which Raspberry V2 and Basler Ace cameras were configured to run at frame rates of 665 fps and 750 fps, respectively. Taking into account that only fluorescence detection was of interest, flow rates of 4 µl/min for water and 8 µl/min for oil were chosen which resulted in a droplet generation frequency of 67 dps.

Due to the shorter exposure times of the sensors (1500 µs for Raspberry V2 and 1330 µs for Basler Ace camera), it was expected that the droplet intensity would be lower than when 5000 microseconds exposure time was used. It is noteworthy that the Raspberry V2 camera performs similarly in both experiments (Figure 26 (a)), but in the case of the Basler Ace camera there is a significant reduction in the brightness of the image (Figure 26 (b)).

3.5.5 Evaluation of image quality using MATLAB PIQE function

So far the images presented in publication [193] and in Figure 20, Figure 21, Figure 24, and Figure 25 have been assessed visually. Evaluation criteria are subjective – they are primarily determined by the sharpness of the objects, the brightness of the image, and the distortion of the object's shape. The criteria have been developed based on previous experience with image processing, especially edge detection. As the aim of the current work was preliminary assessment of open-source camera solutions for droplet microfluidics applications, a neural network-based image detection process, along with objective image quality assessment, was not used in the experiment.

MATLAB's function PIQE (Perception-based Image Quality Evaluator) was also used to evaluate the quality of the images. In addition to being opinion-unaware (requiring no prior training on manually rated datasets), the algorithm is also unsupervised (no training

of models is required). Because the quality score calculation relies on block-wise distortion estimates based on the local variance of perceptibility distorted blocks (the smaller the score, the better), it may not produce the best estimates in neural network-based image processing, where the models are trained on manually rated images.

The PIQE function in MATLAB evaluated three different images captured with different cameras. The score for the Raspberry Pi V2 camera is 8.9607, the score for the Raspberry Pi HQ camera is 30.9641, and the score for the Basler Ace camera is 9.422. As can be seen from the images, the results for the Raspberry Pi V2 camera and the Basler Ace camera appear to be of similar quality.

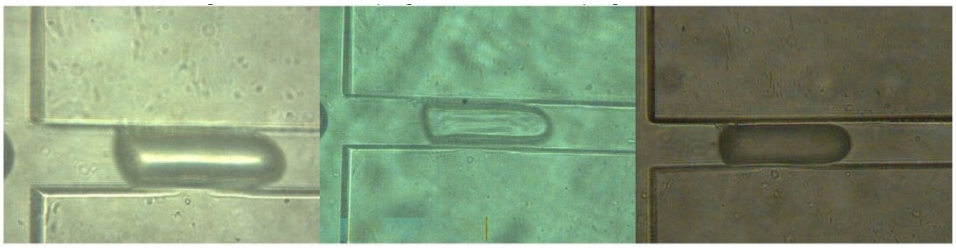

Figure 27. Images of droplets used for MATLAB PIQE function analysis. The results from left to right are 8.9607, 30.9641, and 8.9607 for Raspberry Pi V2, Raspberry Pi HQ, and Basler Ace cameras respectively, where smaller number indicates better image quality.

The MATLAB PIQE function was used in Figure 28 to compare the results from a Raspberry Pi V2 camera recording at 665 fps with a Basler Ace camera recording at 750 fps. The results were 21.24 and 8.8089, respectively. The Raspberry Pi V2 camera's image appears to be blurrier than the Basler Ace camera's image when compared to the two results.

Figure 28. Images of droplets used for MATLAB PIQE function analysis. The result on the left is for Raspberry Pi V2 at 665 fps and resulting PIQE score of 21.24. On the right is the result of Basler Ace camera running at 750 fps and resulting PIQE score of 8.8089.

The MATLAB PIQE function is used in Figure 29 to compare the results of FITC with a concentration of 1 µg/ml and a sensor framerate of 200 fps. The PIQE results are 22.804 for Raspberry Pi V2 camera, 48.2489 for Raspberry Pi HQ camera and 26.7236 for Basler Ace camera. Based on the PIQE function, Basler's results are deemed to be the best and when comparing all three images, it is clear that it is the image with the least amount of noise. However, it may be argued that the Raspberry Pi V2 camera provides the greatest level of detail for the droplet.

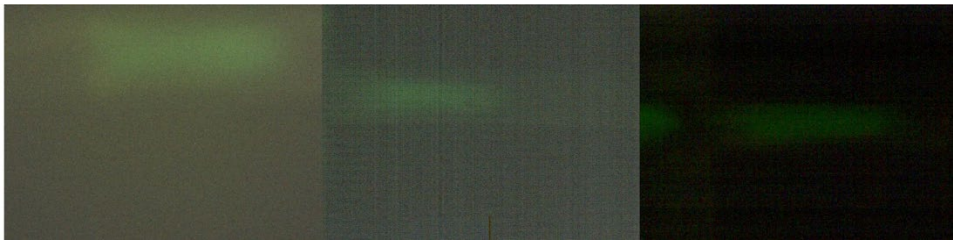

Figure 29. Images of droplets containing FITC used for MATLAB PIQE function analysis. The results from left to right are 22.804, 48.2489, and 26.7236 for Raspberry Pi V2, Raspberry Pi HQ and Basler Ace camera respectively.

The MATLAB PIQE function algorithm is used in Figure 30 to compare the results of FITC at a concentration of 10 µg/ml and at a sensor framerate of 200 frames per second. The results are 19.1907 for Raspberry Pi V2 camera, 47.4599 for Raspberry Pi HQ camera and 25.323 for Basler Ace camera. Here again, the algorithm evaluates the results from Basler to be the best and one can see that there is considerably less noise on the image. Looking at the details of the droplet (brightness and edge contrast), the results from Raspberry Pi V2 camera seems better compared to others.

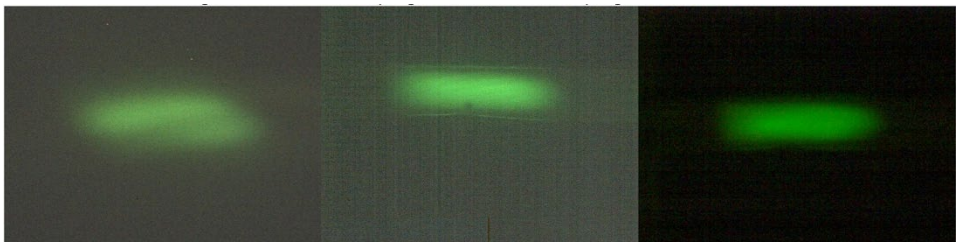

Figure 30. Images of droplets used for MATLAB PIQE function analysis. The results from left to right are 19.1907, 47.4599, and 25,323 for Raspberry Pi V2, Raspberry Pi HQ, and Basler ace cameras respectively.

3.6 Summary of the imaging sensor performance

The experimentation and evaluation of the droplets provided valuable understanding in both the droplet generation parameters, microfluidic chip operation, but mostly provided good understanding about imaging sensor performance. It was interesting to see how it was possible to configure the inexpensive Raspberry Pi camera to work as a high-framerate camera and capture droplets with a width of 90 µm and a generation rate of up to 190 dps. It was disappointing to find that the Raspberry HQ camera performed the worst, as it was unable to go beyond 200 fps and caused the most noise to appear in the images. Basler Ace appeared to perform the best framerate-wise out of all the cameras, however, this was to be expected as the maximum framerate of the camera is 750 fps out of the box. In terms of framerate performance, the Basler Ace camera had the best performance, but when using the most advanced Raspberry Pi 4 B board with the V2 camera, the combination is about five times more affordable than the Basler Ace. While Raspberry platform offers affordability and customization to some degree, the high framerate is not achievable out of the box and the Raspberry V2 lacks a lens mount. Microfluidic applications can also benefit from the Raspberry HQ camera module

when lower framerates are required. In addition, it is compatible with C-mount lenses, which might make it an attractive choice. Furthermore, a MATLAB PIQE function was used to analyse the picture quality of captured droplets, and the results confirmed that previously given subjective results were supported by the MATLAB PIQE function.

This chapter presented a comparison between three open-source and cost-effective imaging sensors and evaluated their performance for droplet microfluidics. The next chapter introduces a novel mathematical model that enables to estimate droplet generation rate based on the flow rates of dispersed and continuous flow.

4 Empirical model for evaluating the droplet generation speed for flow focusing microfluidic chips

In this chapter, a mathematical model is proposed for flow focusing droplet microfluidic chip, that enables to evaluate the droplet generation rate based on the flow rates of dispersed and continuous phases.

This chapter is based on the following publications:

- Pärnamets, K., Udal, A., Koel, A., Pardy, T., Gyimah, N., & Rang, T. (2022). "**Compact Empirical Model for Droplet Generation in a Lab-on-Chip Cytometry System**". *IEEE Access*, *10*, 127708–127717. https://doi.org/10.1109/ACCESS.2022.3226623

The previous chapter showed that when using imaging sensors, there is a clear limit on how many dps can be detected in a microfluidic chip. It is important to distinguish whether the flow of droplets is running at high-speed exceeding the capabilities of the camera sensor or is the flow of liquids jetting when designing a custom setup [88]. For an imaging camera, both of these conditions appear the same. Differentiating the two conditions is important – on the one hand, it is important to know the droplet generation rate, but on the other hand, it could also assist in determining if something is wrong with the chip (e.g., a clog, leak, incorrect flow rate, etc.).

A mathematical model could be used to estimate the droplet generation rate by taking two variables from a microfluidic chip (oil and water flow rates) as inputs. Chip design (channel configuration, channel width and height) also plays an important role, but these values only change when a different chip design is used. Similar research has been conducted in the past, but the focus of previous papers has been primarily on the estimation of droplet sizes [208]. It is true that droplet size is an important parameter, but it does not provide much information in terms of droplet generation rate and camera framerate.

To further emphasize the need for a mathematical model, a specific use case can be considered. When a new chip is introduced to a microfluidic setup, the droplet generation rate of such chip is not known. In order to determine the performance of the chip, one approach would be to conduct a number of experiments and find the droplet generation rate by trial-and-error. It is important to note that while such an approach may be fruitful, it wastes a lot of reagents, some of which can cost in the range of thousands of euros per ml, not to mention the excessive time needed to conduct the numerous experiments. One may use the proposed mathematical model to conduct at least three experiments at different flow rates to estimate the droplet generation rate based on the flow rates of dispersed and continuous phases.

4.1 Evaluation of droplet size based on flow rates

Previously, only droplet length analysis based on the flow rates has been published. It is important to evaluate the existing work and to see how well the droplet size can be estimated based on the existing mathematical formulas. The mathematical formula (Equation 2) is proposed in [208] and requires the input of dispersed and continuous flow rates (Q_d and Q_c). Often water is used as for dispersed phase and oil is used for continuous phase, and their flow rates are represented as Q_W and Q_O, respectively.

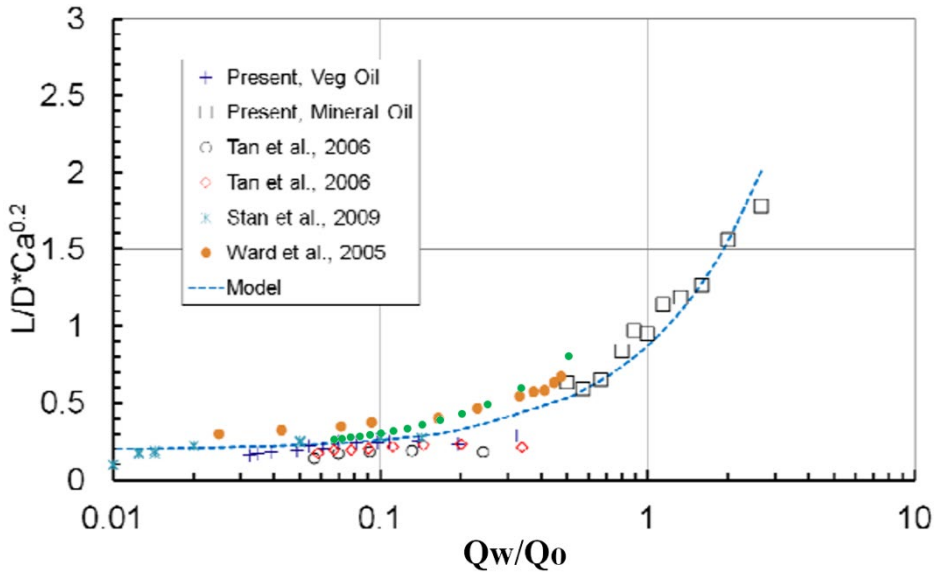

Figure 31. Droplet size of the microfluidic chip used in this work (green dots), plotted against the previously reported works. Figure reproduced from: [208].

$$\frac{L}{D} = \alpha\left(\beta\frac{Q_d}{Q_c}\right)^{0.2} Ca^{-0.2} \tag{2}$$

where D is channel width, α, and β are fitting parameters and *Ca* is the capillary number.

For the microfluidic chip that was used in this work, the fitting parameters in Equation 2 were determined by trial-and-error to be the following: α = 0.1, and β = 0.68. The capillary number (*Ca*) was determined to be 0.05 based on the graph presented in [208]. The results of our model are shown as green dots and are superimposed on the existing graph and show a similar behaviour to previous studies as is seen on Figure 31.

4.2 Analysis of experimental results

The purpose of this study is to develop a compact model for estimating droplet generation rates (dps). To develop a mathematical model, a number of experiments were conducted focusing on recording droplet generation rate and droplet sizes based on the flow rates of continuous and discontinuous phases. For continuous phase mineral oil (Sigma Aldrich 330779) was used and for discontinuous phase deionized water was used. Water flow speeds of 4 µl/min, 8 µl/min, and 12 µl/min were used, and for each water flow speed the ratio of water to oil was changed from 1:2 to 1:8 in steps of 4 µl/min. During the experiment, one-second-long datasets of droplets were recorded at 3000 fps for each flow rate, and the results are presented below (Figure 32). In Figure 32, only single droplets are shown, but other parameters, such as the distance between droplets and the number of droplets generated in one second were extracted from the datasets.

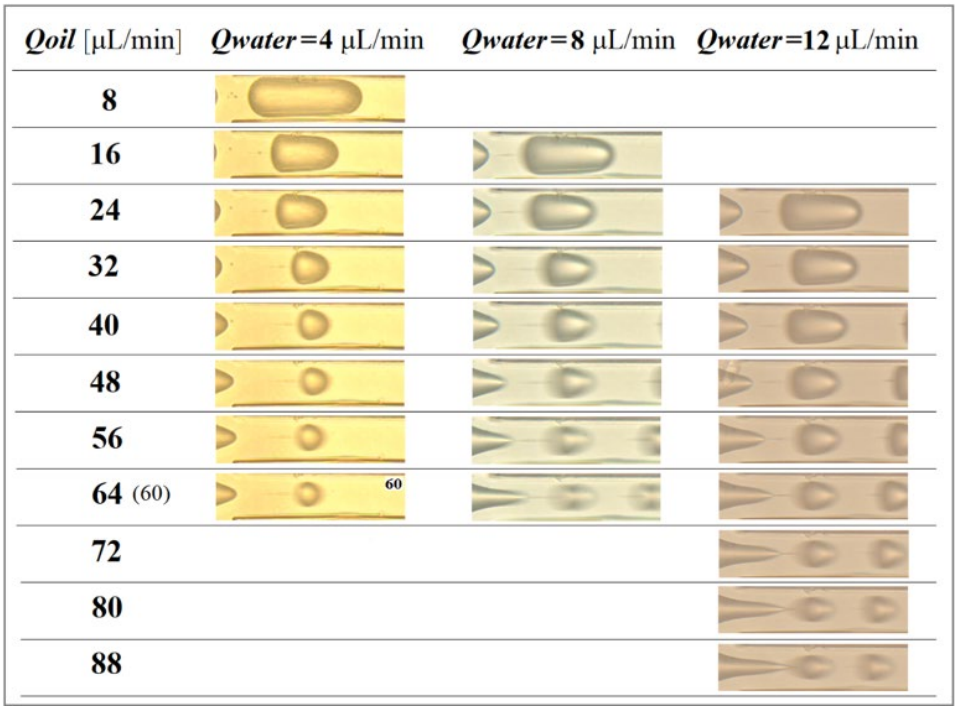

Figure 32. Images of the droplets using different water and oil flow rates. The flow rates used for water were 4 µl/min, 8 µl/min, and 12 µl/min and for oil the flow rates were ranging from 8 µl/min to 88 µl/min. Figure reproduced from: [209].

The droplet generation rate of microfluidic system is determined by manually counting the number of droplets in a dataset containing 3000 frames. The droplets are counted on frames on one tenth of the dataset instead of on the entire dataset, as counting droplets on full datasets is very time-consuming. To obtain the droplet generation rate for one second, the found droplet count was multiplied by 10, resulting in a dps. In order to evaluate and verify this methodology, the dps counts for the full dataset and the tenth of the dataset multiplied by 10 were randomly compared. An accuracy range of +-5% was observed between the results. Such accuracy was accepted as sufficient, as in the literature up to +-8.5% variation in droplet generation rate is reported [210].

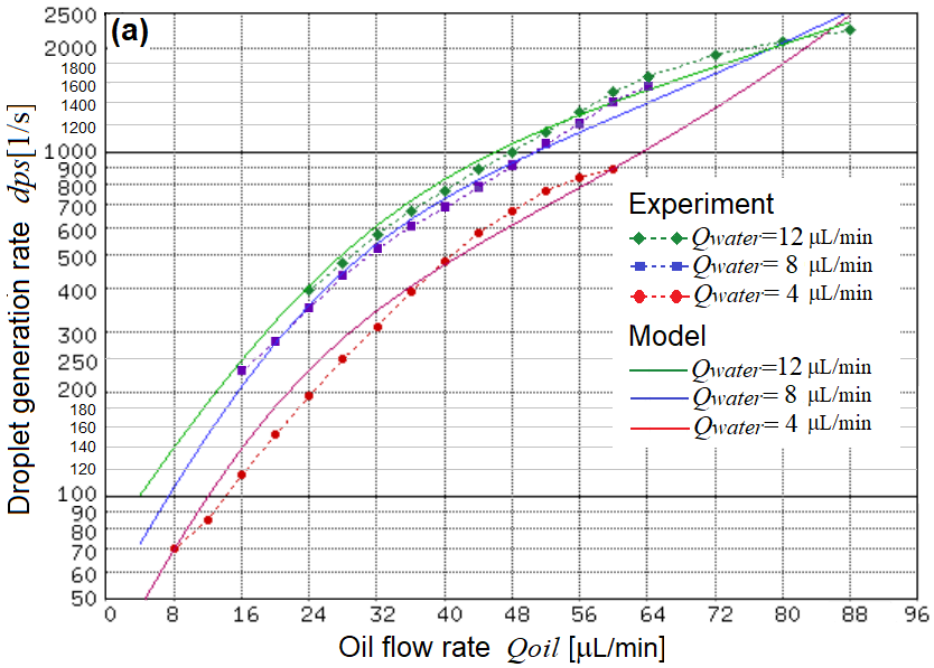

Figure 33. Representation of measurement results plotted against the proposed model of the droplet detection rate. Figure reproduced from: [209].

4.2.1 Proposed mathematical model and application to our system

An in-depth description of the mathematical model can be found in the publication [209] (included in full in Appendix 3 of the thesis). Based on the analysis of experimental results, a mathematical model can be proposed that describes the predicted droplet generation rate (dps_i) (Equation 3). Due to the fact that three different flow rates of water were used, an index *i* was used to distinguish between the experiments. Though the proposed mathematical model should only rely on the flow rates of water and oil (Q_W and Q_O), it needs three additional fitting parameters ($E_{8,i}$, $Q_{E,i}$, and $Q_{D,i}$). Droplet ellipticity *E* can be expressed as droplet length divided by droplet width. Parameter $E_{8,i}$ represents droplet ellipticity at its lowest water to oil ratio (i.e. Q_W = 8 µl/min and Q_O = 16 µl/min). The results indicate that the ellipticity decreases with increasing oil flow rates and variable $Q_{E,i}$ is introduced to account for this change (Equation 5). Moreover a change in droplet diameter is viewed and a variable $Q_{D,i}$ is introduced to account for this change (Equation 4).

$$dps_i = (\,557\ s^{-1}) \left(\frac{Q_{w,i}}{6\ \mu L/min}\right)\left(\frac{1}{E_i}\right)\left(\frac{70\ \mu m}{D_i}\right)^3 \tag{3}$$

$$D_i = (84\ \mu m)\left(1 - \frac{Q_{oil}}{Q_{D,i}}\right) \tag{4}$$

$$E_i = 1 + (E_{8,i} - 1)exp\ (-\frac{(Q_{oil} - 8\ \mu L/min\,)}{Q_{E,i}}) \tag{5}$$

The manual count of droplets is mapped on a graph in Figure 33 for each water flow rates. Moreover, the droplet generation rate predicted by the model (Equation 3) is plotted on the same graph. It can be seen that the model does not follow the experimental results exactly, but comparing the two, the accuracy is within a range of +-10% and is deemed accurate enough. It is important to emphasize that it is not expected for the model to work with utmost accuracy, because being able to predict droplet generation rate with an accuracy of +-10% provides a good starting point for further system fine tuning.

Based on empirical investigation, a mathematical model was developed to estimate the droplet generation rate with an accuracy of +-10% using flow rates of dispersed and continuous phases (water and oil). Following this chapter, a novel approach to non-imaging droplet detection is presented, which exceeds the droplet detection performance of imaging sensors.

5 Proof-of-concept of non-imaging droplet detection

As an extension of Chapter 3 of the thesis, this chapter proposes a low-cost non-imaging setup and method for droplet tracking. Proof-of-concept droplet detection performance evaluation of the setup entails droplet generation rate measurement.

This chapter is based on the following publications:

- Jõemaa, R., Gyimah, N., Ashraf, K., Pärnamets, K., Zaft, A. W., Scheler, O., Rang, T., Pardy, T., "**Cogniflow-Drop: Integrated modular system for automate generation of droplets in microfluidic applications**". *Submitted to IEEE Access by May 2023 - Forthcoming.*

5.1 Background about the non-imaging methods used in droplet microfluidics

A set of experiments was conducted in the previous chapter using a Basler Ace camera, which was capable of recording frame rates up to 3000 fps and detecting droplets at a rate up to 1500 dps. At higher droplet generation rates, it becomes difficult to distinguish whether droplets are being generated at all, or whether the generation has reached a state called jetting [88], [211]. When droplet generation frequency is half or more than the framerate of the camera, the effects of jetting and detecting droplets are remarkably similar. One suitable option would be to switch to even higher performing imaging camera, but sooner or later this approach is not economically viable. Additionally, if only droplet size, speed, and generation frequency are of interest, such a method may not be appropriate. The use of a non-imaging detector could provide a cost-effective alternative to imaging sensors when only the size and speed of the droplet are of concern.

In a typical microfluidic setup, three key components have to be present for droplet generation: the microfluidic chip together with pumps, a source of illumination, and a detector, as illustrated in Figure 3. It is possible to utilize a different combination of illumination and detectors for the same microfluidic chip. In the case of non-imaging detection, a variety of sensors are available (Photomultiplier tube (PMT), avalanche photodiode (APD), photodiode (PD)); however, due to its simplicity of use, a photodiode is frequently chosen (see Section 2.4). A variety of light sources are available for illumination, but due to their low power and ease of use, solid state lasers or LEDs are often preferred (see Section 2.3).

A pinhole is commonly used in confocal microscopy to set a focal plane; however, in the present application, its purpose is different from that in confocal microscopy [212], although it is similarly positioned between the detector and the optical signal coming from the microfluidic chip. The sole purpose of the pinhole is to block out unwanted stray light from uninteresting areas of the microfluidic chip, improving the signal to noise ratio for non-imaging detector. When it comes to non-imaging droplet microfluidic applications, microscope lenses are used primarily to provide optical magnification; however, as magnification increases, the field of interest narrows, preventing the lens from capturing unwanted stray light. When focusing is of interest, often the pinhole is used in photography to provide near infinite focus distance or depth of field. As part of this work, the effects of using a pinhole as a focuser have not been thoroughly explored, but rather the working principles and performance for droplet detection have been evaluated empirically.

It is possible to simplify the overall detection setup by removing the microscope lens from the optical setup and replacing it with the pinhole. As a result, the overall setup becomes less cumbersome and more cost-effective. In addition, it is possible to attach

the pinhole to the microfluidic chip at the time of its manufacture, which will ensure a precise alignment of the pinhole with the microfluidic channel. The use of a photodiode with a relatively large detection area would also make this approach suitable for POCT applications, because alignment of the microfluidic channel to the detector would no longer have to be precise and would no longer be critical.

It is sensible to use readymade modules as much as possible in the very early stages of development, since they allow a quicker evaluation of the overall system. The selection of photodiodes along with the necessary support circuitry should, however, be designed and analysed here. Firstly, it enables the system to be highly customizable, and secondly, the illumination and detection circuits are not overly complicated that would require months of research. It is also necessary to take a closer look at the topic of specialized transimpedance amplifiers for photodiodes when considering the need for high-throughput. It is also essential to select a photodiode that will respond appropriately to both white light and green fluorescent light signals.

5.2 Selection of photodiode

Photodiodes are electronic components that convert photons from incident light into electric current, also known as photocurrent. Diodes are selected primarily based on their spectral range, spectral range of sensitivity, photocurrent, junction capacitance, and architecture. In the non-imaging droplet detector, the photodiode plays a key role, so it is imperative to select the right one. It was indicated in the previous paragraph that for a non-imaging detector based on photodiode to be on par or better compared with current state-of-the-art, as far as droplet detection frequency is concerned, the detector should be capable of detecting droplets at a rate of at least 10 kdps.

In the literature, photodiodes are widely reported to be used for the detection of droplets; however, the manufacturer and model of the diode are often not specified. Furthermore, there is a lack of information about the supporting electronics that are required to convert photocurrent into voltage, making it difficult to replicate and evaluate existing solutions. The evaluation process is further complicated by the fact that different microfluidic chips behave differently with regard to flow rates, droplet size, and frequency of droplet formation. Therefore, it is justified to go through the analysis of selecting a photodiode, aiming for the performance to reach the detection frequency to 10 kdps.

5.2.1 Key parameters for photodiode

The first and foremost consideration when selecting a photodiode is its spectral range, which defines in which range the photodiode can be operational. For droplet microfluidic applications, the choice of a photodiode is primarily determined by the spectrum of the illumination source. In order to count droplets, a white light source can be used. A white power LED with a colour temperature of 3000 K was used to illuminate the setup. Lower colour temperature was preferred as the spectrum has higher red colour intensity around 600 nm. It is possible, however, that droplets that contain FITC may need to be detected. According to chapter 3.5.4, FITC has an excitation spectrum of approximately 490 nm and an emission spectrum of approximately 510 nm. There is a wide variety of photodiodes available that have the spectral range suitable for infrared spectrum (typically around 800–900 nm). In microfluidic droplet detection applications, infrared photodiodes can be used, but they must have a spectral range that also covers wavelengths between 510 nm and 600 nm.

Due to the fact that a photodiode is not a linear component, the previously discussed spectral range of sensitivity does not adequately address how well the photodiode performs over the spectral range. For that, most photodiodes' datasheets include a graph expressing relative spectral sensitivity, which describes how much photocurrent is generated at a specific wavelength within the spectral range. It is typical for photodiode sensitivity spectrums to have only one peak and to have almost linear increases before and linear decreases after the peak wavelength sensitivity. It is possible to use this metric if experiments are conducted using fluorescent emissions, since it allows comparison between different photodiodes operating at a specific wavelength, such as at 510 nm. Photodiodes are also measured by their output current, which is typically defined at a light intensity of 1000 lx and expressed in microamperes. With higher output currents, less gain is required from the amplifier, and therefore, the amplifier design is less challenging. Junction capacitance (C_j) of a photodiode is also important metrics, as it somewhat defines the speed of the detector. An effective way to reduce the junction capacitance is to reverse bias the photodiode (photoconductive mode), however, photodiodes with large photosensitive areas have a large junction capacitance by nature, and reverse biasing only reduces this capacitance to a limited extent. A final factor to consider is the architecture of the photodiode, which may be one of four types, PD, PIN, Schottky or APD, although Schottky and APD-s are not considered as the former have spectral ranges suitable for ultraviolet (UV) and the latter require a high voltage power source. For example, for APD-s the working voltage is considerably higher compared to PD and PIN, reaching tens of volts, posing a challenge to the design or selection of the power supply. Furthermore, they are not as cost effective as PD and PIN. APD-s, on the other hand, provide exceptional sensitivity. As compared to PD and PIN diodes, whose spectral sensitivity ranges from 0.1–1 A/W, APDs have a relative spectral sensitivity of 0.5 to 100 A/W.

5.2.2 The selection of photodiode for droplet microfluidic droplet detection

While there is a wide selection of photodiodes available that meet some or all of the previously mentioned technical criteria, it is not feasible to order and test all of them. A set of photodiodes was selected in order to provide a combination of different parameters in a microfluidic droplet detection application, since it is uncertain how each individual photodiode will perform in a droplet microfluidic droplet detection application. A number of photodiodes are listed in Table 8, each covering all the parameters discussed previously.

To enable evaluation of the photodiodes for fluorescence experiments, a relative spectral performance has also been provided for wavelength of 510 nm. The two parameters that perform best in terms of spectrum, relative spectral sensitivity, photocurrent, and junction capacitance are highlighted in bold. It can be seen that in terms of photocurrent and junction capacitance, the Osram BPW24R has the best performance; however, it has relatively low performance in terms of spectral sensitivity for 510 nm wavelength. The SFH 2240 by Osram is the most sensitive for 510 nm wavelengths and has a peak in spectral range at 620 nm. It has, however, a relatively high junction capacitance, as well as a modest photocurrent. It is also important to note that PIN diodes exhibit a higher level of relative spectral sensitivity than PD diodes. The two photodiodes discussed could possibly be selected for further experiments; but in the end the Osram SFH 2240 was chosen for its very good response at wavelengths of 510 nm and 620 nm.

Table 8. Selection of photodiodes based on the spectral range, relative spectral sensitivity for 510 nm. In the table is also provided the manufacturer, photocurrent, junction capacitance and architecture.

Photodiode	Spectral range	Relative spectral sensitivity [A/W]	Photo-current [µA]	Junction capacitance C_j *[pF]*	Architecture
Ablic S-5420	250-1000, pk@365nm	0.17@365 nm, 0.13@510 nm	-	-	PD
MARKTECH MT03-023	250-1100, pk@950nm	0.22@365 nm, 0.38@633 nm, 0.3@510 nm	-	8-20	PD
MARKTECH MTD5052N	410-580nm, pk@522	0.3@525 nm, 0.275@510 nm	4.5	100	PD
MARKTECH MTD5052W	410-580nm, pk@525	0.3@525 nm, 0.275@510 nm	4	500-700	PD
OSRAM BPW24R	400-1100nm, pk@900nm	0.6@870 nm, 0.12@510 nm	**45-60**	**2.5-11**	PIN
OSRAM BPX 61	400-1100nm, pk@920nm	0.62@850 nm, 0.18@510 nm	55-70	72	PIN
OSRAM BPX 65	350-1100nm, pk@850nm	0.55@850 nm, 0.25@510 nm	10	11	PIN
OSRAM SFH 2240	**400-690nm, pk@620nm**	0.37@550 nm, **0.32@510 nm**	6.6	135	PIN
VISHAY BPW21R	420-675nm, pk@565nm	-	9	400-1200	PD

5.3 Design of transimpedance amplifier

The current that a photodiode generates is in the range of up to 100 µA. Such current is very small and requires an amplifier. Furthermore, most devices (such as microcontrollers and analogue to digital converter (ADCs)) require voltage as an input. It is common to use a transimpedance amplifier (TIA) for such a task, which converts the current from the photodiode into an amplified voltage. Transimpedance amplifier is also preferred as the design is relatively simple, containing only one operational amplifier, resistor and some capacitors. Despite the simplicity of the schematic's design, there are a number of necessary calculations that must be completed before a stable application can be achieved. Fortunately for designers, the TIA design is supported by a wide range of tools that can assist in getting started with TIA design.

5.3.1 The schematic and PCB of transimpedance amplifier

The schematic of the TIA is based on a reference design published by Texas Instruments, which is a photodiode amplifier with a bandwidth of 1 MHz [213]. For the photodiode, an Osram SFH 2240 photodiode is used, having maximum photocurrent of 6.6 µA and junction capacitance of 135 pF. It was previously discussed that the non-imaging approach should achieve the droplet detection rate of up to 10 kdps. Accordingly,

the TIA should also have a bandwidth of at least 10 kHz, but if possible, even higher. The photodiode current of 6.6 µA is specified for a light intensity of 1000 lx (lux), which is roughly equivalent to the light intensity at overcast daylight. The expected photocurrent for the droplet detection system is expected to be less than that, however the exact value is not known. In all cases where photocurrent is required for calculations, the current specified in the datasheet for 1000 lx is used.

The schematic with component values can be seen in Figure 34. Following the previously discussed parameters, the feedback resistor and compensation capacitor were calculated to provide the photodiode amplifier with bandwidth of 40 kHz and with gain of 100 kV/A, meaning for photocurrent of 6.6 µA an output voltage of 0.66 V will be produced. In order to maintain some degree of comparability between the calculations presented here and those presented in the application note, similar operational amplifier (OPA2320) is used as is reported in the application note (OPA320). The performance of this device is similar to that of the OPA320, however, there are two operational amplifiers instead of one. To prevent unwanted use or noise in the other operational amplifier, the unused operational amplifier has been configured as a unity gain amplifier.

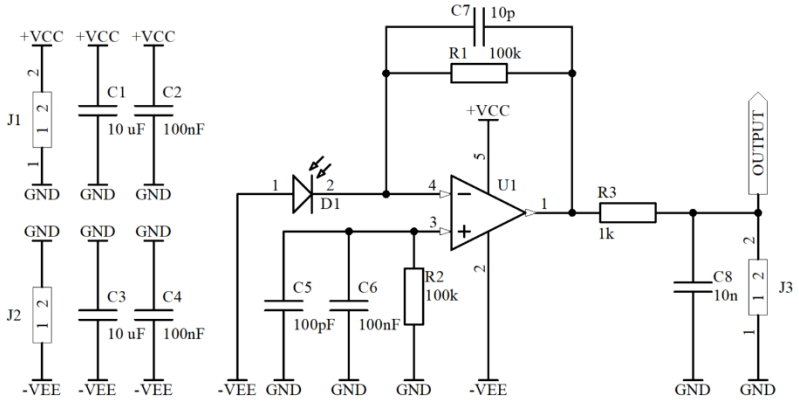

Figure 34. The transimpedance amplifier used non-imaging detection of droplets. The design of the amplifier is based on industry standard transimpedance amplifier design presented in a Texas Instruments application note [213]*, but with feedback and supporting components calculated in accordance with the gain and bandwidth requirements for current work. Moreover, a RC filter is added to the output, to supress noises above 15 kHz.*

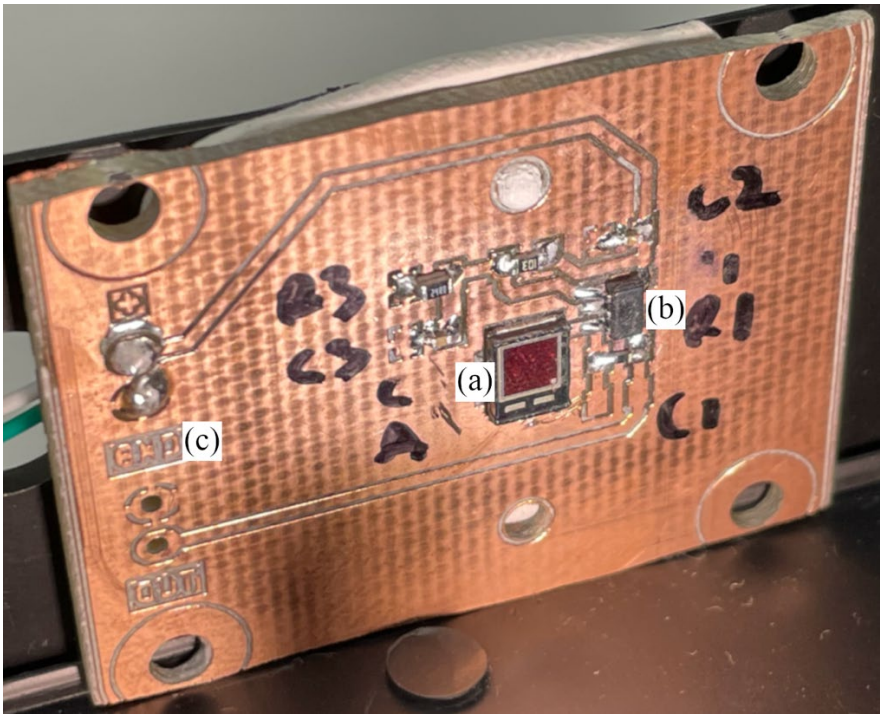

Figure 35. Custom PCB with installed photodiode and transimpedance amplifier. On the board there is (a) a photodiode, (b) a transimpedance amplifier, and (c) connectors for power and output.

It is common for the amplifier to be built separate from the sensor and the photodiode to be connected to the TIA via shielded cable. Keeping portability in mind, it is more reasonable to build the TIA right next to the photodiode. The PCB was manufactured using Protomat, a tool meant for producing prototype PCBs, which is suitable to use here as the circuit is fairly simple. It is also important to note that attaching a photodiode to a PCB and keeping the other components and circuitry close to each other improves mechanical rigidity and minimizes noise induced by otherwise long wires. To even more supress the unwanted noise, a first order RC filter, tuned to 15 kHz cut-off frequency, was used at the output of TIA. The constructed PCB can be seen in Figure 35.

5.3.2 Evaluation of the performance of TIA

As a preliminary step before incorporating a photodiode into the measurement setup, it is sensible to investigate the maximum frequency that the photodiode detector setup will be able to detect. To achieve this, a custom LED light source is assembled, which is capable of switching on and off with rise and fall times of a few µs, and is driven by a signal generator. Rather than evaluating a sensor's performance to a very high level of accuracy, the objective is to determine what order of magnitude of frequency the sensor is capable of detecting. To shield unwanted light from the outside and maintain stable positioning of both PCBs, both the detector and LED were mounted inside a black case (Figure 36).

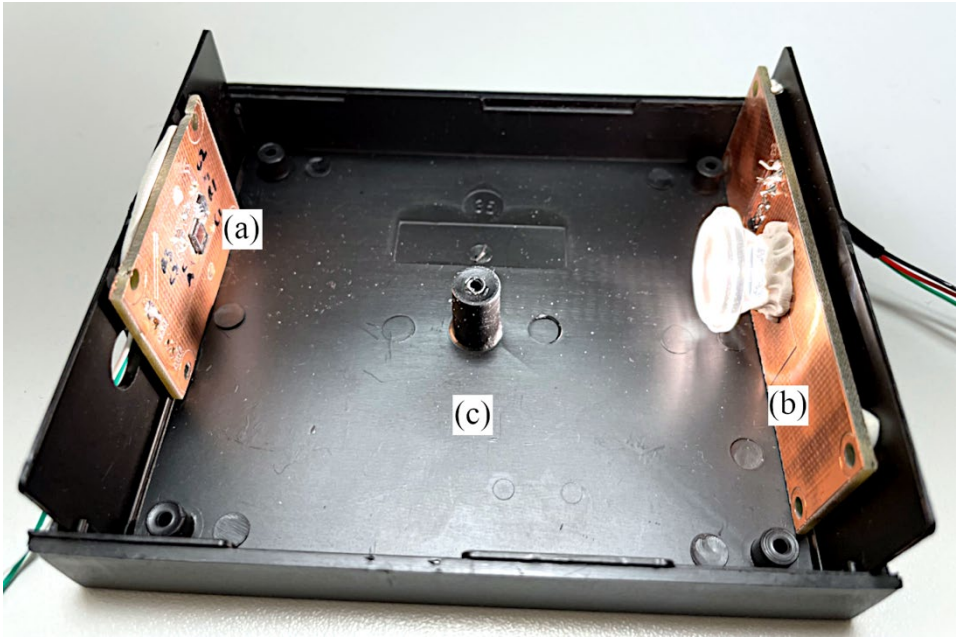

Figure 36. The setup for PD speed determination. The setup contains: (a) the photodiode board, (b) a LED board and (c) a black case to block out external illumination.

An N-channel MOSFET transistor switch was constructed to drive the LED. To limit the LED current, series resistors were used; however, since only one 10 µs pulse is generated in each second, these resistors are not necessary. The LED in this setup is a white power LED (LTW-3030) from Liteon with a colour temperature of 3000 K [214]. It is suitable for this setup as its spectrum peaks at 600 nm wavelength, which is where the Osram SFH 2240 has the highest sensitivity. Due to the fact that this setup is intended only for evaluating the speed of a photodiode, a laboratory power supply is used and pulses are generated by a signal generator in the Keysight DSO-X 2012A oscilloscope. In Figure 37, the oscilloscope channel no 1 (orange) shows a 10 µs pulse from signal generator, while channel no 2 (green) shows a response from the transimpedance amplifier output. The signal rise and fall times can be seen to be around 3 µs. Results indicate a bandwidth limitation of approximately 100 kHz, which is sufficient for a first implementation and should be able to detect droplets at a frequency of 10 kHz.

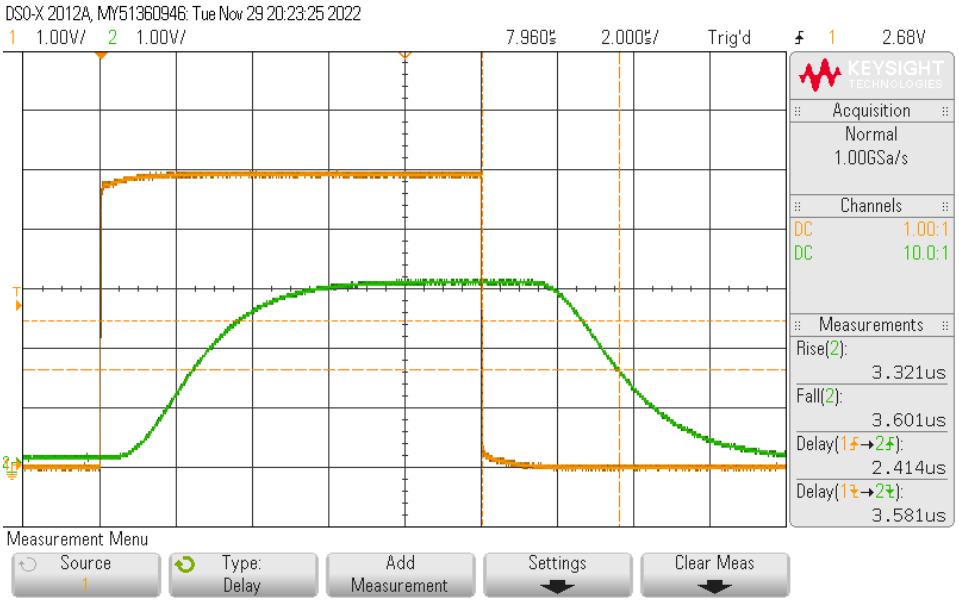

Figure 37. LED driving signal from signal generator and the response signal from photodiode detector. A 10 µs signal from signal generator (orange) is used to drive the LED switching MOSFET. A LED signal is captured by photodiode and the response from the transimpedance amplifier can be seen (green).

5.4 Pinhole add-on for measurement setup

In terms of illumination and detection, it is clear how they will be handled, but once all components have been assembled, the number of detectable droplets will be relatively low (10–20 dps). This is due to the fact that the active area of the Osram SFH 2240 is 2.65 mm x 2.65 mm, while the microfluidic channel has a width of 90 µm. Droplets generated by the generator are estimated to be in the range of 100 µm in size, thus generating a relatively small shadow in comparison with the overall size of the sensor.

A pinhole addon is proposed, which is aligned with the microfluidic channel. Using the pinhole addon, stray light around the droplet generation channel was blocked out, thereby increasing the detection signal to noise ratio. In addition, a lens (Optosupply OEHW2045GF) was added to the LED PCB to narrow the overall wide beam of the LED and increase its intensity at the droplet generation area (Figure 38.). Since the LED board was originally designed to evaluate photodiode performance, it has been modified to operate continuously, by removing the driving transistor, series resistor, and replacing it with a linear constant current LED driver. Section 3.2 has previously evaluated imaging sensors using a microfluidic setup containing LEDs, microfluidic chips, and imaging sensors. In order to install the non-imaging sensor, the imaging sensor was removed from the experimental setup and the LEDs were replaced with the design discussed in this chapter (Figure 39).

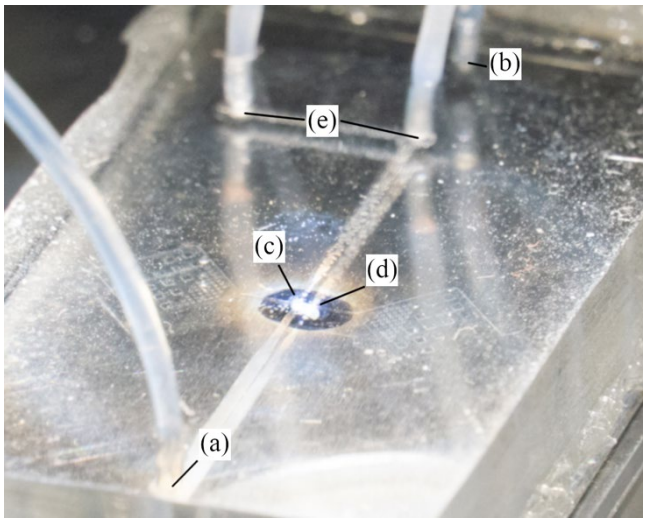

Figure 38. Closeup of microfluidic chip with pinhole add-on. In figure is seen: (a) water and (b) oil are pumped to microfluidic chip via PTFE tubing, resulting in droplets being generated at (c) the junction of microfluidic chip. Right beneath the microfluidic chip is a (d) pinhole add-on, which is aligned with the junction of microfluidic chip. The generated droplets are transported to container via (e) PTFE tubing.

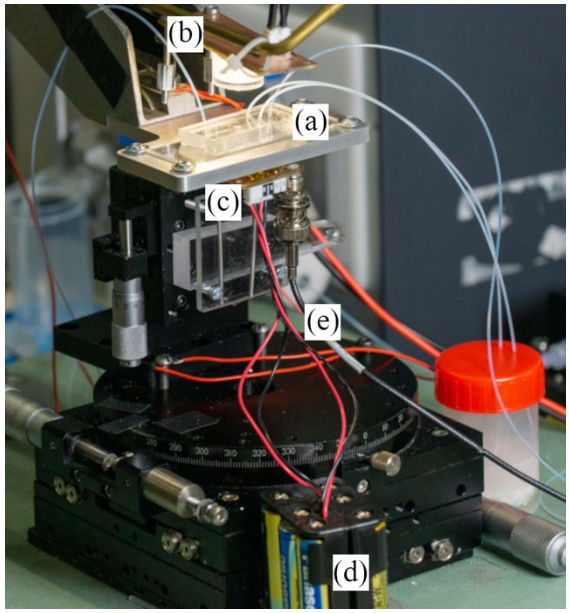

Figure 39. Construction of non-imaging droplet detection setup. The non-imaging detection setup consists of: (a) a microfluidic chip that produces droplets and to where a pinhole addon aligned with microfluidic channel is added, (b) a white LED as light source, (c) a photodiode as a detector, (d) batteries as power supply, and (e) a BNC cable that connects the output of the photodiode sensor to oscilloscope.

5.4.1 Pinhole attached to microfluidic chip

A key component of the proposed microfluidic setup is the pinhole, which aligns with the microfluidic chip channel and serves as a means of blocking out stray light (Figure 40). The microfluidic setup is constructed as follows. On top, there is an illumination source, for which the previously mentioned LED board consisting of LED, lens, and driver is used. An LED illuminates a microfluidic chip beneath which is adhered a pinhole add-on, formed from stainless steel sheet metal with a thickness of 150 microns. A 100 µm hole is laser cut into the sheet metal. A photodiode with a transimpedance amplifier is located directly beneath the pinhole. Compared to previous methods described in the literature, such an approach is much more versatile in terms of alignment.

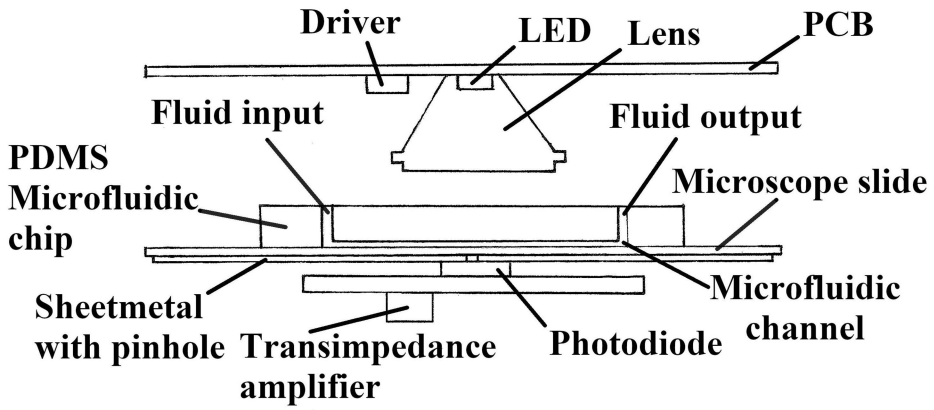

Figure 40. Cross section of the non-imaging microfluidic detection system. The droplets are generated in microfluidic chip, the droplets are illuminated by LED and detected by photodiode. At the centre of the figure is microfluidic chip made out of PDMS, where fluid inputs (for water and oil) and output are represented. The chip is made out of PDMS and is bonded to microscope slide (75 x 25 x 1mm). On top of the chip is a simple illumination board that consists of single LED solution with current limiting resistors. Directly underneath the microscope slide is the pinhole attachment, that is made out sheet metal and the pinhole is laser cut to a size of 100 µm. Directly underneath the pinhole is detector setup, consisting of a photodiode and transimpedance amplifier.

5.5 Performance of droplet detection with the pinhole add-on

The droplet generation rate was previously determined using a camera and counting droplets in images captured over a period of 100 milliseconds and multiplying the number of droplets by 10 to represent dps. As a result of this approach, dps with reasonable accuracy was obtained; however, as mentioned earlier, counting the droplets was time consuming and provided an accuracy of +-5%. In that sense, the non-imaging approach should provide the answer quicker and be more precisely. In current state, an oscilloscope is used to measure the output signal of the transimpedance amplifier. An oscilloscope is preferred at this stage, as it allows the signal to be easily measured by means of amplitude and frequency. Due to the fact that TIA has voltage output, it can be routed to an ADC (separate or internal to the microprocessor) and thus the proposed solution can be implemented on embedded platforms reasonably well.

Based on the droplet count determined using imaging sensors (Table 6), it would be logical to verify the droplet generation rate using non-imaging sensors and compare the results with those determined using imaging sensors. Based on the experiments conducted in Chapter 3 and Chapter 4, it is evident that as the flow rate of oil and water increases, the rate of droplet generation increases, and the size of droplets decreases. It is also necessary to use both imaging and non-imaging approaches for the same experiment in order to obtain the most accurate results. The frequency of droplet generation was first verified using a non-imaging approach after the droplet generation had started. The stable flow of droplets results in a sinewave, whose frequency represents the frequency of droplet generation, and from which the number of droplets generated per second can be extracted. Within a few seconds, the sensor was switched to imaging and a set of images was captured for a period of one second. The camera frame rate was set to be at least five times faster than that detected with the non-imaging approach, i.e. for flow rates of 16/32 (Q_W/Q_O) a frequency of 610 Hz was detected, so the camera frame rate was set to 3000 fps. A set of 3000 images was collected over a period of 1 s. The manual counting of droplets is not viable, so only $1/10^{th}$ of the set is counted to ensure accuracy. To verify that the $1/10^{th}$ method would be effective, the number of droplets for 1 s was counted for flowrates 8/16 (Q_W/Q_O) and 16/32 (Q_W/Q_O).

When imaging and non-imaging methods were compared, similar results were observed and an accuracy of +-3.3% was observed (Table 9). As for flow rates of 1/2 (Q_W/Q_O), where there is a detected flow rate of 12–13 dps, the deviation is the highest (+8.3%), since it is somewhat difficult to accurately determine the number of droplets from the images due to the size of the droplet. For the remaining experiments, the counting is more accurate, as the droplets are considerably smaller in length and are easier to detect and count. Other flowrates show a deviation in range of +-3%.

Table 9. Droplet generation frequency comparison between imaging and non-imaging sensors using different water (Q_W) and oil (Q_O) flow rates.

Flow speeds [Q_W/Q_O], µl/min	1/2	2/4	4/8	8/16	16/32
Dps with imaging	12	30	67	220	630
Dps with non-imaging	13	31	69	213	610
Deviation	+8.3%	+3.3%	+3%	-3.2%	-3,2%

It was confirmed that the non-imaging method provided similar results to the imaging method, and that the droplet count obtained using the non-imaging approach was reliable. It was only reasonable to push the system in terms of droplet generation rate in order to determine the maximum droplet detection rate it is capable of. This was accomplished by gradually increasing the flow rate of oil and water. The proposed method must reach a droplet detection rate of 10 kdps in order to be successful. The water flow rate was increased to 100 µl/min and oil was increased to 200 µl/min. The frequency of droplet generation was observed to be 10.1 kHz. Assuming the system to be accurate to +- 3.3% of droplet count, the detected droplet generation rate is 10.1 kdps +- 333 dps. Compared to the signals captured for droplet generation rates ranging from 13 to 610 dps, the output signal amplitude was two orders of magnitude lower; however, the oscilloscope has sufficient sensitivity to capture the signal, proving the feasibility of the proposed method in principle.

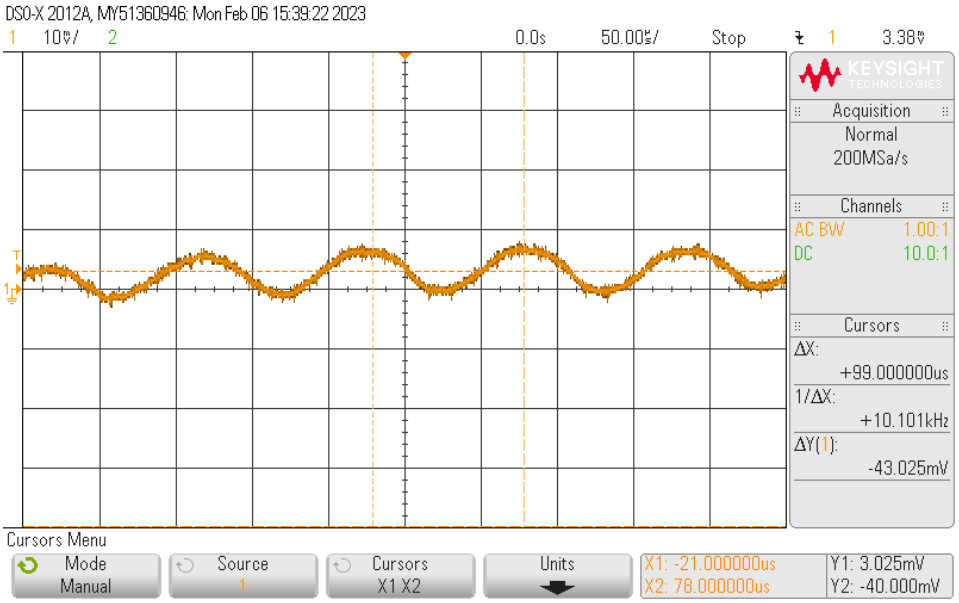

Figure 41. The output of transimpedance amplifier at high droplet generation rate. The droplets are generated using water flow rate of 100 µl/min and oil flow rate of 200 µl/min, resulting in droplet generation rate of 10.1 kdps +- 333 dps.

5.6 Summary

The objectives of this chapter are to assess a photodiode-based non-imaging droplet microfluidic detection setup, including the design of the support circuitry required for the amplification of photodiode signals.

A significant result of this study is the development of a unique way to detect droplets (via the droplet generation rate expressed in droplets/second unit) in microfluidic droplet applications through the integration of a pinhole add-on to the microfluidic droplet device. In this proof-of-concept setup it was possible to improve the existing setup from Chapter 3 by eliminating microscope lenses from the setup, introducing a pinhole to the microfluidic setup, and attaining similar droplet detection rate performance and reaching 10.1 kdps +- 333 dps per second with droplet detection. With the pinhole add-on, the overall detection circuit is less cumbersome, is more cost-effective, and allows the microfluidic setup to be portable. It is relevant to note that the results of the novel method were compared, where appropriate, with the results obtained with the imaging sensors in previous chapters and an accuracy of +-3% was observed. The next chapter presents the conclusions and the future directions of research.

6 Conclusions

6.1 Summary and key findings

The purpose of this thesis is to support the development of portable and cost-effective analytical device that uses droplet microfluidics for sample handling by exploring the existing illumination and detection methods. The focus of this research has been on illumination and detection methods used in biomedical applications, with particular emphasis on the illumination and detection sources used in droplet microfluidics.

Accordingly, this thesis addressed the following research questions (previously formulated Section 1.3):

1. **RQ1** – What are the capabilities of an optical sensors for droplet detection and how does high-throughput limit sensor selection i.e. what are the sensitivity and sensor speed requirements for reliable droplet detection? Also, are the sensor requirements different for droplet detection if the droplets are fluorescently labelled or not?
2. **RQ2** – What possible cost-effective and open-source solutions exist that could be suitable for high-throughput droplet detection with and without fluorescence. Also, what could be the suitable lighting solution, i.e. are LEDs sufficient or should lasers be used instead? How to evaluate the quality of captured images, i.e. which tool to use and which parameters to monitor (sharpness, resolution)?
3. **RQ3** – The question arises, is it possible to model droplet generation to predict stable steady state of generation at high flowrates by knowing the system behaviour at lower flow rates?
4. **RQ4** – Is it possible to find a new approach to achieve non-imaging high-speed droplet detection without requiring the use of conventional microscope lenses, while still achieving a temporal resolution comparable to state-of-the-art solutions?

The thesis employed the applied research method to address the aforementioned research questions. This is, to the best of the author's knowledge, the first experimental study on a suitable combination of detection and illumination in droplet microfluidics that can be used in portable and cost-effective platforms. As a result of this PhD thesis, the following contributions have been made:

Contributing to **RQ1**, a comprehensive study of illumination and detectors was carried out. Throughout Chapter 2, an in-depth review of illumination sources for biomedical applications is provided, along with identification of the sources that are most suitable for cost-effective and portable droplet microfluidic applications. In addition, a similar review is provided for imaging and non-imaging sensors used in biomedical applications with a focus on which of these are suitable for cost-effective and portable droplet microfluidic applications. The results of this study are presented in Publication I.

Having conducted a broad investigation of the field, a more detailed investigation was conducted regarding imaging sensors used in droplet microfluidics that can serve as a portable and cost-effective platform. Contributing to **RQ2**, an analysis and evaluation of cost-effective imaging sensors is presented in Publication II and discussed in Chapter 3.

In a comprehensive study, each imaging sensor is evaluated in order to determine the maximum detectable droplet rate. The suitability of LEDs and lasers is assessed, as well as the detection of droplets containing and without fluorescein.

The contribution of **RQ3** is an empirical model based on experimental results that can be used to determine the droplet generation rate in microfluidic chips by comparing continuous flow rates with dispersed flow rates. The results of this study are presented in Publication III and discussed in Chapter 4.

Contributing to **RQ4**, this thesis proposes an innovative method for non-imaging detection of droplets by incorporating a pinhole into the measurement setup. The proof-of-concept measurement is more compact than existing state-of-the-art setups and provides comparable temporal resolution for droplet generation rate and size measurements. Some results of this study have been presented in Publication V and discussed in Chapter 5.

6.2 Perspectives

The PhD work so far has addressed several challenges and paves the way for further research.

Some of the shorter-term points that directly relate to this topic are:

- Improvements to the detection circuitry proposed in Chapter 5 so that it will provide higher amplification of the output signal. The improved circuitry could enable the signal to be more easily detected (via oscilloscope or microcontroller + analogue to digital converter). The amplified signal would be useful for investigating whether the single channel droplet detection frequency could be advanced even further, as the maximum rate is currently 10 kdps with the setup used.
- A study of illumination sources and their suitability for droplet microfluidics was conducted in this study. The study revealed that a novel automated method for enhancing droplet imaging could be proposed by synchronizing the droplet generation rate with the frequency of illumination flashing. The idea did not fit the timeframe of the study but could be investigated as future work.
- In Chapter 1, a droplet microfluidics module was presented, which included a droplet generation module, a droplet detection module, and a data processing module. This thesis focuses solely on the droplet detection module, while other PhD students were working on other modules. Although the current research aims to integrate illumination and detection modules with other modules that other students are developing, a publication on the full integration is forthcoming at the time of writing this dissertation.
- The current combination of imaging sensors and illumination sources allows for the investigation of only the size and shape of microfluidic droplets; however, it is also important to capture the morphology of droplets (contents). As of now, only a few preliminary experiments have been conducted to verify the concept (Figure 42). So far, the experiments have shown that the current state of the technology shows promise for observing cells within the droplet, however, further research is necessary since the current optical magnification and microfluidic chip cannot be used to analyse cells with high accuracy. Further, since current hardware has been analysed from the perspective that it can be

portable, cost-effective, and ready to be controlled by ML, it would be possible to develop a fully functional imaging flow cytometer that is portable, cost-effective, and enables automatic results analysis using ML.

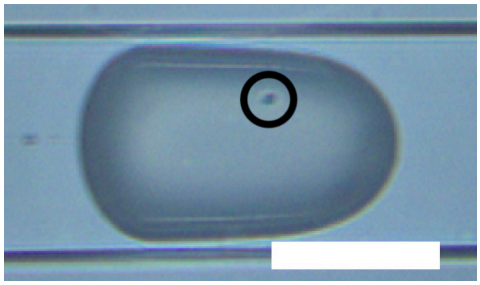

Figure 42. Microfluidic droplet containing algae cell, marked by black circle. A scale of 100 µm is represented by the white horizontal bar at the bottom of the image.

List of Figures

List of Tables

References

[1] D. R. Reyes, D. Iossifidis, P. A. Auroux, and A. Manz, “Micro Total Analysis Systems. 1. Introduction, Theory, and Technology,” *Anal. Chem.*, vol. 74, no. 12, pp. 2623–2636, Jun. 2002, doi: 10.1021/AC0202435.

[2] L. Shang, Y. Cheng, and Y. Zhao, “Emerging Droplet Microfluidics,” *Chemical Reviews*, vol. 117, no. 12. American Chemical Society, pp. 7964–8040, Jun. 28, 2017. doi: 10.1021/acs.chemrev.6b00848.

[3] Z. Chen, S. Kheiri, E. W. K. Young, and E. Kumacheva, “Trends in Droplet Microfluidics: From Droplet Generation to Biomedical Applications,” *Langmuir*, 2022, doi: 10.1021/ACS.LANGMUIR.2C00491/ASSET/IMAGES/LARGE/LA2C00491_0004.JPEG.

[4] N. Khalid, I. Kobayashi, and M. Nakajima, “Recent lab-on-chip developments for novel drug discovery,” *Wiley Interdiscip. Rev. Syst. Biol. Med.*, vol. 9, no. 4, p. e1381, Jul. 2017, doi: 10.1002/WSBM.1381.

[5] T. P. Lagus and J. F. Edd, “A review of the theory, methods and recent applications of high-throughput single-cell droplet microfluidics,” *Journal of Physics D: Applied Physics*, vol. 46, no. 11. Mar. 20, 2013. doi: 10.1088/0022-3727/46/11/114005.

[6] N. Azizipour, R. Avazpour, D. H. Rosenzweig, M. Sawan, and A. Ajji, “Evolution of Biochip Technology: A Review from Lab-on-a-Chip to Organ-on-a-Chip,” *Micromachines 2020, Vol. 11, Page 599*, vol. 11, no. 6, p. 599, Jun. 2020, doi: 10.3390/MI11060599.

[7] D. Wartmann *et al.*, “Automated, miniaturized, and integrated quality control-on-chip (QC-on-a-chip) for cell-based cancer therapy applications,” *Front. Mater.*, vol. 2, p. 60, Sep. 2015, doi: 10.3389/FMATS.2015.00060/BIBTEX.

[8] P. A. Auroux, D. Iossifidis, D. R. Reyes, and A. Manz, “Micro Total Analysis Systems. 2. Analytical Standard Operations and Applications,” *Anal. Chem.*, vol. 74, no. 12, pp. 2637–2652, Jun. 2002, doi: 10.1021/AC020239T.

[9] X. Liu, X. Zhu, G. J. Kost, J. Liu, J. Huang, and X. Liu, “The Creation of Point-of-Careology,” *Point Care*, vol. 18, no. 3, pp. 77–84, Sep. 2019, doi: 10.1097/POC.0000000000000191.

[10] S. Arshavsky-Graham and E. Segal, “Lab-on-a-Chip Devices for Point-of-Care Medical Diagnostics,” *Adv. Biochem. Eng. Biotechnol.*, vol. 179, pp. 247–265, 2022, doi: 10.1007/10_2020_127/FIGURES/9.

[11] Q. Song *et al.*, “Point-of-care testing detection methods for COVID-19,” *Lab Chip*, vol. 21, no. 9, pp. 1634–1660, May 2021, doi: 10.1039/D0LC01156H.

[12] J. Park, D. H. Han, and J. K. Park, “Towards practical sample preparation in point-of-care testing: user-friendly microfluidic devices,” *Lab Chip*, vol. 20, no. 7, pp. 1191–1203, Mar. 2020, doi: 10.1039/D0LC00047G.

[13] S. Sachdeva, R. W. Davis, and A. K. Saha, “Microfluidic Point-of-Care Testing: Commercial Landscape and Future Directions,” *Front. Bioeng. Biotechnol.*, vol. 8, p. 1537, Jan. 2021, doi: 10.3389/FBIOE.2020.602659/BIBTEX.

[14] S. M. Yang, S. Lv, W. Zhang, and Y. Cui, “Microfluidic Point-of-Care (POC) Devices in Early Diagnosis: A Review of Opportunities and Challenges,” vol. 22, no. 4, p. 1620, Feb. 2022, doi: 10.3390/S22041620.

[15] W. Jung, J. Han, J. W. Choi, and C. H. Ahn, “Point-of-care testing (POCT) diagnostic systems using microfluidic lab-on-a-chip technologies,” *Microelectron. Eng.*, vol. 132, pp. 46–57, Jan. 2015, doi: 10.1016/J.MEE.2014.09.024.

[16] T. Nguyen, S. Z. Andreasen, A. Wolff, and D. D. Bang, “From Lab on a Chip to Point of Care Devices: The Role of Open Source Microcontrollers,” *Micromachines*, vol. 9, no. 8, Aug. 2018, doi: 10.3390/MI9080403.

[17] H. Zhu, H. Zhang, S. Ni, M. Korabečná, L. Yobas, and P. Neuzil, “The vision of point-of-care PCR tests for the COVID-19 pandemic and beyond,” *TrAC Trends Anal. Chem.*, vol. 130, p. 115984, Sep. 2020, doi: 10.1016/J.TRAC.2020.115984.

[18] M. A. Chowdury and F. Khalid, “Application of microfluidic paper-based analytical device (µPAD) to detect COVID-19 in energy deprived countries,” *Int. J. Energy Res.*, vol. 45, no. 12, p. 18275, Oct. 2021, doi: 10.1002/ER.6958.

[19] G. Aubry, H. J. Lee, and H. Lu, “Advances in Microfluidics: Technical Innovations and Applications in Diagnostics and Therapeutics,” *Anal. Chem.*, vol. 95, no. 1, pp. 444–467, Jan. 2023, doi: 10.1021/ACS.ANALCHEM.2C04562/ASSET/IMAGES/LARGE/AC2C04562_0008.JPEG.

[20] S. F. Berlanda, M. Breitfeld, C. L. Dietsche, and P. S. Dittrich, “Recent Advances in Microfluidic Technology for Bioanalysis and Diagnostics,” *Anal. Chem.*, vol. 93, no. 1, pp. 311–331, Jan. 2021, doi: 10.1021/ACS.ANALCHEM.0C04366/ASSET/IMAGES/LARGE/AC0C04366_0006.JPEG.

[21] E. M. Payne, D. A. Holland-Moritz, S. Sun, and R. T. Kennedy, “High-throughput screening by droplet microfluidics: perspective into key challenges and future prospects,” *Lab Chip*, vol. 20, no. 13, pp. 2247–2262, Jun. 2020, doi: 10.1039/D0LC00347F.

[22] S. Y. Teh, R. Lin, L. H. Hung, and A. P. Lee, “Droplet microfluidics,” *Lab Chip*, vol. 8, no. 2, pp. 198–220, Jan. 2008, doi: 10.1039/B715524G.

[23] P. S. Dittrich and A. Manz, “Lab-on-a-chip: microfluidics in drug discovery,” *Nat. Rev. Drug Discov. 2006 53*, vol. 5, no. 3, pp. 210–218, Mar. 2006, doi: 10.1038/nrd1985.

[24] W. wen Liu and Y. Zhu, “‘Development and application of analytical detection techniques for droplet-based microfluidics’-A review,” *Anal. Chim. Acta*, vol. 1113, pp. 66–84, May 2020, doi: 10.1016/J.ACA.2020.03.011.

[25] N. M. M. Pires, T. Dong, U. Hanke, and N. Hoivik, “Recent developments in optical detection technologies in lab-on-a-chip devices for biosensing applications,” *Sensors (Switzerland)*, vol. 14, no. 8, pp. 15458–15479, Aug. 2014, doi: 10.3390/s140815458.

[26] C. Yi, Q. Zhang, C. W. Li, J. Yang, J. Zhao, and M. Yang, “Optical and electrochemical detection techniques for cell-based microfluidic systems,” *Anal. Bioanal. Chem.*, vol. 384, no. 6, pp. 1259–1268, Mar. 2006, doi: 10.1007/s00216-005-0252-x.

[27] M. P. Cecchini *et al.*, “Ultrafast surface enhanced resonance raman scattering detection in droplet-based microfluidic systems,” *Anal. Chem.*, vol. 83, no. 8, pp. 3076–3081, Apr. 2011, doi: 10.1021/ac103329b.

[28] L. Shang, Y. Cheng, and Y. Zhao, “Emerging Droplet Microfluidics,” 2017, doi: 10.1021/acs.chemrev.6b00848.

[29] † Honggu Chun, *,‡ and Taek Dong Chung, † Hee Chan Kim*, A. Taek Dong Chung, *, and † Hee Chan Kim*, “Cytometry and Velocimetry on a Microfluidic Chip Using Polyelectrolytic Salt Bridges,” 2005, doi: 10.1021/AC048535O.

[30] M. Tovar *et al.*, "One Sensor for Multiple Colors: Fluorescence Analysis of Microdroplets in Microbiological Screenings by Frequency-Division Multiplexing," *Anal. Chem.*, 2019, doi: 10.1021/acs.analchem.8b05451.

[31] M. Rahimi, S. Yazdanparast, and P. Rezai, "Parametric study of droplet size in an axisymmetric flow-focusing capillary device," *Chinese J. Chem. Eng.*, vol. 28, no. 4, pp. 1016–1022, Apr. 2020, doi: 10.1016/J.CJCHE.2019.12.026.

[32] S. Sohrabi, N. Kassir, and M. Keshavarz Moraveji, "Droplet microfluidics: fundamentals and its advanced applications," *RSC Adv.*, vol. 10, no. 46, pp. 27560–27574, Jul. 2020, doi: 10.1039/D0RA04566G.

[33] X. Yue *et al.*, "Breaking through the Poisson Distribution: A compact high-efficiency droplet microfluidic system for single-bead encapsulation and digital immunoassay detection," *Biosens. Bioelectron.*, vol. 211, p. 114384, Sep. 2022, doi: 10.1016/J.BIOS.2022.114384.

[34] D. J. Collins, A. Neild, A. deMello, A. Q. Liu, and Y. Ai, "The Poisson distribution and beyond: methods for microfluidic droplet production and single cell encapsulation," *Lab Chip*, vol. 15, no. 17, pp. 3439–3459, Aug. 2015, doi: 10.1039/C5LC00614G.

[35] A. C. Hatch *et al.*, "1-Million droplet array with wide-field fluorescence imaging for digital PCR," *Lab Chip*, vol. 11, no. 22, pp. 3838–3845, Oct. 2011, doi: 10.1039/C1LC20561G.

[36] J. Lim, P. Gruner, M. Konrad, and J. C. Baret, "Micro-optical lens array for fluorescence detection in droplet-based microfluidics," *Lab Chip*, vol. 13, no. 8, pp. 1472–1475, Mar. 2013, doi: 10.1039/C3LC41329B.

[37] F. Guo *et al.*, "A droplet-based, optofluidic device for high-throughput, quantitative bioanalysis," *Anal. Chem.*, vol. 84, no. 24, pp. 10745–10749, Dec. 2012, doi: 10.1021/ac302623z.

[38] H. Jiang *et al.*, "Droplet-based light-sheet fluorescence microscopy for high-throughput sample preparation, 3-D imaging and quantitative analysis on a chip," *Lab Chip*, vol. 17, no. 13, pp. 2193–2197, Jul. 2017, doi: 10.1039/c7lc00164a.

[39] V. R. Yelleswarapu, H. H. Jeong, S. Yadavali, and D. Issadore, "Ultra-high throughput detection (1 million droplets per second) of fluorescent droplets using a cell phone camera and time domain encoded optofluidics," *Lab Chip*, vol. 17, no. 6, pp. 1083–1094, Mar. 2017, doi: 10.1039/c6lc01489e.

[40] E. Schonbrun, A. R. Abate, P. E. Steinvurzel, D. A. Weitz, and K. B. Crozier, "High-throughput fluorescence detection using an integrated zone-plate array," *Lab Chip*, vol. 10, no. 7, pp. 852–856, 2010, doi: 10.1039/b923554j.

[41] J. C. Baret *et al.*, "Fluorescence-activated droplet sorting (FADS): Efficient microfluidic cell sorting based on enzymatic activity," *Lab Chip*, vol. 9, no. 13, pp. 1850–1858, Jul. 2009, Accessed: May 03, 2020. [Online]. Available: https://pubs.rsc.org/en/content/articlehtml/2009/lc/b902504a

[42] D. K. Kang *et al.*, "3D Droplet Microfluidic Systems for High-Throughput Biological Experimentation," *Anal. Chem.*, vol. 87, no. 21, pp. 10770–10778, Nov. 2015, doi: 10.1021/acs.analchem.5b02402.

[43] H. Mikami *et al.*, "Virtual-freezing fluorescence imaging flow cytometry," *Nat. Commun.*, vol. 11, no. 1, pp. 1–11, Dec. 2020, doi: 10.1038/s41467-020-14929-2.

[44] M. E. Piyasena and S. W. Graves, "The Intersection of Flow Cytometry with Microfluidics and Microfabrication," *Lab Chip*, vol. 14, no. 6, p. 1044, Mar. 2014, doi: 10.1039/C3LC51152A.

[45] J. Riordon, D. Sovilj, S. Sanner, D. Sinton, and E. W. K. Young, “Deep Learning with Microfluidics for Biotechnology,” *Trends Biotechnol.*, vol. 37, no. 3, pp. 310–324, Mar. 2019, doi: 10.1016/J.TIBTECH.2018.08.005.

[46] L. Weng and J. E. Spoonamore, “Droplet microfluidics-enabled high-throughput screening for protein engineering,” *Micromachines*, vol. 10, no. 11. MDPI AG, p. 734, Nov. 01, 2019. doi: 10.3390/mi10110734.

[47] Y. Li, A. Mahjoubfar, C. L. Chen, K. R. Niazi, L. Pei, and B. Jalali, “Deep Cytometry: Deep learning with Real-time Inference in Cell Sorting and Flow Cytometry,” *Sci. Reports 2019 91*, vol. 9, no. 1, pp. 1–12, Jul. 2019, doi: 10.1038/s41598-019-47193-6.

[48] J. Demagny *et al.*, “Combining imaging flow cytometry and machine learning for high-throughput schistocyte quantification: A SVM classifier development and external validation cohort,” *eBioMedicine*, vol. 83, p. 104209, Sep. 2022, doi: 10.1016/J.EBIOM.2022.104209.

[49] S. Luo *et al.*, “Machine-Learning-Assisted Intelligent Imaging Flow Cytometry: A Review,” *Adv. Intell. Syst.*, vol. 3, no. 11, p. 2100073, Nov. 2021, doi: 10.1002/AISY.202100073.

[50] Y. Zhu and Q. Fang, “Analytical detection techniques for droplet microfluidics-A review,” *Anal. Chim. Acta*, vol. 787, pp. 24–35, Jul. 2013, doi: 10.1016/j.aca.2013.04.064.

[51] K. Pärnamets *et al.*, “Optical Detection Methods for High-Throughput Fluorescent Droplet Microflow Cytometry,” *Micromachines 2021, Vol. 12, Page 345*, vol. 12, no. 3, p. 345, Mar. 2021, doi: 10.3390/MI12030345.

[52] S. Lv *et al.*, “A Microfluidic Detection System for Bladder Cancer Tumor Cells,” *Micromachines*, vol. 10, no. 12, p. 871, Dec. 2019, doi: 10.3390/mi10120871.

[53] F. S. Ligler and J. S. Kim, *The microflow cytometer*. Pan Stanford Publishing, 2010.

[54] R. Uhl, “Arc Lamps and Monochromators for Fluorescence Microscopy,” *Cold Spring Harb. Protoc.*, vol. 2012, no. 9, p. pdb.top071001, Sep. 2012, doi: 10.1101/PDB.TOP071001.

[55] D. C. Peters, “A comparison of mercury arc lamp and laser illumination for flow cytometers.,” *http://dx.doi.org/10.1177/27.1.374581*, vol. 27, no. 1, pp. 241–245, Jan. 2017, doi: 10.1177/27.1.374581.

[56] K. Hölz, J. Lietard, and M. M. Somoza, “High-Power 365 nm UV LED Mercury Arc Lamp Replacement for Photochemistry and Chemical Photolithography,” *ACS Sustain. Chem. Eng.*, vol. 5, no. 1, pp. 828–834, Jan. 2017, doi: 10.1021/acssuschemeng.6b02175.

[57] V. I. Batshev, A. A. Blokhin, and A. S. Belov, “LED illumination module for fluorescence and spectroscopic studies in microscopy,” *J. Phys. Conf. Ser.*, vol. 1421, no. 1, Dec. 2019, doi: 10.1088/1742-6596/1421/1/012036.

[58] J. Picot, C. L. Guerin, C. Le Van Kim, and C. M. Boulanger, “Flow cytometry: retrospective, fundamentals and recent instrumentation,” *Cytotechnology*, vol. 64, no. 2, pp. 109–130, Mar. 2012, doi: 10.1007/s10616-011-9415-0.

[59] T. Regan Baird, D. Kaufman, and C. M. Brown, “Mercury Free Microscopy: An Opportunity for Core Facility Directors,” *J. Biomol. Tech.*, vol. 25, no. 2, p. 48, 2014, doi: 10.7171/JBT.14-2502-001.

[60] D. Caputo *et al.*, “Microfluidic chip with integrated a-Si:H photodiodes for chemiluminescence-based bioassays,” *IEEE Sens. J.*, vol. 13, no. 7, pp. 2595–2602, 2013, doi: 10.1109/JSEN.2013.2256889.

[61] J. M. Cooper, “Challenges in lab-on-a-chip technology,” *Front. Lab a Chip Technol.*, vol. 1, p. 1, Sep. 2022, doi: 10.3389/FRLCT.2022.979398.

[62] H. Zhu, Z. Fohlerová, J. Pekárek, E. Basova, and P. Neužil, “Recent advances in lab-on-a-chip technologies for viral diagnosis,” *Biosens. Bioelectron.*, vol. 153, p. 112041, Apr. 2020, doi: 10.1016/J.BIOS.2020.112041.

[63] Y. Gong, N. Fan, X. Yang, B. Peng, and H. Jiang, “New advances in microfluidic flow cytometry,” *Electrophoresis*, vol. 40, no. 8, pp. 1212–1229, Apr. 2019, doi: 10.1002/ELPS.201800298.

[64] “Coulter Electronics (1976 - 2009).” https://www.beckman.fr/resources/technologies/flow-cytometry/history/coulter-electronics (accessed Feb. 15, 2023).

[65] Exceder Scientific Leasing Company, “How Much Does A Flow Cytometer Cost in 2022 | Excedr,” 2022. https://www.excedr.com/blog/how-much-does-a-flow-cytometer-cost/ (accessed Jan. 10, 2023).

[66] S. Zhang, Z. Li, and Q. Wei, “Smartphone-based cytometric biosensors for point-of-care cellular diagnostics,” *Nanotechnol. Precis. Eng.*, vol. 3, no. 1, pp. 32–42, Jan. 2020, doi: 10.1016/j.npe.2019.12.004.

[67] T. Kremers, S. Thelen, N. Bosbach, and U. Schnakenberg, “PortaDrop: A portable digital microfluidic platform providing versatile opportunities for Lab-On-A-Chip applications,” *PLoS One*, vol. 15, no. 9, p. e0238581, Sep. 2020, doi: 10.1371/JOURNAL.PONE.0238581.

[68] T. Xie, P. Wang, L. Wu, B. Sun, Q. Zhao, and G. Li, “A hand-powered microfluidic system for portable and low-waste sample discretization,” *Lab Chip*, vol. 21, no. 18, pp. 3429–3437, Sep. 2021, doi: 10.1039/D1LC00448D.

[69] A. Suea-Ngam, P. D. Howes, M. Srisa-Art, and A. J. Demello, “Droplet microfluidics: from proof-of-concept to real-world utility?,” *Chem. Commun.*, vol. 55, no. 67, pp. 9895–9903, Aug. 2019, doi: 10.1039/C9CC04750F.

[70] L. Zhao *et al.*, “Smartphone-Based Quantitative Fluorescence Detection of Flowing Droplets Using Embedded Ambient Light Sensor,” *IEEE Sens. J.*, vol. 21, no. 4, pp. 4451–4461, Feb. 2021, doi: 10.1109/JSEN.2020.3029261.

[71] L. F. Capitán-Vallvey and A. J. Palma, “Recent developments in handheld and portable optosensing-A review,” *Analytica Chimica Acta*, vol. 696, no. 1–2. Elsevier, pp. 27–46, Jun. 24, 2011. doi: 10.1016/j.aca.2011.04.005.

[72] T. Blasi *et al.*, “Label-free cell cycle analysis for high-throughput imaging flow cytometry,” *Nat. Commun. 2016 71*, vol. 7, no. 1, pp. 1–9, Jan. 2016, doi: 10.1038/ncomms10256.

[73] J. Howell, T. C. Hammarton, Y. Altmann, and M. Jimenez, “High-speed particle detection and tracking in microfluidic devices using event-based sensing,” *Lab Chip*, vol. 20, no. 16, pp. 3024–3035, Aug. 2020, doi: 10.1039/D0LC00556H.

[74] B. Damit, “Droplet-based microfluidics detector for bioaerosol detection,” *Aerosol Sci. Technol.*, vol. 51, no. 4, pp. 488–500, Apr. 2017, doi: 10.1080/02786826.2016.1275515/SUPPL_FILE/UAST_A_1275515_SM4643.ZIP.

[75] C. J. Hsiao *et al.*, “Enhancement of the stability of chlorophyll using chlorophyll-encapsulated polycaprolactone microparticles based on droplet microfluidics,” *Food Chem.*, vol. 306, p. 125300, Feb. 2020, doi: 10.1016/J.FOODCHEM.2019.125300.

[76] A. Baccouche *et al.*, "Massively parallel and multiparameter titration of biochemical assays with droplet microfluidics," *Nat. Protoc. 2017 129*, vol. 12, no. 9, pp. 1912–1932, Aug. 2017, doi: 10.1038/nprot.2017.092.

[77] M. Grafton *et al.*, "Design of a multi-stage microfluidics system for high-speed flow cytometry and closed system cell sorting for cytomics," *Proc. SPIE 6859, Imaging, Manip. Anal. Biomol. Cells, Tissues VI, 68590V*, vol. 6859, pp. 187–198, Feb. 2008, doi: 10.1117/12.764037.

[78] M. M. Islam, A. Loewen, and P. B. Allen, "Simple, low-cost fabrication of acrylic based droplet microfluidics and its use to generate DNA-coated particles," *Sci. Rep.*, vol. 8, no. 1, p. 8763, Dec. 2018, doi: 10.1038/s41598-018-27037-5.

[79] X. Huang, J. Guo, X. Wang, M. Yan, and Y. Kang, "A Contact-Imaging Based Micro uidic Cytometer with Machine-Learning for Single-Frame Super-Resolution Processing," vol. i, 2014.

[80] Y. Ding, P. D. Howes, and A. J. Demello, "Recent advances in droplet microfluidics," *Anal. Chem.*, vol. 92, no. 1, pp. 132–149, Jan. 2020, doi: 10.1021/ACS.ANALCHEM.9B05047/ASSET/IMAGES/LARGE/AC9B05047_0009.JPEG.

[81] M. T. Guo, A. Rotem, J. A. Heyman, and D. A. Weitz, "Droplet microfluidics for high-throughput biological assays," *Lab on a Chip*, vol. 12, no. 12. Royal Society of Chemistry, pp. 2146–2155, Jun. 21, 2012. doi: 10.1039/c2lc21147e.

[82] R. M. Maceiczyk, D. Hess, F. W. Y. Chiu, S. Stavrakis, and A. J. DeMello, "Differential detection photothermal spectroscopy: Towards ultra-fast and sensitive label-free detection in picoliter & femtoliter droplets," *Lab Chip*, vol. 17, no. 21, pp. 3654–3663, Nov. 2017, doi: 10.1039/c7lc00946a.

[83] A. M. Kaushik, K. Hsieh, and T. H. Wang, "Droplet microfluidics for high-sensitivity and high-throughput detection and screening of disease biomarkers," *Wiley Interdisciplinary Reviews: Nanomedicine and Nanobiotechnology*, vol. 10, no. 6. Wiley-Blackwell, Nov. 01, 2018. doi: 10.1002/wnan.1522.

[84] J. Yang, R. Tu, H. Yuan, Q. Wang, and L. Zhu, "Recent advances in droplet microfluidics for enzyme and cell factory engineering," *Crit. Rev. Biotechnol.*, vol. 41, no. 7, pp. 1023–1045, 2021, doi: 10.1080/07388551.2021.1898326.

[85] M. W. Davidson and M. Abramowitz, "OPTICAL MICROSCOPY", Accessed: Feb. 18, 2023. [Online]. Available: http://microscopy.fsu.edu

[86] P. Zhou, H. He, H. Ma, S. Wang, and S. Hu, "A Review of Optical Imaging Technologies for Microfluidics," *Micromachines 2022, Vol. 13, Page 274*, vol. 13, no. 2, p. 274, Feb. 2022, doi: 10.3390/MI13020274.

[87] S. Sarkar, N. Cohen, P. Sabhachandani, and T. Konry, "Phenotypic drug profiling in droplet microfluidics for better targeting of drug-resistant tumors," *Lab Chip*, vol. 15, no. 23, pp. 4441–4450, Nov. 2015, doi: 10.1039/C5LC00923E.

[88] T. Fu, Y. Wu, Y. Ma, and H. Z. Li, "Droplet formation and breakup dynamics in microfluidic flow-focusing devices: From dripping to jetting," *Chem. Eng. Sci.*, vol. 84, pp. 207–217, Dec. 2012, doi: 10.1016/J.CES.2012.08.039.

[89] T. Pirbodaghi, D. Vigolo, S. Akbari, and A. DeMello, "Investigating the fluid dynamics of rapid processes within microfluidic devices using bright-field microscopy," *Lab Chip*, vol. 15, no. 9, pp. 2140–2144, Apr. 2015, doi: 10.1039/C5LC00175G.

[90] Y. C. Tung, M. Zhang, C. T. Lin, K. Kurabayashi, and S. J. Skerlos, "PDMS-based opto-fluidic micro flow cytometer with two-color, multi-angle fluorescence detection capability using PIN photodiodes," *Sensors Actuators, B Chem.*, vol. 98, no. 2–3, pp. 356–367, Mar. 2004, doi: 10.1016/j.snb.2003.10.010.

[91] K. M. McKinnon, “Flow cytometry: An overview,” *Curr. Protoc. Immunol.*, vol. 2018, no. 1, pp. 5.1.1-5.1.11, Feb. 2018, doi: 10.1002/cpim.40.

[92] J. Teimour Maleki, T. Fricke, J. T. Quesenberry, P. W. Todd, and J. F. Leary, “Point-of-care, portable microfluidic blood analyzer system,” *https://doi.org/10.1117/12.909051*, vol. 8251, pp. 96–108, Feb. 2012, doi: 10.1117/12.909051.

[93] M. Sun, Z. Li, and Q. Yang, “µdroPi: A Hand-Held Microfluidic Droplet Imager and Analyzer Built on Raspberry Pi,” *J. Chem. Educ.*, vol. 96, no. 6, pp. 1152–1156, Jun. 2019, doi: 10.1021/acs.jchemed.8b00975.

[94] M. Sesen and G. Whyte, “Image-Based Single Cell Sorting Automation in Droplet Microfluidics,” *Sci. Rep.*, vol. 10, no. 1, pp. 1–14, Dec. 2020, doi: 10.1038/s41598-020-65483-2.

[95] M. Vaithiyanathan, N. Safa, and A. T. Melvin, “FluorocellTrack: An algorithm for automated analysis of high-throughput droplet microfluidic data,” *PLoS One*, vol. 14, no. 5, May 2019, doi: 10.1371/journal.pone.0215337.

[96] Y. Saeys, S. Van Gassen, and B. N. Lambrecht, “Computational flow cytometry: Helping to make sense of high-dimensional immunology data,” *Nature Reviews Immunology*, vol. 16, no. 7. Nature Publishing Group, pp. 449–462, Jul. 01, 2016. doi: 10.1038/nri.2016.56.

[97] H. Yang *et al.*, “A droplet-based microfluidic flow cytometry enabling absolute quantification of single-cell proteins leveraging constriction channel,” *Microfluid. Nanofluidics*, vol. 25, no. 4, pp. 1–11, Apr. 2021, doi: 10.1007/S10404-021-02427-W/FIGURES/5.

[98] A. Adan, G. Alizada, Y. Kiraz, Y. Baran, and A. Nalbant, *Flow cytometry: basic principles and applications*, vol. 37, no. 2. Taylor and Francis Ltd, 2017, pp. 163–176. doi: 10.3109/07388551.2015.1128876.

[99] Y. Han, Y. Gu, A. C. Zhang, and Y. H. Lo, “Review: Imaging technologies for flow cytometry,” *Lab on a Chip*, vol. 16, no. 24. Royal Society of Chemistry, pp. 4639–4647, Nov. 29, 2016. doi: 10.1039/c6lc01063f.

[100] H. M. Shapiro, *Practical Flow Cytometry*, Fourth Edi. New York: a John Wiley & Sons, Inc, 2003. [Online]. Available: https://ia801608.us.archive.org/23/items/PracticalFlowCytometryShapiro/Practical Flow Cytometry_Shapiro.pdf

[101] S. Stavrakis, G. Holzner, J. Choo, and A. DeMello, “High-throughput microfluidic imaging flow cytometry,” *Curr. Opin. Biotechnol.*, vol. 55, pp. 36–43, Feb. 2019, doi: 10.1016/j.copbio.2018.08.002.

[102] A. S. Rane, J. Rutkauskaite, A. deMello, and S. Stavrakis, “High-Throughput Multi-parametric Imaging Flow Cytometry,” *Chem*, vol. 3, no. 4, pp. 588–602, Oct. 2017, doi: 10.1016/j.chempr.2017.08.005.

[103] H. M. Shapiro and W. G. Telford, “Lasers for Flow Cytometry: Current and Future Trends,” *Curr. Protoc. Cytom.*, vol. 83, no. 1, pp. 1.9.1-1.9.21, Jan. 2018, doi: 10.1002/cpcy.30.

[104] D. V. Voronin *et al.*, “Detection of rare objects by flow cytometry: Imaging, cell sorting, and deep learning approaches,” *International Journal of Molecular Sciences*, vol. 21, no. 7. MDPI AG, p. 2323, Apr. 01, 2020. doi: 10.3390/ijms21072323.

[105] A. Adan, G. Alizada, Y. Kiraz, Y. Baran, and A. Nalbant, “Flow cytometry: basic principles and applications,” *https://doi.org/10.3109/07388551.2015.1128876*, vol. 37, no. 2, pp. 163–176, Feb. 2016, doi: 10.3109/07388551.2015.1128876.

[106] X. Yuan, T. Darcie, J. J. D. McKendry, M. D. Dawson, M. J. Strain, and J. Stewart Aitchison, “LED Excitation of an Imaging Cytometer for Bead-Based Immunoassay,” *IEEE Photonics Technol. Lett.*, vol. 33, no. 16, pp. 892–895, Aug. 2021, doi: 10.1109/LPT.2021.3070079.

[107] “PRODUCT FAMILY DATA SHEET XLamp ® XQ-E LEDs,” 2013, Accessed: Feb. 27, 2023. [Online]. Available: www.cree-led.com

[108] A. R. Miller *et al.*, “Portable, Battery-Operated, Low-Cost, Bright Field and Fluorescence Microscope,” *PLoS One*, vol. 5, no. 8, p. e11890, 2010, doi: 10.1371/JOURNAL.PONE.0011890.

[109] X. Qian *et al.*, “Improved optical imaging of high aspect ratio nanostructures using dark-field microscopy,” *Nanotechnology*, vol. 30, no. 28, p. 285301, Apr. 2019, doi: 10.1088/1361-6528/AB13DE.

[110] P. F. Gao, G. Lei, and C. Z. Huang, “Dark-Field Microscopy: Recent Advances in Accurate Analysis and Emerging Applications,” *Anal. Chem.*, vol. 93, no. 11, pp. 4707–4726, Mar. 2021, doi: 10.1021/ACS.ANALCHEM.0C04390/ASSET/IMAGES/LARGE/AC0C04390_0012.JPEG.

[111] D. A. Bui and P. C. Hauser, “Analytical devices based on light-emitting diodes - A review of the state-of-the-art,” *Analytica Chimica Acta*, vol. 853, no. 1. Elsevier, pp. 46–58, Jan. 01, 2015. doi: 10.1016/j.aca.2014.09.044.

[112] K. K. Aswani, “Emerging LED Technologies for Fluorescence Microscopy,” *Micros. Today*, vol. 24, no. 4, pp. 22–27, Jul. 2016, doi: 10.1017/S1551929516000407.

[113] K. Aswani, T. Jinadasa, and C. M. Brown, “Fluorescence Microscopy Light Sources,” *Micros. Today*, vol. 20, no. 4, pp. 22–28, Jul. 2012, doi: 10.1017/S1551929512000399.

[114] “Zeiss HAL 100 Light Source – Nanodyne Measurement Systems.” https://www.nano-dyne.com/led-microscope-lights/zeiss-hal-100-light-source/ (accessed Feb. 26, 2023).

[115] “ZEISS Colibri: Multicolor LED Light Source.” https://www.zeiss.com/microscopy/en/products/accessories/colibri.html#downloads (accessed Feb. 27, 2023).

[116] M. Macka, T. Piasecki, and P. K. Dasgupta, “Light-Emitting Diodes for Analytical Chemistry,” *Annu. Rev. Anal. Chem.*, vol. 7, no. 1, pp. 183–207, Jun. 2014, doi: 10.1146/annurev-anchem-071213-020059.

[117] “PRODUCT FAMILY DATA SHEET XLamp ® XP-E LEDs PRODUCT DESCRIPTION,” 2008, Accessed: Feb. 27, 2023. [Online]. Available: www.cree-led.com

[118] V. Bormuth, J. Howard, and E. Schäffer, “LED illumination for video-enhanced DIC imaging of single microtubules,” *J. Microsc.*, vol. 226, no. 1, pp. 1–5, Apr. 2007, doi: 10.1111/J.1365-2818.2007.01756.X.

[119] G. Martin, H. T. Agostini, and L. L. Hansen, “Light emitting diode microscope illumination for green fluorescent protein or fluorescein isothiocyanate epifluorescence,” *Biotechniques*, vol. 38, no. 2, pp. 204–206, May 2005, doi: 10.2144/05382BM06/ASSET/IMAGES/LARGE/FIGURE2.JPEG.

[120] P. Herman, B. P. Maliwal, H. J. Lin, and J. R. Lakowicz, “Frequency-domain fluorescence microscopy with the LED as a light source,” *J. Microsc.*, vol. 203, no. 2, pp. 176–181, Aug. 2001, doi: 10.1046/J.1365-2818.2001.00943.X.

[121] D. F. Albeanu, E. Soucy, T. F. Sato, M. Meister, and V. N. Murthy, “LED Arrays as Cost Effective and Efficient Light Sources for Widefield Microscopy,” *PLoS One*, vol. 3, no. 5, p. e2146, May 2008, doi: 10.1371/JOURNAL.PONE.0002146.
[122] H. M. Shapiro, “The evolution of cytometers,” *Cytometry*, vol. 58A, no. 1, pp. 13–20, Mar. 2004, doi: 10.1002/cyto.a.10111.
[123] O. Svelto, *Principles of lasers*. Springer US, 2010. doi: 10.1007/978-1-4419-1302-9.
[124] W. G. G. Telford, “Lasers in Flow Cytometry,” 2011, pp. 373–409. doi: 10.1016/B978-0-12-374912-3.00015-8.
[125] “How semiconductor laser diodes work - Explain that Stuff.” https://www.explainthatstuff.com/semiconductorlaserdiodes.html (accessed Mar. 03, 2023).
[126] J. Panwar, A. Autour, and C. A. Merten, “Design and construction of a microfluidics workstation for high-throughput multi-wavelength fluorescence and transmittance activated droplet analysis and sorting,” *Nat. Protoc. 2023*, pp. 1–57, Jan. 2023, doi: 10.1038/s41596-022-00796-2.
[127] Y. Zhou, Z. Yu, M. Wu, Y. Lan, C. Jia, and J. Zhao, “Single-cell sorting using integrated pneumatic valve droplet microfluidic chip,” *Talanta*, vol. 253, p. 124044, Feb. 2023, doi: 10.1016/j.talanta.2022.124044.
[128] H. T. Nguyen, M. Marquis, M. Anton, and S. Marze, “Studying the real-time interplay between triglyceride digestion and lipophilic micronutrient bioaccessibility using droplet microfluidics. 2 application to various oils and (pro)vitamins,” *Food Chem.*, vol. 275, pp. 661–667, Mar. 2019, doi: 10.1016/J.FOODCHEM.2018.09.126.
[129] “Difference between gas lasers, solid-state lasers, and semiconductor lasers | Laser welding | Automated Welding Basics | KEYENCE America.” https://www.keyence.com/ss/products/measure/welding/laser/difference.jsp (accessed Mar. 03, 2023).
[130] “OSRAM Metal Can TO56, PLT5 488 Color Lasers (EEL) | ams OSRAM.” https://ams-osram.com/products/lasers/color-lasers-eel/osram-metal-can-to56-plt5-488 (accessed Mar. 02, 2023).
[131] F. Mubaid *et al.*, “Fluorescence microscope light source stability,” *Histochem. Cell Biol.*, vol. 151, no. 4, pp. 357–366, Apr. 2019, Accessed: Jan. 16, 2023. [Online]. Available: https://link.springer.com/article/10.1007/s00418-019-01776-6
[132] “Microscope Illuminating System HBO 100”, Accessed: Jan. 18, 2023. [Online]. Available: www.zeiss.de
[133] “HBO 100 W/2 Mercury Bulb.” https://microscopecentral.com/collections/osram/products/hbo-100-w-2-mercury-bulb-for-fluorescence-microscopes (accessed Feb. 21, 2023).
[134] J. Lim, J. Vrignon, P. Gruner, C. S. Karamitros, M. Konrad, and J. C. Baret, “Ultra-high throughput detection of single cell β-galactosidase activity in droplets using micro-optical lens array,” *Appl. Phys. Lett.*, vol. 103, no. 20, p. 203704, Nov. 2013, doi: 10.1063/1.4830046.
[135] “Operating Manual N HBO 103 and N XBO 75 Microscope Illuminating Systems”, Accessed: Feb. 24, 2023. [Online]. Available: www.zeiss.de/micro
[136] “XBO 75 W/2 OFR | OSRAM PIA.” https://www.osram.com/ecat/XBO Xenon short-arc lamps without reflector-XBO Xenon short-arc lamps-Discharge lamps-Industry-Specialty Lighting/com/en/GPS01_1028545/ZMP_56401/ (accessed Feb. 25, 2023).

[137] “ZEISS Microscopy Online Campus | Xenon Arc Lamps.” https://zeiss-campus.magnet.fsu.edu/articles/lightsources/xenonarc.html (accessed Feb. 20, 2023).
[138] Y. J. Y. Wang, D. I. Adeoye, Y. J. Y. Wang, and M. G. Roper, “Increasing insulin measurement throughput by fluorescence anisotropy imaging immunoassays,” *Anal. Chim. Acta*, vol. 1212, p. 339942, Jun. 2022, doi: 10.1016/J.ACA.2022.339942.
[139] R. E. Gerver *et al.*, “Programmable microfluidic synthesis of spectrally encoded microspheres,” *Lab Chip*, vol. 12, no. 22, pp. 4716–4723, Oct. 2012, doi: 10.1039/C2LC40699C.
[140] F. Mekki-Berrada, J. Xie, and S. A. Khan, “High-throughput and High-speed Absorbance Measurements in Microfluidic Droplets using Hyperspectral Imaging,” *Chem. - Methods*, vol. 2, no. 5, p. e202100086, May 2022, doi: 10.1002/CMTD.202100086.
[141] J. Probst, P. Howes, P. Arosio, S. Stavrakis, and A. Demello, “Broad-Band Spectrum, High-Sensitivity Absorbance Spectroscopy in Picoliter Volumes,” *Anal. Chem.*, vol. 93, no. 21, pp. 7673–7681, Jun. 2021, doi: 10.1021/ACS.ANALCHEM.1C00587/ASSET/IMAGES/MEDIUM/AC1C00587_M002.GIF.
[142] “ZEISS Microscopy Online Campus | Tungsten-Halogen Lamps.” https://zeiss-campus.magnet.fsu.edu/articles/lightsources/tungstenhalogen.html (accessed Feb. 20, 2023).
[143] H. Zhang *et al.*, “An ultra high-efficiency droplet microfluidics platform using automatically synchronized droplet pairing and merging,” *Lab Chip*, vol. 20, no. 21, pp. 3948–3959, Oct. 2020, doi: 10.1039/D0LC00757A.
[144] “Nikon Eclipse LV100N.” https://www.microscope.healthcare.nikon.com/products/polarizing-microscopes/eclipse-lv100n-pol (accessed Feb. 18, 2023).
[145] G. P. Rutkowski, I. Azizov, E. Unmann, M. Dudek, and B. A. Grimes, “Microfluidic droplet detection via region-based and single-pass convolutional neural networks with comparison to conventional image analysis methodologies,” *Mach. Learn. with Appl.*, vol. 7, p. 100222, Mar. 2022, doi: 10.1016/J.MLWA.2021.100222.
[146] “Specifications | ECLIPSE Ti2 Series | Nikon Instruments Inc.” https://www.microscope.healthcare.nikon.com/products/inverted-microscopes/eclipse-ti2-series/specifications (accessed Feb. 18, 2023).
[147] “ZEISS Microscopy Online Campus | Metal Halide Lamps.” https://zeiss-campus.magnet.fsu.edu/articles/lightsources/metalhalide.html (accessed Feb. 20, 2023).
[148] J. E. Ortiz-Cárdenas *et al.*, “Towards spatially-organized organs-on-chip: Photopatterning cell-laden thiol-ene and methacryloyl hydrogels in a microfluidic device,” *Organs-on-a-Chip*, vol. 4, p. 100018, Dec. 2022, doi: 10.1016/J.OOC.2022.100018.
[149] A. Banerjee, A. Pais, I. Papautsky, and D. Klotzkin, “A polarization isolation method for high-sensitivity, low-cost on-chip fluorescence detection for microfluidic lab-on-a-chip,” *IEEE Sens. J.*, vol. 8, no. 5, pp. 621–627, May 2008, doi: 10.1109/JSEN.2008.918961.

[150] P. Guang *et al.*, "Development of microfluidic flow cytometry capable of characterization of single-cell intrinsic structural and electrical parameters," *J. Micromechanics Microengineering*, vol. 32, no. 3, p. 035007, Feb. 2022, doi: 10.1088/1361-6439/AC5171.
[151] "Sharp GH04850B2G laser diode datasheet," 2020.
[152] "ZEISS Axiocam Microscope Cameras for Science and Research." https://www.zeiss.com/microscopy/en/products/cameras.html (accessed Mar. 05, 2023).
[153] "Digital Microscope Color Camera | Olympus LS." https://www.olympus-lifescience.com/en/camera/color/ (accessed Mar. 05, 2023).
[154] H. Mikami, T. Miura, Y. Ozeki, and K. Goda, "High-throughput fluorescence imaging flow cytometry with light-sheet excitation and machine learning (Conference Presentation)," in *High-Speed Biomedical Imaging and Spectroscopy III: Toward Big Data Instrumentation and Management*, Mar. 2018, vol. 10505, p. 15. doi: 10.1117/12.2289708.
[155] N. Smith *et al.*, "EMCCD technology and its impact on rapid low-light photometry," in *Optical and Infrared Detectors for Astronomy*, Sep. 2004, vol. 5499, p. 162. doi: 10.1117/12.549789.
[156] D. Dussault and P. Hoess, "Noise performance comparison of ICCD with CCD and EMCCD cameras," in *Infrared Systems and Photoelectronic Technology*, Oct. 2004, vol. 5563, p. 195. doi: 10.1117/12.561839.
[157] N. Bardiya, J. W. Choi, and S. I. Chang, "Analysis of single nucleotide polymorphism in human angiogenin using droplet-based microfluidics," *Biochip J.*, vol. 8, no. 1, pp. 15–21, Mar. 2014, doi: 10.1007/s13206-014-8103-5.
[158] M. Kim *et al.*, "Optofluidic ultrahigh-throughput detection of fluorescent drops," *Lab Chip*, vol. 15, no. 6, pp. 1417–1423, Mar. 2015, doi: 10.1039/c4lc01465k.
[159] "Photomultiplier tube R7205-01 | Hamamatsu Photonics." https://www.hamamatsu.com/eu/en/product/type/R7205-01/index.html (accessed Feb. 09, 2020).
[160] "Microchannel plate photomultiplier tube R3809U-50 | Hamamatsu Photonics." https://www.hamamatsu.com/eu/en/product/type/R3809U-50/index.html (accessed Feb. 09, 2020).
[161] R. H. Cole, N. de Lange, Z. J. Gartner, and A. R. Abate, "Compact and modular multicolour fluorescence detector for droplet microfluidics," *Lab Chip*, vol. 15, no. 13, pp. 2754–2758, Jul. 2015, doi: 10.1039/C5LC00333D.
[162] LaserComponents, "Silicon Avalanche Photodiodes." https://www.lasercomponents.com/fileadmin/user_upload/home/Datasheets/lc/application-reports/lc-apd/si-apds.pdf (accessed May 02, 2020).
[163] "Si APD (avalanche photodiode)."
[164] B. Nabet, *Photodetectors: Materials, Devices and Applications*. Elsevier Inc., 2015. doi: 10.1016/C2014-0-01868-0.
[165] A. M. Kaushik, K. Hsieh, L. Chen, D. J. Shin, J. C. Liao, and T. H. Wang, "Accelerating bacterial growth detection and antimicrobial susceptibility assessment in integrated picoliter droplet platform," *Biosens. Bioelectron.*, vol. 97, pp. 260–266, Nov. 2017, doi: 10.1016/J.BIOS.2017.06.006.
[166] Z. Gao *et al.*, "A Facile Strategy for Visualizing and Modulating Droplet-Based Microfluidics," *Micromachines*, vol. 10, no. 5, p. 291, Apr. 2019, doi: 10.3390/mi10050291.

[167] J. Yu, G. Sun, N. W. Lin, S. V. Vadanan, S. Lim, and C. H. Chen, "Intelligent optofluidic analysis for ultrafast single bacterium profiling of cellulose production and morphology," *Lab Chip*, vol. 20, no. 3, pp. 626–633, Feb. 2020, doi: 10.1039/c9lc01105f.

[168] J. W. Choi, D. K. Kang, H. Park, A. J. Demello, and S. I. Chang, "High-throughput analysis of protein-protein interactions in picoliter-volume droplets using fluorescence polarization," *Anal. Chem.*, vol. 84, no. 8, pp. 3849–3854, Apr. 2012, doi: 10.1021/ac300414g.

[169] D. Vercruysse *et al.*, "Three-part differential of unlabeled leukocytes with a compact lens-free imaging flow cytometer," *Lab Chip*, vol. 15, no. 4, pp. 1123–1132, 2015, doi: 10.1039/c4lc01131g.

[170] J. Zhao and Z. You, "A microflow cytometer with a rectangular Quasi-flat-top laser spot," *Sensors (Switzerland)*, vol. 16, no. 9, Sep. 2016, doi: 10.3390/s16091474.

[171] J. Clausell-Tormos *et al.*, "Droplet-Based Microfluidic Platforms for the Encapsulation and Screening of Mammalian Cells and Multicellular Organisms," *Chem. Biol.*, vol. 15, no. 5, pp. 427–437, 2008, doi: 10.1016/j.chembiol.2008.04.004.

[172] B. L. Fiedler *et al.*, "Droplet Microfluidic Flow Cytometer For Sorting On Transient Cellular Responses Of Genetically-Encoded Sensors.," *Anal. Chem.*, vol. 89, no. 1, pp. 711–719, 2017, doi: 10.1021/acs.analchem.6b03235.

[173] Y. Qin *et al.*, "A Fluorescence-Activated Single-Droplet Dispenser for High Accuracy Single-Droplet and Single-Cell Sorting and Dispensing," *Anal. Chem.*, 2019, doi: 10.1021/acs.analchem.9b01017.

[174] X. Zhu *et al.*, "A 'quasi' confocal droplet reader based on laser-induced fluorescence (LIF) cytometry for highly-sensitive and contamination-free detection," *Talanta*, vol. 206, p. 120200, Jan. 2020, doi: 10.1016/J.TALANTA.2019.120200.

[175] J.-L. Fu, Q. Fang, T. Zhang, X.-H. Jin, and Z.-L. Fang, "Laser-Induced Fluorescence Detection System for Microfluidic Chips Based on an Orthogonal Optical Arrangement," 2006, doi: 10.1021/ac060153q.

[176] X. Geng, M. Shi, H. Ning, C. Feng, and Y. Guan, "A compact and low-cost laser induced fluorescence detector with silicon based photodetector assembly for capillary flow systems," *Talanta*, vol. 182, pp. 279–284, May 2018, doi: 10.1016/J.TALANTA.2018.01.076.

[177] N. T. Nguyen, S. Lassemono, and F. A. Chollet, "Optical detection for droplet size control in microfluidic droplet-based analysis systems," *Sensors Actuators, B Chem.*, vol. 117, no. 2, pp. 431–436, Oct. 2006, doi: 10.1016/j.snb.2005.12.010.

[178] G. Aubry *et al.*, "A multicolor microfluidic droplet dye laser with single mode emission," *Appl. Phys. Lett.*, vol. 98, no. 11, p. 111111, Mar. 2011, doi: 10.1063/1.3565242.

[179] Y. R. Smith *et al.*, "Heterogenous integration of a thin-film GaAs photodetector and a microfluidic device on a silicon substrate," *J. Micromechanics Microengineering*, vol. 21, no. 3, p. 035008, Feb. 2011, doi: 10.1088/0960-1317/21/3/035008.

[180] L. M. Lee, X. Cui, and C. Yang, "The application of on-chip optofluidic microscopy for imaging Giardia lamblia trophozoites and cysts," *Biomed. Microdevices*, vol. 11, no. 5, pp. 951–958, Oct. 2009, doi: 10.1007/S10544-009-9312-X/FIGURES/3.

[181] S. Hengoju *et al.*, "Optofluidic detection setup for multi-parametric analysis of microbiological samples in droplets," *Biomicrofluidics*, vol. 14, no. 2, p. 024109, Apr. 2020, doi: 10.1063/1.5139603.
[182] "TOP 10 COMPANIES IN FLOW CYTOMETRY MARKET | Meticulous Blog." https://meticulousblog.org/top-10-companies-in-flow-cytometry-market/ (accessed Mar. 06, 2023).
[183] "Top 5 Vendors in the Global Flow Cytometry Market from 2016 to 2020: Technavio | Business Wire." https://www.businesswire.com/news/home/20161004005171/en/Top-5-Vendors-in-the-Global-Flow-Cytometry-Market-from-2016-to-2020-Technavio (accessed Mar. 06, 2023).
[184] "FACSymphony™ A5 | High-Parameter Cell Analyzer." https://www.bdbiosciences.com/en-us/products/instruments/flow-cytometers/research-cell-analyzers/bd-facsymphony-a5 (accessed Mar. 06, 2023).
[185] "BD FACSymphony™ A5 SE Flow Cytometer User's Guide," 2021.
[186] "BD FACSymphony ™ A5 Cell Analyzer Special Order Research Product".
[187] "ZE5 Cell Analyzer | Bio-Rad." https://www.bio-rad.com/en-ee/product/ze5-cell-analyzer?ID=OC62Q015 (accessed Mar. 06, 2023).
[188] "ZE5 Cell Analyzer and Everest Software Quick Guide Flow Cytometry".
[189] "Attune Flow Cytometer Models | Thermo Fisher Scientific - EE." https://www.thermofisher.com/ee/en/home/life-science/cell-analysis/flow-cytometry/flow-cytometers/attune-nxt-flow-cytometer/models.html (accessed Mar. 06, 2023).
[190] "Attune CytPix Flow Cytometer | Thermo Fisher Scientific - EE." https://www.thermofisher.com/ee/en/home/life-science/cell-analysis/flow-cytometry/flow-cytometers/attune-nxt-flow-cytometer/models/cytpix.html#specifications (accessed Mar. 06, 2023).
[191] "Beckman Coulter - CytoFlexLX documents." https://www.beckman.com/search#q=CytoFLEX LX&t=coveo-tab-othercontent (accessed Mar. 06, 2023).
[192] Basler, "Basler Ace ac640-750uc - Area Scan Camera," *Basler2*, 2021. https://www.baslerweb.com/en/products/cameras/area-scan-cameras/ace/aca640-750uc/ (accessed Jan. 28, 2023).
[193] K. Parnamets, A. Koel, T. Pardy, and T. Rang, "Open Source Hardware Cost-Effective Imaging Sensors for High-Throughput Droplet Microfluidic Systems," *Proc. 2022 26th Int. Conf. Electron. Electron. 2022*, 2022, doi: 10.1109/IEEECONF55059.2022.9810383.
[194] J. Merrin, "Frontiers in Microfluidics, a Teaching Resource Review," *Bioeng. 2019, Vol. 6, Page 109*, vol. 6, no. 4, p. 109, Dec. 2019, doi: 10.3390/BIOENGINEERING6040109.
[195] "SpinSplit. Lab equipment for academic research." https://spinsplit.com/spincube/ (accessed May 03, 2022).
[196] "Fluorescein isothiocyanate-dextran, FD10S." https://www.sigmaaldrich.com/EE/en/product/sigma/fd10s (accessed Mar. 07, 2023).
[197] J. W. Choi *et al.*, "A droplet-based microfluidic immunosensor for high efficiency melamine analysis," *Biosens. Bioelectron.*, vol. 80, pp. 182–186, Jun. 2016, doi: 10.1016/J.BIOS.2015.12.023.

[198] C. I. Rogers, J. V. Pagaduan, G. P. Nordin, and A. T. Woolley, “Single-monomer formulation of polymerized polyethylene glycol diacrylate as a nonadsorptive material for microfluidics,” *Anal. Chem.*, vol. 83, no. 16, pp. 6418–6425, Aug. 2011, doi: 10.1021/AC201539H/SUPPL_FILE/AC201539H_SI_001.PDF.

[199] S. W. Hu, B. Y. Xu, W. K. Ye, X. H. Xia, H. Y. Chen, and J. J. Xu, “Versatile microfluidic droplets array for bioanalysis,” *ACS Appl. Mater. Interfaces*, vol. 7, no. 1, pp. 935–940, Jan. 2015, doi: 10.1021/AM5075216/SUPPL_FILE/AM5075216_SI_001.PDF.

[200] J. B. Harmon, H. K. Gray, C. C. Young, and K. J. Schwab, “Microfluidic droplet application for bacterial surveillance in fresh-cut produce wash waters,” *PLoS One*, vol. 15, no. 6, p. e0233239, Jun. 2020, doi: 10.1371/JOURNAL.PONE.0233239.

[201] S. W. Lim and A. R. Abate, “Ultrahigh-throughput sorting of microfluidic drops with flow cytometry,” *Lab Chip*, vol. 13, no. 23, pp. 4563–4572, Oct. 2013, doi: 10.1039/C3LC50736J.

[202] “3M Novec 7500 Engineered Fluid - Properties.”

[203] “FluoSurf Surfactant in Fluorinated Oil– Darwin Microfluidics.” https://darwin-microfluidics.com/products/fluosurf-high-performance-surfactant-for-droplet-generation?variant=29556657487917 (accessed Mar. 13, 2023).

[204] “Phantom Model: v2640 support.” https://phantomhighspeed.my.site.com/PhantomCommunity/s/detail/a1p3m000003pVzGAAU (accessed Mar. 14, 2023).

[205] “VEO & VEO4K CAMERAS”, Accessed: Mar. 14, 2023. [Online]. Available: www.phantomhighspeed.com

[206] “GitHub - raspberrypi/raspiraw:” https://github.com/raspberrypi/raspiraw (accessed Jan. 08, 2022).

[207] “GitHub - Hermann-SW/fork-raspiraw.” https://github.com/Hermann-SW/fork-raspiraw (accessed Jan. 08, 2022).

[208] F. Lapierre, N. Wu, and Y. Zhu, “Influence of flow rate on the droplet generation process in a microfluidic chip,” *Smart Nano-Micro Mater. Devices*, vol. 8204, p. 8, Dec. 2011, doi: 10.1117/12.903271.

[209] K. Parnamets, A. Udal, A. Koel, T. Pardy, N. Gyimah, and T. Rang, “Compact Empirical Model for Droplet Generation in a Lab-on-Chip Cytometry System,” *IEEE Access*, vol. 10, pp. 127708–127717, 2022, doi: 10.1109/ACCESS.2022.3226623.

[210] S. Wiedemeier *et al.*, “Parametric studies on droplet generation reproducibility for applications with biological relevant fluids,” *Eng. Life Sci.*, vol. 17, no. 12, pp. 1271–1280, Dec. 2017, doi: 10.1002/ELSC.201700086.

[211] A. Dewandre, J. Rivero-Rodriguez, Y. Vitry, B. Sobac, and B. Scheid, “Microfluidic droplet generation based on non-embedded co-flow-focusing using 3D printed nozzle,” *Sci. Reports 2020 101*, vol. 10, no. 1, pp. 1–17, Dec. 2020, doi: 10.1038/s41598-020-77836-y.

[212] A. R. Hibbs, *Confocal Microscopy for Biologists | Alan R. Hibbs | Springer*. 2004. Accessed: Feb. 10, 2023. [Online]. Available: https://www.springer.com/gp/book/9780306484681

[213] J. Caldwell, “1 MHz, Single-Supply, Photodiode Amplifier Reference Design,” 2014, Accessed: Feb. 12, 2023. [Online]. Available: https://www.ti.com/lit/ug/tidu535/tidu535.pdf

[214] “LTW3030 Series Datasheet.” https://optoelectronics.liteon.com/en-global/light/lighting_led/Content/197 (accessed Feb. 13, 2023).

Acknowledgements

To begin with, I wish to extend my gratitude to the Thomas Johann Seebeck Department of Electronics at Taltech for providing me with the opportunity to pursue a PhD.

As well, I would like to acknowledge the assistance I received from my supervisor, Tamás Pardy, who guided me through the topics of lab-on-a-chip, helped me organize my thoughts, and has been a tremendous help at the beginning of my academic career.

Further, I would like to express my gratitude to my co-supervisor, Ants Koel, who was not only my supervisor for this PhD topic, but also my supervisor for my first PhD topic. Over the years, he guided me through the process from beginning to end and provided me with valuable learning experiences throughout the journey.

In addition, I would like to thank Professor Yannick Le Moullec for his assistance in writing and organizing my thesis at the end of my studies.

I would like to thank everybody in Taltech, Thomas Johann Seebeck Department of Electronics who have helped me with their skills and knowledge throughout my studies. Specifically, I would like to thank Andres Eek, who enabled me to achieve a balance between teaching activities and learning activities in order to be successful in my academic endeavours. As well, I wish to thank Professor Toomas Rang for his support and motivation throughout the years.

I would also like to thank all the PhD students whom I have met over the years. It has been a pleasure to have many stimulating discussions with you, which have contributed to the development of new ideas for my studies and research. In particular, I wish to thank recently graduated student Hip Kõiv, a friend and colleague, for the engaging and invigorating discussions. Further, I would like to thank a fellow PhD student, Rauno Jõemaa, for the awesome and fruitful technical discussions we had.

I thank my family and friends for always encouraging me to continue and supporting me with moral support.

Most importantly, I would like to express my gratitude to my wife, Eva, who has been supportive throughout the highs and lows of my studies. It would not have been possible for me to achieve success without your encouragement, positive thinking and energy.

As a PhD candidate, I am grateful for the funding provided by the various projects that supported me financially during my research. Funding for this project has been provided by the following sources:

- Estonian Science Agency ETAg under Grant, PRG620, MOTP109, IUT1911, and TAR16013;
- Estonian Science Agency ETAg under grant PUT1435;
- European Union's Horizon 2020 Research and innovation program under grant 668995;
- DoRa programme.

Abstract
Optical detection methods for droplet microfluidic applications

The purpose of the thesis is to investigate cost-effective and portable illumination and detection circuits for droplet microfluidics. First, the dissertation examines the current state-of-the-art of illumination sources and detectors for biomedical applications, with particular emphasis on droplet microfluidics. It is then evaluated and analysed the performance of open-source, cost-effective, and portable imaging optical detectors for droplet microfluidics. To overcome the limitations of imaging sensor detection capabilities in terms of droplet generation rate, a mathematical model is proposed to evaluate the theoretical droplet generation rate based on the flow rates of dispersed and continuous phases. Lastly, a non-imaging method is proposed which is less cumbersome in comparison to current state-of-the-art devices yet has similar performance in terms of detection of droplets per second.

Over the past few years, there has been an increase in the demand for rapid, cost-effective, and portable methods of detecting viruses, which could be used by untrained personnel and at home (known as point-of-care-technologies). Another trend emerging over the past decade or two is to improve single cell handling of flow cytometry using droplet microfluidics. Droplet microfluidics enables to encapsulate single cells in separate droplets, and enables to do it at high throughputs. Although much research has been conducted in both fields, the existing solutions are often cumbersome and not portable in fashion. Additionally, some parts of a system may be suitable for portable and cost-effective solutions, while other parts may not be. In addition, a large number of data collected from high-throughput droplet generation systems cannot be automatically detected and analysed, since it is often necessary to use a separate system for analysis. This leads to a problem, that it is likely there exists a combination of readout frequency, excitation, and sensing technologies that can be combined to detect fluorescence of cells using a portable and cost-effective method. In order to investigate how such a problem may be resolved, an applied research method is employed.

In previous state-of-the-art works of droplet microfluidics, that use imaging sensors for capturing droplets at high throughputs (ca 1000 droplets per second or more), often a high performing camera is used. While such solutions have excellent performance in terms of maximum frames per second, they are often expensive and cumbersome, and are not suitable for cost-effective and portable solutions. As a comparison with the existing state of the art, a set of open-source, cost-effective, and portable sensors is compared, and their performance and suitability for droplet microfluidic applications is analysed. Once the rate of droplet generation reaches half the maximum frame rate, the droplets are no longer visible in the image and the captured images resemble an effect found in microfluidic chips called jetting. However, based on the captured images, it is not possible to determine whether the droplets are being produced or if the microfluidic chip is jetting. It may be possible to overcome this issue by applying a mathematical model that estimates the theoretical droplet generation rate. In current state-of-the-art literature, droplet sizes are being estimated based on flow rates of oil and water. An innovative mathematical model is proposed in this work to estimate the rate at which droplets are generated based on the flow rates of water and oil. In contrast to approaches that use imaging sensors, a non-imaging approach may be utilized. For such an approach, typical state-of-the-art solutions utilize either a photodiode or a

photomultiplier tube. In order to focus the excitation and emission wavelengths to and from the microfluidic chip, a microscope is usually used, which provides a suitable optical magnification and a proper illumination. It is also possible to use a set of microscope lenses to achieve the desired magnification. By using such an approach, state-of-the-art solutions become cumbersome and expensive. In this study, a novel approach is proposed in which a pinhole is attached to the microfluidic chip in order to block stray light and focus the sensor on only one droplet at a time. This system is evaluated and found to be on par with current state-of-the-art setups, with a detection rate of 10000 droplets per second.

Lühikokkuvõte
Optilised tuvastamismeetodid tilkade mikrofluidiliste rakenduste jaoks

Lõputöö eesmärgiks on uurida tilkade mikrofluidika kuluefektiivseid ja kaasaskantavaid valgustus- ja tuvastusahelaid. Esiteks uuritakse lõputöös biomeditsiiniliste rakenduste valgusallikate ja detektorite hetkeseisu, pöörates erilist tähelepanu tilkade mikrofluidikale. Seejärel hinnatakse ja analüüsitakse tilkade mikrofluidika jaoks mõeldud avatud lähtekoodiga, kulutõhusate ja kaasaskantavate optiliste pildidetektorite toimivust. Kujutise anduri tuvastamise võimaluste piirangute ületamiseks tilkade tekkekiiruse osas pakutakse välja matemaatiline mudel, mis hindab teoreetilise tilkade tekkekiiruse hajutatud ja pidevate faaside voolukiirustel. Lõpuks pakutakse välja mittepildistamismeetod, mis on praeguste tipptasemel seadmetega võrreldes vähem tülikas, kuid millel on samasugune jõudlus tilkade tuvastamisel sekundis.

Viimastel aastatel on kasvanud nõudlus kiirete, kulutõhusate ja kaasaskantavate viiruste tuvastamise meetodite järele, mida saaksid kasutada nii koolitamata töötajad kui ka kodus (tuntud kui hoolduspunktide tehnoloogiad). Veel üks viimase kümnendi või kahe aasta jooksul ilmnenud suundumus on parandada voolutsütomeetria üherakulist käsitsemist tilkade mikrofluidika abil. Piiskade mikrofluidika võimaldab kapseldada üksikuid rakke eraldi tilkadesse ja võimaldab seda teha suure läbilaskevõimega. Kuigi mõlemas valdkonnas on tehtud palju uuringuid, on olemasolevad lahendused sageli tülikad ega ole moes kaasaskantavad. Lisaks võivad mõned süsteemi osad sobida kaasaskantavateks ja kulutõhusateks lahendusteks, teised aga mitte. Lisaks ei saa suurt hulka suure läbilaskevõimega tilkade genereerimise süsteemidest kogutud andmeid automaatselt tuvastada ja analüüsida, kuna sageli on analüüsiks vaja kasutada eraldi süsteemi. See toob kaasa probleemi, et tõenäoliselt on olemas lugemissageduse, ergastuse ja tundlikkuse tehnoloogiate kombinatsioon, mida saab kombineerida rakkude fluorestsentsi tuvastamiseks kaasaskantava ja kulutõhusa meetodi abil. Et uurida, kuidas sellist probleemi saab lahendada, kasutatakse rakendusuuringu meetodit.

Varasemates tipptasemel tilkade mikrofluidika töödes, mis kasutavad pildiandureid tilkade hõivamiseks suure läbilaskevõimega (ca 1000 tilka sekundis või rohkem), kasutatakse sageli suure jõudlusega kaamerat. Kuigi sellised lahendused on suurepärase jõudlusega maksimaalsete kaadrite arvu sekundis, on need sageli kallid ja tülikad ning ei sobi kulutõhusate ja kaasaskantavate lahenduste jaoks. Võrdluseks olemasoleva tehnika tasemega võrreldakse avatud lähtekoodiga, kulutõhusate ja kaasaskantavate andurite komplekti ning analüüsitakse nende jõudlust ja sobivust tilkade mikrofluidilisteks rakendusteks. Kui tilkade tekkekiirus jõuab poole maksimaalsest kaadrisagedusest, ei ole tilgad enam pildil nähtavad ja jäädvustatud kujutised meenutavad mikrofluidkiipides leiduvat efekti, mida nimetatakse jugamiseks. Jäädvustatud piltide põhjal ei ole aga võimalik kindlaks teha, kas tilgad tekivad või mikrofluidkiip pihustub. Sellest probleemist võib olla võimalik üle saada, rakendades matemaatilist mudelit, mis hindab tilkade teoreetilise tekkekiirust. Praeguses nüüdisaegses kirjanduses hinnatakse tilkade suurust õli ja vee voolukiiruste põhjal. Selles töös pakutakse välja uuenduslik matemaatiline mudel, et hinnata tilkade tekke kiirust vee ja õli voolukiiruste põhjal. Erinevalt pildiandureid kasutavatest lähenemisviisidest võib kasutada mittekujundavat lähenemisviisi. Sellise lähenemisviisi jaoks kasutavad tüüpilised tipptasemel lahendused kas fotodioodi või fotokordisti toru. Ergastus- ja emissioonilainepikkuste fokuseerimiseks mikrofluidkiibile ja sealt tagasi kasutatakse tavaliselt mikroskoopi, mis tagab sobiva

optilise suurenduse ja korraliku valgustuse. Soovitud suurenduse saavutamiseks on võimalik kasutada ka mikroskoobi läätsede komplekti. Sellist lähenemist kasutades muutuvad tipptasemel lahendused tülikaks ja kulukaks. Selles uuringus pakutakse välja uudne lähenemine, mille kohaselt mikrofluidkiibile kinnitatakse nööpnõelauk, et blokeerida hajuvat valgust ja fokuseerida andur korraga ainult ühele tilgale. Seda süsteemi hinnatakse ja leiti, et see on võrdne praeguste tipptasemel seadistustega, tuvastamissagedusega 10 000 tilka sekundis.

Appendix 1

Publication I

K. Pärnamets et al., “Optical Detection Methods for High-Throughput Fluorescent Droplet Microflow Cytometry,” Micromachines 2021, Vol. 12, Page 345, vol. 12, no. 3, p. 345, Mar. 2021, doi: 10.3390/MI12030345.

micromachines

MDPI

Review

Optical Detection Methods for High-Throughput Fluorescent Droplet Microflow Cytometry

Kaiser Pärnamets [1,*], Tamas Pardy [2], Ants Koel [1], Toomas Rang [1], Ott Scheler [2], Yannick Le Moullec [1] and Fariha Afrin [1]

[1] Thomas Johann Seebeck Department of Electronics, Tallinn University of Technology, 19086 Tallinn, Estonia; ants.koel@taltech.ee (A.K.); toomas.rang@taltech.ee (T.R.); yannick.lemoullec@taltech.ee (Y.L.M.); fariha.afrin@taltech.ee (F.A.)

[2] Department of Chemistry and Biotechnology, Tallinn University of Technology, 19086 Tallinn, Estonia; tamas.pardy@taltech.ee (T.P.); ott.scheler@taltech.ee (O.S.)

* Correspondence: kaiser.parnamets@taltech.ee

Abstract: High-throughput microflow cytometry has become a focal point of research in recent years. In particular, droplet microflow cytometry (DMFC) enables the analysis of cells reacting to different stimuli in chemical isolation due to each droplet acting as an isolated microreactor. Furthermore, at high flow rates, the droplets allow massive parallelization, further increasing the throughput of droplets. However, this novel methodology poses unique challenges related to commonly used fluorometry and fluorescent microscopy techniques. We review the optical sensor technology and light sources applicable to DMFC, as well as analyze the challenges and advantages of each option, primarily focusing on electronics. An analysis of low-cost and/or sufficiently compact systems that can be incorporated into portable devices is also presented.

Keywords: droplet microfluidics; optical sensors; light sources; microflow cytometry

Citation: Pärnamets, K.; Pardy, T.; Koel, A.; Rang, T.; Scheler, O.; Le Moullec, Y.; Afrin, F. Optical Detection Methods for High-Throughput Fluorescent Droplet Microflow Cytometry. *Micromachines* **2021**, *12*, 345. https://doi.org/10.3390/mi12030345

Academic Editor: Eui-Hyeok Yang

Received: 25 February 2021
Accepted: 19 March 2021
Published: 23 March 2021

1. Introduction

Microfluidics is today a rapidly increasingly active research field due to numerous advantages over batch chemistry and benchtop instrumentation, especially for the implementation of miniaturized, automated analytical and diagnostic devices [1–3]. To analyze the sample, microfluidic devices consist of four main components (Figure 1): microfluidic chip, detection, power supply, and communication. The microfluidic section itself can be divided into multiple different subsections (separation, mixing, focusing, droplet generation, etc.) that take care of sample preparation. Due to the small particle and volume size, precise and highly sensitive sensors are used. The most widely used detection method is optical, but electrochemical and mechanical methods also exist. The detected information is either analyzed on the device itself (e.g., smartphone-based devices) or the data is communicated to separate devices (e.g., personal computer). For additional information about detection methods and power supplies, please see the following reviews [4,5].

Droplet microfluidics, as a subfield of microfluidics, is particularly active as it allows analyzing biological organisms, e.g., cells in chemical isolation, enabling more complex assays and/or higher throughput than state-of-the-art methods [6–9]. In essence, each droplet acts as a separate microreactor, allowing massive parallelization of different reactions and analyses with different types of cells and reagents. Droplet microfluidics relies on two-phase flows of immiscible phases [10], typically oil and water, one of which is discontinuous and forms droplets. Highly monodisperse droplets with <2% coefficient of variation (CV) in size can be generated at frequencies higher than 10 kHz, providing a tool for high-throughput, isolated flow cytometry assays [6,11]. One of the key challenges related to droplet microflow cytometry (DMFC) is the throughput of the sensor: high-throughput analysis is possible only with sensors that have a readout speed the same

or higher than the droplet generation frequency. Typically, flow cytometry is conducted by fluorescence spectroscopy that combines laser excitation of fluorophores with photomultiplier tubes for measuring emissions. This yields a high-throughput and highly sensitive system at the expense of physical dimensions and cost, as shown in [9,12–15]. To make a compact, portable system at a lower price point than widely used benchtop fluorescent flow cytometers, alternative technologies are preferable. However, with more compact alternatives, additional challenges and risks related to (i) signal-to-noise ratio (SNR), (ii) sensitivity, and (iii) spatial and temporal resolution need to be addressed.

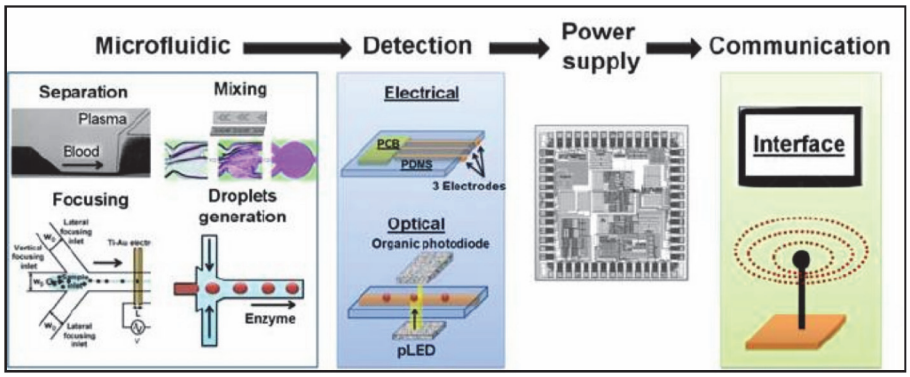

Figure 1. Typical setup of a self-contained microfluidic system that consists of four major sections: microfluidic chip where a type of microfluidic process occurs (mixing, separation, focusing, droplet generation, etc.); detection—optical, electrochemical, or mechanical detection methods are used to detect cells in the microfluidic chip; power supply to power the device; communication—gathered data is either analyzed on the device or communicated to separate device. Reproduced with permission from [16].

Commonly used sensors in microfluidic applications (both experimental and commercial) rely on optical [5] or electrochemical sensing methods [17,18]. Electrochemical sensors (impedance sensors with coplanar or parallel electrode layouts) can be made compact and low-cost, but have limited spatial resolution and issues with SNR [19]. High-throughput flow cytometry typically relies on fluorometry for cell counting and fluorescent microscopy for imaging analyses, e.g., [20]. For both methods, the commonly used setups include (i) lasers as excitation sources, (ii) an optical path consisting of waveguides, mirrors, lenses, etc., and (iii) photomultiplier tubes (PMTs) as detectors. While these setups are reliable, fast, sensitive, and have a good spatiotemporal resolution (including imaging applications), they are also complex and expensive (typically $\geq$100 k€) [21–23]. Therefore, there is a need for research focusing on low-cost, simpler, and more compact detection setups to make measurement setups more available for a wider population and/or speed up the analysis process [24]. For example, relying on light-emitting diodes (LEDs) as excitation sources and photodiodes or Complementary Metal Oxide Semiconductor (CMOS) cameras as detectors, and at the same time including fewer low-cost components in the optical path. While these systems need improvements in sensitivity to be comparable to laser-PMT setups, they can be (i) low-cost, (ii) have small physical dimensions, and (iii) can easily be multiplexed to greatly increase their throughput [25]. Thus, optical systems can be made competitive compared to electrochemical sensors in complexity, dimensions, and cost.

To date, several reviews have focused on biosensors and detection methods in general, as well as on electrochemical and optical sensors in particular, to be applied in Lab-on-a-Chip systems. For instance, in [14,26], high-throughput imaging microflow cytometry is discussed. In [27] detection techniques applicable to droplet microfluidics, including electrochemical and spectroscopic means along with optical ones are reviewed. In [5] optical sensor technology is reviewed and compared to electrochemical and mechanical sensors. In [28] the technology behind optofluidic microflow cytometry is detailed (this

method combines micro-optical and microfluidic components). In [29] the focus is primarily on sensor technology, providing a detailed overview of sensor structure, performance characteristics, and limitations from an electronics perspective. Our understanding is that previous reviews can be grouped into two categories: (1) reviews that focus on the analytical performance of experimental setups, and (2) reviews that focus on the specific electronics aspects of sensor technology. Papers in category (1) analyze analytical performance metrics (limit of detection (LOD), sensitivity, analysis speed, sample labelling, etc.). They also discuss the biological and chemical aspects of the experimental setup (types of biological organisms studied, reagents used). These papers only briefly discuss the sensor setups used and the electronics aspects are not discussed in detail. A few review papers cover microflow cytometry or droplet microfluidics, but rarely the combination of the two. Papers in category (2) discuss the details of the electronic sensor technology in general but do not discuss how they are applied in experimental setups in microfluidics or microflow and droplet microflow cytometry. While optical sensor technology is discussed in several papers, light sources and the construction of the optical path are typically not discussed in detail in either category. There is no review giving a balanced overview of the electronic side of optical detection for droplet microflow cytometry.

In contrast to the above, in our review we (i) discuss sensor and light source technology, focusing on electronics, and (ii) discuss how they are applied in experimental setups to detect and analyze droplets, which may contain (a) a set of reagents, (b) cells, or (c) combinations of cells and reagents. We do not discuss the analytical performance, but cover the throughput and characterize the advantages and challenges related to each discussed technology, in light of how they are used in existing experimental setups.

In Table 1, we compare how much detail is provided in the aforementioned review papers on various aspects, and how our paper is positioned compared to them.

Table 1. Comparison of reviews on detection techniques in microflow cytometry. The level of detail of the various aspects discussed is rated from low to high (*–***).

Ref.	Sensor Technology	Light Source Technology	Optical Path Construction	Analytical Performance	Droplet Microfluidics?
[14]	**	*	***	**	No
[5]	**	*	***	**	No
[26]	**	**	**	*	No
[27]	**	*	***	***	Yes
[28]	**	**	**	**	No
[30]	*	*	*	**	Yes
[31]	*	**	*	**	Yes
Our paper	***	**	**	*	Yes

The rest of the paper is divided into four main sections. In Section 2, we give an overview of commonly used optical paths in DMFC detection setups. In Section 3, we review the light sources used in DMFC setups and discuss their advantages and challenges related to DMFC detection setup. In Section 4, we review the sensor technology used in DMFC detection setups, in the context of the detection setup as well as in terms of electronics. Finally, in Section 4, we summarize our findings and any potential commercial devices, and we outline the remaining open challenges.

2. Light Sources

The focus of this review is on sensors for DMFC; however, a brief look at light sources and optical paths first provides well-needed additional information to better understand the construction of a measurement setup and the choice of the sensor type. Flow cytometry in general and DMFC in particular, require a light source to illuminate the fluorophores in the sample with an appropriate wavelength range and intensity [27]. After conducting a Boolean search in Google Scholar, we concluded that lasers were the most

commonly used light sources with about 287 search results. A laser is a light source that produces monochromatic, coherent, and unidirectional light [32–40], making it excellent for single-wavelength excitation and thus for DMFC. In this review, we do not focus on the detailed properties and working principles of lasers. For more detailed information about lasers see [35,41]. For benchtop flow cytometers, argon-ion (gas) lasers are commonly used (488 nm wavelength), but their driving circuitry is complex and large [14,37,42]. To overcome this, solid-state lasers, especially semiconductor lasers, can be used. They are lower cost, smaller, and have less complex driving circuits, which makes them more suitable for low-cost and portable applications, as shown in [13,14,38,42,43]. Due to their monochromatic, coherent, and unidirectional light, lasers are suitable light sources for laser-induced fluorescence (LIF) detection in DMFC. With high-throughput, droplets are excited with light for only a fraction of a second. The intensity of the emitted light from fluorescence depends on the intensity of the incident light. The laser beam is guided to the microfluidic chip through an optical fiber, and a set of dichroic mirrors, filters, and lenses to filter and focus the emitted light into 1–3 photomultiplier tubes (PMT) and will lose some of its optical power due to optical parts in the optical pathway. The PMTs convert the light into an electrical signal for the detection of fluorescent events (Figure 2a). This configuration typically results in a high-throughput benchtop instrument. While an overwhelming majority of papers use this approach, this configuration has a lower potential for massive parallelization (i.e., of readout zones, increasing throughput) and portability [14,26,42–47]. However, lasers themselves enable focusing high-intensity light beams to fast-moving droplets. Therefore, they are widely used in DMFC applications. For example, the current and future trends for lasers in flow cytometry are reviewed in [48].

Although lasers provide excellent SNR for optical detection, they are not always the optimal technology. In recent years, light-emitting diodes (LEDs) are more commonly used instead. After conducting a Boolean search in Google Scholar, we concluded that LEDs were the second most commonly used light sources with about 136 search results. A low-cost, compact setup can be achieved by using an LED for excitation, with a set of filters and lenses before and after the microfluidic chip, and a photodetector or a camera (e.g., with a CMOS sensor) for detection (Figure 2c). LEDs are the most energy-efficient light sources on the market today [49]. Furthermore, they are compact and capable of producing monochromatic light between the UV (240 nm) and mid-wave infrared (5 µm) ranges, and the light output increases as the technology advances [42,48,50,51]. This makes them suitable as a replacement for xenon arc and halogen lamps [52]. Due to their low energy consumption, LEDs are widely used in handheld instrumentation [53]. In recent years, LEDs have found more use in DMFC applications as they enable decreasing the overall price and size of the measurement device [54]. Furthermore, as LEDs cover the full visible spectrum, they enable matching the absorption wavelength more closely to the fluorophore to achieve maximum excitation efficiency [54]. On the other hand, compared to lasers, LEDs have some disadvantages: the light of the LED is non-collimated, which makes it difficult to focus on the microfluidic channel, whereas lasers usually have collimated light output with spot diameters in the range of a few millimeters. However, this can be overcome by using a lens between the light and the microfluidic channel. The spectrum of the LEDs is narrow and is best described by the manufacturer specification of full width at half maximum (FWHM). Their FWHM is usually in the range of 20–70 nm [55], [56]. Lasers have FWHM in the range of 5–10 nm [57]. Depending on the fluorophore used, this may necessitate additional filters [54]. Compared to lasers, LEDs are less susceptible to overcurrent and simple current regulation circuits are sufficient for driving circuits. Usually, simple resistor-based current limiting circuits are used for low-power LEDs [58] but for higher driving currents a switch-mode constant current driver is more suitable [58,59]. The typical lifespan for LEDs is 50,000 h, and depending on operating conditions, at least 20,000 h [60]. All of these properties make LEDs highly attractive to implement DMFC applications.

For fluorescent imaging and fluorescent microscopy, setups commonly rely on existing microscopy equipment (Figure 2b) or modified versions thereof. This means that the light source will most commonly be a lamp, e.g., a mercury short-arc lamp [61]. Such lamps have a wide emission spectrum, short lifetime [62,63], and may need filtering (e.g., an ultraviolet (UV) filter) [62]. Filtering is specifically needed to reduce the UV emissions harmful to living organisms [62]. They are most suitable for wide spectrum excitation, but due to the wide emission spectrum, monochromators and filters are required to select the appropriate excitation wavelengths [52,53,64]. Compared to lasers or LEDs, the power source is usually high voltage [65,66]. Minimally, the setup needs to include an objective lens and a mirror beside the filters, to direct and focus the light beam into the camera for detection [67]. Alternatively, a laser or high-power LED can be used for excitation, using an objective and a set of filters and optionally additional lenses to filter and focus the light into the camera for detection [26,68]. The popularity of lasers and LEDs is likely due to their long lifetime, easy handling, and inherently monochromatic light beam output.

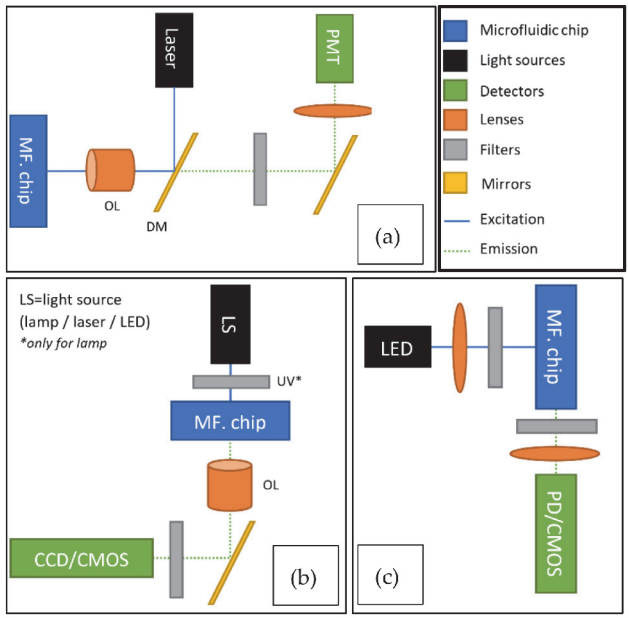

Figure 2. Typical light path configurations applicable in droplet microflow cytometry (DMFC) setups, using lasers, light-emitting diodes (LEDs), and arc discharge lamps as light sources. Setups are fine-tuned by the addition of filters and lenses of various types to focus and filter excitation and emission beams. (**a**) Typical fluorescent event counting setup with a laser as the light source and objective lens (OL) and two dichroic mirrors (DM) to focus and direct fluorescent emission [14,43–46]. (**b**) Typical fluorescent microscopy setup using a mercury arc or halogen lamp and a set of filters to select the appropriate excitation wavelength [61,69]. Alternatively, laser/LED excitation can be used without excitation filtering [70,71]. (**c**) Compact LED-based fluorescent imaging/microscopy setup [25,72]. Only narrow-band LEDs are suitable for use without excitation filtering. By combining the setups shown in (**a**,**b**), one can increase the spatial or temporal resolution of the imaging system.

3. Detection Setups and Optical Sensor Technology

Detection in flow cytometry typically relies on optical sensors, primarily fluorescence-based detection methods [73]. In this section, we first review the technology behind the detection setups demonstrated in DMFC applications, and then we discuss the sensors themselves from an electronics perspective. In terms of performance as detection setups, we analyze and compare the throughput of different setups with a specific focus on novel,

more compact, and portable setups that can offer similar performance to their widely used, highly sensitive, but large and expensive counterparts. In the case of droplet microfluidic examples are not available for a particular technology, we instead discuss setups using regular microflow cytometry as the optical sensor technology and the construction of the detection setup does not differ (droplets are larger in diameter than individual cells, and are thus easier to detect). Our analysis covers the following aspects: (1) sensor technology, (2) layout of the optical detection setup, (3) droplet counting/imaging throughput. Table 2 summarizes the findings reported in this section and provides a comparison of the performance metrics and setups reported in the literature. Section 4.1 provides an overview of the detection setups used in DMFC and Section 4.2 characterizes and compares the optical sensors available to DMFC.

Table 2. Comparison of the complexity and performance of detection setups used in droplet microflow cytometry (DMFC) systems.

Optical Sensor	Light Source	Max. Throughput (Dps) *	Excitation Wavelength (nm)	Complexity (No. of Optical Components **)	Portable/Compact?	Imaging?	Ref.
APD	laser	50	488	>10	no	no	[74]
CCD	LED	1150	~440	4	no	yes	[75]
CCD	lamp	100	470–495	>10	no	yes	[76]
EM-CCD	laser	40	488	6	no	yes	[71]
CMOS	LED	1,000,000	530	3	yes	no	[77]
CMOS	LED	254,000	490	3	yes	no	[72]
CMOS	laser/LED	96,000	488/640	>10	no	yes	[78]
CMOS	laser	70	532	2	yes	yes	[79]
sCMOS	laser	184,000	532	5	no	no	[80]
sCMOS	laser	10,000	488/560	>10	no	yes	[81]
PMT	laser	100,000	488	5	no	no	[82]
PMT	laser	10,000	405/488/561/639	6	no	no	[83]
PMT	laser	500	488	3	no	no	[43]
PMT	laser	50	405/473	7	no	no	[84]
PMT	laser	10	445	7	no	no	[85]

* dps = droplets or cells per second. ** includes all mirrors, filters, lenses, waveguides, apertures, etc., in the optical path, but not the microfluidic chip, the sensor, nor the excitation source.

3.1. Detection Setups

Relevant optical sensors can be divided into two major groups: imaging and non-imaging. Imaging sensors can natively record the morphology besides the emitted fluorescent light intensity, and thus are easily applicable to fluorescent microscopy, whereas non-imaging sensors only detect the emitted light intensity and by themselves cannot be used to construct a two-dimensional image. In the group of imaging sensors, there are two major sensor types: Charge-Coupled Device (CCD) and Complementary Metal Oxide Semiconductor (CMOS). For non-imaging optical sensors, there are two major groups: photodiodes and photomultiplier tubes (PMTs). Subtypes exist for both groups. Figure 3 shows a classification chart of the different optical sensors discussed in this section.

To determine which sensors have been most commonly used, we again conducted a Boolean search using Google Scholar. Search results are shown in Figure 4 and are overlaid by the maximum throughput of each sensor to compare popularity with performance. The search indicated that CCD sensors were the most popular (128 results), while PMT sensors came second (101 results). The popularity of CCD sensors is likely because most fluorescent microscopes integrate well with CCD cameras and indicate that most reported setups were used for imaging applications. The relatively high popularity of PMTs was likely due to their high light sensitivity, as is further discussed below. In the following analysis, we discuss the performance of each sensor in more detail. We analyze the performance in terms of (1) quantum efficiency, (2) response time, (3) resolution (spatial/temporal, where applicable), and (4) spectral response. Quantum efficiency (QE) is an essential performance metric of optical sensors, as it expresses the ratio of incident photons to generated electrons [86,87].

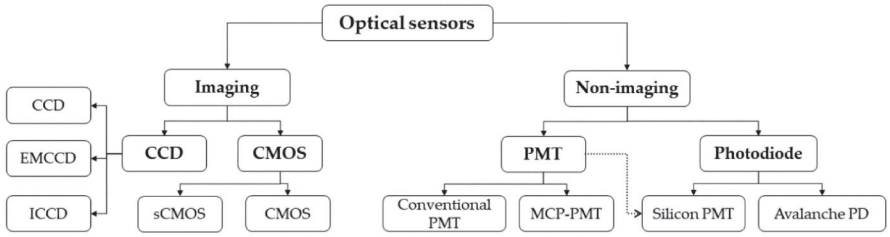

Figure 3. Based on the operating methods, the optical sensors for droplet microfluidic setups can be divided into two major categories—imaging and non-imaging. Photomultiplier tubes or photodiodes are widely used for non-imaging detection setups in droplet microflow cytometry (DMFC) where they detect the light level. If morphological and/or spatial information about cells is required, Charge-Coupled Device (CCD) or Complementary Metal Oxide Semiconductor (CMOS) type imaging sensors are preferred.

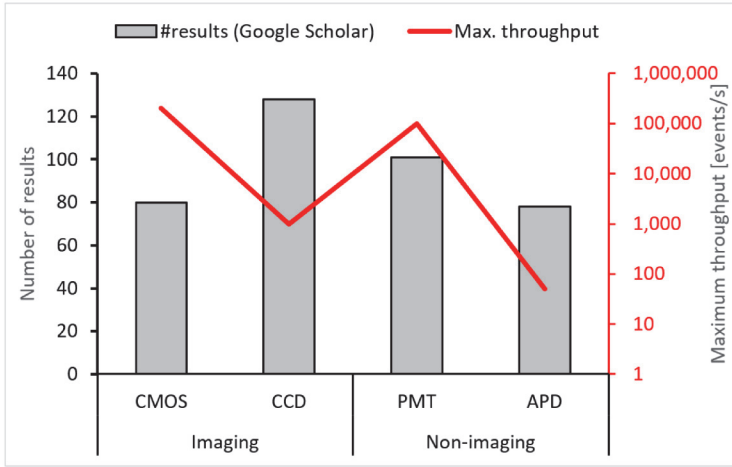

Figure 4. Sensor types and their relevance to droplet microflow cytometry (DMFC). On the vertical axis, there are several results for each sensor type based on a Boolean search from Google Scholar. The red line shows the maximum reported throughput of each sensor type.

CCDs are popular choices for droplet microfluidic devices due to their high light sensitivity, as indicated in [76,88–90]. Although CCD sensors are widely used in DMFC, they are not ideal for high-throughput applications. The readout noise for CCD sensors is low, but the maximum frames per second (fps) is limited, which in turn limits the throughput to 100–1000 droplets/s in imaging applications [81,91].

CMOS cameras have 10 times higher framerates than CCD cameras, and therefore are more suitable for high-throughput imaging [91]. In DMFC, CMOS cameras are often used to detect the morphology and textural information of individual cells [14]. Furthermore, CMOS cameras are excellent for massively parallelized applications due to their high spatial resolution and high imaging throughput. The throughput can be increased further by microfluidic channel splitting. Besides their ultrahigh-throughput, these setups were also among the most compact.

PMTs are the most sensitive detectors available for DMFC and are also the most common detectors for high-throughput cell counting applications [31,92,93]. However, they cannot natively resolve 2D images and are fragile and large, which makes them difficult to integrate with a microchannel. Thus, a complex optical path with lenses, filters, waveguides, optical fibers, etc., is needed to direct and focus the light to the microchannel. Furthermore, they can only detect a single color. To detect multiple colors, typically multiple sensors and filters are used, which makes the setup complex and expensive. The

throughput of PMT-based non-imaging setups can easily go up to 100,000 events/s in fluorescent event counting applications.

Avalanche photodiodes (APD) can be used to construct highly sensitive, yet more compact and less complex detection setups than those with PMTs; a laser for excitation, an APD, a microscope objective (both for focusing excitation and collecting emissions), and two mirrors [74,94].

3.2. Charge-Coupled Device Based Sensors in Droplet Microflow Cytometry (DMFC)

Fluorescence-based detection is most frequently used in conjunction with droplets [31]. Microfluidic chip channel widths are in the range of 50–100 micrometers, and to focus on fluorescent emissions, a lens system is needed, as shown in [95]. Based on the Boolean analysis conducted earlier in Section 2, the CCD sensor is the most widely used sensor in droplet microfluidics. When referred to as a sensor, it is either a camera with a CCD sensor or a standalone CCD sensor with additional acquisition electronics. To capture the emission spectrum from a microfluidic channel, a microscope objective or a set of lenses together with filters and dichroic mirrors are used to filter and focus the emitted light on the sensor [95]. In this review, we do not go into detail on CCD sensor technology, as numerous publications have been published on that subject. Secondly, the state-of-the-art of sensor technology is proprietary to manufacturers and little or no information is present about the latest technologies. More detailed information about CCD technologies is available in [96].

In a CCD sensor, there is an array of biased P-Channel Metal Oxide Semiconductor (PMOS) or N-Channel Metal Oxide Semiconductor (NMOS) photodiodes, each acting as an individual pixel of the sensor. When photons hit the biased photodiode, the photons are turned into an electrical charge. For an array of pixels, there are only a few readout amplifiers, and here lies one of the biggest shortcomings of standard CCD technology in terms of high-throughput droplet analysis. The low number of amplifiers per sensor limits the maximum frames per second (fps) the sensor can achieve [97]. Moreover, the sensitivity of the sensor is limited to the charge-to voltage conversion process, and the readout noise increases if the data is acquired faster [98]. Thus, the readout rate is lowered to minimize the noise [99].

In addition to CCD, intensified CCD sensor (ICCD) and electron multiplication CCD (EMCCD) technologies are used that offer light sensitivity down to a single photon level [100,101]. ICCD sensors have image intensifiers in front of the sensor to boost the number of incoming photons [102]. This improves sensitivity in low-light scenarios at the cost of a higher supply voltage (1 kV) and reduced dynamic range [103,104]. EMCCD sensors have a similar gain performance to ICCD. Instead of the intensifier, an on-chip electron-multiplier is used to achieve the gain [98]. EMCCD has good sensitivity in poor lighting, has little dark current, and better readout noise than ICCD, but also inherits noise from the amplification registry and clock-induced charge [98,99]. A comparison of the noise performance of ICCD, CCD, and EMCCD sensors is presented in [97]. CCD sensors are generally characterized by higher light sensitivity than CMOS sensors, at the cost of imaging throughput. ICCD and EMCCD sensors perform even better in low-light situations [105–108], but cost more and consume more power. Figure 5 shows the common detection setups for CCD sensor-based measurement devices.

In one demonstrated example, a 488 nm laser was used for excitation and an EM-CCD sensor for detection [39]. Droplets of about 350 pL volume were detected in a polydimethylsioxane (PDMS) chip at about 40 Hz droplet generation frequency. Using an LED strobe-light excitation at variable frequency, it was possible to detect droplets at 1150 Hz frequency without the need for a trigger or a synchronizer [75]. Another similar setup was reported in [109] where a 488 nm laser was used for excitation and a camera with an EMCCD sensor was used as a detector. Microdroplets filled with fluorescence were generated at a rate of 30 Hz. When compared to CMOS-based detection setups, the throughput is the most lacking aspect.

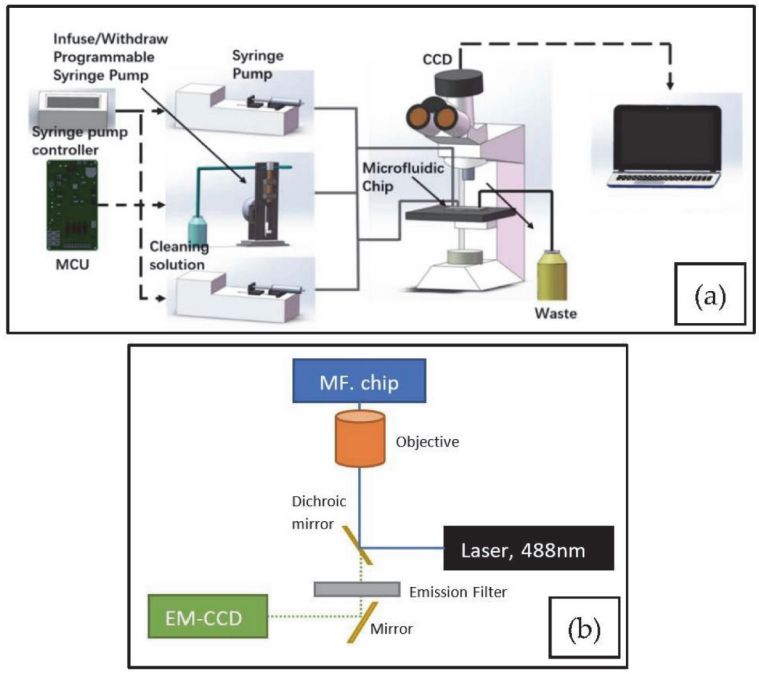

Figure 5. Detection setups used in droplet microflow cytometry (DMFC) using Charge Coupled Device (CCD) sensors as a detector. (**a**) A typical solution for microscope-based microfluidic measurement setup. A microscope with an integrated camera is used to zoom and focus on a microfluidic chip. Two syringe pumps with a controller are responsible for the continuous flow of sheath (carrier) fluid and sample fluid. (**b**) A laser Electron Multiplying Charge Coupled Device (EMCCD) sensor system capable of detecting fluorescence-induced droplets at the rate of 30 Hz. The optical setup consists of a 20× objective lens, dichroic mirror, emission filter, mirror, camera, laser, and a microfluidic device. Reproduced with permission from [110].

3.3. Complementary Metal Oxide Semiconductor (CMOS) Based Sensors in DMFC

CMOS sensors are active pixel sensors, as the captured photons are converted to an electrical voltage by photodiodes and amplified in the pixel itself [111,112]. This improves the detection speed at the cost of losing the detection area and sensitivity. Additionally, the pixel fill factor (PFF) can be increased and microlenses can be used [113–115]. Compared to CCD sensors, CMOS sensors are typically lower cost, offer lower power consumption, and require lower input voltages [112,116]. Thus, CMOS sensors are more suitable for compact or portable applications, as demonstrated by the literature analysis in the first half of this section. Although CCD sensors have higher light sensitivity, they have a much faster conversion characteristic, making them more suited for high-throughput imaging applications [117]. Sensitivity can be increased by external filtering and focusing or increasing the excitation light intensity. Beyond a certain droplet generation rate or flow rate, motion blur will occur. This can be compensated by increasing the imaging throughput (framerate) of the sensor. However, this reduces the exposure time and therefore the sensitivity, so a more sensitive sensor will be needed.

For high-throughput applications, CMOS sensors are more suitable. From the scientific literature, many high-throughput applications can be found. For instance, a zone-plate array of 64 output channels was demonstrated, capable of counting cells at 184,000 droplets/s throughputs by running an sCMOS camera at 16,000 fps [80]. In another demonstrated setup, the camera and the chip were integrated [72]. By spin coating a filter onto the CMOS sensor and bonding a 16-channel PDMS droplet generator chip, a 100,000 events/s

detection rate was achieved. For excitation, a 250 mW LED with 490 nm peak wavelength was used. The filter blocked most of the excitation light and only a 4-pixel wide area of the sensor aligned with the chip was used for detection. The CMOS camera was run at up to 2150 fps. Image stabilization by optomechanical means could also improve the throughput: in one demonstrated setup, a polygon scanner counteracted the movement of a cell in the measured channel. This technique allowed a 1000 times increase in exposure and was suitable for applications where the fluorescent emission intensity was low, as shown in [81]. Figure 6 shows the CMOS-based setups with the highest reported throughput.

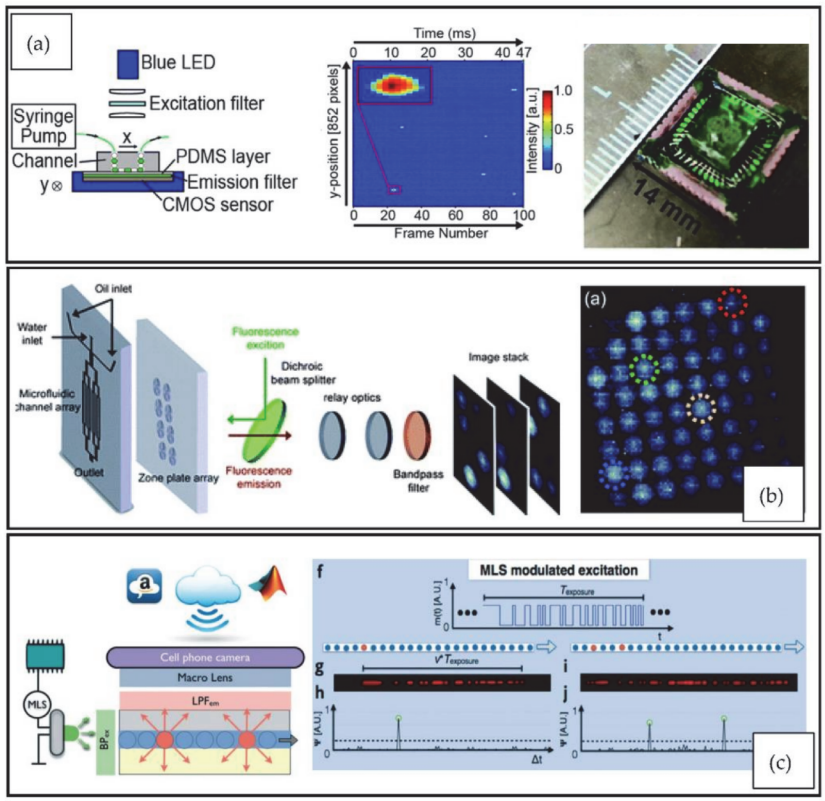

Figure 6. Demonstrated ultrahigh-throughput detection setups in DMFC. (**a**) A compact LED-CMOS system, which could detect fluorescent droplets at 254,000 dps throughput. The system used a simple and compact optical path and microfluidic channels branching into 16 parallel channels to increase throughput [72]. (**b**) A laser-CMOS system, which could detect droplets at 184,000 dps throughput. In this application, microfluidic channels were split into 64 parallel branches and imaged through an 8 × 8 zone-plate array. The resultant image is shown on the right [80]. (**c**) An LED-CMOS system capable of detecting droplets at up to 1,000,000 dps throughput. This was achieved by splitting the microfluidic channels into 120 parallel branches. Additionally, pseudorandom maximum length sequences (MLS) were used for excitation that prevented droplets overlapping due to framerate limitations of CMOS cameras [77]. Reproduced with permission from [72,77,80].

Due to the advances in the smartphone industry and specifically smartphone cameras, extremely compact optical paths can be fabricated from low-cost components. Furthermore, it is possible to use an existing smartphone camera with its built-in lens system. One has only to add filters to restrict emissions to the required wavelengths. This setup, using an aperture, can adjust the focal length and focus, as it is shown in [14]. The exact number of filters and lenses may vary from paper to paper, as can be seen in [14,25]. The described

setup has the highest potential for physically parallel realization and system-level integration in low-cost, portable instruments because the readout area can be extended by using multiple readers, and the microfluidic throughput can be increased by channel splitting, as shown in [25]. Smartphones have high-performance CMOS cameras, which makes them excellent candidates for use in droplet microfluidics applications due to their low-cost and portability, e.g., [75,90,91,95,118]. Recently, smartphone-based flow cytometry has reached a level where high-throughput can be achieved with low-cost microfluidic setups, as shown in [119]. The solution offers a similar resolution to benchtop microscopes commonly used for droplet analyses and microflow cytometry [120]. Furthermore, they can run software applications that automate analytical workflows and evaluation of results [119,120]. In [77], a theoretical maximum fluorescent event detection rate of up to 1,000,000 events/s was reported using a smartphone camera. In this setup, an ultra-bright LED was flashed in a pseudorandom sequence to excite droplets that would have otherwise overlapped. The system also used a massively parallelized droplet generator structure with 120 channels.

3.4. Photomultiplier Tube (PMT)-Based Sensors in DMFC

A PMT is a vacuum tube with a window that consists of a photocathode, an electron-multiplier or dynode, focusing electrodes, and an anode that outputs a current proportional to the incident light [86,121]. The QE of PMTs, defined as the ratio of photoelectrons emitted by the photocathode to the number of incident photons on the window, is usually ~35% [122]. PMTs have response times in the range of nanoseconds, e.g., 26 ns for the Hamamatsu R7205-01. Microchannel plate photomultiplier tubes (MCP-PMT) are advanced PMTs where dynodes are replaced with microchannels of 6–20 μm diameter, decreasing the response time to the picosecond range (e.g., the Hamamatsu R3809U50 has a 0.55 ns response time) and increasing gain to 10^4–10^7, while allowing 2D images to be reconstructed [86,123,124]. This comes at the cost of a higher supply voltage (up to 3 kV compared to 0.5–2 kV for a regular PMT). PMTs have a lower power efficiency than CCD and CMOS sensors, require a high voltage power supply (which means a complex power supply unit), are sensitive to magnetic fields, require heating up before operation (takes 30–60 min), and are difficult to handle due to their fragility [125]. Furthermore, due to their high sensitivity, they require a shielding or dark box to operate, adding to the size and complexity [86]. Finally, the performance of PMTs degrades over time: it was found with MCP-PMT that after 5 months of operation, QE dropped by 16% and gain by 50% [126].

For non-imaging sensors, PMTs that have inherently high gain are used, which makes them able to detect fluorescence signals that are weak and have a short lifetime. For many commercial flow cytometers, the PMTs are also used as a sensor (e.g., two widely used BD Accuri C6 and Attune NxT). Multi-parameter measurements have been a challenge with PMTs. To overcome this deficiency, multiple lasers can be switched on separately, varying the excitation and detection wavelength without the use of filters or multiple sensors [84] or single-sensor setups can be used by modulating the laser frequency and using frequency-division multiplexing [83]. Both the aforementioned setups included only the PMT, lasers, optical fibers, and microfluidic chips in their optical path, which is the minimum number of parts achievable with PMT-based setups. Figure 7 shows the common detection setups for PMT-based measurement devices.

3.5. Photodiode-Based Sensors in DMFC

In recent years, more versatile and lower-cost silicon-based counterparts, e.g., avalanche photodiodes (APDs), are replacing PMTs. Photodiodes are semiconductor devices that directly convert photons into electrical current. Avalanche photodiodes (APD) are the most closely comparable in performance to the PMTs. They are high-speed and high-sensitivity photodiodes that have internal photocurrent amplification. APDs are physically more robust than PMTs, but still require a higher operating voltage in the range of a few hundred volts, which makes them unsuitable for portable applications [127–129]. APDs are sensitive to high ambient temperatures: in one study, a gain reduction of 15% was observed when

the sensor temperature increased from room temperature to 80 °C [128]. To overcome that, APD modules with internal temperature compensation circuits might be more suitable for DMFC. Hamamatsu offers multiple modules that have an internal high voltage generator with temperature monitoring and compensation, e.g., the C12702 series [128]. When the diode is operated above the breakdown voltage, it is in Geiger-mode (GM-APD), where it can detect light down to a single photon level [130]. However, due to the avalanche process, the output is not proportional to the incident light. To overcome that, multi-pixel photon counters (MPPC) or silicon photomultipliers (SiPM) were created. In a SiPM device, an array of micro-cells consisting of GM-APD diodes in parallel sums the signal of all cells [130]. The output of SiPM sensors depends on the selected supply voltage that is in the range of 30–60 V [103]. Increasing the supply voltage increases the gain, but also increases the dark count, crosstalk, and after-pulses, which all lower the SNR [130–133].

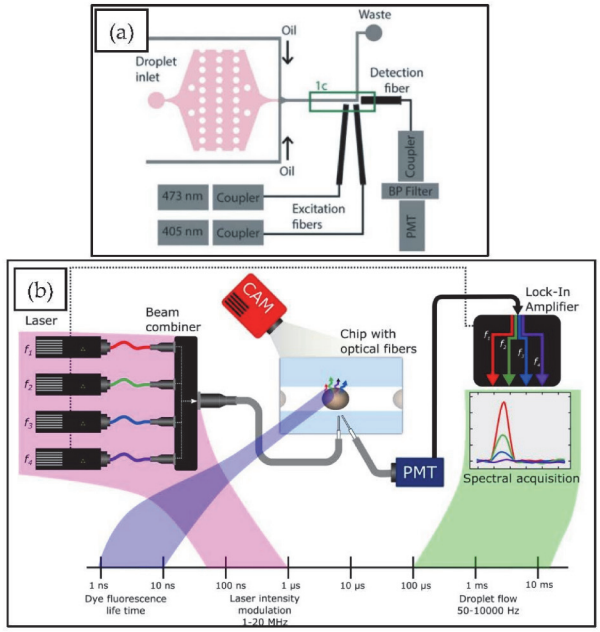

Figure 7. Detection setups used in droplet microflow cytometry (DMFC) using photomultiplier tubes (PMT) as a detector. (**a**) Measurement system where multiple lasers are used and coupled into the microfluidic chip. Knowing the flow speed, multiple analyses of droplets can be done using only one PMT tube [84]; (**b**) a measurement setup consisting of one PMT capable of measuring four parameters at the same time, using lasers for light sources, beam combiner, and lock-in amplifier to demodulate the result [83]. Reproduced from with permission from [83,84].

In one demonstration, an argon-ion laser was used along with two sets of dichroic mirrors and filters and two APDs to detect two fluorescent signals at a 50 Hz droplet generation rate [134]. It is also possible to combine CCD cameras and APDs to perform rapid kinetic measurements [94]. In another experiment, APD was used for fluorescence emission detection to detect bacteria growth. Additionally, a CCD camera was used to verify droplet generation [74]. Usually, fluorescence is used to label cells, but this can lead to cytotoxicity, nonspecific binding, and other problems. In some cases, high-throughput measurement setups have been provided to measure live cells at a high-throughput rate, using a photodiode as the detector [135–137]. Figure 8 shows the common detection setups for the photodiode-based measurement setup.

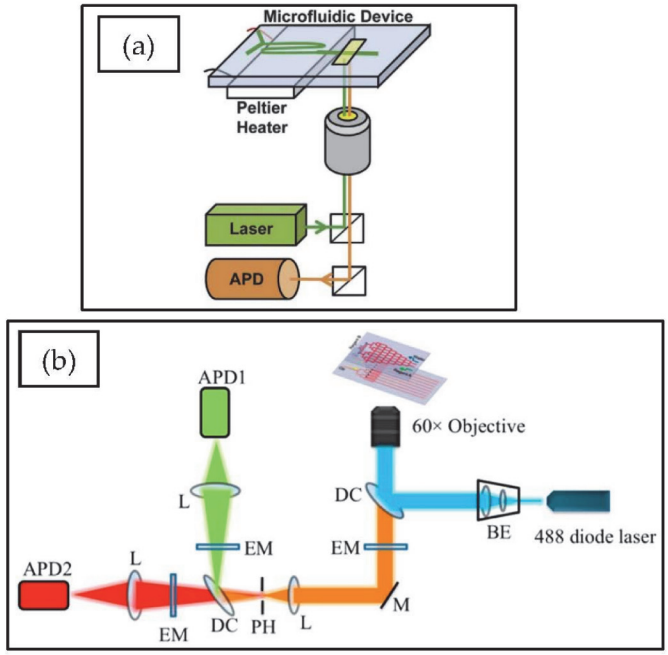

Figure 8. Detection setups used in droplet microflow cytometry (DMFC) using photodiodes or avalanche photodiodes (APD) as a detector. (**a**) Microfluidic measurement system where a laser is used for excitation and APD is used as a detector. Additionally, optics are used to focus light on the sample. (**b**) Microfluidic measurement system where Differential Detection Photothermal Interferometry is used and two photodiodes collect the data that is collected with a lock-in amplifier and analyzed in PC. Reproduced from with permission from [74,134].

4. Discussion

In this paper, we reviewed the light sources, optical paths (Section 2), and optical sensor technologies (Section 3) applied in the DMFC detection setup. The technology review was focused on the electronics aspect of sensors and light sources and the technology aspects (construction) of detection setups. We focused on fluorometry or fluorescent microscopy as the detection method. In this discussion section, we summarize the findings of Sections 2 and 3, then highlight existing commercial products, and finally highlight perspectives. The summary combines findings from all previous sections and groups them by the type of detection setup.

Fluorescent counting and microscopy are the leading applications of DMFC technology, and thus setups can be divided into two distinct groups: non-imaging and imaging. Non-imaging detection setups will typically employ lasers as light sources and PMTs as sensors to maximize light sensitivity. This approach requires a highly complex optical path with specialized components, a minimally objective or equivalent lens system, dichroic mirrors, emission filter, and lens (typically 5–10 components). The fluorescent event counting throughput of PMT-based sensors is commonly in the range of 100,000 events per second (eps). This is achieved by fine-tuning the optical path to improve sensitivity. Furthermore, more compact, potentially lower-cost setups can be constructed by using APDs and semiconductor diode lasers while retaining a similar sensitivity. The light sensitivity of PMTs has been achieved thanks to their inherently high gain (10^4–10^7). They also have a fast response time (nanosecond–picosecond range). The smaller size and lower input voltage requirements of SiPM sensors can also offer gains up to 10^6. It is possible to construct more compact yet highly sensitive setups with LEDs and photodiodes, e.g., APDs.

Fluorescent imaging setups commonly rely on existing technology, that is, a fluorescent microscope. These systems typically come with receptacles for CCD/CMOS cameras and use arc lamps (mercury, xenon, or metal halide) as the light source. They also have built-in objectives for magnification. For event counting applications, UV filters are necessary in case lamps are used. Alternatively, lasers and high-power LEDs (250 mW) are used for focused and highly monochromatic excitation. CCD cameras have inherently higher light sensitivity than CMOS cameras, especially ICCD and EMCCD sensors. The optical path minimally consists of a lamp with a UV filter or a laser/LED as the light source, and an objective with or without additional filtering after the microfluidic chip to filter and focus emissions into the sensor. The light source and sensor can be installed at 90 degrees, or a mirror can be used to reflect emissions towards the sensor from the microfluidic chip. With CCD sensors, the maximum imaging throughput is ~1000 frames per second or droplets per second (fps/dps). CMOS cameras have higher framerates than CCDs, with some setups achieving framerates more than a million frames per second [138,139]. They are also more compact and can be equipped with compact lens systems. Due to their high spatial resolution, they can also scan a wider area and thus allow increasing throughput by parallel readouts of branching microfluidic channels (up to 120 channels reported). This yields ultrahigh throughputs of 100,000–200,000 eps in fluorescent event counting applications, and up to 10,000 dps in imaging and morphology analysis. Detection setups most commonly use lasers in conjunction with CMOS sensors. CMOS sensors are excellent for portable applications, with optical paths reported that had only two components in the optical path (lenses and filter). To increase portability and lower cost, it is also possible to use LEDs as light sources. Such setups can reach throughputs between ~1000–2000 dps. Smartphone cameras are also commonly used in portable setups and can yield similarly high throughputs. Furthermore, they are equipped with integrated lens systems and the image processing can be directly implemented on the smartphone, further reducing dimensions and complexity. CCD sensors and CMOS sensors are both pixel sensors and rely on photodiodes but employ different methods for signal amplification. CCD sensors employ charge shifting and a single amplifier, which results in a more consistent (more noise-free), but slower readout than CMOS sensors. On the contrary, CMOS sensors have amplifiers as a part of each pixel, which results in faster but noisier readouts, thus the difference in light sensitivity. However, as CMOS sensor technology improves, the noise and sensitivity cap is narrowing. Increasing the PFF and employing integrated microfabricated lenses on the CMOS sensor are methods to improve sensitivity. Integrating microlenses has led to a reported 30% sensitivity increase in the visible range.

4.1. Commercial Platforms

Some benchtop droplet analyzers are commercially available. The Amnis ImageStreamx MKII can detect up to 5000 cells/s. By using multiple lasers, it can detect up to 12 channels of cellular imagery [54]. They probably use a CCD sensor with Time Delay Integration (TDI) readout technology to increase the throughput and maximize the sensitivity [26,140]. Amnis also offers a scaled-down version, FlowSight, that has a CCD camera and can take 10 simultaneous fluorescent pictures up to 4000 events per second [141]. The OptoReader platform (Elveflow, Paris, France) promises a counting throughput of 100,000 events/s [142]. The system relies on multi-wavelength LED/laser excitation and uses a compact, low-cost digital microscope with up to $\times$100 magnification for imaging. Although not clearly stated in the documentation, the microscope likely uses a CMOS camera. The system is reported to weigh 10 kg and is considered a candidate for Point-of-Care applications [143]. The CytoMine system (Sphere Fluidics Ltd., Cambridge, UK) is a high-throughput benchtop droplet analyzer. It relies on a 488 nm laser for excitation and a CMOS camera for detection [144]. Their droplet sorter is capable of 300 dps throughput [145]. Droplet digital polymerase chain reaction (PCRs) are also high-throughput droplet-based systems, where nucleic acid samples are partitioned into thousands of droplets. The readout is based on fluorescent event counting, using a laser/LED as a light source and a PMT for detection [146]. A more

detailed comparison of four commercially available (Accuri™ C6 (BD Biosciences, San Jose, CA, USA), NovoCyte ® (ACEA Biosciences, San Diego, CA, USA), Attune™ NxT (Thermo Fisher Scientific, Waltham, MA, USA), and MACSQuant 10 (Miltenyi Biotec, Bergish Gladbach, Germany)) cytometers is available here [147]. The flow cytometry buyers guide can also be helpful when selecting a platform [141].

4.2. Perspectives

We can conclude that with recent developments in semiconductor sensor technology (photodiodes and CMOS sensors), it is possible to construct high-throughput fluorescent counting and microscopy setups that are on par in performance with well-established benchtop counterparts (PMTs and traditional fluorescent microscopy setups). Using compact detection setups relying on lasers for excitation and CMOS sensors for detection, it is possible to reach counting throughputs above 100,000 eps, and imaging throughputs above 10,000 dps. With even more compact setups that only employ a lens and a filter in conjunction with LEDs for excitation and CMOS sensors for detection, it is possible to reach above 1000 dps. Thus, highly portable and high-throughput imaging and counting setups are achievable. These setups commonly rely on the parallelized readout of branching microfluidic channels with thousands of droplets passing through each.

In the future, we can expect further development in CMOS sensor technology, increasing the sensitivity and decreasing the cost of sensors. With the rapid development of parallelized image processing architectures, the computational overhead will also continue to drop, increasing the throughput of the system further. Image quality can be increased dramatically using machine learning for de-noising and pre-processing. Neural networks can also be taught to detect and classify cells in a completely automated manner. With the cost and power requirements of such systems dropping rapidly, fully automated portable analyzers are on the horizon and can greatly aid in the fight against novel and recurring bacterial pathogens. There is a pronounced need for a high number of portable analyzers to decentralize diagnostics and increase diagnostic coverage. Early detection can greatly aid preventive measures and targeted isolation of cases to prevent community spread. Although there is a significant scientific and commercial interest in portable droplet analyzers, several open challenges remain. To make such detection setups competitive compared to benchtop instruments, CMOS sensors still need to become more sensitive. The bottleneck of the analog-to-digital (ADC) conversion also remains an issue for portable applications. The miniaturization of lenses and filters is an ongoing process, but the highly specialized fabrication methodology required for them is a limit. If the optical path could be fabricated with lower costs, e.g., 3D printing, that would greatly reduce the overall complexity and cost (as well as shorten the supply chain for instrument fabrication).

Author Contributions: Conceptualization, T.P.; methodology, T.P., O.S., and A.K.; formal analysis, K.P., T.P., and O.S.; investigation, K.P., T.P.; resources, T.R.; writing—original draft preparation, K.P. and T.P.; writing—review and editing, O.S., Y.L.M., A.K., and T.R.; writing–revisions and final editing, K.P.; visualization, T.P., K.P.; supervision, T.P., A.K., O.S., and Y.L.M.; project administration, T.R.; funding acquisition, T.R.; finding latest relevant articles, F.A. All authors have read and agreed to the published version of the manuscript.

Funding: This research was funded by the Estonian Science Agency ETAg, grant numbers PRG620, PUT1435, MOBTP109, IUT1911, and TAR16013 Center of Excellence "EXCITE IT" and European Union's Horizon 2020 Research and Innovation Program under Grant 668995.

Acknowledgments: The authors thank the Estonian Science Agency ETAg and the European Commission for supporting the research work.

Conflicts of Interest: The authors declare no conflict of interest.

References

1. Liu, Y.; Jiang, X. Why microfluidics? Merits and trends in chemical synthesis. *Lab Chip* **2017**, *17*, 3960–3978. [CrossRef]
2. Whitesides, G.M. The origins and the future of microfluidics. *Nature* **2006**, *442*, 368–373. [CrossRef]

3. Zhang, J.; Yan, S.; Yuan, D.; Alici, G.; Nguyen, N.T.; Ebrahimi Warkiani, M.; Li, W. Fundamentals and applications of inertial microfluidics: A review. *Lab Chip* **2016**, *16*, 10–34. [CrossRef] [PubMed]
4. Yi, C.; Zhang, Q.; Li, C.W.; Yang, J.; Zhao, J.; Yang, M. Optical and electrochemical detection techniques for cell-based microfluidic systems. *Anal. Bioanal. Chem.* **2006**, *384*, 1259–1268. [CrossRef]
5. Pires, N.M.M.; Dong, T.; Hanke, U.; Hoivik, N. Recent developments in optical detection technologies in lab-on-a-chip devices for biosensing applications. *Sensors* **2014**, *14*, 15458–15479. [CrossRef] [PubMed]
6. Kaminski, T.S.; Scheler, O.; Garstecki, P. Droplet microfluidics for microbiology: Techniques, applications and challenges. *Lab Chip* **2016**, *16*, 2168–2187. [CrossRef] [PubMed]
7. Joensson, H.N.; Andersson Svahn, H. Droplet Microfluidics—A Tool for Single-Cell Analysis. *Angew. Chem. Int. Ed.* **2012**, *51*, 12176–12192. [CrossRef]
8. Lagus, T.P.; Edd, J.F. A review of the theory, methods and recent applications of high-throughput single-cell droplet microfluidics. *J. Phys. D Appl. Phys.* **2013**, *46*, 114005. [CrossRef]
9. Teh, S.Y.; Lin, R.; Hung, L.H.; Lee, A.P. Droplet microfluidics. *Lab Chip* **2008**, *8*, 198–220. [CrossRef]
10. Baroud, C.N.; Gallaire, F.; Dangla, R. Dynamics of microfluidic droplets. *Lab Chip* **2010**, *10*, 2032–2045. [CrossRef] [PubMed]
11. Yelleswarapu, V.; Buser, J.R.; Haber, M.; Baron, J.; Inapuri, E.; Issadore, D. Mobile platform for rapid sub–picogram-per-milliliter, multiplexed, digital droplet detection of proteins. *Proc. Natl. Acad. Sci. USA* **2019**, *116*, 4489–4495. [CrossRef]
12. Fang, X.-X.; Li, H.-Y.; Fang, P.; Pan, J.-Z.; Fang, Q. A handheld laser-induced fluorescence detector for multiple applications. *Talanta* **2016**, *150*, 135–141. [CrossRef]
13. Geng, X.; Shi, M.; Ning, H.; Feng, C.; Guan, Y. A compact and low-cost laser-induced fluorescence detector with silicon based photodetector assembly for capillary flow systems. *Talanta* **2018**, *182*, 279–284. [CrossRef]
14. Stavrakis, S.; Holzner, G.; Choo, J.; DeMello, A. High-throughput microfluidic imaging flow cytometry. *Curr. Opin. Biotechnol.* **2019**, *55*, 36–43. [CrossRef]
15. Regmi, R.; Mohan, K.; Mondal, P.P. Light sheet based imaging flow cytometry on a microfluidic platform. *Microsc. Res. Tech.* **2013**, *76*, 1101–1107. [CrossRef]
16. Colomer-Farrarons, J.; Miribel, P.; Rodríguez-Villarreal, A.; Samitier, J.; Ll., P.; Ivon, A.; Samitier, J. Portable Bio-Devices: Design of electrochemical instruments from miniaturized to implantable devices. In *New Perspectives in Biosensors Technology and Applications*; InTech: London, UK, 2011; ISBN 978-953-307-448-1.
17. Saateh, A.; Kalantarifard, A.; Celik, O.T.; Asghari, M.; Serhatlioglu, M.; Elbuken, C. Real-time impedimetric droplet measurement (iDM). *Lab Chip* **2019**, *19*, 3815–3824. [CrossRef]
18. Guan, J.-G.; Miao, Y.-Q.; Zhang, Q.-J. Impedimetric biosensors. *J. Biosci. Bioeng.* **2004**, *97*, 219–226. [CrossRef]
19. Yang, R.-J.; Fu, L.-M.; Hou, H.-H. Review and perspectives on microfluidic flow cytometers. *Sens. Actuators B Chem.* **2018**, *266*, 26–45. [CrossRef]
20. Jiang, H.; Zhu, T.; Zhang, H.; Nie, J.; Guan, Z.; Ho, C.M.; Liu, S.; Fei, P. Droplet-based light-sheet fluorescence microscopy for high-throughput sample preparation, 3-D imaging and quantitative analysis on a chip. *Lab Chip* **2017**, *17*, 2193–2197. [CrossRef] [PubMed]
21. BD Accuri™ C6 Plus | BD Biosciences-US. Available online: https://www.bdbiosciences.com/en-us/instruments/research-instruments/research-cell-analyzers/accuri-c6-plus (accessed on 15 April 2020).
22. Cell Analysis at the Bench: Benchtop Flow Cytometers | Biocompare: The Buyer's Guide for Life Scientists. Available online: https://www.biocompare.com/editorial-articles/146008-cell-analysis-at-the-bench-benchtop-flow-cytometers/ (accessed on 15 April 2020).
23. Attune NxT Flow Cytometer | Thermo Fisher Scientific—EE. 2020. Available online: https://www.thermofisher.com/ee/en/home/life-science/cell-analysis/flow-cytometry/flow-cytometers/attune-acoustic-focusing-flow-cytometer.html (accessed on 15 April 2020).
24. Shrirao, A.B.; Fritz, Z.; Novik, E.M.; Yarmush, G.M.; Schloss, R.S.; Zahn, J.D.; Yarmush, M.L. Microfluidic flow cytometry: The role of microfabrication methodologies, performance and functional specification. *Technology* **2018**, *6*, 1–23. [CrossRef]
25. Schonbrun, E.; Gorthi, S.S.; Schaak, D. Microfabricated multiple field of view imaging flow cytometry. *Lab Chip* **2012**, *12*, 268–273. [CrossRef] [PubMed]
26. Han, Y.; Gu, Y.; Zhang, A.C.; Lo, Y.H. Review: Imaging technologies for flow cytometry. *Lab Chip* **2016**, *16*, 4639–4647. [CrossRef]
27. Zhu, Y.; Fang, Q. Analytical detection techniques for droplet microfluidics—A review. *Anal. Chim. Acta* **2013**, *787*, 24–35. [CrossRef] [PubMed]
28. Zhang, Y.; Watts, B.; Guo, T.; Zhang, Z.; Xu, C.; Fang, Q. Optofluidic Device Based Microflow Cytometers for Particle/Cell Detection: A Review. *Micromachines* **2016**, *7*, 70. [CrossRef]
29. Yotter, R.A.; Wilson, D.M. A review of photodetectors for sensing light-emitting reporters in biological systems. *IEEE Sens. J.* **2003**, *3*, 288–303. [CrossRef]
30. Samiei, E.; Tabrizian, M.; Hoorfar, M. A review of digital microfluidics as portable platforms for lab-on a-chip applications. *Lab Chip* **2016**, *16*, 2376–2396. [CrossRef]
31. Liu, W.; Zhu, Y. "Development and application of analytical detection techniques for droplet-based microfluidics"—A review. *Anal. Chim. Acta* **2020**, *1113*, 66–84. [CrossRef]
32. Elliott, D.J. *Ultraviolet Laser Technology and Applications*; Academic Press: New York NY, USA, 1995; ISBN 9781483296517.
33. Rawicz, A.H. Theodore Harold Maiman and the invention of laser. In *Proceedings of the Photonics, Devices, and Systems IV*; Tománek, P., Senderáková, D., Hrabovský, M., Eds.; SPIE: Bellingham, WA, USA, 2008; Volume 7138, p. 713802.

34. Schawlow, A.L.; Townes, C.H. Infrared and optical masers. *Phys. Rev.* **1958**, *112*, 1940–1949. [CrossRef]
35. Svelto, O. *Principles of Lasers*; Springer: New York, NY, USA, 2010; ISBN 9781441913012.
36. Ready, J.F. *Industrial Applications of Lasers*; Elsevier: Amsterdam, The Netherlands, 1997; ISBN 9780125839617.
37. Laser Diode Tutorial. Available online: https://www.thorlabs.com/newgrouppage9.cfm?objectgroup_id=1832 (accessed on 21 March 2020).
38. Lai, M.H.; Lim, K.S.; Gunawardena, D.S.; Lee, Y.S.; Ahmad, H. CO2 Laser Applications in Optical Fiber Components Fabrication and Treatment: A Review. *IEEE Sens. J.* **2017**, *17*, 2961–2974. [CrossRef]
39. Types of Lasers—Solid State Laser, Gas Laser, Liquid Laser & Semiconductor Laser. Available online: https://www.physics-and-radio-electronics.com/physics/laser/differenttypesoflasers.html (accessed on 25 May 2020).
40. Legres, L.G.; Chamot, C.; Varna, M.; Janin, A. The Laser Technology: New Trends in Biology and Medicine. *J. Mod. Phys.* **2014**, *5*, 267–279. [CrossRef]
41. Silfvast, W.T. *Laser Fundamentals*, 2nd ed.; Cambridge University Press: Cambridge, UK, 2004; ISBN 9780521541053.
42. Frot, C.; Taccoen, N.; Baroud, C.N. Frugal droplet microfluidics using consumer opto-electronics. *PLoS ONE* **2016**, *11*, e161490. [CrossRef]
43. Clausell-Tormos, J.; Lieber, D.; Baret, J.C.; El-Harrak, A.; Miller, O.J.; Frenz, L.; Blouwolff, J.; Humphry, K.J.; Köster, S.; Duan, H.; et al. Droplet-Based Microfluidic Platforms for the Encapsulation and Screening of Mammalian Cells and Multicellular Organisms. *Chem. Biol.* **2008**, *15*, 427–437. [CrossRef]
44. Sjostrom, S.L.; Bai, Y.; Huang, M.; Liu, Z.; Nielsen, J.; Joensson, H.N.; Andersson Svahn, H. High-throughput screening for industrial enzyme production hosts by droplet microfluidics. *Lab Chip* **2014**, *14*, 806–813. [CrossRef]
45. Isozaki, A.; Mikami, H.; Hiramatsu, K.; Sakuma, S.; Kasai, Y.; Iino, T.; Yamano, T.; Yasumoto, A.; Oguchi, Y.; Suzuki, N.; et al. A Practical Guide to Intelligent Image-Activated Cell Sorting. *Nat. Protoc.* **2019**, *14*, 2370–2415. [CrossRef]
46. Hung, S.-T.; Mukherjee, S.; Jimenez, R. Enrichment of rare events using a multi-parameter high throughput microfluidic droplet sorter. *Lab Chip* **2020**, *15*, 332–335. [CrossRef] [PubMed]
47. Sciambi, A.; Abate, A.R. Accurate microfluidic sorting of droplets at 30 kHz. *Lab Chip* **2015**, *15*, 47–51. [CrossRef]
48. Shapiro, H.M.; Telford, W.G. Lasers for Flow Cytometry: Current and Future Trends. *Curr. Protoc. Cytom.* **2018**, *83*, 1–9. [CrossRef] [PubMed]
49. Pavlovic, T. (Ed.) *The Sun and Photovoltaic Technologies*; Green Energy and Technology; Springer International Publishing: Cham, Switzerland, 2020; ISBN 978-3-030-22402-8.
50. Powering Lasers: Evaluating Bench Power Supplies | Lasers | Photonics Handbook | Photonics Buyers' Guide. Available online: https://www.photonics.com/Articles/Powering_Lasers_Evaluating_Bench_Power_Supplies/a57160 (accessed on 30 April 2020).
51. Denker, B.; Shklovsky, E. *Handbook of Solid-State Lasers: Materials, Systems and Applications*; Elsevier: Amsterdam, The Netherlands, 2013; ISBN 978-0-85709-272-4.
52. Light-Emitting Diodes: A Primer | Light Sources | Photonics Handbook | Photonics Buyers' Guide. Available online: https://www.photonics.com/Articles/Light-Emitting_Diodes_A_Primer/a36706 (accessed on 17 March 2020).
53. Capitán-Vallvey, L.F.; Palma, A.J. Recent developments in handheld and portable optosensing—A review. *Anal. Chim. Acta* **2011**, *696*, 27–46. [CrossRef] [PubMed]
54. Gong, Y.; Fan, N.; Yang, X.; Peng, B.; Jiang, H. New advances in microfluidic flow cytometry. *Electrophoresis* **2018**. [CrossRef] [PubMed]
55. ZEISS Microscopy Online Campus | Light-Emitting Diodes. Available online: http://zeiss-campus.magnet.fsu.edu/print/lightsources/leds-print.html (accessed on 9 March 2020).
56. Bui, D.A.; Hauser, P.C. Analytical devices based on light-emitting diodes—A review of the state-of-the-art. *Anal. Chim. Acta* **2015**, *853*, 46–58. [CrossRef]
57. Zhou, S.; Pan, Y.; Li, N.; Xu, B.; Liu, J.; Song, Q.; Xu, J.; Li, D.; Liu, P.; Xu, X.; et al. Spectroscopy and diode-pumped laser operation of Pr:LaMgAl11O19 crystal. *Opt. Mater.* **2019**, *89*, 14–17. [CrossRef]
58. Van Der Broeck, H.; Sauerländer, G.; Wendt, M. Power driver topologies and control schemes for LEDs. In Proceedings of the APEC 07—Twenty-Second Annual IEEE Applied Power Electronics Conference and Exposition, Anaheim, CA, USA, 25 February–1 March 2007; pp. 1319–1325.
59. Wang, Y.; Alonso, J.M.; Ruan, X. A Review of LED Drivers and Related Technologies. *IEEE Trans. Ind. Electron.* **2017**, *64*, 5754–5765. [CrossRef]
60. Hölz, K.; Lietard, J.; Somoza, M.M. High-Power 365 nm UV LED Mercury Arc Lamp Replacement for Photochemistry and Chemical Photolithography. *ACS Sustain. Chem. Eng.* **2017**, *5*, 828–834. [CrossRef] [PubMed]
61. Lim, J.; Vrignon, J.; Gruner, P.; Karamitros, C.S.; Konrad, M.; Baret, J.C. Ultra-high throughput detection of single cell β-galactosidase activity in droplets using micro-optical lens array. *Appl. Phys. Lett.* **2013**, *103*, 203704. [CrossRef] [PubMed]
62. Aswani, K.; Jinadasa, T.; Brown, C.M. Fluorescence Microscopy Light Sources. *Microsc. Today* **2012**, *20*, 22–28. [CrossRef]
63. Mubaid, F.; Kaufman, D.; Wee, T.L.; Nguyen-Huu, D.S.; Young, D.; Anghelopoulou, M.; Brown, C.M. Fluorescence microscope light source stability. *Histochem. Cell Biol.* **2019**, *151*, 357–366. [CrossRef] [PubMed]
64. Elvidge, C.D.; Keith, D.M.; Tuttle, B.T.; Baugh, K.E. Spectral Identification of Lighting Type and Character. *Sensors* **2010**, *10*, 3961–3988. [CrossRef]
65. Osram Metal Halide Lamp—Osram. Available online: https://www.osram.de/media/resource/hires/334186/Metal-halide-lamps.-Instructions-for-the-use-and-application.pdf (accessed on 15 April 2020).

66. Chang, Y.N.; Yang, T.H.; Chan, S.Y.; Cheng, H.L. Design of electronic ballast for short-arc Xenon lamps. In Proceedings of the IEEE International Symposium on Industrial Electronics, Hangzhou, China, 28–31 May 2012; pp. 309–314.
67. Seo, S.; Mastiani, M.; Mosavati, B.; Peters, D.M.; Mandin, P.; Kim, M. Performance evaluation of environmentally benign nonionic biosurfactant for enhanced oil recovery. *Fuel* **2018**, *234*, 48–55. [CrossRef]
68. Utharala, R.; Tseng, Q.; Furlong, E.E.M.; Merten, C.A. A versatile, low-cost, multi-way microfluidic sorter for droplets, cells and embryos. *Anal. Chem.* **2018**, *90*, 5982–5988. [CrossRef]
69. Leman, M.; Abouakil, F.; Griffiths, A.D.; Tabeling, P. Droplet-based microfluidics at the femtolitre scale. *Lab Chip* **2015**, *15*, 753–765. [CrossRef]
70. Hess, D.; Rane, A.; DeMello, A.J.; Stavrakis, S. High-Throughput, Quantitative Enzyme Kinetic Analysis in Microdroplets Using Stroboscopic Epifluorescence Imaging. *Anal. Chem.* **2015**, *87*, 4965–4972. [CrossRef] [PubMed]
71. Choi, J.W.; Kang, D.K.; Park, H.; Demello, A.J.; Chang, S.I. High-throughput analysis of protein-protein interactions in picoliter-volume droplets using fluorescence polarization. *Anal. Chem.* **2012**, *84*, 3849–3854. [CrossRef]
72. Kim, M.; Pan, M.; Gai, Y.; Pang, S.; Han, C.; Yang, C.; Tang, S.K.Y. Optofluidic ultrahigh-throughput detection of fluorescent drops. *Lab Chip* **2015**, *15*, 1417–1423. [CrossRef] [PubMed]
73. Shapiro, H.M. *Practical Flow Cytometry*; Wiley: Hoboken, NJ, USA, 2003; ISBN 9780471411253.
74. Kaushik, A.M.; Hsieh, K.; Chen, L.; Shin, D.J.; Liao, J.C.; Wang, T.H. Accelerating bacterial growth detection and antimicrobial susceptibility assessment in integrated picoliter droplet platform. *Biosens. Bioelectron.* **2017**, *97*, 260–266. [CrossRef]
75. Gao, Z.; Peng, H.; Zhu, M.; Wu, L.; Jia, C.; Zhou, H.; Zhao, J. A Facile Strategy for Visualizing and Modulating Droplet-Based Microfluidics. *Micromachines* **2019**, *10*, 291. [CrossRef] [PubMed]
76. Yu, J.; Sun, G.; Lin, N.W.; Vadanan, S.V.; Lim, S.; Chen, C.H. Intelligent optofluidic analysis for ultrafast single bacterium profiling of cellulose production and morphology. *Lab Chip* **2020**, *20*, 626–633. [CrossRef]
77. Yelleswarapu, V.R.; Jeong, H.H.; Yadavali, S.; Issadore, D. Ultra-high throughput detection (1 million droplets per second) of fluorescent droplets using a cell phone camera and time domain encoded optofluidics. *Lab Chip* **2017**, *17*, 1083–1094. [CrossRef]
78. Rane, A.S.; Rutkauskaite, J.; deMello, A.; Stavrakis, S. High-Throughput Multi-parametric Imaging Flow Cytometry. *Chem* **2017**, *3*, 588–602. [CrossRef]
79. Vercruysse, D.; Dusa, A.; Stahl, R.; Vanmeerbeeck, G.; de Wijs, K.; Liu, C.; Prodanov, D.; Peumans, P.; Lagae, L. Three-part differential of unlabeled leukocytes with a compact lens-free imaging flow cytometer. *Lab Chip* **2015**, *15*, 1123–1132. [CrossRef]
80. Schonbrun, E.; Abate, A.R.; Steinvurzel, P.E.; Weitz, D.A.; Crozier, K.B. High-throughput fluorescence detection using an integrated zone-plate array. *Lab Chip* **2010**, *10*, 852. [CrossRef]
81. Mikami, H.; Kawaguchi, M.; Huang, C.-J.; Matsumura, H.; Sugimura, T.; Huang, K.; Lei, C.; Ueno, S.; Miura, T.; Ito, T.; et al. Virtual-freezing fluorescence imaging flow cytometry. *Nat. Commun.* **2020**, *11*, 1162. [CrossRef] [PubMed]
82. Zhao, J.; You, Z. A Microflow Cytometer with a Rectangular Quasi-Flat-Top Laser Spot. *Sensors* **2016**, *16*, 1474. [CrossRef] [PubMed]
83. Tovar, M.; Hengoju, S.; Weber, T.; Mahler, L.; Choudhary, M.; Becker, T.; Roth, M. One Sensor for Multiple Colors: Fluorescence Analysis of Microdroplets in Microbiological Screenings by Frequency-Division Multiplexing. *Anal. Chem.* **2019**, *91*, 3055–3061. [CrossRef] [PubMed]
84. Cole, R.H.; de Lange, N.; Gartner, Z.J.; Abate, A.R. Compact and modular multicolour fluorescence detector for droplet microfluidics. *Lab Chip* **2015**, *15*, 2754–2758. [CrossRef] [PubMed]
85. Fiedler, B.L.; Van Buskirk, S.; Carter, K.P.; Qin, Y.; Carpenter, M.C.; Palmer, A.E.; Jimenez, R. Droplet Microfluidic Flow Cytometer For Sorting On Transient Cellular Responses Of Genetically-Encoded Sensors. *Anal. Chem.* **2017**, *89*, 711–719. [CrossRef]
86. Hamamatsu Photonics. *Photomultiplier Tubes—Basics and Applications*, 3rd ed.; Word Tehcnical Writing, Ed.; Hamamatsu Photonics K.K.: Hamamatsu, Japan, 2007.
87. Ibsen Quick Note: Calculating Quantum Efficiency from A/W. Available online: https://ibsen.com/wp-content/uploads/Tech-Note-Quantum-efficiency-conversion-note.pdf (accessed on 16 April 2020).
88. Larsen, A.C.; Dunn, M.R.; Hatch, A.; Sau, S.P.; Youngbull, C.; Chaput, J.C. A general strategy for expanding polymerase function by droplet microfluidics. *Nat. Commun.* **2016**, *7*, 11235. [CrossRef]
89. Gao, R.; Cheng, Z.; Demello, A.J.; Choo, J. Wash-free magnetic immunoassay of the PSA cancer marker using SERS and droplet microfluidics. *Lab Chip* **2016**, *16*, 1022–1029. [CrossRef]
90. Shi, W.; Wen, H.; Lu, Y.; Shi, Y.; Lin, B.; Qin, J. Droplet microfluidics for characterizing the neurotoxin-induced responses in individual Caenorhabditis elegans. *Lab Chip* **2010**, *10*, 2855–2863. [CrossRef]
91. Mikami, H.; Miura, T.; Ozeki, Y.; Goda, K. High-throughput fluorescence imaging flow cytometry with light-sheet excitation and machine learning (Conference Presentation). In Proceedings of the High-Speed Biomedical Imaging and Spectroscopy III: Toward Big Data Instrumentation and Management; Goda, K., Tsia, K.K., Eds.; SPIE: Bellingham, WA, USA, 2018; p. 15.
92. Chen, W.P.; Eivar, P.B.; Petersen, T.; Gandhi, D.; Liu, K.; Luo, N. The sub-system validation of solid-state detector in BD Accuri C6 plus flow cytometer. In Proceedings of the Design and Quality for Biomedical Technologies XII; Liang, R., Pfefer, T.J., Hwang, J., Eds.; SPIE: Bellingham, WA, USA, 2019; Volume 10870, p. 9.
93. Bonar, M.M.; Tilton, J.C. High sensitivity detection and sorting of infectious human immunodeficiency virus (HIV-1) particles by flow virometry. *Virology* **2017**, *505*, 80–90. [CrossRef]

94. Srisa-Art, M.; Dyson, E.C.; deMello, A.J.; Edel, J.B. Monitoring of Real-Time Streptavidin−Biotin Binding Kinetics Using Droplet Microfluidics. *Anal. Chem.* **2008**, *80*, 7063–7067. [CrossRef]
95. Nguyen, N.T. Micro-optofluidic Lenses: A review. *Biomicrofluidics* **2010**, *4*, 031501. [CrossRef]
96. Holst, G.C.; Lomheim, T.S. *CMOS/CCD Sensors and Camera Systems*, 2nd ed.; JCD Publishing: Winter Park, FL, USA, 2018; ISBN 978-0-9707-7498-9.
97. Dussault, D.; Hoess, P. Noise performance comparison of ICCD with CCD and EMCCD cameras. In Proceedings of the Infrared Systems and Photoelectronic Technology; Dereniak, E.L., Sampson, R.E., Johnson, C.B., Eds.; SPIE: Bellingham, WA, USA, 2004; Volume 5563, p. 195.
98. Smith, N.; Coates, C.; Giltinan, A.; Howard, J.; O'Connor, A.; O'Driscoll, S.; Hauser, M.; Wagner, S. EMCCD technology and its impact on rapid low-light photometry. In Proceedings of the Optical and Infrared Detectors for Astronomy; Garnett, J.D., Beletic, J.W., Eds.; SPIE: Bellingham, WA, USA, 2004; Volume 5499, p. 162.
99. Robbins, M.S.; Hadwen, B.J. The noise performance of electron multiplying charge-coupled devices. *IEEE Trans. Electron Devices* **2003**, *50*, 1227–1232. [CrossRef]
100. Qi, L.; Just, F.; Leuchs, G.; Chekhova, M.V. Autonomous absolute calibration of an ICCD camera in single-photon detection regime. *Opt. Express* **2016**, *24*, 26444. [CrossRef] [PubMed]
101. Daigle, O.; Turcotte, J.; Gosselin, Y.; Lamy, A.S.A. Time-delay integration EMCCD. In Proceedings of the 2019 Photonics North, PN 2019, Quebec City, QC, Canada, 21–23 May 2019.
102. Schühle, U. Intensified solid state sensor cameras: ICCD and IAPS. In *Observing Photons in Space*; Springer: New York, NY, USA, 2013; pp. 455–465.
103. Introduction to SiPM Technical Note. Available online: https://www.sensl.com/downloads/ds/TN-IntrotoSPMTech.pdf (accessed on 3 May 2020).
104. Lindén, J.; Knappe, C.; Richter, M.; Aldén, M. Limitations of ICCD detectors and optimized 2D phosphor thermometry. *Meas. Sci. Technol.* **2012**, *23*, 035201. [CrossRef]
105. Yamada, M.; Nakashima, M.; Seki, M. Pinched flow fractionation: Continuous size separation of particles utilizing a laminar flow profile in a pinched microchannel. *Anal. Chem.* **2004**, *76*, 5465–5471. [CrossRef] [PubMed]
106. Wang, W.-H.; Zhang, Z.-L.; Xie, Y.-N.; Wang, L.; Yi, S.; Liu, K.; Liu, J.; Pang, D.-W.; Zhao, X.-Z. Flow-Focusing Generation of Monodisperse Water Droplets Wrapped by Ionic Liquid on Microfluidic Chips: From Plug to Sphere. *Langmuir* **2007**, *23*, 11924–11931. [CrossRef] [PubMed]
107. Oh, D.W.; Jin, J.S.; Choi, J.H.; Kim, H.Y.; Lee, J.S. A microfluidic chaotic mixer using ferrofluid. *J. Micromech. Microeng.* **2007**, *17*, 2077–2083. [CrossRef]
108. Cecchini, M.P.; Hong, J.; Lim, C.; Choo, J.; Albrecht, T.; DeMello, A.J.; Edel, J.B. Ultrafast surface enhanced resonance raman scattering detection in droplet-based microfluidic systems. *Anal. Chem.* **2011**, *83*, 3076–3081. [CrossRef]
109. Bardiya, N.; Choi, J.W.; Chang, S.I. Analysis of single nucleotide polymorphism in human angiogenin using droplet-based microfluidics. *Biochip J.* **2014**, *8*, 15–21. [CrossRef]
110. Lv, S.; Yu, J.; Zhao, Y.; Li, H.; Zheng, F.; Liu, N.; Li, D.; Sun, X. A Microfluidic Detection System for Bladder Cancer Tumor Cells. *Micromachines* **2019**, *10*, 871. [CrossRef] [PubMed]
111. Kemeny, S.E.; Fossum, E.R. CMOS Active Pixel Image Sensor. *IEEE Trans. Electron Devices* **1994**, *41*, 452–453. [CrossRef]
112. Fossum, E.R. Active pixel sensors: Are CCDs dinosaurs? In Proceedings of the Charge-Coupled Devices and Solid State Optical Sensors III; SPIE: Bellingham, WA, USA, 1993; Volume 1900, pp. 2–14.
113. Eid, S.I.; Dickinson, A.G.; Inglis, D.A.; Ackland, B.D.; Fossum, E.R. 256 × 256 CMOS active pixel image sensor. In Proceedings of the Charge-Coupled Devices and Solid State Optical Sensors V; SPIE: Bellingham, WA, USA, 1995; Volume 2415, p. 265.
114. Bermak, A.; Bouzerdoum, A.; Eshraghian, K. High fill-factor native logarithmic pixel: Simulation, design and layout optimization. In Proceedings of the IEEE International Symposium on Circuits and Systems, Geneva, Switzerland, 28–31 May 2000; Volume 5.
115. Joy, T.; Pyo, S.; Park, S.; Choi, C.; Palsule, C.; Han, H.; Feng, C.; Lee, S.; McKee, J.; Altice, P.; et al. Development of a production-ready, back-illuminated CMOS image sensor with small pixels. In Proceedings of the 2007 IEEE International Electron Devices Meeting, Washington, DC, USA, 10–12 December 2007; pp. 1007–1010.
116. Williams, J.B.; Williams, J.B. Introduction. In *The Electronics Revolution*; Springer International Publishing: Berlin/Heidelberg, Germany, 2017; pp. 1–4.
117. Bigas, M.; Cabruja, E.; Forest, J.; Salvi, J. Review of CMOS image sensors. *Microelectron. J.* **2006**, *37*, 433–451. [CrossRef]
118. Yang, H.; Gijs, M.A.M. Micro-optics for microfluidic analytical applications. *Chem. Soc. Rev.* **2018**, *47*, 1391–1458. [CrossRef]
119. Li, Z.; Zhang, S.; Wei, Q. Smartphone-based flow cytometry. In *Smartphone Based Medical Diagnostics*; Elsevier: Amsterdam, The Netherlands, 2020; pp. 67–88.
120. Skandarajah, A.; Reber, C.D.; Switz, N.A.; Fletcher, D.A. Quantitative Imaging with a Mobile Phone Microscope. *PLoS ONE* **2014**, *9*, e96906. [CrossRef]
121. Lubsandorzhiev, B.K. On the history of photomultiplier tube invention. *Nucl. Instrum. Methods Phys. Res. Sect. A* **2006**, *567*, 236–238. [CrossRef]
122. Photonis. Photomultiplier Tube Basics. Available online: https://psec.uchicago.edu/library/photomultipliers/Photonis_PMT_basics.pdf (accessed on 4 April 2020).

123. Anashin, V.V.; Golubev, V.B.; Beschastnov, P.M.; Golubev, V.B.; Mironenko, L.A.; Salnikov, A.A.; Serednyakov, S.I. Nuclear Instruments and Methods in Physics Research Section A Accelerators Spectrometers Detectors and Associated Equipment April 1995 ELSEVIER Nuclear Instruments and Methods. *Phys. Res. A* **1995**, *357*, 103–109. [CrossRef]
124. Dhawan, S. Introduction to microchannel plate photomultipliers. *IEEE Trans. Nucl. Sci.* **1981**, *28*, 672–676. [CrossRef]
125. Kishimoto, N.; Nagamine, M.; Inami, K.; Enari, Y.; Ohshima, T. Lifetime of MCP-PMT. *Nucl. Instrum. Methods Phys. Res. Sect. A* **2006**, *564*, 204–211. [CrossRef]
126. Britting, A.; Eyrich, W.; Lehmann, A.; Uhlig, F. Lifetime-issues of MCP-PMTs. *J. Instrum.* **2011**, *6*, C10001. [CrossRef]
127. Cheng, Z.; Xu, H.; Chen, Y. Design of low noise silicon reach-through avalanche photodiodes. In Proceedings of the Hard X-Ray, Gamma-Ray, and Neutron Detector Physics XX; Fiederle, M., Burger, A., James, R.B., Payne, S.A., Eds.; SPIE: Bellingham, WA, USA, 2018; Volume 10762, p. 19.
128. LaserComponents Silicon Avalanche Photodiodes. Available online: https://www.lasercomponents.com/fileadmin/user_upload/home/Datasheets/lc/application-reports/lc-apd/si-apds.pdf (accessed on 2 May 2020).
129. Hamamatsu APD Modules. Available online: https://www.hamamatsu.com/resources/pdf/ssd/apd_modules_kacc9010e.pdf (accessed on 2 May 2020).
130. Nabet, B. *Photodetectors: Materials, Devices and Applications*; Elsevier Inc.: Amsterdam, The Netherlands, 2015; ISBN 9781782424680.
131. Bruschini, C.; Homulle, H.; Antolovic, I.M.; Burri, S.; Charbon, E. Single-photon avalanche diode imagers in biophotonics: Review and outlook. *Light Sci. Appl.* **2019**, *8*, 1–28. [CrossRef]
132. Engelmann, E.; Popova, E.; Vinogradov, S. Spatially resolved dark count rate of SiPMs. *Eur. Phys. J. C* **2018**, *78*. [CrossRef]
133. Nakamura, Y.; Okumura, A.; Tajima, H.; Yamane, N.; Zenin, A. Characterization of SiPM Optical Crosstalk and its Dependence on the Protection-Window Thickness. In Proceedings of the 5th International Workshop on New Photon-Detectors (PD18), Tokyo, Japan, 27–29 November 2019. [CrossRef]
134. Kang, D.K.; Gong, X.; Cho, S.; Kim, J.Y.; Edel, J.B.; Chang, S.I.; Choo, J.; Demello, A.J. 3D Droplet Microfluidic Systems for High-Throughput Biological Experimentation. *Anal. Chem.* **2015**, *87*, 10770–10778. [CrossRef]
135. Suzuki, Y.; Kobayashi, K.; Wakisaka, Y.; Deng, D.; Tanaka, S.; Huang, C.J.; Lei, C.; Sun, C.W.; Liu, H.; Fujiwaki, Y.; et al. Label-free chemical imaging flow cytometry by high-speed multicolor stimulated Raman scattering. *Proc. Natl. Acad. Sci. USA* **2019**, *116*, 15842–15848. [CrossRef]
136. Guo, B.; Lei, C.; Kobayashi, H.; Ito, T.; Yalikun, Y.; Jiang, Y.; Tanaka, Y.; Ozeki, Y.; Goda, K. High-throughput, label-free, single-cell, microalgal lipid screening by machine-learning-equipped optofluidic time-stretch quantitative phase microscopy. *Cytom. Part A* **2017**, *91*, 494–502. [CrossRef]
137. Guo, B.; Lei, C.; Wu, Y.; Kobayashi, H.; Ito, T.; Yalikun, Y.; Lee, S.; Isozaki, A.; Li, M.; Jiang, Y.; et al. Optofluidic time-stretch quantitative phase microscopy. *Methods* **2018**, *136*, 116–125. [CrossRef]
138. Suzuki, M.; Suzuki, M.; Kuroda, R.; Kumagai, Y.; Chiba, A.; Miura, N.; Kuriyama, N.; Sugawa, S. An over 1 Mfps global shutter CMOS image sensor with 480 frame storage using vertical analog memory integration. In Proceedings of the Technical Digest—International Electron Devices Meeting, IEDM, San Francisco, CA, USA, 3–7 December 2016; pp. 8.5.1–8.5.4.
139. Suzuki, M.; Sugama, Y.; Kuroda, R.; Sugawa, S. Over 100 Million Frames per Second 368 Frames Global Shutter Burst CMOS Image Sensor with Pixel-wise Trench Capacitor Memory Array. *Sensors* **2020**, *20*, 1086. [CrossRef] [PubMed]
140. Amnis® ImageStream®XMark II. Available online: https://www.luminexcorp.com/imagestreamx-mk-ii/#overview (accessed on 16 March 2021).
141. Fung, P.A. 2016 Flow Cytometry Buyer's Guide: A Researcher's Guide to Selecting a Flow Cytometer. Available online: https://www.biocompare.com/186616-2016-Flow-Cytometry-Buyer-s-Guide/ (accessed on 14 March 2021).
142. Elveflow Optical Reader for Microfluidics—Elveflow. Available online: https://www.elveflow.com/microfluidic-flow-control-archives/optical-reader-for-microfluidics/ (accessed on 27 April 2020).
143. Houssin, T.; Cramer, J.; Grojsman, R.; Bellahsene, L.; Colas, G.; Moulet, H.; Minnella, W.; Pannetier, C.; Leberre, M.; Plecis, A.; et al. Ultrafast, sensitive and large-volume on-chip real-time PCR for the molecular diagnosis of bacterial and viral infections. *Lab Chip* **2016**, *16*, 1401–1411. [CrossRef]
144. "Sphere Fluidics" Cyto-Mine® The Single Cell Analysis and Monoclonality Assurance System. 2018. Available online: https://spherefluidics.com/wp-content/uploads/2018/12/Cyto-Mine-Brochure-12-page-Version-October-2018.pdf?v=a57b8491d1d8 (accessed on 27 April 2020).
145. Josephides, D.; Davoli, S.; Whitley, W.; Ruis, R.; Salter, R.; Gokkaya, S.; Vallet, M.; Matthews, D.; Benazzi, G.; Shvets, E.; et al. Cyto-Mine: An Integrated, Picodroplet System for High-Throughput Single-Cell Analysis, Sorting, Dispensing, and Monoclonality Assurance. *SLAS Technol.* **2020**, *25*, 177–189. [CrossRef]
146. *BioRad. QX200 Droplet Reader and QuantaSoft Software Instruction Manual*; Bio-Rad: Hercules, CA, USA, 2019.
147. Safford, H.R.; Bischel, H.N. Performance comparison of four commercially available cytometers using fluorescent, polystyrene, submicron-scale beads. *Data Br.* **2019**, *24*. [CrossRef] [PubMed]

Appendix 2

Publication II

K. Parnamets, A. Koel, T. Pardy, and T. Rang, “Open Source Hardware Cost-Effective Imaging Sensors for High-Throughput Droplet Microfluidic Systems,” *Proc. 2022 26th Int. Conf. Electron. Electron. 2022*, 2022, doi: 10.1109/IEEECONF55059.2022.9810383.

Open Source Hardware Cost-Effective Imaging Sensors for High-Throughput Droplet Microfluidic Systems

Kaiser Parnamets[1, *], Ants Koel[1], Tamas Pardy[2], Toomas Rang[1, 2]
[1]*Thomas Johann Seebeck Department of Electronics, Tallinn University of Technology, Ehitajate tee 5, 19086, Tallinn, Estonia*
[2]*Department of Chemistry and Biotechnology, Tallinn University of Technology, Ehitajate tee 5, 19086, Tallinn, Estonia*
kaiser.parnamets@taltech.ee

2022 26th International Conference Electronics | 978-1-6654-8321-6/22/$31.00 ©2022 IEEE | DOI: 10.1109/IEECONF55059.2022.9810383

***Abstract*—Microfluidic systems have been and continue to be very attractive to scientific community. In a typical droplet microfluidic measurement setup, a microscope and a camera attached to it are used for observing the droplets. The throughput of droplets has increased over time, and high-throughput systems require sensors with high framerates per second. With the increase of the required speed, also the price of the cameras increases. To avoid the use of expensive cameras, many unusual cameras such as webcams and smartphone cameras have found their way to droplet microfluidics. Additionally, the droplet microfluidic systems tend to grow more complex and autonomous and need more customization than the closed hardware can provide. This leads to the need for highly customisable, cost-effective, and open-source hardware. In this article, we compare three cost-effective imaging sensors, two of them open-hardware, that could be considered to be used in high-throughput droplet microfluidic systems. During the tests two different entry-level open-source systems based on Raspberry Pi were tested and the results compared to slightly more expensive mid-range Basler camera results. The entry-level systems were able to reach 200 and 665 frames per second and the mid-range comparison reference to 750 fps.**

***Index Terms*—Image sensors; Microfluidics; Open source hardware.**

I. Introduction

To date lab-on-a-chip and microfluidic devices have been around for almost half a century [1]. In the recent decades, the microfluidic devices have gained interest as they handle sample fluid volumes in the ranges from microliters to picolitres, allowing users to reduce biological waste and minimize the use of expensive reagents [2]–[4]. Droplet microfluidics is often used in experiments to isolate single cells from the bulk, allowing faster results, achieving better control over the contents of each droplet and allowing massive parallel experimentation [5]–[8]. The latter usually requires droplets to be generated at high speeds, resulting in high-throughput (1000> droplets per second (dps)) [2], [9], [10]. To see and visualise static results, some form of bright-field microscopy can be used [11], however when droplets are generated at high speeds, then visual inspection by eye is not suitable anymore and some form of automated analytical approach should be used. There are multiple sensors available to acquire data for general microfluidics (optical, chemical, electric), but two types of optical sensors, imaging and non-imaging, both having their advantages and disadvantages [12], [13], clearly stand out as preferred ones for the various droplet microfluidics applications. For imaging sensors, especially if high-throughput performance is aimed, the cameras quickly move out from the cost-effective price range and in the majority of cases the software included with cameras is proprietary and not free [14]–[19]. During the recent years open source hardware has gained more and more attraction in the scientific field. The Boolean search for the *open source hardware* search term was conducted in Google Scholar to see the trend of the last 10 years. Over the period, the results have increased from 73 800 to 96 500. A similar search was conducted for *open source hardware lab-on-a-chip* and the results increased from 304 to 5 160. These searches clearly indicate the rising interest and use of open source hardware in scientific and lab-on-a-chip applications.

The top of the line equipment for droplet microfluidic flow cytometry are the commercial flow cytometers. Out of many companies, two have gained popularity as their devices have been reported the most in scientific studies. Thermo Fisher Attune Nxt (Thermo Fisher Scientific, Waltham, MA, USA) has been on the market for some years and allows users to quantitatively analyse their sample up to 65000 events per second (eps) [20]. Some sources report the list price to be near 100000 USD [21]. Another device, the BD Accuri C6 (BD Biosciences, San Jose, CA, USA), allows users to quantitatively analyse their sample at maximum of 10000 eps [22]. The price is reported to be around 50000 USD [21]. Both of the devices include multiple light sources and optical filters to enable up to 16 different measurements. Next to the commercial devices are

Manuscript received 10 January, 2022; accepted 5 April, 2022.
This research was funded by the Estonian Science Agency ETAg, grant number PRG620, MOBTP109 and by the European Union's Horizon 2020 Research and Innovation Program under Grant 668995.

experimental microfluidic imaging setups using high speed cameras in combination with microscope or microscope lenses. Often these setups are tuned to one specific experiment and use only one type of light source and optical filtering. The flow rate of conventional imaging flow cytometers is estimated to be around 1000 dps [17], [23]–[25]. The high speed cameras reach framerates of tens of thousands of frames per second [18], [19]. For such devices the price is not publicly available and has to be quoted for each camera, however some sources estimate it to be in range of tens of thousands of dollars [26]. For experiments, where high throughput (1000> dps) is not needed, the cameras with lower framerates can be used. During the recent years the development of open hardware solutions have been promising as they allow the end user to customize the camera to their need. In such applications Raspberry Pi has been very interesting as it is a low-cost microcomputer system with camera interface and has three different camera modules available. In literature such systems are reported and typically cameras are used at the resolution of 640x480 pixels and the framerate up to 120 fps [27], [28].

The aim of this article is to compare open-hardware imaging sensors for droplet microfluidic applications. In droplet microfluidic typically the following two kinds of experiments are recorded: i) droplets in some sort of backlight (similar to brightfield microscopy) and ii) droplets that contain some sort of fluorescein excited by narrow frequency range light, usually laser. Based on the most common experiments found in literature [13], [27], [29], [30], we have conducted three tests for each sensor and determined the maximum framerate performance using: i) white light emitting diode (LED) as the light source and diluted water as aqueous sample (brightfield microscopy analogue) ii) 488nm laser light and 1 µg/ml fluorescein isothiocyanate-dextran (FITC) as aqueous sample (first fluorescence experiment); iii) 488nm laser light and 10 µg/ml FITC as aqueous sample (second fluorescence experiment). The novelty of our setup is to use the combination of open source hardware (Raspberry Pi) and software that is cheaper than high speed cameras (Basler Ace) and achieve recording speeds for images (200 fps and 665 fps) that are higher than previously reported (120 fps).

II. Material and Methods

A. Materials

In the experiment, two main liquids are used, water and mineral oil. For water, deionized water is used, which for some experiments is mixed with FITC to get two different solution concentrations of 1 µg/ml and 10 µg/ml. For oil mineral oil is used. The components for experimental setup are purchased from following suppliers, from Sigma Aldrich (USA): FITC-dextran, mineral oil (code: 33779), surfactant (Span 80, code: 8.40123), microscope slides, Eppendorf tubes, polydimethylsiloxane (PDMS). From Darwin Microfluidics (France) the following components were obtained: syringes, polytetrafluoroethylene (PTFE) tubing and needles. From Farnell UK the following components are obtained: Raspberry Pi 4B, Raspberry Pi V2 camera and 5.1 V / 3.0 A USB-C power supply, SD card. From Mouser (USA) the following components were obtained: Raspberry Pi High Quality (HQ) camera, high power white LEDs and heatsink for LEDs. The Basler Ace camera was obtained directly from the manufacturer's website. From Ebay or similar source the following components were obtained: laser diode (Sharp 488 nm), housing for laser diode with lens and heatsink, XY positioning table with microadjustments and single axis positioning table for Z axis with microadjustment. To filter out the blue light form the laser and pass the expected green light emission from FITC, a colored glass long-pass filter with 495 nm cut-off wavelength was obtained from Thor labs. Some components are not listed here, but can be found in any electronics laboratory like personal computer (PC), wiring, soldering iron, and laboratory power supply.

B. Setting up Software for Cameras

Out-of-the-box Raspberry Pi 4B comes without an SD card and the software. There are many distributions of software available for Raspberry and in this experiment the native distribution of software (Raspberry Pi OS) was installed, using Raspberry Pi Imager available from the manufacturers webpage [31]. After initial startup, some minor configuration should be done where I^2C and Camera interface are enabled from Raspberry configuration. To make sure that camera system is working, *raspivid* and *raspistill* commands are used.

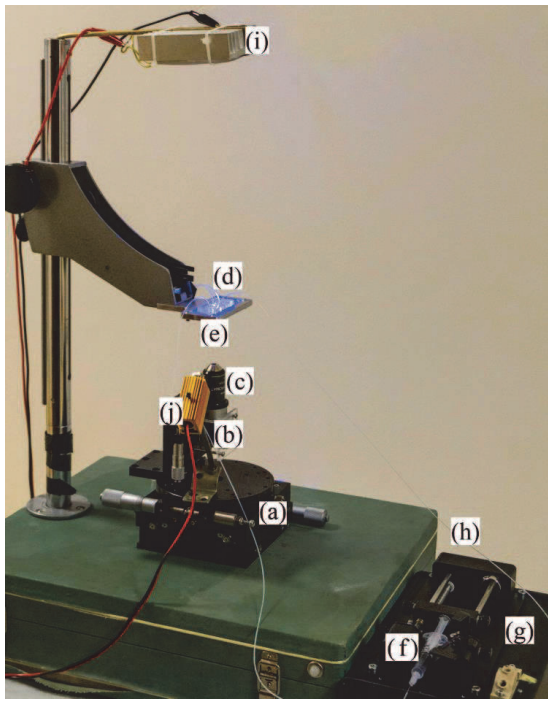

Fig. 1. The construction of a measurement setup. (a) on the base is a XYZ table (a) to which is connected camera (b) with 20x microscope lens (c). Microfluidic chip (d) is connected to custom made aluminum holder (e) that accepts 75x25mm microscope slides, syringes (f) and pumps (g) are apart from the measurement setup and are connected to PDMS chip by PTFE tubing (h). LED light (i) is directly above the microfluidic chip. Not used in the experiment currently being conducted, but laser light (j) is also present.

Yet unpublished research has shown, that the best results can be obtained if images of droplets are acquired, as the

results are sharper and contain more details compared to compressed video. Raspberry Pi allows to take pictures but does not allow to do that at high framerates. Few open-source developments are published on Github named raspiraw, which allow the version 2 camera to achieve 1000 frames per second (fps) [32]. This version of raspiraw unfortunately doesn't allow to communicate with HQ camera and another version of raspiraw is used instead [33]. An USB keyboard and a mouse are also needed and a monitor with HDMI input. In this work a generic 2 A and 5 V USB power supply is used for power and there were no issues, however the manufacturer suggests to use the 3 A and 5 V model. Despite the availability of graphical user interfaces (GUI) available for Raspberry Pi cameras, the decision was taken to work with raspiraw, which requires some knowledge about how to use terminal but offers more flexibility and detailed access to camera configuration. The documentation found in Github is sufficient to set up the camera system. However, without any previous knowledge about UNIX systems, it can be bit tedious. For Basler camera, the software that includes a GUI and a driver is available on manufacturer's website [34]. There are no steps with the setup process that need extra notion.

C. The Setup of Experiment

The base of the measurement is mechanically built around an old portable photo enlarger. The enlarger has a movable arm that enables to coarsely set the chip to the required distance from the camera lens and enables the chip to be moved away from the camera, if the lenses need to be replaced. Additionally, this coarse movement greatly helps in the prototyping phase as different lenses of different focal lengths need to be mounted at different distances from the microfluidic chip.

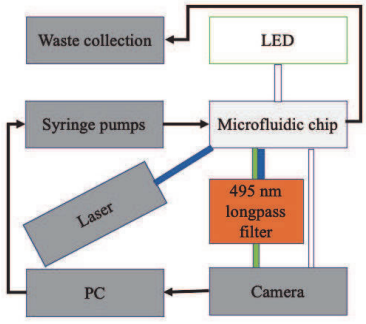

Fig. 2. Block diagram of measurement system. Two syringes (one for oil and other for water) are actuated using syringe pumps. Water and oil are pumped into Microfluidic chip where oil and water are combined into droplets. The droplets are illuminated by LED and results are captured by camera. Alternatively, laser can be used to excite FITC diluted with water. In that case longpass filter is used to filter out laser light and green emission from droplets are captured with camera.

Final adjustment can be done with the Z axis micrometre. As the initial use of the device was intended for photo-enlarging, the arm holding the microfluidic chip is fairly stable; however, a more rigid system could help to decrease vibration movements in the system. The different components of the measurement setup can be seen in Figure 1.

In addition to the measurement system there are syringes and pumps that create a constant flow of oil and water. As with different cameras the installation distances change, light sources are not attached to the rigid measurement system and are finally mounted before each test.

D. Image quality assessment

For the current paper the quality of images has been assessed visually. Thus, the evaluation criteria are subjective – mainly depending on the sharpness of objects, image brightness and object shape distortions. The criteria has been obtained through the previous experience with following image processing, mainly edge detection. The quality of images was alternatively evaluated by MATLAB function *PiQE* (Perception based Image Quality Evaluator). More detailed information can be seen in Supplementary document. The algorithm is opinion-unaware (does not need previous training on manually rated dataset) and unsupervised (model training is not needed at all). As the quality score calculation (the smaller the better) is based on block-wise distortion estimation based on the local variance of perceptibility distorted blocks, it might not produce the best estimate for neural networks-based image processing, where the models are derived by training on manually prepared datasets.

III. Results and Discussion

Three experiments were conducted with all three cameras. During the first experiment, a LED was used for illumination, and deionized water and oil were pumped into the chip. During the second and third experiments, instead of deionized water, a mixture of deionized water and FITC was used. Two different dilutions of 1 µg/ml and 10 µg/ml were used as these are the most commonly used dilutions according to literature [35]–[38] and offer the best value for the scientific community due to the similarity to practical biochemistry measurements. In the latter experiments the LED was replaced by a laser with peak wavelength of 488 nm that was used to excite the FITC and a 495 nm long-pass filter was added in front of the cameras to filter out the blue light from the laser. A usage of a LED with 480-490 nm peak emission wavelength was considered, but the idea was discarded as a typical LED has full width half maximum (FWHM) around 20-40 nm, which crosses with the emission wavelength of FITC (around 510 nm). The FWHM of the laser is typically below 5 nm. The experiments focused on achieving the maximum possible framerate by the hardware, where the droplets would still be visually distinguishable. The major bottlenecks could be in data acquisition speed from sensor and sensor capabilities. Secondary, but still important factors influencing the speed, are the computing capabilities of the acquisition system and the functionality (and speed) of the software. From the maximum framerate perspective, out of the three tested cameras, the Raspberry Pi HQ camera was the least suitable as the locked-in software didn't allow to set the resolution below 1020x760 pixels and was able to achieve framerate maximum of 200 fps. It should be stressed, that the suitability was based on the closed code for the camera, not the capabilities of the sensor it uses. For the other two cameras, due to the functionality in software that enabled to define lower resolution, the framerate of 665 fps was achievable by Raspberry V2 camera and 3000 fps by Basler

camera.

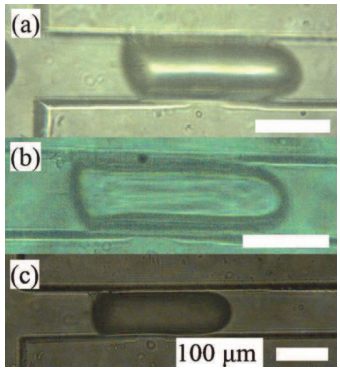

Fig. 3. Comparison of droplets using LED light. The results are recorded using (a) Raspberry Pi V2 camera, (b) Raspberry Pi HQ camera and (c) Basler Ace camera. In all cases flow rate of 2 µL/min for water and 4 µL/min for were used. Camera framerates are set to 200 fps and exposure time is reduced to 500 µs.

However, to keep the results comparable, the resolution for Raspberry Pi V2 and Basler camera was set to 640x480 pixels and for Raspberry Pi HQ camera was set to 1020x760 pixels which was later cropped to 480x640 pixels. For higher framerates the resolution was were lowered. For the pumping setup the flow rates of 2 µl/min was used for water and 4 µl/min was used for oil. In that case the expected droplet generation rate was 30 dps. Additionally, in some cases the flow rate of 4 µl/min for water and 8 µl/min was used for oil with expected droplet generation rate of 67 dps. With those flow rates, the droplet generation rate was experimentally evaluated over multiple experiments to be around second (dps). Additionally, the image quality of the droplets was evaluated to be sufficient if the camera framerate was set 3 or more times higher than the droplet generation rate.

A. Deionized Water and LED Light

Using a LED as the light source the droplets had high contrast and were fairly easy to distinguish. The results gathered with Basler Ace camera (Figure 3 (c)) were used as reference when comparing with two different cameras attached to Raspberry Pi. On Figure 3 three cameras were compared where the flowrate of liquids was 2 µl/min for water and 4 µl/min. The droplet generation rate was 29 dps. For framerate, a 200 frames per second was used for each camera. With each test, data was gathered over 1 second time period, resulting in ca 200 images per camera, though in some cases Raspberry cameras dropped some frames

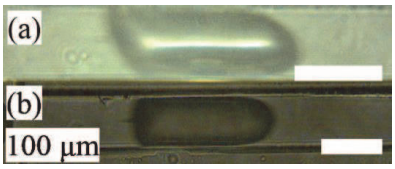

Fig. 4. Comparison of droplets using LED light. The results are recorded using (a) Raspberry Pi V2 camera running at 665 fps and (b) Basler Ace camera running at 750 fps. A flow rate of 4 µl/min for water and 8 µl/min for oil were used.

The collected images are combined to .gif file format to illustrate the droplet moving in the PDMS chip and are slowed down 10 times for better visualisation. The results for each camera can be found in supplementary files (Fig_3_a_supp.gif, Fig_3_b_supp.gif and Fig_3_c_supp.gif). The maximum theoretical exposure time with such framerate is 5000 µs, however it usually is lower due to the time consumed with data acquisition. In this experiment, the exposure time was set to 500 µs. Though Basler Ace result (Figure 3 (c)) seems dim, the droplet shows sharp edges and little to no ghosting providing the sharpest image and possibility for detailed analysis. The image from Raspberry Pi HQ camera (Figure 3 (b)) has the biggest droplet, as the image is cropped from 1020x760 pixels to 480x640 pixels. However, the edges are blurry and there is also some odd ghosting visible inside the droplet. The Raspberry Pi V2 (Figure 3 (a)) camera yielded a surprisingly clear results with bright image and only little ghosting visible near the edges of droplet. However, the sensors used for Raspberry Pi HQ and Raspberry V2 camera implement the rolling shutter compared to Basler Ace camera, which has global shutter. Droplets on Figure 3 (a) and (b) are clearly skewed compared to Basler Ace 3. The skewing effect might be less pronounced on lower flow rates, but one has to take it into account when analysing results. It is interesting to see how the Raspberry Pi V2 and Basler Ace camera perform at higher framerates. Compared to previous experiment, the flow rate of water was increased to 4 µl/min and the flow rate of oil was increased to 8 µl/min. Compared to previous experiment, the droplet generation rate is twice as high, 67 dps instead of 29 dps. The Raspberry Pi V2 camera was running at 665 fps and Basler Ace camera was running at 750 fps. The dataset of 566 and 762 images were captured. The results for each camera, which are slowed down 60 times, can be found in supplementary files (Fig_4_a_supp.gif and Fig_4_b_supp.gif). The previously seen skewing effect from rolling shutter is still present for Raspberry Pi (Figure 4 (a)) and compared to earlier (Figure 3 (a)) it is more distinct. The results from Basler Ace camera (Figure 4 (b)) seem only a little bit blurrier around the edges of droplets compared to previous (Figure 3 (c)).

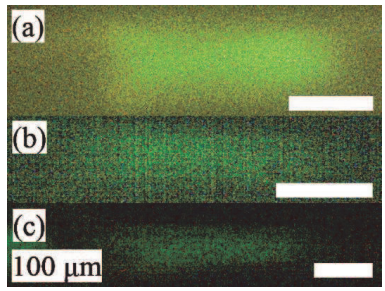

Fig. 5. Comparison of droplets using laser light and water with 1 µg/ml FITC dilution. The results are recorded using (a) Raspberry Pi V2 camera, (b) Raspberry Pi HQ camera and (c) Basler Ace camera at 200 fps. Images are cropped from 640x480 pixel frame. Ace image (Figure 4 (c)). All images are quite blurry and the results are difficult to use for any droplet morphology analysis. However, the results are sufficiently bright and sharp for droplet counting.

From the results, it can be seen, that the global shutter has its benefits when moving objects are being recorded. For

lower flowrates and lower framerates, all cameras seem suitable, as each camera captured droplets, however the images from Raspberry Pi HQ camera images were bit blurrier compared to other two.The Basler camera produces the sharpest images however with same lighting conditions the images are considerably darker compared to both Raspberry Pi cameras. With higher framerates in mind only two cameras are suitable. If one can take the skewing effect into account, the Raspberry Pi V2 camera is fairly on par with Basler Ace Camera.

A. 1 μg/ml FITC Dilution and Laser Light

Compared to previous setup, instead LED a laser is used. Additionally, a longpass filter is added to the optical pathway between the microfluidic chip and the microscope lens which considerably decreases the sharpness of droplets. Unfortunately, the filter is crucial in this setup as it cuts out the blue light and passes the green emission from FITC to sensor. Otherwise, the intense laser light oversaturates the sensor and the droplets are not detectable. The raw images from camera are unfortunately very dim and hard to distinguish. The images on Figure 5 are altered, where exposure, brightness, contrast, and shadow detail were increased to increase the visibility of droplets. Datasets of 200 images per test were collected and the results are slowed down 10 times for better visualisation. The results for each camera can be found in supplementary files (Fig_5_a_supp.gif, Fig_5_b_supp.gif and Fig_5_c_supp.gif). When compared to previous brightfield images seen on Figure 3 and 4, it is clear, that the droplets are not as clear and sharp anymore. The intensity of FITC is weak and makes it hard to distinguish droplets from the sensor noise, especially for Raspberry Pi V2 (Figure 5(a)) and Raspberry Pi HQ camera (Figure 5 (b)). The sensor noise was lower for Basler Ace camera (Figure 5 (c)), which makes the droplet to stand out better. The exposure time for each camera is set near 5000 μs and framerate was set to 200 fps. However, such results are not suitable for morphology analysis, but are good enough for droplet counting, as droplets are still recognizable.

A. 10 μg/ml FITC Dilution and Laser Light

In this experiment, the concentration of FITC was increased to 10 μg/ml. For Raspberry Pi sensors and Basler Ace camera, the framerate was set to 200 fps and exposure time was set near 5000 μs. A noticeable increase in droplet brightness can be seen for each camera. Data was gathered similarly with earlier, where every camera produced ca 200 images per test. The collected results are slowed down 10 times for better visualisation. The results for each camera can be found in supplementary files (Fig_6_a_supp.gif, Fig_6_b_supp.gif and Fig_6_c_supp.gif). For Raspberry Pi V2 camera (Figure 6 (a)) the droplet shape resembles with the size and shape seen on Figure 3 (a) with noticeable edges for
droplets. For Raspberry Pi HQ camera (Figure 6 (b)) the droplet size is similar as seen on Figure 3 (b), but the edges are less distinguished. However, these results are bit expected, as the results with LED light were also blurry. For the Basler Ace camera (Figure 6 (c)), the droplet has distinguishable edges and resembles what was seen on Fig. 3 (c).

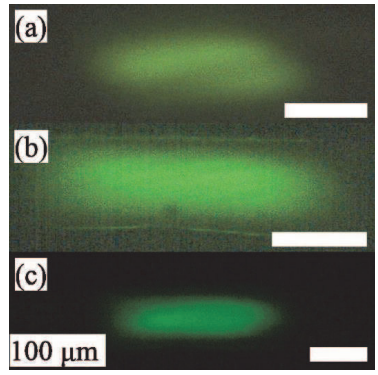

Fig. 6. Comparison of droplets using laser light and water with 10 μg/ml FITC dilution. The results are recorded using (a) Raspberry Pi V2 camera, (b) Raspberry Pi HQ camera at 200 fps and (c) Basler Ace camera at (c) 200 fps. Images are cropped from 640x480 pixel frame

The results obtained with the Raspberry Pi HQ camera are bit blurry and might not be sufficient for droplet morphology but Raspberry Pi V2 and Basler Ace show acceptable details in the results, are suitable for droplet counting and perhaps even for morphology analysis.

IV. Conclusions

In this paper we compare two open-source and one mid-range cost-effective cameras for droplet microfluidic systems. Over time different camera options have been used for droplet microfluidic systems which are ready-made modules that don't fall into the section of open source hardware. Previously some setups have used Raspberry Pi cameras, reporting framerate as high as 120 fps. In our work, two of the imaging sensors were used, Raspberry Pi V2 and High Quality camera, which were tested out using Raspberry Pi 4B, an open source small single-board computer widely used among the hobbyist and scientific community. Raspberry Pi HQ camera was able to achieve maximum framerate of 200 fps at resolution of 1020x760 pixels. This was the highest framerate we were able to set due to the software limitations of sensor resolution settings. The V2 achieved 200 fps at resolution of 480x680, but we were able to push it to 665 fps using lower resolution of 128x640 pixels. Additionally, a Basler Ace camera was used which by default can achieve up to 750 fps framerate at resolution of 640x480 pixels, but with the reduction of resolution it can go up to 4500 fps. The images captured with all three cameras were compared to one another, and based on the sharpness, brightness and of the droplet, all three cameras were able to capture droplets. However, the Raspberry Pi V2 camera produced sharper images compared to HQ camera. Additionally, the V2 camera can go higher with framerates (665 fps compared to 200 fps) and is thus more suitable for high throughput microfluidic applications. The Basler Ace produced the sharpest images of the three, even at the same settings, probably because it is using global shutter instead of rolling shutter. Additionally, Basler Ace can go up to 4500 fps at lower resolutions. Going up with the camera frame rate from 200fps (Figure 3) to 665+fps for (Figure 4) the results are still acceptable. Based on the

comparison between fps and dps (Figure 3 all are at 200fps and droplets at 67dps), the prognosis is, that both cameras could handle droplet speeds at least up to 220 dps. Though the Basler produces sharp images, the Raspberry Pi V2 camera could be considered as fair open source alternative. Basler Ace is a camera module that doesn't fill the open-hardware criteria, however the information about sensor in the module (Onsemi Python 300) is readily available on the manufacturer's web page and open hardware can be built based on the same sensor. All compared cameras are substantially cheaper that the high-speed cameras used for taking high-speed images from high droplet flow rates.

Conflicts of Interest

The authors declare that they have no conflicts of interest.

References

[1] "Lab-on-a-Chip Devices and Micro-Total Analysis Systems," Lab-on-a-Chip Devices Micro-Total Anal. Syst., 2015, doi: 10.1007/978-3-319-08687-3.

[2] M. Leman, F. Abouakil, A. D. Griffiths, and P. Tabeling, "Droplet-based microfluidics at the femtolitre scale," Lab Chip, vol. 15, no. 3, pp. 753–765, Feb. 2015, doi: 10.1039/c4lc01122h.

[3] K. Hu, B. N. Hsu, A. Madison, K. Chakrabarty, and R. Fair, "Fault detection, real-time error recovery, and experimental demonstration for digital microfluidic biochips," in Proceedings -Design, Automation and Test in Europe, DATE, 2013, pp. 559–564, doi: 10.7873/date.2013.124.

[4] S. Hassan, "Droplet-Based Microfluidics: Formation, Detection and Analytical Characterization," Res. Dev. Mater. Sci., vol. 11, no. 5, Sep. 2019, doi: 10.31031/rdms.2019.11.000774.

[5] T. S. Kaminski, O. Scheler, and P. Garstecki, "Droplet microfluidics for microbiology: Techniques, applications and challenges," Lab on a Chip, vol. 16, no. 12. Royal Society of Chemistry, pp. 2168–2187, Jun. 07, 2016, doi: 10.1039/c6lc00367b.

[6] M. T. Guo, A. Rotem, J. A. Heyman, and D. A. Weitz, "Droplet microfluidics for high-throughput biological assays," Lab on a Chip, vol. 12, no. 12. Royal Society of Chemistry, pp. 2146–2155, Jun. 21, 2012, doi: 10.1039/c2lc21147e.

[7] A. M. Kaushik, K. Hsieh, and T. H. Wang, "Droplet microfluidics for high-sensitivity and high-throughput detection and screening of disease biomarkers," Wiley Interdisciplinary Reviews: Nanomedicine and Nanobiotechnology, vol. 10, no. 6. Wiley-Blackwell, Nov. 01, 2018, doi: 10.1002/wnan.1522.

[8] M. Leman, F. Abouakil, A. D. Griffiths, and P. Tabeling, "Droplet-based microfluidics at the femtolitre scale," Lab Chip, vol. 15, no. 3, pp. 753–765, Feb. 2015, doi: 10.1039/c4lc01122h.

[9] E. Schonbrun, A. R. Abate, P. E. Steinvurzel, D. A. Weitz, and K. B. Crozier, "High-throughput fluorescence detection using an integrated zone-plate array," Lab Chip, vol. 10, no. 7, pp. 852–856, 2010, doi: 10.1039/b923554j.

[10] L. Shang, Y. Cheng, and Y. Zhao, "Emerging Droplet Microfluidics," Chemical Reviews, vol. 117, no. 12. American Chemical Society, pp. 7964–8040, Jun. 28, 2017, doi: 10.1021/acs.chemrev.6b00848.

[11] R. C. Prado and E. R. Borges, "MICROBIOREACTORS AS ENGINEERING TOOLS FOR BIOPROCESS DEVELOPMENT," Brazilian J. Chem. Eng., vol. 35, no. 4, pp. 1163–1182, Dec. 2018, doi: 10.1590/0104-6632.20180354S20170433.

[12] K. Pärnamets et al., "Optical Detection Methods for High-Throughput Fluorescent Droplet Microflow Cytometry," Micromachines 2021, Vol. 12, Page 345, vol. 12, no. 3, p. 345, Mar. 2021, doi: 10.3390/MI12030345.

[13] Y. Han, Y. Gu, A. C. Zhang, and Y. H. Lo, "Review: Imaging technologies for flow cytometry," Lab on a Chip, vol. 16, no. 24. Royal Society of Chemistry, pp. 4639–4647, Nov. 29, 2016, doi: 10.1039/c6lc01063f.

[14] N. Tottori and T. Nisisako, "High-throughput production of satellite-free droplets through a parallelized microfluidic deterministic lateral displacement device," Sensors Actuators B Chem., vol. 260, pp. 918–926, May 2018, doi: 10.1016/J.SNB.2018.01.112.

[15] S. S. Schütz, T. Beneyton, J. C. Baret, and T. M. Schneider, "Rational design of a high-throughput droplet sorter," Lab Chip, vol. 19, no. 13, pp. 2220–2232, Jun. 2019, doi: 10.1039/C9LC00149B.

[16] O. Caen et al., "High-throughput multiplexed fluorescence-activated droplet sorting," Microsystems Nanoeng. 2018 41, vol. 4, no. 1, pp. 1–10, Oct. 2018, doi: 10.1038/s41378-018-0033-2.

[17] M. H. Loo, Y. Nakagawa, S. H. Kim, A. Isozaki, and K. Goda, "High-throughput sorting of nanoliter droplets enabled by a sequentially addressable dielectrophoretic array," Electrophoresis, vol. 43, no. 3, pp. 477–486, Feb. 2022, doi: 10.1002/ELPS.202100057.

[18] H. Zhang et al., "An ultra high-efficiency droplet microfluidics platform using automatically synchronized droplet pairing and merging," Lab Chip, vol. 20, no. 21, pp. 3948–3959, Oct. 2020, doi: 10.1039/D0LC00757A.

[19] C. Lee et al., "Microfluidic droplet sorting with a high frequency ultrasound beam," Lab Chip, vol. 12, no. 15, pp. 2736–2742, Jul. 2012, doi: 10.1039/C2LC21123H.

[20] "SPECIFICATION SHEET Attune NxT Flow Cytometer Attune NxT Flow Cytometer."

[21] "Cell Analysis at the Bench: Benchtop Flow Cytometers | Biocompare: The Buyer's Guide for Life Scientists." https://www.biocompare.com/editorial-articles/146008-cell-analysis-at-the-bench-benchtop-flow-cytometers/ (accessed Mar. 18, 2022).

[22] "BD AccuriTM C6 Flow Cytometer Technical Specifications."

[23] A. S. Rane, J. Rutkauskaite, A. deMello, and S. Stavrakis, "High-Throughput Multi-parametric Imaging Flow Cytometry," Chem, vol. 3, no. 4, pp. 588–602, Oct. 2017, doi: 10.1016/j.chempr.2017.08.005.

[24] G. Holzner et al., "High-throughput multiparametric imaging flow cytometry: toward diffraction-limited sub-cellular detection and monitoring of sub-cellular processes," Cell Rep., vol. 34, no. 10, p. 108824, Mar. 2021, doi: 10.1016/j.celrep.2021.108824.

[25] C. Lei et al., "High-throughput imaging flow cytometry by optofluidic time-stretch microscopy," Nat. Protoc. 2018 137, vol. 13, no. 7, pp. 1603–1631, Jul. 2018, doi: 10.1038/s41596-018-0008-7.

[26] "The 'Entry-Level' Phantom TMX 5010 Can Shoot 1.16 Million FPS | PetaPixel." https://petapixel.com/2021/07/20/the-entry-level-phantom-tmx-5010-can-shoot-1-16-million-fps/ (accessed Mar. 18, 2022).

[27] Z. Wang et al., "A High-Resolution Minimicroscope System for Wireless Real-Time Monitoring," IEEE Trans. Biomed. Eng., vol. 65, no. 7, pp. 1524–1531, Jul. 2018, doi: 10.1109/TBME.2017.2749040.

[28] V. Jain and R. M. Patrikar, "A Low-Cost Portable Dynamic Droplet Sensing System for Digital Microfluidics Applications," IEEE Trans. Instrum. Meas., vol. 69, no. 6, pp. 3623–3630, Jun. 2020, doi: 10.1109/TIM.2019.2932526.

[29] K. Loizou, V. L. Wong, and B. Hewakandamby, "Examining the Effect of Flow Rate Ratio on Droplet Generation and Regime Transition in a Microfluidic T-Junction at Constant Capillary Numbers," Invent. 2018, Vol. 3, Page 54, vol. 3, no. 3, p. 54, Aug. 2018, doi: 10.3390/INVENTIONS3030054.

[30] P. Hadikhani, N. Borhani, S. M. H. Hashemi, and D. Psaltis, "Learning from droplet flows in microfluidic channels using deep neural networks," Sci. Reports 2019 91, vol. 9, no. 1, pp. 1–7, May 2019, doi: 10.1038/s41598-019-44556-x.

[31] "Raspberry Pi OS – Raspberry Pi." https://www.raspberrypi.com/software/ (accessed Jan. 08, 2022).

[32] "GitHub - Hermann-SW/fork-raspiraw: my raspiraw working fork for high framerate stuff (up to 750/1007 fps for v1/v2 camera)." https://github.com/Hermann-SW/fork-raspiraw (accessed Jan. 08, 2022).

[33] "GitHub - raspberrypi/raspiraw: Example app directly receiving raw data from CSI2 sensors." https://github.com/raspberrypi/raspiraw (accessed Jan. 08, 2022).

[34] "Software Download | Basler." https://www.baslerweb.com/en/sales-support/downloads/software-downloads/ (accessed Jan. 08, 2022).

[35] S. Bartkova, M. Vendelin, I. Sanka, P. Pata, and O. Scheler, "Droplet image analysis with user-friendly freeware CellProfiler," Anal. Methods, vol. 12, no. 17, pp. 2287–2294, May 2020, doi: 10.1039/D0AY00031K.

[36] J. B. Harmon, H. K. Gray, C. C. Young, and K. J. Schwab, "Microfluidic droplet application for bacterial surveillance in fresh-cut produce wash waters," PLoS One, vol. 15, no. 6, p. e0233239, Jun. 2020, doi: 10.1371/JOURNAL.PONE.0233239.

[37] S. W. Lim and A. R. Abate, "Ultrahigh-throughput sorting of microfluidic drops with flow cytometry," Lab Chip, vol. 13, no. 23, pp. 4563–4572, Oct. 2013, doi: 10.1039/C3LC50736J.

[38] M. Y. H. Tang and H. C. Shum, "One-step immunoassay of C-reactive protein using droplet microfluidics," Lab Chip, vol. 16, no. 22, pp. 4359–4365, Nov. 2016, doi: 10.1039/C6LC01121G.

Appendix 3

Publication III

K. Parnamets, A. Udal, A. Koel, T. Pardy, N. Gyimah, and T. Rang, “Compact Empirical Model for Droplet Generation in a Lab-on-Chip Cytometry System,” *IEEE Access*, vol. 10, pp. 127708–127717, 2022, doi: 10.1109/ACCESS.2022.3226623.

IEEE Access
Multidisciplinary ⋮ Rapid Review ⋮ Open Access Journal

Received 3 November 2022, accepted 21 November 2022, date of publication 2 December 2022, date of current version 9 December 2022.

Digital Object Identifier 10.1109/ACCESS.2022.3226623

RESEARCH ARTICLE

Compact Empirical Model for Droplet Generation in a Lab-on-Chip Cytometry System

KAISER PÄRNAMETS[1], (Graduate Student Member, IEEE), ANDRES UDAL[2], (Member, IEEE), ANTS KOEL[1], (Member, IEEE), TAMÁS PARDY[3], (Member, IEEE), NAFISAT GYIMAH[1], AND TOOMAS RANG[1,3], (Senior Member, IEEE)

[1]Thomas Johann Seebeck Department of Electronics, Tallinn University of Technology, 19086 Tallinn, Estonia
[2]Department of Software Science, Tallinn University of Technology, 19086 Tallinn, Estonia
[3]Department of Chemistry and Biotechnology, Tallinn University of Technology, 19086 Tallinn, Estonia

Corresponding author: Kaiser Pärnamets (kaiser.parnamets@taltech.ee)

This work was supported by the Estonian Science Agency ETAg under Grant PRG620 and Grant MOBTP109, and in part by the European Union's Horizon 2020 Research and Innovation Program under Grant 668995.

ABSTRACT This study describes the construction of a droplet generation speed compact empirical mathematical model for a flow-focusing microfluidic droplet generator. The application case is a portable, low-cost flow cytometry system for microbiological applications, with water droplet sizes of 50-70 micrometer range and droplet generation rates of 500-1500 per second. In this study, we demonstrate that for the design of reliable microfluidic systems, the availability of an empirical model of droplet generation is a mandatory precondition that cannot be achieved by time-consuming simulations based on detailed physical models. When introducing the concept of a compact empirical model, we refer to a mathematical model that considers general theoretical estimates and describes experimental behavioral trends with a minimal set of easily measurable parameters. By interpreting the experimental results for different water- and oil-phase flow rates, we constructed a minimal 3-parameter droplet generation rate model for every fixed water flow rate by relying on submodels of the water droplet diameter and effective ellipticity. As a result, we obtained a compact model with an estimated 5-10% accuracy for the planned typical application modes. The main novelties of this study are the demonstration of the applicability of the linear approximation model for droplet diameter suppression by the oil flow rate, introduction of an effective ellipticity parameter to describe the droplet form transformation from a bullet-like shape to a spherical shape, and introduction of a machine learning correction function that could be used to fine-tune the model during the real-time operation of the system.

INDEX TERMS Compact empirical model, droplet cytometry, droplet generation, flow-focusing junction, microfluidic chip.

I. INTRODUCTION

Bacterial threats have been a noticeable challenge of this century, and a delayed response due to the lack of field-testing options poses risks to human lives and can cause epidemics. Classical microbiological methods are relatively slow, while cytometric methods allow measuring the number and morphology of cells easily, reliably, and quickly. Droplet microfluidics, a new technology developed over the last dozen years, offers breakthrough solutions for creating low-cost, fully portable cytometers for field analysis of bacteria based on very small sample volumes and the possibility of seeking single-cell resolutions.

The present study discusses model-based design of portable cytometer devices based on the concepts of lab-on-a-chip [1], [2], [3], microfluidics [4], [5], and droplet cytometry [6], [7], [8], [9], [10]. Specifically, we describe the construction of an empirical mathematical model for the calculation of droplet generation rates and dimensions in the water-in-oil flow-focusing-type [11] droplet generation node of a lab-on-a-chip cytometer. This study was partly based on the digital twin model developed by our group [12].

Figure 1 illustrates the topicality trends of the considered research areas based on the publication statistics of the

The associate editor coordinating the review of this manuscript and approving it for publication was Kin Fong Lei.

Clarivate Web of Science database [13]. As demonstrated in Figure 1, the concept of lab-on-a-chip has become popular since the beginning of the 21st century, and is presently showing a saturation trend. The overall area of droplet microfluidics became popular slightly later in years 2003-2004 and has demonstrated linear growth until the present time. The most vital concept is droplet cytometry, for which exponential growth with a doubling time of 4-5 years started approximately 12 years ago. An overall comparison of regions over the last decade demonstrated the approximate equality of Western Europe, North America, and the People's Republic of China (PRC) [13].

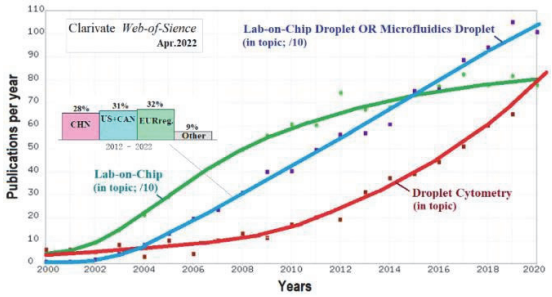

FIGURE 1. Research intensity trends on basis of Clarivate Web of Science publication statistics [13]. Dynamics of the most relevant subfields as Lab-on-Chip, droplet microfluidics and droplet cytometry is compared. Inlet compares contributions from People's Republic of China, North America and European region (incl. Turkey and Israel).

Model-based design has become a mandatory methodology for system design in various applications, including microfluidics [14], [15], [16], [17]. In the present use case, a model of the droplet generation node is required for the prediction of droplet generation parameters, such as generation rates and diameters, both during the cytometer construction and exploitation phases, to improve the control quality via model predictive control.

An important issue in the construction of a mathematical model for any object is the selection of a detailed physical or formal empirical approach [18], [19], [20], [21]. The physical approach can be time consuming for both the computer and developer but can yield reliable results for a wide range of operation conditions, provided that the physical mechanisms and relevant key parameter values are known and modelled correctly. In the case of droplet microfluidics, physical models rely on well-known equations and methods of computational fluid mechanics (CFD), which must be supplemented with less reliable multicomponent fluid flow methods [22], [23]. Thus, in addition to the high computational workload, the major problem of the physical approach is often the presence of non-measurable physical parameters and the hidden influence of numerical factors such as reduced spatial dimensionality and mesh step sizes. Although many authors have illustrated their studies with simulated droplet images, for example, [23], [24], [25], [26], several respected research groups, for example, [24], [27], [28], [29], emphasize the unreliability of numerical physical modelling, particularly if the droplet size, generation rate, and monodispersity characteristics must all be reliably calculated simultaneously. Moreover, considering the three main droplet generation geometry types – co-axial, T-junction and flow-focused [27], [30], the third option, which is also analyzed in the present study, has been estimated most difficult for the point of view of accurate modelling [20], [30], [31]. Our simulation results with the COMSOL Multiphysics®5.6 Two-Phase Flow Level Set module [32], described below in the simulation section, confirm the unreliability claims regarding the detailed physical modelling approach. To illustrate the relevant difficulties, it is reasonable to point out that to overcome the aforementioned uncertainties and obtain a reliable practical tool for flow-focusing droplet generator design, a large-scale experimental study was recently conducted by the group of Boston University [24], [28]. In this study, a generalized flow-focusing structure with an orifice was described using six geometrical parameters: 25 orthogonal structure variants were manufactured using the Taguchi formal scheme, over 30 operation modes for each structure were tested, and a statistical empirical model was obtained to cover a reasonably wide range of droplet diameters and generation rates. In comparison with [24], [28], the present study discusses only one flow-focusing structure without nozzle (orifice) section but, on the other hand, the droplet geometry description includes also the ellipticity factor, droplet generation rates are of 2-3 times higher range and the formula-based analytic formulation having a better transparency and real-time adjustability is used.

In contrast to detailed physical models, the alternative empirical approach is characterized by a formal generalization of experimental data [20], [27], [30]. The empirical approach is usually less labor-intensive and often more accurate, but only for the parameter space covered by the experiments. In practice, the most useful real models are semi-empirical, which means that they combine theoretical principles with available experimental data. In droplet microfluidics, it is reasonable to build all droplet generation models based on the mass conservation principle for the dispersed phase (i.e., droplet fluid-like water), which allows a state connection between three main variables: droplet fluid flow rate, droplet diameter, and droplet generation rate [20], [21], [28], [31]. Some authors, who have investigated the formation of relatively large non-spherical droplets that fill all cross-sections of the generation channel, have added a fourth parameter, the droplet length, for example, [20], [21], [30]. In this study, we introduce an original approach using an effective ellipticity parameter that maintains droplet volume conservation and accounts for experimentally observed droplet shape changes from bullet-like shapes at low continuous-phase flow rates to spherical shapes at high continuous-phase flow rates.

When discussing the droplet diameter empirical models, many authors have used the ratio of dispersed and continuous phase flow rates Q_d/Q_c, for example, [21], [25], [26].

Our droplet image recording results, presented below in the experimental section, do not support the use of this ratio parameter, and demonstrate that for higher water flow values, a proportional oil flow increase is required to achieve a comparable diameter suppression effect.

An important characteristic for the practical applicability of mathematical models is their compactness. We recommend defining compactness based on the following features:1) the minimal number of adjustment parameters, 2) measurability of the adjustment parameters, 3) low computational workload, and 4) transparency of the set of equations [33]. The concept of a compact model is widely used in the field of electronic and semiconductor microchip design [34] for two main reasons: lowering the computational workload and operation with measurable parameters. In droplet microfluidics, the need for compact models has not yet been explicitly recognized and only a few studies have used this term. However these studies have focused solely on estimating the length of droplets based on the ratio of dispersed and continuous phase flowrates [35], [36], [37], [38]. At the same time, nearly 1000 publications (see Figure 1) contain some approximate formulas for the calculation of droplet sizes or generation rates that may be interpreted as compact models for solving some subproblems of droplet microfluidic system design tasks.

An important question in droplet generation model construction is the description of the droplet diameter suppression effect owing to continuous phase (oil) flow. The majority of published results and models, for example, [25], [26], [39], predict a less-than-proportional diameter suppressing effect owing to the increasing continuous phase flow rate Q_c. Few studies support either a proportional decrease in diameter, for example, [31], or a stronger than proportional increase [26]. The present experimental study confirmed the applicability of the linear approximation of the dependence of the water droplet diameter on the oil flow rate. Thus, a linear droplet diameter model may be offered that uses only one proportionality factor for a fixed water flow rate and given droplet generation channel width. If completed with two parameters for the description of effective ellipticity changes, a compact 3-parameter model for the calculation of droplet diameters, ellipticities, and generation rate dependencies on the oil flow rate may be constructed.

In recent years, there has been an urgent need to accelerate and simplify the development of microfluidic droplet generators with desired output parameters via automatization and the application of machine learning methods [24], [40], [41]. To realize these goals via empirical statistical modelling by applying artificial neural networks, large-scale experimental testing [24], [28] or sophisticated computer vision methods for additional droplet data collection [40] have been proposed. In this study, a much narrower task scope was considered and only the desired droplet parameters were obtained by adjusting the water and oil flow rates for a fixed microfluidic chip. However, formula-based transparent presentation of mathematical models offers much better possibilities for solving system optimization and real-time model adjustment (i.e., machine learning) tasks. Although the modification of neural-network-based statistical models [24], [40] requires significant effort and time for the collection of additional data and retraining (transfer learning), the empirical model considered here, in the form of mathematical formulas with adjustable coefficients, offers possibilities for the realization of real-time model adjustment and a cytometer system with an extremely simple feedback loop containing an elementary optical sensor.

The remainder of this paper is organized as follows. In Section 2, the microfluidic chip and the measurement setup are described. In Section 3, a short summary of the detailed numerical simulation results and a discussion of the problems that occurred are presented. Section 4 summarizes the experimental results for the different water and oil flow rates. In section 5, the construction principles, formulas, and fitting results of the compact mathematical model are presented. Section 6 discusses the scope of the application of the proposed model. Section 7 presents the main results of the study.

II. DESCRIPTION OF DROPLET GENERATION CHIP AND MEASUREMENT SETUP

Microfluidic droplets were generated inside a polydimethylsiloxane (PDMS) chip, as shown in Figure 2. The full thickness of the PDMS chip was 5 mm, and it had a microfluidic channel structure with a depth of 100 μm on one surface (Figure 2a), which was covered by a 1 mm thick glass plate (microscope slide plate). From the three main droplet generation geometries, the T-junction, co-flow, and flow-focusing junction [11], the last geometry variant, where water flows with biological agents, is cut into droplets by a continuous oil flow entering the junction area from the two opposite sides (Figure 2a and 2c). Thus, water droplets were formed in the junction area and in the generation channel with cross-sectional dimensions of 84 μm width and 100 μm height. An overview of the droplet generation unit with the inlet and outlet tubes is shown in Figure 2b. Deionized water was used as the dispersed phase (droplets). For the continuous phase, Sigma-Aldrich 330779 mineral oil [42] with a 2% surfactant [43] was used. The water and oil flow rates were maintained using syringe pumps and software manufactured by SpinSplit [44]. The lighting of the droplet generation junction area was realized from the PDMS side of the chip using a white LED group consisting of two LEDs with cold-color temperatures and two LEDs with warm-color temperatures. Photorecording was accomplished using a Basler Ace acA640-750um camera in a reduced resolution mode that allowed a frame rate of up to 3300 per second at an exposure time of 100 μs. Thus, as the experiment shows, a droplet per second (*dps*) generation rate of up to 1600 s^{-1} can be directly determined from the sequence of the recorded images. Additionally, *dps* values up to 2300 s^{-1} can be extrapolated based on the droplet separation distances (see Figure 7).

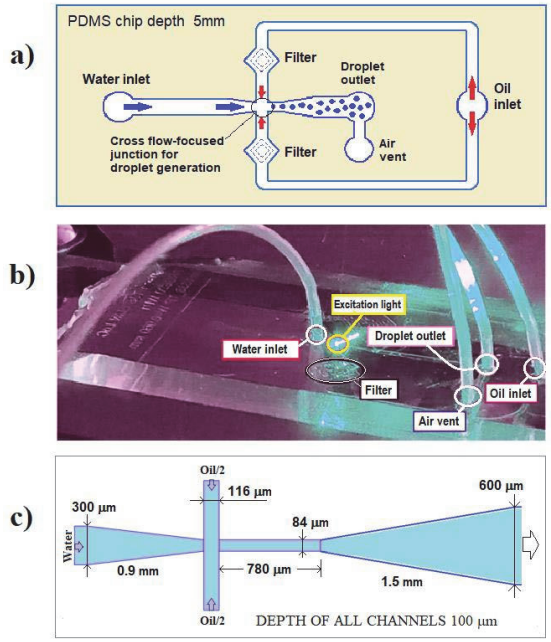

FIGURE 2. Description of the droplet generation PDMS chip: a) Water droplets generation scheme in the flow focusing cross-junction; b) Photo of the setup with inlet and outlet tubes and photorecording area; c) Exact dimensions of channels near the flow focusing junction.

III. INTRODUCTORY SIMULATIONS OF UNDERLYING PHYSICS

In general, the prerequisite for the construction of a compact model may be the availability of experimental data or, as an alternative, the availability of a sufficiently reliable detailed physical model with necessary input data. In the case of flow-focused droplet generation junctions, the choice of the detailed physical approach can be complicated by the complex nature of the task, that is, the need for accurate modelling of the balance of competing processes of separation and encapsulation of droplets. Another serious problem is the high computational time required for realistic three-dimensional calculations. Therefore, all affordable two-dimensional calculations, even if the parameters of the physical processes are correctly estimated, can only serve as predictions that need to be confirmed by real experiments. Figure 3 shows the critical competing processes that must be accurately modelled in a flow-focused junction. Figure 3 emphasizes the importance of accurately modelling the surface tension forces, viscosities of both liquids, wall friction effects, channel dimensions, and other factors to obtain a realistic picture of both the liquid flow and droplet formation processes.

To test the possibility of using detailed physical modelling to formulate the basis of the droplet generation model, we performed several numerical simulation series using the COMSOL Multiphysics®5.6 Two-Phase Flow Level Set

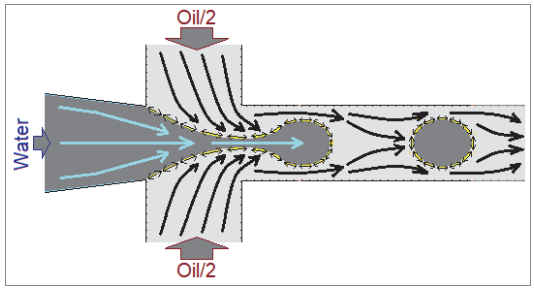

FIGURE 3. Illustration of competing processes of water droplets generation in a flow-focusing cross-junction. The incoming water stream tries to maintain the minimum surface area due to the surface tension forces but is divided into droplets by the "oil pliers" acting from both sides. After that the surface tension helps to maintain the size of droplets already formed, provided that the adjacent droplets are at a sufficient distance. At that all flow speeds are decelerated near the walls because of the wall friction effect.

module [32] in the traditional two-dimensional (2D) axisymmetric approximation of geometry [11]. It is important to emphasize that the crucial point for the accuracy of all modelling approaches is the correct handling of water volumes in the task specification. Oil can be considered an auxiliary substance that splits the incoming water stream and suppresses the diameters of the formed water droplets. Because in the 2D-simulation the droplets are cylindrical rather than spherical, the first question in the specification of the 2D-simulation task is to correctly select the effective size of the simulated structure towards the third dimension. Considering the realistic situation of the 3D-experiment (at high oil flow rates), it can be assumed that the droplets are spheres with a volume

$$V_{exp} = \frac{\pi}{6} D_{exp}^3 \tag{1}$$

where D_{exp} is the droplet diameter used in this experiment. In the 2D simulations, the volume of the droplet was defined using the cylinder formula

$$V_{sim} = \pi \cdot \left(\frac{D_{sim}}{2}\right)^2 \cdot H_{eff} \tag{2}$$

where H_{eff} is the introduced effective size of the structure towards the third dimension (see Figure 4).

The diameter and volume of the droplets must be equal to match the water volume counts in the experiments and simulations. Figure 4 shows the methodology for achieving the aforementioned water volume balance conditions when the auxiliary parameter H_{eff} of the 2D-simulation is specified as follows:

$$H_{eff} = \frac{2}{3} D_{exp}. \tag{3}$$

Specifically, if the actual expected droplet diameter is 60 μm (in the 84 μm channel), then a reasonable measure for the structure depth in 2D-simulations should be 40 μm.

Figure 5 summarizes the main results of the COMSOL 2D-simulations with the Two-Phase Flow Level

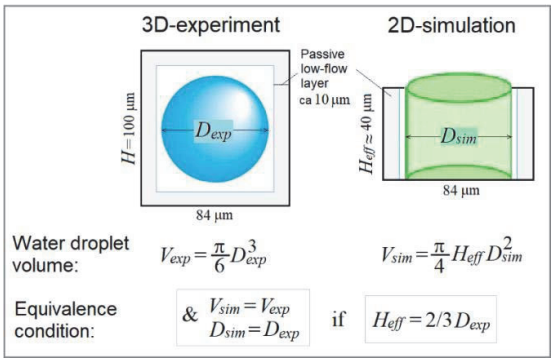

FIGURE 4. Graphical representation of droplet volumes in real life 3D-experiment and in simplified 2D-simulation.

Set module [32] for the droplet generation area described in Figure 2c. For the first adjustment parameter, the effective depth of the structure in the third dimension was specified as 40 μm based on the considerations explained above. For the second essential adjustment parameter, the surface tension coefficient values of $\sigma = 40 \div 50$mN/m were used to avoid the jetting effect and ensure the acceptable stability of the formed droplets. High surface tension values in a similar range have been recommended for water-to-mineral oil interfaces, for example, in [45] and [46]. Next, in presented simulations the "no-slip" sub model of high friction walls was used. Other models, such as the Navier slip model with several additional adjustment parameters, did not cause essential changes.

For the main computational parameters, that is, the spatial mesh size, the two standard cases of "Fine" with 9536 finite elements and "Finer" with 36626 elements were compared. The computational times for the relatively short 20 ms process calculation ranged from 2 h to 14 h on a powerful desktop 16-core Intel i9-computer.

The main results of the COMSOL simulations are shown in Figure 5. The results demonstrate the difficulty of achieving stable droplet diameters and droplet generation rates. When the spatial mesh size was increased to a very high number of final elements, instead of the expected stabilization of the main output parameters, the chaotic behavior of the results demonstrated a remarkable increase, and the definition of certain values of droplet diameters and droplet generation rates became impossible. This emerging instability and uncertainty may be caused by the difficulty of the task, as shown in Figure 3. In summary, detailed physics-based numerical simulations provide supporting explanations for the underlying physical processes. However, the expected results for building a compact model for droplet generation have not been obtained.

IV. SUMMARY OF EXPERIMENTAL RESULTS

For the actual microfluidic chip, the expected droplet generation rates were in the range of 500-1500 per second, with droplet diameters of 50-70 micrometer range. Based on these design goals, three test series with constant water flow rates $Q_w = 4, 8$, and 12μL/min and varying oil flow rates from value $Q_{oil} = 2Q_w$ to value $Q_{oil} = 60 \div 88\mu$L/min in steps of 4 μL/min were performed. The selection of droplet images recorded in the beginning section of the 84 μm generation channel is presented in Figure 6. The results in Figure 6 show that at low oil flow rates, the droplets resemble bullets (modelled by the effective ellipsoids below in this study). With an increase in the oil flow rate, the droplets begin to resemble spheres. Simultaneously, the diameter can be suppressed by increasing the oil flow rate. The increasing blurring of droplet fronts and backs at higher droplet formation rates is due to camera exposure settings (100 μs).

An overall summary of the experimental results, including the directly recorded and extrapolated *dps* values from the droplet separation distances, is shown in Figure 7. The experimental diameters of droplet D were obtained by carefully comparing the droplet lateral sizes with a channel width of 84 μm and smoothing the dependencies with the neighboring points. Thus, the estimated accuracy of the diameters was of the order of ± 2 μm. The effective ellipticity numbers, E (approximate ratio of the vertical and horizontal sizes of the droplets in the images), were estimated from the principle of equivalent volumes of the imaginary ellipsoidal and real bullet-like droplets. Additionally, minor smoothing of the experimental diameter and effective ellipticity values was performed to ensure correlation with the real water flow rates.

Owing to the camera frame rate limit, the high droplet rate values over $dps > 1600$ s^{-1} were difficult to define from video recordings but were extrapolated on the basis of the observed decrease in droplet distances (see inlet in the upper part of Figure 7). Regarding this extrapolation, it should be mentioned that because of the increasing influence of the friction of the channel walls at higher Q_{oil} rates, the size of the effective high-flow-speed center area of the channel may be smaller at high Q_{oil} values; thus, the extrapolated *dps* numbers may be underestimated.

V. CONSTRUCTION OF THE COMPACT EMPIRICAL MODEL

In the present microfluidic system design, the main purpose of developing a compact droplet generation model is to obtain a tool for estimating the droplet generation rate *dps*. The latter depends directly on the droplet volume estimation by the sub-models for the droplet size parameters, such as the diameter D and effective ellipticity E, if the water flow rate Q_w is given. The oil flow rate Q_{oil} can be interpreted as an auxiliary factor that suppresses D compact model and can be constructed based on the following approximations:

1) For droplet generation rate *dps*, recalculation from a single ellipsoidal droplet volume formula $V = E\,(\pi/6)\,D^3$ can be applied if the diameter and ellipticity are estimated with reasonable accuracy.

2) Initially, it is reasonable to consider all three water flow rate values $Q_{w,i}$ separately. The final result for any Q_w value

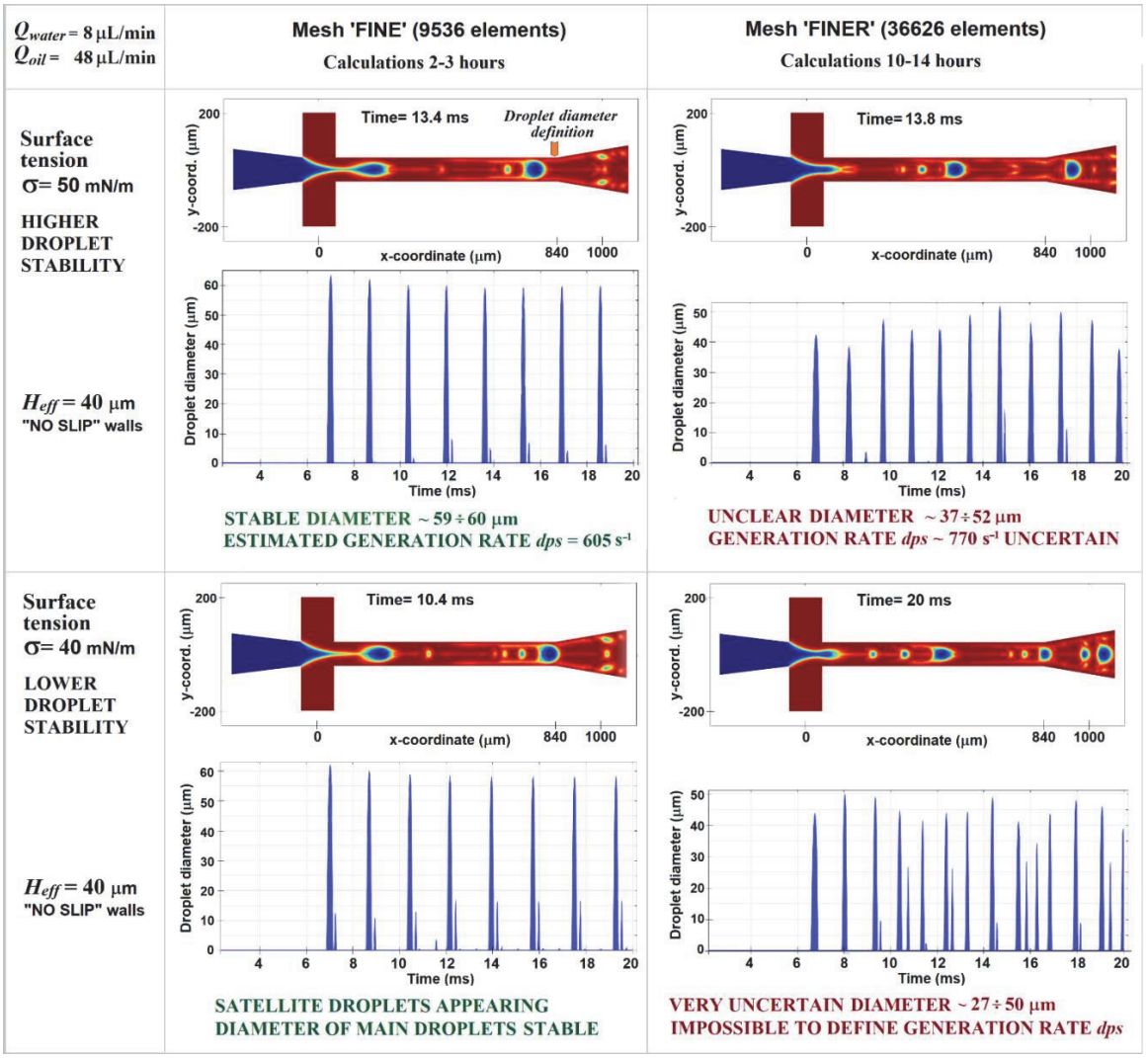

FIGURE 5. Illustration of appearance of droplet generation instabilities in detailed physical 2D-simulations with COMSOL 5.6 [32].

can be interpolated based on three separate results for dps_i, D_i, and E_i.

3) Relying on Figure 7 and seeking the principle of minimal complexity, for diameter dependence on oil flow rate $D(Q_{oil})$ the simplest single-parameter linear dependences may be applied; for the zero-oil origin point, the actual channel width value of 84 μm can be used as a common constant. The changes in *dps* in the 10% range were acceptable for an approximate adjustable model.

4) For E, the decreasing exponent law can be applied with a final level at high oil rate values close to one, which corresponds to the spherical limit form.

5) For machine learning readiness one real-time adjustable correction function $C_{ML}(Q_w, Q_{oil})$ may be added.

Considering the principles described above, the following set of mathematical equations can be proposed for the compact model (for every water flow rate value $Q_{w,i}$, i= 1, 2, 3):

$$dps_i = \left(557\ \mathrm{s}^{-1}\right)\left(\frac{Q_{w,i}}{6\ \mu\mathrm{L/min}}\right)\left(\frac{1}{E_i}\right)\left(\frac{70\ \mu\mathrm{m}}{D_i}\right)^3 \quad (4)$$

$$D_i = (84\ \mu\mathrm{m})\left(1 - \frac{Q_{oil}}{Q_{D,i}}\right) \quad (5)$$

$$E_i = 1 + (E_{8,i} - 1)\exp\left(-\frac{(Q_{oil} - 8\ \mu\mathrm{L/min})}{Q_{E,i}}\right) \quad (6)$$

where, following the goal of minimizing the number of adjustable parameters, only three fitting parameters, $E_{8,i}$, $Q_{E,i}$, $Q_{D,i}$ were introduced for each of the tested water

TABLE 1. Best fit compact model parameter values for considered 3 water flow rates.

Water rate series index i	Water flow rate $Q_{w,i}$, μL/min	Ellipticity $E_{8,i}$ at low oil rate Q_{oil} = 8 μL/min	Exponential decay parameter of ellipticity $Q_{E,i}$, μL/min	Linear decay parameter of droplet diameter $Q_{D,i}$, μL/min
1	4	2.6	9.9	157
2	8	3.6	10.4	196
3	12	4.15	12.4	248

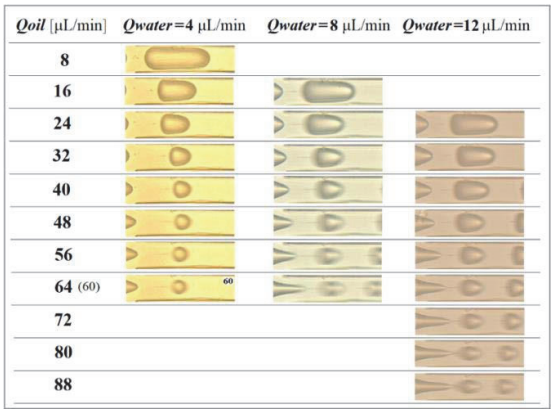

FIGURE 6. Summary of droplet photos for different water and oil flow rate values in beginning section of 84 μm generation channel. Different coloring is caused by slightly changed LED lighting between experimental series. The transform from bullet-like shapes at low oil flow rates to spherical shapes at high oil flow rates may be observed. Increasing blur of photos at high oil flow rates is caused by camera shutter time 100 μs.

flow rate values: $Q_{w,1} = 4$ μL/min $Q_{w,2} = 8$ μL/min, and $Q_{w,3} = 12$ μL/min (see Figure 6).

In systems (4)–(6), equation (4) is constructed to transform the value of the water flow rate to the number of droplets per second, considering the lateral diameter of droplets D_i and the effective ellipticity E_i as key parameters for the calculation of a single droplet volume. Equation (5) postulates the simplest linear decrease law for droplet diameters by introducing only one adjustable parameter $Q_{D,i}$ for every water rate, and using an actual channel width of 84 μm as a fixed constant for the low oil flow limit. Equation (6) approximates the exponential decrease in effective ellipticity from the initial high value at $Q_{oil} = 8$ μL/min to the final unit value using two adjustment parameters: $E_{8,i}$ and $Q_{E,i}$.

For the general case of any water flow rate between 4 and 12 μL/min, the simplest reliable piecewise linear approximation may be offered, considering that higher-order approximations such as parabolic approximations may distort the monotony of the dependences. In addition, an advanced feature of machine learning readiness may be included in the real-time empirical adjustment function $C_{ML}(Q_w, Q_{oil})$ for dps. In the minimal model formulation, the droplet size parameters may be excluded from the real-time adjustment because they droplet size parameters are difficult to measure during real-time operation.

Thus, the piecewise linear interpolation-based generalization of the droplet generation rate calculation for any water rate value can be performed using equations (7) and (8) given below.

The mathematical formulation of the linear approximation with machine learning adjustment for the first interval $Q_{w,1} \le Q_w \le Q_{w,2}$ can be written as

$$dps = C_{ML}(Q_w, Q_{oil})\left(A_{21} dps\left(Q_{w,1}\right) + B_{21} dps\left(Q_{w,2}\right)\right),$$
$$A_{21} = \frac{Q_{w,2} - Q_w}{Q_{w,2} - Q_{w,1}}, B_{21} = 1 - A_{21} \quad (7)$$

and for the second interval $Q_{w,2} \le Q_w \le Q_{w,3}$ as

$$dps = C_{ML}(Q_w, Q_{oil})\left(A_{32} dps\left(Q_{w,2}\right) + B_{32} dps\left(Q_{w,3}\right)\right),$$
$$A_{32} = \frac{Q_{w,3} - Q_w}{Q_{w,3} - Q_{w,2}}, B_{32} = 1 - A_{32}. \quad (8)$$

The fitting of the three parameters of models (4)–(6) to determine the best agreement between the model and experimental points in Figure 7 was performed by separately minimizing the root-mean-square (RMS) difference between the experiment and simulation for the three water rate values. The weight scalers for the three main output parameters, dps, D, E were 20 s^{-1}, 2 μm, and 0.1, respectively. In addition, the weights of the low oil rate endpoints for the high water rate curves $Q_{w,2}$, $Q_{w,3}$ were increased to obtain a reasonable balance with the low water $Q_{w,1}$ curve. The overall results of the fitting are shown in Figure 8. The values obtained for the model coefficients are listed in Table 1.

VI. DISCUSSION AND APPLICATION AREA

The definition of the application area is an important issue in empirical models. The general principle is that the reliability of the results can only be assumed in the range of parameter values covered by the experimental results. The application area of the proposed compact empirical model is illustrated in Figure 9. In addition, we compared our experimental results with existing droplet length estimation models and found that existing models are also suitable for our microfluidic setup after some modifications to microfluidic chip-dependent parameters [35], [36], [37], [38]. It is important to emphasize that previous studies have solely focused on estimating the length of droplets.

As shown in Figure 8, the droplet rate calculation accuracy of the proposed compact model remained in the range of 20% when considering the all-parameter area. However, it is

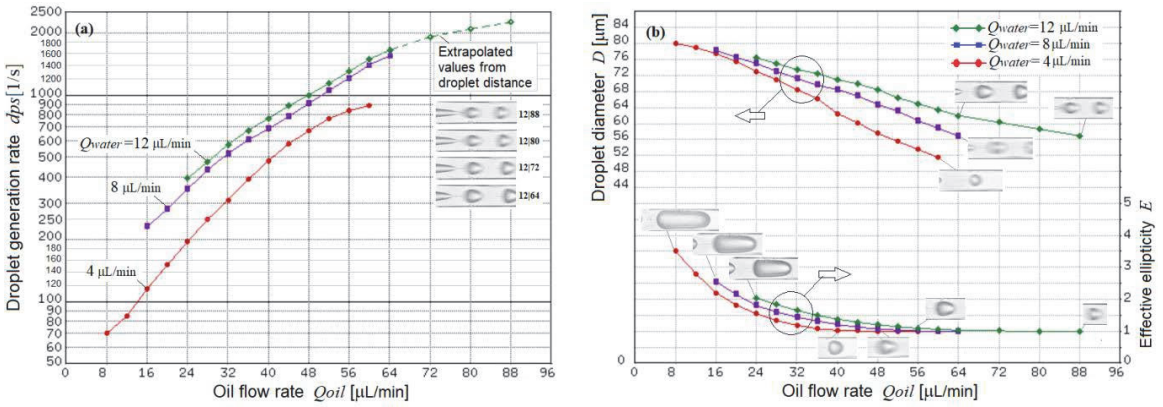

FIGURE 7. Overall summary of experimental results for droplet generation rates (a) and droplet diameters and ellipticities (b).

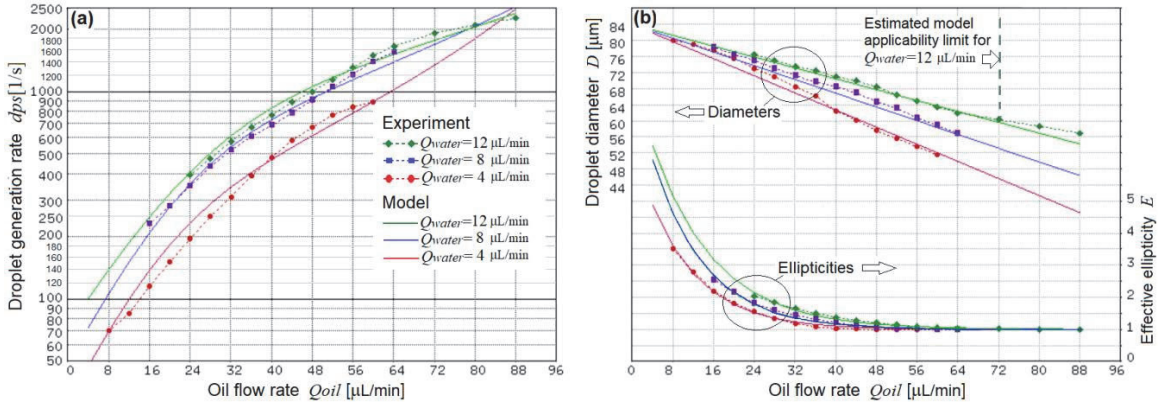

FIGURE 8. Summary of fitting results of compact empirical model (4)-(6) against experimental points for 3 water flow rate values: droplet generation rates (a); droplet diameters and ellipticities (b). Model results are presented by solid lines, experimental points by marker symbols and dotted lines.

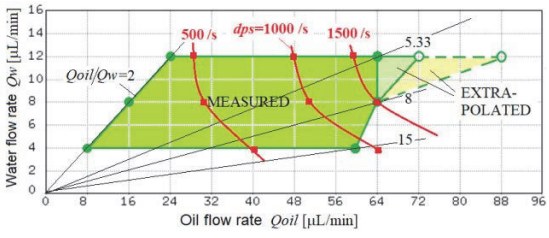

FIGURE 9. Illustration of application area of compact empirical model on the plane of water and oil flow rates.

important to emphasize that the trends of changes due to water and oil flow rate changes were modelled correctly. Additionally, for the central region of the planned operation around dps = 500-1500 s^{-1} the accuracy is much better and is already in the 5-10% range. Moreover, this number can be improved by machine-learning adjustments during real operations if the droplet generation rates are measured using optical measurements.

The reason for the moderate accuracy of the proposed simple 3-parameter model is the simplicity of modelling the droplet diameter using the simplest 1-parameter linear dependence. Since the droplet formation rate depends on the droplet diameter according to the cubic law, small differences in diameters of about 3% were increased to 10% when the formation rates were taken into account. It is possible to introduce a sub-model of a more precise diameter; however, the accompanying increase in the number of model parameters may require additional complex measurements.

From a technical viewpoint, it seems more reasonable to use a simpler model with the possibility of real-time adjustment.

VII. CONCLUSION

Compact models are a well-established approach in electronics and microelectronics but are not yet sufficiently appreciated in the relatively young field of droplet microfluidics. Although for design of any technical system, like droplet cytometry portable apparatus in the present use case, the availability of compact models for all subsystems is a highly

desirable precondition for the successful design of the system as well for later exploitation of the system. In addition, as demonstrated in the present study, the alternative approach of detailed physical modelling may not yield usable results in the case of the droplet generation task of microfluidics, where the competing balances of different physical mechanisms must be accurately modelled.

The original new results presented in the present study may be summarized as follows:

1) For the first time, a compact empirical model of droplet generation speed has been developed.
2) The applicability of the linear approximation of the dependence of the droplet diameter on the oil flow rate for the actual flow-focusing microfluidic water droplet generator task (droplet sizes in the 50-70 micrometer range and generation rates in the 500-1500 per second range) was demonstrated.
3) The concept of effective ellipticity was introduced to describe a unified model for the change of droplet geometry from a bullet-like to a spherical shape.
4) The methodology for the construction of a minimized compact 3-parameter droplet generation rate model with 5-10% accuracy for the calculation of the oil flow rate dependence at fixed water flow rates for the desired operation region was described.
5) A machine learning extension to the basic model for further adjustment using real-time measurement results was proposed.
6) The droplet-volume-based equivalence condition to make 2D-simulations comparable to the real 3D experimental geometry is discussed.

REFERENCES

[1] P. S. Dittrich and A. Manz, "Lab-on-a-chip: Microfluidics in drug discovery," *Nature Rev. Drug Discovery*, vol. 5, no. 3, pp. 210–218, Mar. 2006, doi: 10.1038/nrd1985.

[2] J.-Y. Yoon and B. Kim, "Lab-on-a-chip pathogen sensors for food safety," *Sensors*, vol. 12, no. 8, pp. 10713–10741, Aug. 2012, doi: 10.3390/S120810713.

[3] H. Craighead, "Future lab-on-a-chip technologies for interrogating individual molecules," *Nature*, vol. 442, no. 7101, pp. 387–393, Jul. 2006. [Online]. Available: https://www.nature.com/articles/nature05061, doi: 10.1038/nature05061.

[4] S. Haeberle and R. Zengerle, "Microfluidic platforms for lab-on-a-chip applications," *Lab Chip*, vol. 7, no. 9, pp. 1094–1110, Apr. 2007, doi: 10.1039/B706364B.

[5] R. Pol, F. Céspedes, D. Gabriel, and M. Baeza, "Microfluidic lab-on-a-chip platforms for environmental monitoring," *Trends Anal. Chem.*, vol. 95, pp. 62–68, Oct. 2017, doi: 10.1016/J.TRAC.2017.08.001.

[6] M. Grafton, L. M. Reece, P. P. Irazoqui, B. Jung, H. D. Summers, R. Bashir, and J. F. Leary, "Design of a multi-stage microfluidics system for high-speed flow cytometry and closed system cell sorting for cytomics," *Proc. SPIE*, vol. 6859, pp. 187–198, Feb. 2008, doi: 10.1117/12.764037.

[7] J. Fattaccioli, J. Baudry, J.-D. Émerard, E. Bertrand, C. Goubault, N. Henry, and J. Bibette, "Size and fluorescence measurements of individual droplets by flow cytometry," *Soft Matter*, vol. 5, no. 11, pp. 2232–2238, May 2009, doi: 10.1039/B814954B.

[8] M. Li, H. Liu, S. Zhuang, and K. Goda, "Droplet flow cytometry for single-cell analysis," *RSC Adv.*, vol. 11, no. 34, pp. 20944–20960, Jun. 2021, doi: 10.1039/D1RA02636D.

[9] M. Vitelli, H. Budman, M. Pritzker, and M. Tamer, "Applications of flow cytometry sorting in the pharmaceutical industry: A review," *Biotechnol. Prog.*, vol. 37, no. 4, p. 17, Apr. 2021, doi: 10.1002/BTPR.3146.

[10] H. Yang, Y. Wei, B. Fan, L. Liu, T. Zhang, D. Chen, J. Wang, and J. Chen, "A droplet-based microfluidic flow cytometry enabling absolute quantification of single-cell proteins leveraging constriction channel," *Microfluidics Nanofluidics*, vol. 25, no. 4, pp. 1–11, Apr. 2021, doi: 10.1007/S10404-021-02427-W.

[11] W. Han and X. Chen, "A review on microdroplet generation in microfluidics," *J. Brazilian Soc. Mech. Sci. Eng.*, vol. 43, no. 5, pp. 1–12, May 2021, doi: 10.1007/S40430-021-02971-0.

[12] N. Gyimah, O. Scheler, T. Rang, and T. Pardy, "Digital twin for controlled generation of water-in-oil microdroplets with required size," in *Proc. 23rd Int. Conf. Thermal, Mech. Multi-Phys. Simulation Exp. Microelectron. Microsyst.*, Apr. 2022, pp. 1–7, doi: 10.1109/EuroSimE54907.2022.9758876.

[13] Web of Science. (2022). *The Clarivate Web of Science™ Publisher-Independent Global Citation Database*. Accessed: Apr. 24, 2022. [Online]. Available: https://clarivate.com/webofsciencegroup/solutions/web-of-science/

[14] H. Hjalmarsson, M. Gevers, and F. De Bruyne, "For model-based control design, closed-loop identification gives better performance," *Automatica*, vol. 32, no. 12, pp. 1659–1673, Dec. 1996, doi: 10.1016/S0005-1098(96)80003-3.

[15] J. C. Jensen, D. H. Chang, and E. A. Lee, "A model-based design methodology for cyber-physical systems," in *Proc. 7th Int. Wireless Commun. Mobile Comput. Conf. (IWCMC)*, Jul. 2011, pp. 1666–1671, doi: 10.1109/IWCMC.2011.5982785.

[16] C. K. Harnett, J. Templeton, K. A. Dunphy-Guzman, Y. M. Senousy, and M. P. Kanouff, "Model based design of a microfluidic mixer driven by induced charge electroosmosis," *Lab Chip*, vol. 8, no. 4, pp. 565–572, Mar. 2008, doi: 10.1039/B717416K.

[17] A. Savran and G. Kahraman, "A fuzzy model based adaptive PID controller design for nonlinear and uncertain processes," *ISA Trans.*, vol. 53, no. 2, pp. 280–288, Mar. 2014, doi: 10.1016/J.ISATRA.2013.09.020.

[18] J. R. Thompson, *Empirical Model Building: Data, Models, and Reality*, 2nd ed. Hoboken, NJ, USA: Hoboken, NJ, USA: Wiley, 2011.

[19] P. A. Fritzson, *Introduction to Modeling and Simulation of Technical and Physical Systems With Modelica*. Hoboken, NJ, USA: Wiley, 2011.

[20] X. Chen, T. Glawdel, N. Cui, and C. L. Ren, "Model of droplet generation in flow focusing generators operating in the squeezing regime," *Microfluid. Nanofluidics*, vol. 18, nos. 5–6, pp. 1341–1353, May 2015, doi: 10.1007/s10404-014-1533-5.

[21] A. Biral, D. Zordan, and A. Zanella, "Modeling, simulation and experimentation of droplet-based microfluidic networks," *IEEE Trans. Mol., Biol. Multi-Scale Commun.*, vol. 1, no. 2, pp. 122–134, Jun. 2015, doi: 10.1109/TMBMC.2015.2500569.

[22] M. Wörner, "Numerical modeling of multiphase flows in microfluidics and micro process engineering: A review of methods and applications," *Microfluidics Nanofluidics*, vol. 12, no. 6, pp. 841–886, Mar. 2012, doi: 10.1007/S10404-012-0940-8.

[23] J. Kim, "Phase-field models for multi-component fluid flows," *Commun. Comput. Phys.*, vol. 12, no. 3, pp. 613–661, Sep. 2012, doi: 10.4208/CICP.301110.040811A.

[24] A. Lashkaripour, C. Rodriguez, L. Ortiz, and D. Densmore, "Performance tuning of microfluidic flow-focusing droplet generators," *Lab Chip*, vol. 19, no. 6, pp. 1041–1053, Mar. 2019, doi: 10.1039/C8LC01253A.

[25] M. Rahimi, S. Yazdanparast, and P. Rezai, "Parametric study of droplet size in an axisymmetric flow-focusing capillary device," *Chin. J. Chem. Eng.*, vol. 28, no. 4, pp. 1016–1022, Apr. 2020, doi: 10.1016/J.CJCHE.2019.12.026.

[26] A. Khater, M. Mohammadi, A. Mohamad, and A. S. Nezhad, "Dynamics of temperature-actuated droplets within microfluidics," *Sci. Rep.*, vol. 9, no. 1, pp. 1–11, Mar. 2019, doi: 10.1038/s41598-019-40069-9.

[27] S. L. Anna, "Droplets and bubbles in microfluidic devices," *Annu. Rev. Fluid Mech.*, vol. 48, no. 1, pp. 285–309, Jan. 2016, doi: 10.1146/ANNUREV-FLUID-122414-034425.

[28] A. Lashkaripour, C. Rodriguez, N. Mehdipour, R. Mardian, D. McIntyre, L. Ortiz, J. Campbell, and D. Densmore, "Machine learning enables design automation of microfluidic flow-focusing droplet generation," *Nature Commun.*, vol. 12, no. 1, pp. 1–14, Jan. 2021, doi: 10.1038/s41467-020-20284-z.

[29] A. Grimmer, M. Hamidović, W. Haselmayr, and R. Wille, "Advanced simulation of droplet microfluidics," *ACM J. Emerg. Technol. Comput. Syst.*, vol. 15, no. 3, pp. 1–16, Jul. 2019, doi: 10.1145/3313867.

[30] C. N. Baroud, F. Gallaire, and R. Dangla, "Dynamics of microfluidic droplets," *Lab Chip*, vol. 10, no. 16, pp. 2032–2045, Aug. 2010, doi: 10.1039/C001191F.
[31] W. Lee, L. M. Walker, and S. L. Anna, "Role of geometry and fluid properties in droplet and thread formation processes in planar flow focusing," *Phys. Fluids*, vol. 21, no. 3, Mar. 2009, Art. no. 032103, doi: 10.1063/1.3081407.
[32] *COMSOL Multiphysics 5.6, Laminar Flow and Two-Phase Flow, Level Set Modules. Two-Phase Flow Modeling Guidelines*. Accessed: May 3, 2022. [Online]. Available: https://www.comsol.com/support/knowledgebase/1239
[33] A. Udal, M. Jurise, J. Kaugerand, and R. Sell, "COMSPECT: A compact model of green vegetation reflectance spectra in the 400–900 nm wavelength range," *Proc. Estonian Acad. Sci.*, vol. 69, no. 4, pp. 277–286, 2022.
[34] G. Gildenblat, *Compact Modeling: Principles, Techniques and Applications*. Amsterdam, The Netherlands: Springer, 2010, doi: 10.1007/978-90-481-8614-3.
[35] A. S. Bedekar, Y. Wang, S. Krishnamoorthy, S. S. Siddhaye, and S. Sundaram, "System-level simulation of flow-induced dispersion in lab-on-a-chip systems," *IEEE Trans. Comput. Design Integr. Circuits Syst.*, vol. 25, no. 2, pp. 294–303, Feb. 2006, doi: 10.1109/TCAD.2005.858354.
[36] F. Lapierre, N. Wu, and Y. Zhu, "Influence of flow rate on the droplet generation process in a microfluidic chip," *Proc. SPIE*, vol. 8204, p. 8, Dec. 2011, doi: 10.1117/12.903271.
[37] F. Ender, M. Németh, P. Pálovics, A. Drozdy, and A. Poppe, "Thermal compact modeling approach of droplet microreactor based lab-on-a-chip devices," *Microelectron. J.*, vol. 45, no. 12, pp. 1786–1794, Dec. 2014, doi: 10.1016/J.MEJO.2014.07.005.
[38] A. Bonament, M. Madec, and C. Lallement, "Compact modeling of reaction-diffusion-advection mechanisms for the virtual prototyping of lab-on-chip," in *Proc. IEEE Int. Symp. Circuits Syst. (ISCAS)*, May 2021, pp. 1–5, doi: 10.1109/ISCAS51556.2021.9401396.
[39] K. I. Belousov, N. A. Filatov, I. V. Kukhtevich, V. Kantsler, A. A. Evstrapov, and A. S. Bukatin, "An asymmetric flow-focusing droplet generator promotes rapid mixing of reagents," *Sci. Rep.*, vol. 11, no. 1, pp. 1–10, Apr. 2021, doi: 10.1038/s41598-021-88174-y.
[40] A. E. Siemenn, E. Shaulsky, M. Beveridge, T. Buonassisi, S. M. Hashmi, and I. Drori, "A machine learning and computer vision approach to rapidly optimize multiscale droplet generation," *ACS Appl. Mater. Interfaces*, vol. 14, no. 3, pp. 4668–4679, Jan. 2022, doi: 10.1021/ACSAMI.1C19276.
[41] S. Srikanth, S. K. Dubey, A. Javed, and S. Goel, "Droplet based microfluidics integrated with machine learning," *Sens. Actuators A, Phys.*, vol. 332, Dec. 2021, Art. no. 113096, doi: 10.1016/J.SNA.2021.113096.
[42] *Sigma-Aldrich Mineral Oil. Sigma-Adrich Mineral Oil 330779-1L Data Page*. Accessed: May 3, 2022. [Online]. Available: https://www.sigmaaldrich.com/EE/en/product/sial/330779
[43] *Sigma-Aldrich Surfactant. Sigma-Adrich Span 80 (Code 840123100) Data Page*. Accessed: May 3, 2022. [Online]. Available: https://www.sigmaaldrich.com/EE/en/product/mm/840123
[44] SpinSplit. *Lab Equipment for Academic Research*. Accessed: May 3, 2022. [Online]. Available: https://spinsplit.com/spincube/
[45] W.-L. Ong, J. Hua, B. Zhang, T.-Y. Teo, J. Zhuo, N.-T. Nguyen, N. Ranganathan, and L. Yobas, "Experimental and computational analysis of droplet formation in a high-performance flow-focusing geometry," *Sens. Actuators A, Phys.*, vol. 138, no. 1, pp. 203–212, Jul. 2007, doi: 10.1016/J.SNA.2007.04.053.
[46] *Surface Tension Values of Some Common Test Liquids for Surface Energy Analysis*. Accessed: May 3, 2022. [Online]. Available: http://www.surface-tension.de/

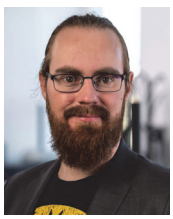

KAISER PÄRNAMETS (Graduate Student Member, IEEE) was born in Tallinn, Estonia, in January 1989. He received the Bachelor of Science and Master of Science degrees in engineering from the Tallinn University of Technology, in 2013 and 2016, respectively, where he is currently pursuing the Ph.D. degree. From 2014 to 2017, he was a Hardware Engineer at the electronics industry. Since 2018, he has been an Electronics Lecturer for bachelor's and master's students. His research interests include lab-on-a-chip and microfluidics.

ANDRES UDAL (Member, IEEE) received the Ph.D. degree in electronic engineering from the Tallinn University of Technology, Tallinn, Estonia, in 1999. From 1990 to 1995, he was acting as a Visiting Researcher and a TCAD Software Designer at Silvaco Inc., Santa Clara, CA, USA; Darmstadt University of Technology, Germany; and Uppsala University, Sweden. He is currently a Senior Research Fellow with the Laboratory for Proactive Technologies, Department of Software Science, Tallinn University of Technology.

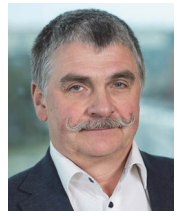

ANTS KOEL (Member, IEEE) was born in Tallinn, Estonia, in August 1962. He received the Engineer Diploma degree in industrial electronics from the Tallinn Polytechnic Institute, Estonia, in 1985, the master's degree, in 1998, and the Ph.D. degree from the Tallinn University of Technology, Tallinn, Estonia, in 2014. His research interests include semiconductor electronics and devices, TCAD simulations, and circuit design. He has been the Chairperson of the Steering Committee of the IEEE-Sponsored Baltic Electronics Conference, in 2020 and 2022, participated in ERA Chair projects COEL and 5GSOLAR, led electronics in-kind contribution projects of Estonia in European Spallation Source.

TAMÁS PARDY (Member, IEEE) received the M.Sc. degree in info-bionics engineering from Pázmáany Péter Catholic University, Budapest, Hungary, in 2014, and the Ph.D. degree in electronics and telecommunication from the Tallinn University of Technology, Tallinn, Estonia, in 2018. He is currently a Senior Researcher with the Tallinn University of Technology. He has supervised one Ph.D. thesis and three M.Sc. theses and has authored or coauthored 20 scientific publications. His research interests include flow- and temperature-control of lab-on-a-chip devices.

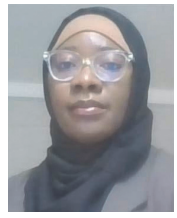

NAFISAT GYIMAH received the B.S. degree in electrical and electronic engineering from the Kwame Nkrumah University of Technology, Kumasi, Ghana, in 2013, and the M.S. degree in communicative electronics from the Tallinn University of Technology, Tallinn, Estonia, in 2020, where she is currently pursuing the Ph.D. degree in high-speed droplet microfluidics sorting and encapsulation. She was a Cognitronics Engineer at the Tallinn University of Technology, from June 2020 to December 2020. From November 2021 to January 2022, she worked at Selfdiagnostics Deutschland GmbH on the thermal and electrical characterization of SARS-CoV2 microfluidic multitest kits. Her research interests include lab-on-a-chip, droplet microfluidic system control, and flow control simulations using computational fluid dynamics (CFD).

TOOMAS RANG (Senior Member, IEEE) received the Ph.D. degree in semiconductor electronics from the Hungarian Academy of Sciences, in 1981. He is currently a Professor Emeritus with the Thomas Johann Seebeck Department of Electronics, and a Senior Research Fellow with the Department of Chemistry and Biotechnologies, Tallinn University of Technology, Estonia. His research activities related to research and development in the field of applied microfluidic approaches for lab-on-a-chip applications. He supervised 15 Ph.D. Students and fulfilled the PI position on several European and domestic research and industrial projects. He was the Initiator and an Honor Chairperson of the Baltic Electronics Conferences (BEC) series, in 1987, and has been supported by IEEE, since 1996.

Curriculum vitae

Personal data

Name:	Kaiser Pärnamets
Date of birth:	05.01.1989
Place of birth:	Keila
Citizenship:	Estonia

Contact data

E-mail:	kaiser.parnamets@ttu.ee

Education

2016–2023	Tallinn University of Technology, Information and Communication Technology, PhD
2014–2016	Tallinn University of Technology, Information and Communication Technology, MsC, *cum laude*
2008–2013	Tallinn University of Technology, Electronics and bionics, Bsc
2005–2008	Tallinn Nõmme Gymnasium

Language competence

Estonian	Native
English	Fluent
Russian	Basic

Professional employment

2018– …	Tallinn University of Technology, School of Information Technologies, Thomas Johann Seebeck Department of Electronics, Lecturer
2013–2017	The Systems LLC, Hardware engineer

Elulookirjeldus

Isikuandmed

Nimi:	Kaiser Pärnamets
Sünniaeg:	05.01.1989
Sünnikoht:	Keila
Kodakondsus:	Eesti

Kontaktandmed

E-post:	kaiser.parnamets@ttu.ee

Hariduskäik

2016–2023	Tallinna Tehnikaülikool, Info- ja kommunikatsioonitehnoloogia, doktoriõpe
2014–2016	Tallinna Tehnikaülikool, Info- ja kommunikatsioonitehnoloogia, magistriõpe, *cum laude*
2008–2013	Tallinna Tehnikaülikool, Elektroonika ja bioonika, bakalaureuseõpe
2005–2008	Tallinna Nõmme Gümnaasium

Keelteoskus

Eesti keel	emakeel
Inglise keel	kõrgtase
Vene keel	algtase

Teenistuskäik

2018–...	Tallinna Tehnikaülikool, Infotehnoloogiateaduskond, Thomas Johann Seebecki elektroonikainstituut, lektor
2013–2017	The Systems OÜ, Riistvara insener

ISSN 2585-6901 (PDF)
ISBN 978-9916-80-023-2 (PDF)